NORTHWESTERN UNIVERSITY

Effects of Nanoscale Confinement and Interfaces on the Structural Relaxation of Amorphous Polymers Monitored at the Molecular Scale by Fluorescence and Dielectric Spectroscopy

A DISSERTATION

SUBMITTED TO THE GRADUATE SCHOOL IN PARTIAL FULFILLMENT OF THE REQUIREMENTS

for the degree

DOCTOR OF PHILOSOPHY

Field of Chemical Engineering

By

Rodney Dewayne Priestley

EVANSTON, ILLINOIS

June 2008

ABSTRACT

Effects of Nanoscale Confinement and Interfaces on the Structural Relaxation of Amorphous Polymers Monitored at the Molecular Scale by Fluorescence and Dielectric Spectroscopy

Rodney Dewayne Priestley

Over the past decade and a half, there has been considerable interest in the effect confinement and interfaces have on the properties of glass forming materials. With the emergence of nanotechnology, some glass formers, in particular polymeric glass formers, will be used at increasingly smaller length scales. An understanding of how polymeric properties are impacted by confinement and interfaces is essential to their full utilization in nanotechnology applications. The focus of this work was to investigate how confinement and interfaces impact the α-relaxation dynamics, the glass transition temperature (T_g), and physical aging of polymers.

In this work, a unique fluorescence / multilayer method was employed to investigate confinement and interfacial effects on the T_g of a series of poly(n-methacrylate) films. Fluorescent probe-labeled polymer was selectively placed at known locations within a multilayer film. It was demonstrated that there exists a correlation between the observed deviation in T_g with confinement for single layer films and the relative strength of the deviation in T_g of free surface and substrate interface layers of the films.

In addition, a novel dielectric / multilayer technique was developed allowing for measurements of the α-relaxation dynamics at surfaces and interfaces. The technique is analogous to the fluorescence / multilayer technique except for the choice of probe. It was illustrated that the reorientation and rotational dynamics of molecular dipole probes were coupled to the α-relaxation dynamics of polymer. Studies show for the first time that the α-relaxation dynamics at the aluminum-polymer interface are faster and broader compared to the film interior.

Lastly, work presented within the dissertation investigated confinement and interfacial effects on physical aging. It was shown for the first time that physical aging could be strongly suppressed via attractive interactions between a polymer and an inorganic interface. Dielectric relaxation spectroscopy provided evidence that the suppression of physical aging with confinement is related to the reduction of β-relaxation dynamics with confinement.

In summary, this work investigated confinement and interfacial effects on the relaxation dynamics of polymer at the glass transition (T_g), above the glass transition (α-relaxation dynamics), and below the glass transition (physical aging).

ACKNOWLEDGEMENTS

To my advisors Linda Broadbelt and John Torkelson – Thank you for all your support and encouragement over the last five years, I really appreciate it. I have learned a great deal from each of you. I look forward to being your colleagues in the future.

To all Broadbelt and Torkelson research group members – Thanks for the support and good times. Perla, Simon, Jim, Seth, Xinrui, Amanda, Manish, Kat, and Connie – it has been a lot of fun. Chris and Andrew (Chobix) - Thanks for the fun memories.

To my engineering BGSA family Ashley, Cynthia, Ade, Stacey, James, Rassia, Yalonda, Michele, Dedra, Laura and Lexyene – it has been real! Ashley (Docbix) and Cynthia – Thanks for the special friendships. Stacey and James – my runner partners, hopefully one day I will be as fast as you.

To my parents Wanda and Steve Thompson – Thanks for instilling in me the values and hard work required to be successful and the love and encouragement. We will reap the benefits together! I did this for you, Terrence and myself.

To my brother Terrence Priestley – We will always hold each other down, much much love.

À mon fiancée, Anny Flory - merci de votre amour, appui, et pendant d'encouragement ce processus. Vous avez facilité terminant ces travaux beaucoup et avez rempli ma vie avec joie. J'attends avec intérêt de passer nos vies ensemble, de goûter le vin à Paris, et de l'absorber le soleil dans Gaudeloupe.

À ma plus nouvelle famille Mary Odile et Maruice et leurs enfants - mercis de l'amour et de l'appui et de rendre toujours me la sensation distante de la famille.

To everyone I did not directly name – Thank you very much.

To the Ronald E. McNair Scholars Program at Texas Tech University

TABLE OF CONTENTS

LIST OF TABLES

LIST OF FIGURES

1 INTRODUCTION

With nanoscale confinement, it has been observed that the properties of materials can deviate substantially from the bulk. In particular, for polymeric systems, changes in glass transition temperature (T_g), physical aging, elastic modulus, creep compliance, crystallization, and α-relaxation time distribution have been observed with confinement. Here, the term *confinement* refers to the physical confinement of polymer to the nanometer length scale.

The reasons for investigating nanoscale confinement effects on the properties of polymers are driven by both technology and scientific inquiry. The future of nanotechnology will require the use of polymers confined to dimensions less than 100 nm (the National Science Foundation defines the *nanoscale* length to be less than 100 nm). Further understanding of important macroscopic polymeric properties is believed to be accessible via studies of polymer confined to the length scale at which the properties themselves are defined, that is the nanoscale.

Polymers are considered an enabling material for nanotechnology as they have found use in many applications. For example, in the area of separations, 20 to 80 nm thick polymeric skin layers are used in the production of asymmetric membranes (Koros 1993). In the area of microelectronics, future devices will require the development of photoresists with feature sizes less than 100 nm (Mundra 2007a). Nanoconfined polymer is also critical in materials development (Winey 2007). For polymer nanocomposites, in which the nanofiller load level is only several volume percent, all polymer chains reside less than 100 nm from a nanofiller interface; thus, polymer in nanocomposites is nanoconfined. Polymer nanocomposites are very

interesting because they are bulk materials; however, their properties can be controlled by nanoconfined polymer. Critical to the optimal use of polymers in nanotech applications is an understanding of how their properties are impacted by nanoconfinement.

Two polymer relaxation phenomena of critical technical importance are the T_g and physical aging response. The T_g is the temperature at which a polymer exhibits a transition from a rubber to a glass. Physical aging is the spontaneous structural relaxation in the glassy state that results in a time dependence of material properties. Work presented in this thesis addresses the impact of nanoscale confinement on the T_g and physical aging of polymers. In addition, the impact of confinement on the α-relaxation dynamics (relaxation process associated with the glass transition) will be investigated. It will be presented that nanoscale confinement can lead to dramatic changes in the properties discussed above. Reasons for why such dramatic changes are observed will also be presented. A general conclusion from this work is that nanoconfinement effects are a result of interfacial effects.

From a historical point of view, Keddie *et al*. (Keddie 1994a; Keddie 1994b) were the first to measure a change in T_g of ultrathin polymer films (less than 80 nm) compared to T_g(bulk). It was observed that T_g of polystyrene (PS) films supported on silica decreased with confinement while that of poly(methyl methacrylate) (PMMA) increased with confinement. Conversely, PMMA films supported on gold exhibited a decrease in T_g with confinement. In 1996, Forrest *et al*. (Forrest 1996) showed that freely standing films of PS and PMMA exhibited reductions in T_g with confinement. The results were generally understood to result from interfacial effects. In those cases in which T_g decreased with confinement, it was hypothesized that the effect was associated with the presence of the free surface enhancing the dynamics associated with T_g. In

those cases in which T_g increased with confinement, it was hypothesized that the effect was associated with how attractive polymer-substrate interactions reduced the dynamics associated with T_g. Using a fluorescence / multilayer approach, Ellison and Torkelson provided valuable insight into the effect of confinement on T_g for those cases in which T_g decreased with confinement (Ellison 2003).

Studies by Hall *et al*. (Hall 1997b) and Fukao *et al*. (Fukao 1999; Fukao 2000) were the first to show that the α-relaxation dynamics of thin polymer films were impacted by nanoconfinement. In agreement with T_g studies of PS, the α-relaxation dynamics were enhanced with confinement (Fukao 1999). In addition, there was an observed broadening of the α-relaxation time distribution of PS with confinement (Fukao 1999).

The first studies that investigated the effect of confinement on physical aging were those from the membrane research literature (Pfromm 1995). Pfromm and Koros observed that the physical aging response of polyimide films was accelerated compared to the bulk at thicknesses approaching the micron length scale. Work by Huang and Paul (Huang 2004) conducted nearly a decade later is in agreement with work from Pfromm and Koros.

This thesis will present work that adds to our understanding of the impact of confinement on T_g, the α-relaxation dynamics, and physical aging of thin polymer films. After the Introduction, Section I (which includes Chapters 2-4) will provide necessary background information required for understanding the work presented. Chapter 2 will provide an overview of the physics of the glass transition. Topics discussed in Chapter 2 include glass formation, models of the glass transition, dynamic heterogeneity and physical aging.

This work was preceded by many studies aimed at characterizing and understanding

confinement effects on the properties of polymers. Properties of interest include T_g, physical aging, elastic modulus, creep compliance, crystallization, etc. Chapter 3 provides a survey of selected important literature done prior to completion of this thesis.

Fluorescence spectroscopy and dielectric relaxation spectroscopy are employed in novel ways to investigate confinement and interfacial effects on the relaxation dynamics of polymers above, below, and at T_g. Chapter 4 provides fundamental information about fluorescence spectroscopy and dielectric relaxation spectroscopy as well as practical information for using the techniques to probe polymer dynamics.

Section II, which includes Chapters 5 and 6, details the impact of confinement and interfaces on T_g of thin polymer films supported on silica for which there exist attractive polymer-substrate interactions. In agreement with previous studies, Chapter 5 shows that the values T_g of PMMA films supported on silica increase with confinement. Chapter 5 illustrates for the first time that the observed increase in T_g with confinement for PMMA films supported on silica is a result of competing interfacial effects. The free surface leads to a reduction in T_g, while the substrate leads to an increase in T_g. A major conclusion from Chapter 5 is that the stronger substrate effects result in an overall increase in T_g of PMMA films supported on silica. In addition, the results will be considered in the context of the Adam-Gibbs theory.

Chapter 6 investigates the impact of confinement and interfaces on T_g of a series of poly(n-methacrylate)s: PMMA, poly(ethyl methacrylate) (PEMA), poly(propyl methacrylate) (PPMA), and poly(isobutyl methacrylate) (PIBMA). It is observed T_g of PMMA increases with confinement, T_g of PEMA and PPMA decreases with confinement, and T_g of PIBMA is independent of confinement. A key conclusion from the chapter is that there exists a correlation

between the observed deviation in T_g with confinement for single layer films and the relative strength of the deviation in T_g of free surface and substrate interface layers of the films.

Section III, which includes Chapters 7 and 8, focuses on the impact of confinement and interfaces on the α-relaxation dynamics of PS. Chapter 7 shows that PS labeled with the molecular dipole, Disperse Red 1 (DR1), serves as an excellent system to investigate confinement effects on the α-relaxation dynamics. While PS labeled with DR1 exhibits enhanced (strength of signal) α-relaxation dynamics compared to neat PS, the impact of confinement on the dynamics is similar. Work by Fukao *et al*. (Fukao 2000) has suggested that confinement effects on the α-relaxation dynamics are a result of interfacial effects.

Chapter 8 illustrates for the first time the ability to measure the interfacial α-relaxation dynamics of a polymer using a multilayer / dielectric relaxation spectroscopy (DRS) technique. The technique is analogous to the multilayer / fluorescence technique presented in Chapter 5 and work by Ellison and Torkelson (Ellison 2003) with the difference being the choice of label. Results presented in Chapter 8 show that the α-relaxation dynamics are faster at the aluminum (Al)-polymer interface (DRS measurements require the presence of an Al electrode atop the free surface of the polymer; however, it has been shown that the interface behaves as a free surface (Fukao 2000)).

Section IV, which includes Chapters 9, 10, 11, and 12, focuses on the impact of confinement and interfaces on the physical aging behavior of polymer films and nanocomposites. Chapter 9 illustrates the importance of polymer-substrate interactions on the physical aging response of ultrathin polymer films. When aged deep in the glassy state, PS supported on silica exhibits no aging-confinement effect (deviation in physical aging rate with confinement), while

PMMA films supported on silica exhibit a dramatic reduction in their physical aging rate with confinement. The difference in the impact that confinement has on the physical aging response of PS and PMMA is rationalized via differences in polymer-substrate interactions. Polystyrene and silica have no attractive interactions, while PMMA and silica exhibit hydrogen bonding interactions with one another. The attractive polymer-substrate interactions are thought to reduce the molecular mobility associated with physical aging.

Chapter 10 provides the first direct measurement of physical aging at the interfaces of a polymer film using the fluorescence / multilayer technique. For PMMA films supported on silica, when aged deep in the glassy state, aging is reduced near the free surface and strongly suppressed near the substrate interface. When aged at a temperature near the bulk T_g (T_g (bulk) – 5 K), physical aging does not occur near the free surface as a result of a reduced T_g at the free surface of approximately 7-8 K. Thus, under the appropriate conditions there can exist an equilibrium rubbery layer at the free surface of a glassy polymer.

While Chapters 9 and 10 explore the aging response of polymers by monitoring the fluorescence emission intensity as a function of aging time, Chapter 11 provides the first demonstration of monitoring physical aging via a ratio of fluorescence intensities. The advantage of monitoring aging via a ratio of intensities is that the extent of aging toward equilibrium can be determined. With this approach, it was observed for the first time that both glass formation and the extent of aging toward equilibrium are impacted by confinement.

Chapter 12, the last chapter in Section IV, provides a molecular-scale origin for the suppression of aging in PMMA / silica systems (PMMA films supported on silica or silica-PMMA nanocomposites). Dielectric relaxation spectroscopy is used to investigate the strength

of the β process of silica-PMMA nanocomposites with varying amounts of silica nanoparticles. It is observed that with increasing silica content in the nanocomposite, the strength of the β process decreases. From such a result it is concluded that the suppression of physical aging in PMMA / silica systems results from a reduced β process (dynamics) that results from hydrogen bonding interactions between PMMA and silica.

Section V, which includes Chapter 13, provides key conclusions from this study as well as potential future work.

(The author developed a novel model nanocomposite geometry to investigate confinement and interfacial effects on T_g and physical aging that complimented similar measurements undertaken on real nanocomposites. See reference Rittigstein 2007 for details of the work.)

PART I: BACKGROUND

2 PHYSICS OF THE GLASS TRANSITION FOR AMORPHOUS POLYMERS

2.1 Introduction

This chapter provides background information necessary to understand the research presented in this work. The important features of glass formation and glassy behavior will be presented. The chapter presents the thermodynamics of the glass transition, kinetics of the glass transition, models of the glass transition, dynamic heterogeneity and physical aging.

2.2 Dynamics and Thermodynamics of the Glass Transition

Although significantly studied for well over half a century, the physics of the glass transition are still of great scientific interest and remain one of the deepest and most interesting unsolved problems in physics (Anderson 1995). The glass transition exhibits certain aspects of a second-order thermodynamic transition but is experimentally observed to be a kinetic phenomenon. Extensive reviews have been written about the glass transition (Kauzmann 1948; Tant 1981; McKenna 1989; Angell 1995; Hutchinson 1995; Angell 2000; Ediger 2000; Debenedetti 2001; McKenna 2002). Rather than attempting to do justice to the entire field of glass formation and glass behavior, a brief overview will be given here. The overview will discuss glass formation and behavior in three temperature domains: above, below, and at the glass transition temperature (T_g).

2.2.1 Glass Formation and the Glass Transition Temperature

As stated by Angell, "a glass in the popular and basically correct conception is a liquid that has lost its ability to flow" (Angell 1995). Structurally, there is virtually no difference between the supercooled liquid and its glassy state. Upon cooling of a glass-forming liquid, the molecular motions undergo a dramatic slowing down in the cooperative segmental dynamics. At a particular temperature, the molecules will lose the ability to rearrange structurally into thermodynamic equilibrium. Subsequent cooling results in the formation of a non-equilibrium glass. The temperature at which an equilibrium liquid passes into its non-equilibrium glassy state is defined as the glass transition temperature. Thus, T_g is the temperature at which there is a transition from the liquid state to the glassy state.

Figure 2-1 illustrates the specific volume or specific enthalpy as a function of temperature for a non-crystallizable supercooled liquid (polymer). The intersection of the liquid state and glassy state lines provides one measure of T_g. However, the behavior depicted in Figure 2-1 (for one particular curve) is not that of a true second-order thermodynamic transition since there is no discontinuity in specific volume or specific enthalpy as a function of temperature (McKenna 1989; Debenedetti 2001).

As shown in Figure 2-1, T_g depends on the cooling rate. The faster a glass-forming liquid is cooled, the shorter is the time allowed for the molecules to rearrange structurally into thermodynamic equilibrium. As a result, the higher the cooling rate, the higher the T_g. Typically, one order of magnitude change in cooling rate will result in a 3-5 K change in T_g (Ediger 1996). The observation that T_g depends on the rate of cooling illustrates a key phenomenon of glasses, that is, the properties of glasses depend on the manner in which they are formed.

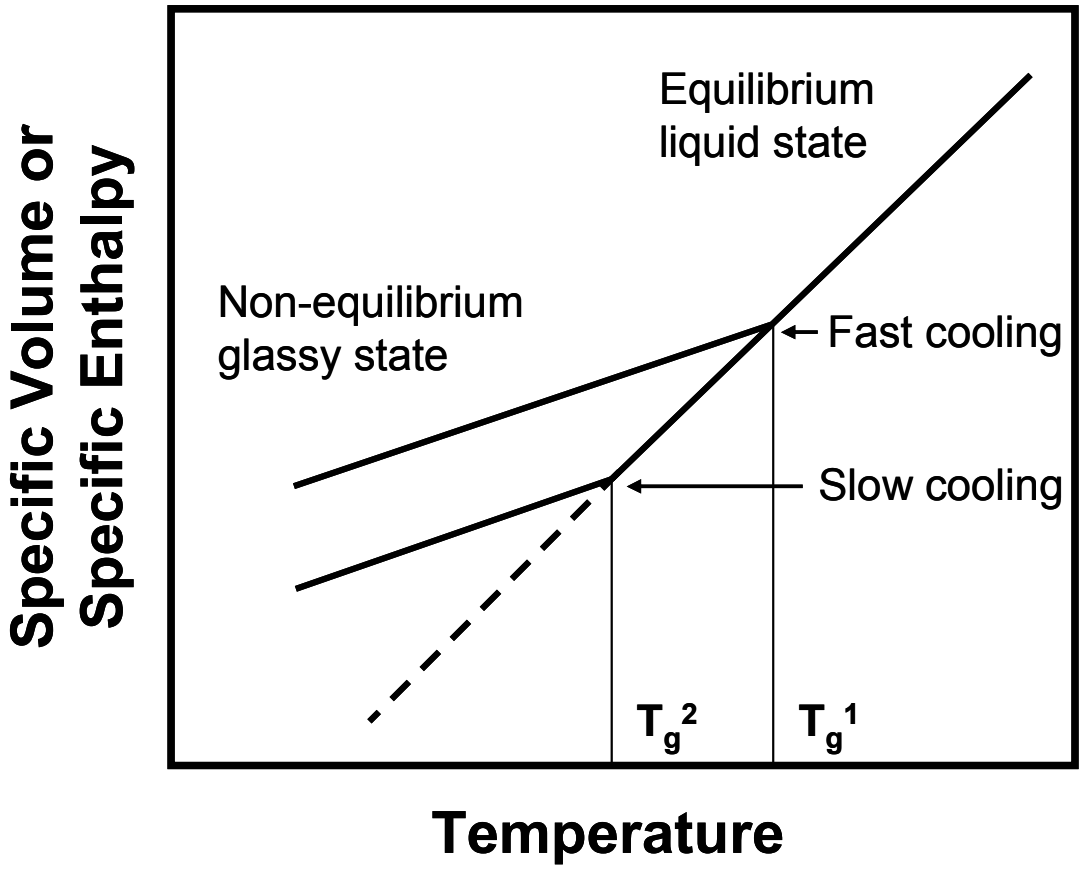

Figure 2-1: Temperature dependence of specific volume or specific enthalpy for an amorphous polymer. The vertical lines denote the glass transition temperatures determined using a fast cooling rate and a slow cooling rate.

2.2.1.1 The Kauzmann Paradox

The specific volume or specific enthalpy of a liquid is higher than that of its corresponding crystal. However, Kauzmann noticed that such a situation would not be true if the equilibrium liquid properties of glass-forming systems could be extrapolated below T_g but still above 0 K (Kauzmann 1948). Experimentally, this would imply the cooling of a liquid at an infinitely slow rate such that the glass transition does not occur. The Kauzmann paradox is illustrated in Figure 2-2. If the liquid were cooled at an infinitely slow rate, its specific volume and specific enthalpy would become less than that of the corresponding crystal at a nonzero temperature (the Kauzmann temperature). In addition, since the entropy of a crystal approaches zero at 0 K, the entropy of the liquid would become negative if the liquid could be cooled at an infinitely slow rate (Kauzmann 1948). Such a situation is a violation of the third law of thermodynamics. However, such a phenomenon has never been experimentally observed because the kinetic glass transition intervenes. Thus, "kinetics save the thermodynamic day" (DiMarzio 1981).

2.2.1.2 Molecular-Scale Motions of the Glass Transition

The molecular-scale motions associated with the glass transition of polymers are those of cooperative segmental motions. The relaxation process of the cooperative segmental motions of the glass transition is known as the alpha-relaxation (α-relaxation) process. At the glass transition, the length scale of a cooperative segmental motion is believed to be 1-4 nm, and the average α-relaxation time is approximately 100 seconds (see Section 2.2.3).

The α-relaxation process is represented by a distribution of relaxation times. In time-

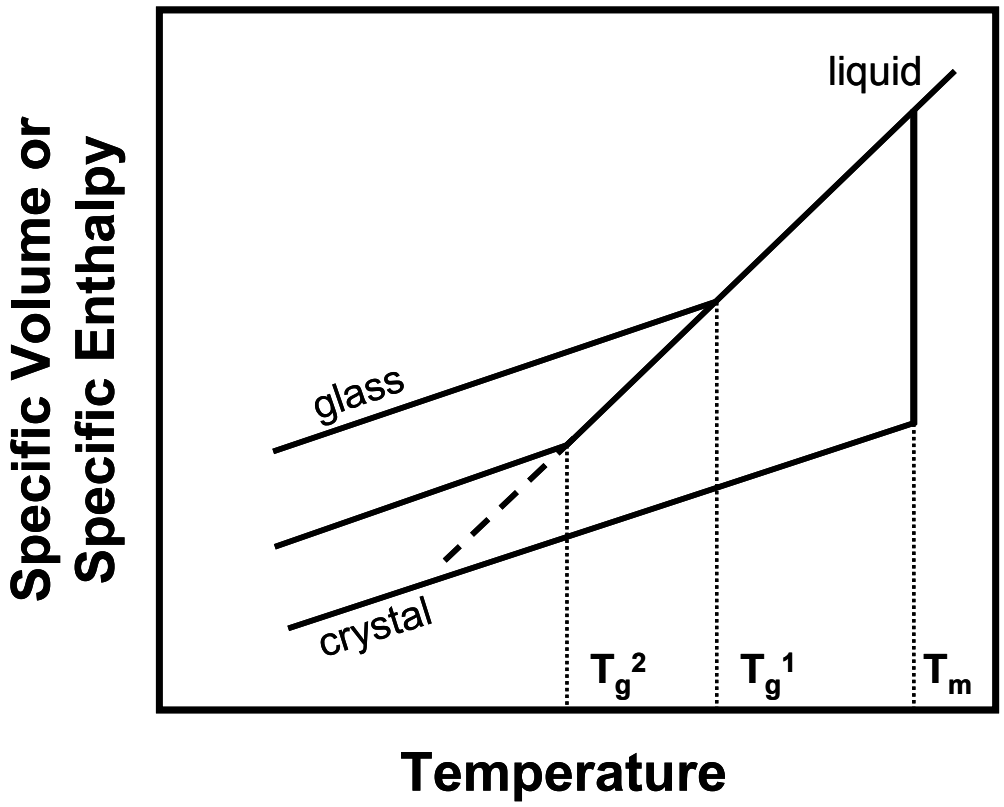

Figure 2-2: Temperature dependence of specific volume and specific enthalpy for a glass-forming liquid and its corresponding crystalline phase**.**

domain measurements (for example, depolarization after removal of an applied electric field or stress relaxation in response to a deformation), the α-relaxation is non-exponential and can be described by a series of single-exponential functions with different relaxation times or a stretched-exponential function. The most common function used to describe the α-process is that of the Kohlraush-Williams-Watts (KWW) (Kohlrausch 1874; Williams 1970) equation:

$$F(t) = \exp\left[-\left(\frac{t}{\tau}\right)^{\beta}\right] \qquad 2\text{-}1$$

where $F(t) = [\sigma(t) - \sigma(\infty)] / [\sigma(0) - \sigma(\infty)]$ and σ is the measured quantity (for example, the capacitance following the removal of a voltage), t is time, τ is the apparent relaxation time, and β is the stretching parameter which describes the width of the distribution of α-relaxation times. The stretching parameter, β, can vary between 0 and 1. When the value of β is near 0, the distribution of α-relaxation times is very broad; when β is near 1, the distribution of α-relaxation times is narrow, and near a single exponential (Gaussian distribution). Ngai has suggested from the so called "Ngai Coupling Model" that the stretching parameter β in the KWW function is a measure of the extent of cooperative motion of the α-process (Ngai 2007). (In the "Ngai Coupling Model", β is expressed as 1-n.) As β decreases, the extent of cooperative motion increases. Thus, a lower β value represents a broad α-process. The average α-relaxation time, $<\tau>$, can be determined from the fitting parameters of the KWW function by the following equation:

$$<\tau> = \int_0^{\infty} \exp\left[-\left(\frac{t}{\tau}\right)^{\beta}\right] dt \qquad 2\text{-}2$$

Such an approach has been used to determine the average α-relaxation time based on second

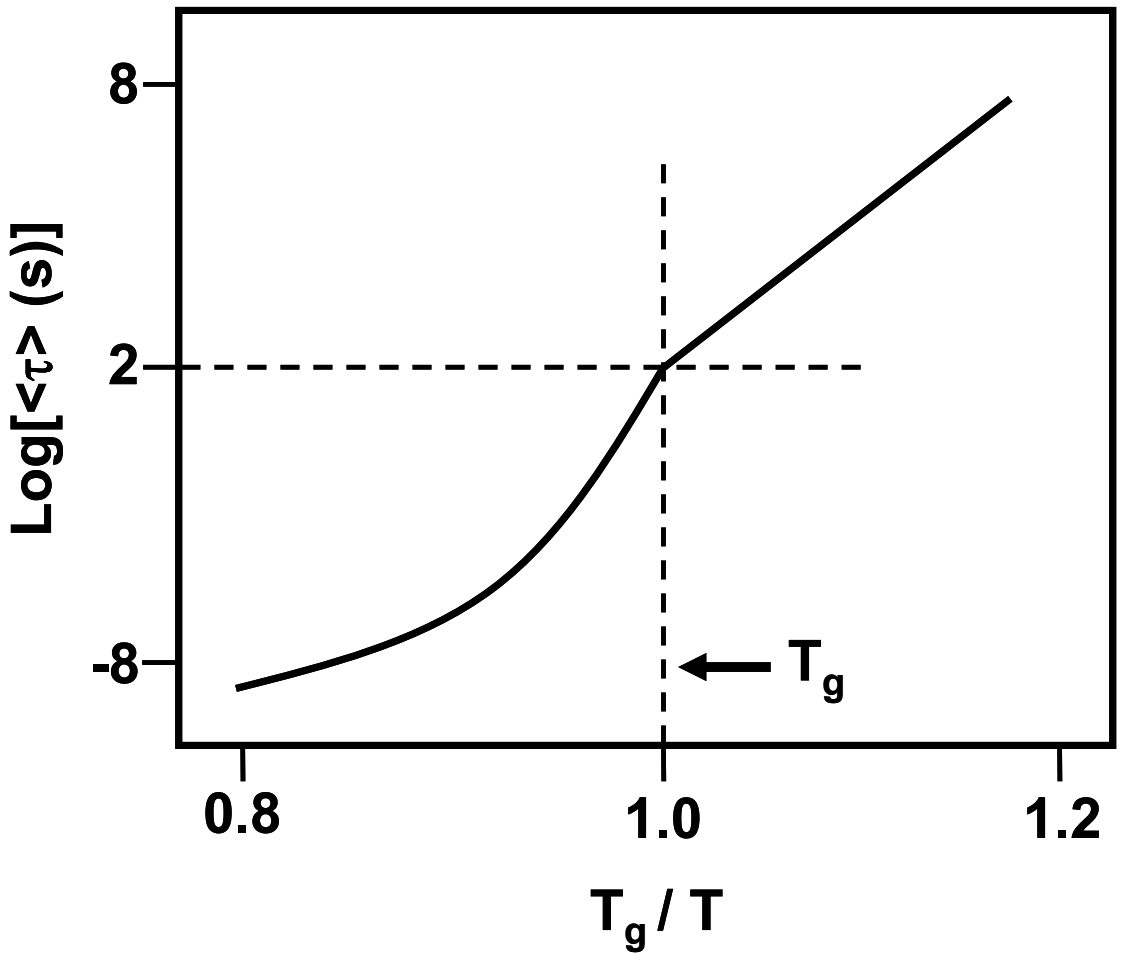

Figure 2-3: Arrhenius representation of the average α-relaxation time for a typical amorphous polymer. The data is scaled to the glass transition temperature. Above the glass transition temperature, polymer relaxation exhibits a non-Arrhenius temperature dependence while below the glass transition temperature, polymer relaxation exhibits an Arrhenius temperature dependence.

harmonic generation measurements (Dhinojwala 1993; Dhinojwala 1994b) and fluorescence recovery after pattern photobleaching measurements (Thurau 2002a; Thurau 2002b).

Upon cooling, the average α-relaxation time of polymers exhibit a dramatic sensitivity to temperature as T_g is approached. Figure 2-3 shows the temperature dependence of the average α-relaxation time as a function of inverse temperature scaled to T_g for a typical amorphous polymer. For polymers and other glass-forming liquids, the temperature dependence of the average α-relaxation (or viscosity) can be well described by the Vogel-Fulcher-Tamann-Hess (VFTH) equation (Vogel 1921; Fulcher 1925; Tammann 1926):

$$\tau = A \cdot \exp\left[\frac{B}{(T - T_o)}\right] \qquad 2\text{-}3$$

where A and B are temperature independent constants. The value of T_o is typically found to be approximately 50 K below the experimentally determined T_g (McKenna 1989). Although purely empirical, the VFTH equation describes polymer data over ten orders of magnitude for the average α-relaxation time. The temperature range over which the VFTH equation is valid is approximately T_g + 10 K < T_g < T_g + 100 K (McKenna 1989). An understanding of the dramatic slowing down of the α-relaxation dynamics of polymeric glass-formers near the glass transition (as depicted in Figure 2-3) is a central challenge in polymeric physics. Free volume concepts and thermodynamic theories will be briefly described that attempt to explain the dramatic slowing down of α-relaxation dynamics and / or other relaxation processes near T_g.

2.2.2 Models of the Glass Transition

2.2.2.1 Free Volume Concepts

The idea of resistance to flow being controlled by free space (free volume) instead of temperature was first introduced by Doolittle (Doolittle 1951). Doolittle found that the temperature dependence of viscosity could be described by the following equation:

$$\ln(\eta) = \ln(A) + B\left(\frac{(\upsilon - \upsilon_f)}{\upsilon_f}\right) \qquad 2\text{-}4$$

where A and B are fitting parameters, η is viscosity, υ is specific volume, and υ_f is free volume. As defined by Doolittle, free volume, υ_f, equal to

$$\upsilon_f = \upsilon - \upsilon_o \qquad 2\text{-}5$$

where υ_o is the occupied volume of the liquid.

Free volume concepts were subsequently applied to explain the temperature dependence of relaxation mechanisms for polymers above the glass transition by Williams, Landel and Ferry (Williams 1955). The empirical equation known as the WLF equation can describe well the temperature dependence of relaxation mechanisms (φ) (for example, φ could be the average α-relaxation time) above T_g:

$$\log\left(\frac{\varphi(T)}{\varphi(T_S)}\right) = \frac{-C_1 \cdot (T - T_S)}{C_2 + T - T_S} \qquad 2\text{-}6$$

In the WLF equation, C_1 and C_2 are fitting parameters that are dependent on the polymer (Tant 1981; McKenna 1989), and T_s is a reference temperature and is often taken to be T_g.

Williams, Landel and Ferry (Williams 1955) showed that equation 2-6 can be rationalized from equation 2-4 if free volume is assumed to increase linearly with the

temperature:

$$f = f_g + \Delta\alpha(T - T_g) \qquad 2\text{-}7$$

where f is the fractional free volume = $\upsilon_f / (\upsilon_f + \upsilon_o)$, f_g is the fractional free volume at T_g and $\Delta\alpha$ is the difference in thermal expansion coefficients above and below the glass transition. The Doolittle expression and the WLF expression are equivalent when

$$C_1 = \frac{B}{2.303 f_g} \qquad 2\text{-}8$$

$$C_2 = \frac{f_g}{\Delta\alpha} \qquad 2\text{-}9$$

Based on equation 2-8, when B is considered to have a value of unity, the fractional free volume at the glass transition is between 0.013 and 0.034 for many polymers (Williams 1955).

Both the Doolittle and WLF equations can describe well the temperature dependence of a relaxation mechanism invoking free volume arguments. With decreasing temperature, free volume decreases; thus, molecular mobility decreases. At a particular temperature, the time required for molecular rearrangement for the achievement of equilibrium is longer than the experimental time scale, and the liquid falls out of equilibrium. This particular temperature is the glass transition temperature. Thus, the glass transition is purely a kinetic phenomenon.

Free volume concepts also provide a resolution to the Kauzmann paradox (McKenna 1989). With decreasing temperature, the WLF expression predicts that the relaxation time of an equilibrium state polymer approaches infinity at a temperature approximately 50 K below T_g, which corresponds to a fractional free volume of zero. Therefore, a liquid would never reach equilibrium if cooled extremely slowly such that the liquid properties approach that of the corresponding crystal. Thus, the Kauzmann paradox is solved for kinetic reasons.

Arguments against the free volume concepts arise from the inability to determine the fractional free volume *a priori* (McKenna 1989). In addition, when free volume is held constant by changing temperature and pressure simultaneously, viscosity is not constant (McKenna 1989). Despite these arguments, free volume concepts allow for the description of molecular mobility of polymers. Attempts to provide a more quantitative interpretation of free volume have been carried out by Cohen and Turnbull (Turnbull 1961). The reader is referred to reviews by Tant and Wilkes (Tant 1981) and McKenna (McKenna 1989) for an analysis of the model.

2.2.2.2 Gibbs-DiMarzio Theory

The Gibbs-DiMarzio theory (Gibbs 1958; DiMarzio 1981) of the glass transition is derived from the Flory-Huggins (Flory 1953) lattice model for a polymer. Polymer chains are placed on a Flory-Huggins lattice along with vacant sites. Each polymer chain on the lattice has a lowest energy shape. The internal energy of the molecule is calculated based on the amount its shape deviates from its lowest energy shape. The model predicts the existence of a second-order thermodynamic transition at a temperature T_2. At the temperature T_2, which is greater than 0 K, the configurational entropy of the system becomes zero. The reduction in configurational entropy with temperature results from two factors. First, at lower temperatures the chains prefer lower energy states. Secondly, as the temperature is lowered, the number of vacant sites decreases, i.e., the volume of the system decreases. The Gibbs-DiMarzio theory considers the glass transition to be a true thermodynamic transition. The experimentally observed T_g is a reflection of the true transition at T_2. Gibbs and DiMarzio suggested that the experimentally observed T_g would equal T_2 in long time experiments. Since the theory predicts the existence of a true second-order transition at T_2, extrapolation of the liquid state properties below the glass

transition is not permitted; thus, the theory resolves the Kauzmann paradox for thermodynamic reasons rather than kinetic reasons (McKenna 1989). In fact, the theory defines the glassy state as a fourth state of matter, with an internal energy between that of a liquid phase and a crystalline phase.

2.2.2.3 Adam-Gibbs Theory

In an effort to unite free volume concepts and the thermodynamic theory of Gibbs-DiMarzio, Adam and Gibbs (Adams 1965) developed a model of the glass transition in which the relaxation time of a cooperatively rearranging region (CRR) was inversely proportional to the configurational entropy. The polymer is defined as an ensemble of cooperative regions. The cooperatively rearranging region is large enough to allow for rearrangement of the region to take place without affecting neighboring regions. As the temperature is lowered, the size of the regions increases and by definition at temperature T_2 is equal to the sample size. The relaxation time of the system is given by

$$\frac{1}{\tau(T)} = A \cdot \exp\left(\frac{-\Delta\mu S_c^*}{kTS_c}\right) \qquad 2\text{-}10$$

where $\Delta\mu$ is the activation energy for cooperative rearrangement, k is Boltzmann's constant, S_c^* is the critical configurational entropy for the smallest size capable of having two configurations, and S_c is the macroscopic configurational entropy. Therefore, the smaller the size of CRRs (lesser cooperativity), the smaller the relaxation time of the system. It is important to note that equations 2-4 and 2-6 rationalized from free volume concepts can also be obtained from the Adam-Gibbs theory if

$$C_1 = \frac{2.303\Delta\mu S_c^*}{k\Delta C_p T_S \ln(T_S/T_2)} \quad 2\text{-}11$$

$$C_2 = \frac{T_S \ln(T_S/T_2)}{1+\ln(T_S/T_2)} \quad 2\text{-}12$$

where ΔC_p is the change in heat capacity between the liquid state and glassy state. The fact that a thermodynamics approach to the glass transition can lead to the WLF equation shows that both approaches are compatible.

2.2.3 Dynamic Heterogeneity

A compelling reason to investigate the existence of dynamic heterogeneity in glass-forming systems is to explain the non-exponential relaxation of the α-process and the dramatic slowing down of the α-relaxation dynamics with decreasing temperature. In a system in which there exists dynamic heterogeneity, individual homogeneous domains have been hypothesized to relax exponentially; the dynamic heterogeneity of the system as a whole would result from each homogeneous domain having a different relaxation time (Ediger 2000). The dramatic slowing of the α-relaxation dynamics with decreasing temperature could result from a growth of and a slowing of individual relaxing domains within a heterogeneous system (Ediger 2000). The concepts and experimental evidence for dynamic heterogeneity in glass-forming systems have been reviewed by Ediger (Ediger 2000) and Sillescu (Sillescu 1999). The existence of dynamic heterogeneity has been used to explain the difference in the temperature dependence of translational and rotational diffusion as the glass transition is approached (this phenomenon is often called the translation-rotation paradox) (Hall 1997b; Thurau 2002a; Thurau 2002b).

Dynamic heterogeneity has been observed experimentally by dielectric spectroscopy

(Russell 2000; Sinnathamby 2005), dynamic susceptibility measurements (Berthier 2005; Merolle 2005), 3-D imaging (Weeks 2000), second harmonic generation measurements (Jerome 1997; Hall 1997a), and nuclear magnetic resonance (Tracht 1998). Dynamic heterogeneity has also been observed through molecular dynamics simulation studies (Donati 1998; Smith 2003; Baljon 2004). As determined by several different techniques, the size scale of dynamic heterogeneous regions is approximately 1-4 nm (Tracht 1998; Ediger 2000; Berthier 2005). The shape of dynamic heterogeneous regions as proposed by Ediger (Ediger 2000) and Spiess (Tracht 1998) was elliptical; however, simulations (Donati 1998) and experiments (Weeks 2000) have shown the shape to be more string-like. Both experimental and simulation studies have provided evidence for the growth of heterogeneous domains as the glass transition is approached (Russell 2000; Berthier 2005). This growth in relaxing domains with decreasing temperature provides a possible mechanism by which the dramatic slowing down of relaxation dynamics originates. Ediger has provided a connection between a dynamic heterogeneous region and a CRR; that is, a dynamic heterogeneous region should serve as the upper size limit for a CRR (Ediger 2000).

2.2.4 Physical Aging

The experimentally observed kinetic glass transition results in the formation of a non-equilibrium glass. As a result, when a glass is annealed below T_g, it will spontaneously relax toward its equilibrium state that would be obtained if the glass transition did not intervene. This relaxation process is known as physical aging or structural recovery. (The term structural recovery is often referred to as volume or enthalpy relaxation while physical aging is often used to express the change in mechanical properties that accompanies volume/enthalpy relaxation (McKenna 1989; McKenna 2002). The terms will be used interchangeably here.) Physical aging

leads to many time-dependent property changes such as specific volume, specific enthalpy, yield stress, elastic modulus, and ultimate elongation (Struik 1978; Kovacs 1979; Tant 1981; Greiner 1984; McKenna 1989; Hodge 1995; Hutchinson 1995). The prefix "physical" is placed before aging to distinguish the difference between "chemical" aging and degradation (Struik 1978; Hutchinson 1995). Chemical aging leads to irreversible changes in properties as a result of permanent changes to the material structure. The property changes that accompany physical aging are reversible. This is because there are no permanent changes to the material structure with physical aging. The property changes that result from physical aging can be erased by heating the glass above T_g; thus, physical aging is thermoreversible.

Physical aging is of concern for any technology that requires the use of polymer glasses slated for long-term applications. The time-dependent property changes that accompany physical aging must be taken into account in the design and use of polymer glasses. For example, most thermoplastics are melt processed via extrusion and injection molding and then rapidly quenched to the glassy state. The quenching should initiate physical aging. An understanding of the accompanying property changes with physical aging is important (Hutchinson 1995). Another example of the technological importance of physical aging is from the separations industry. Glassy membranes provide a route to develop energy efficient methods for the separation of gases (Nagai 2001). The problem with glassy membranes is that the inevitable physical aging results in a dramatic reduction in permeation with time (Pfromm 1995).

Figure 2-4 shows the most common situation of physical aging for an amorphous polymer. When quenched below T_g to an aging temperature T_a (at a constant pressure), the glass has an excess of thermodynamic quantities (e.g. specific volume). Annealing the glass at T_a

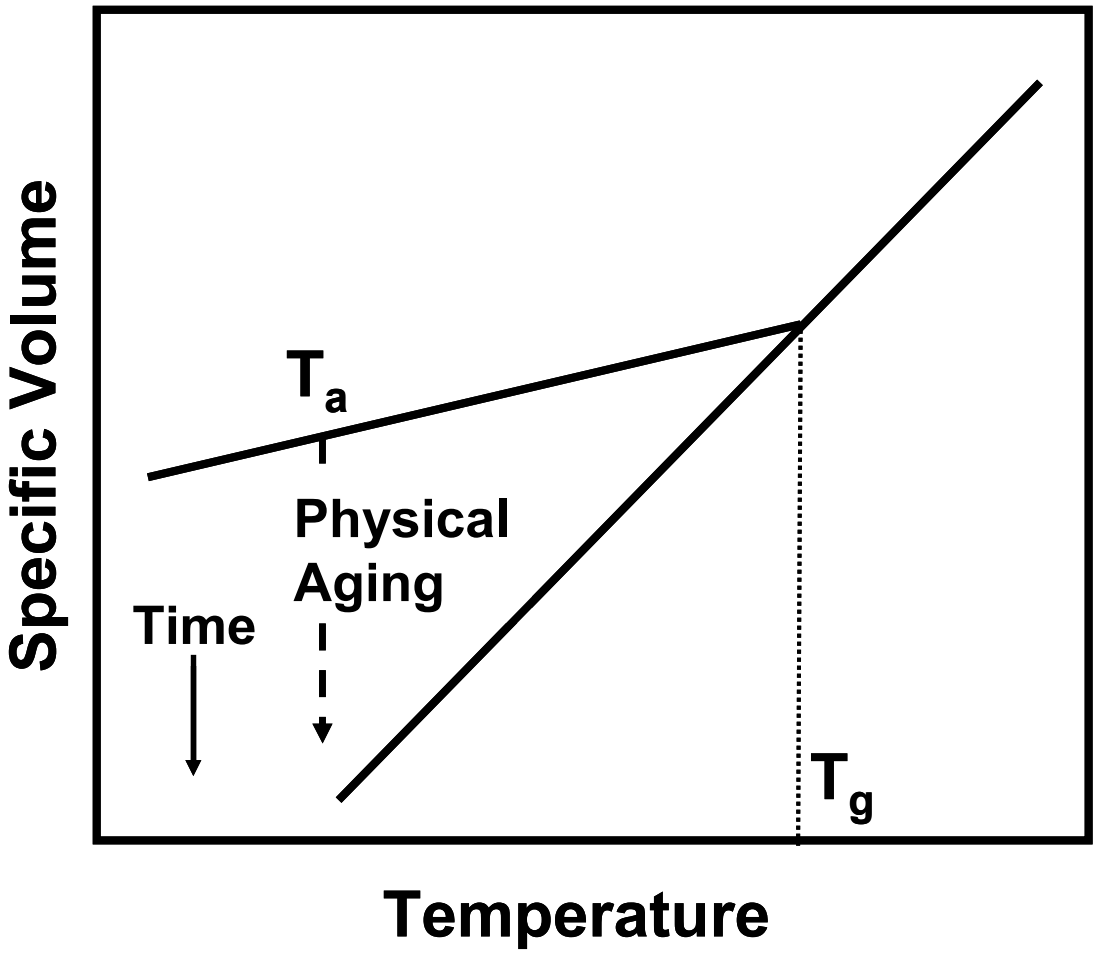

Figure 2-4: Physical aging of an amorphous polymer. With time there is a reduction in specific volume during physical aging.

results in the relaxation of the excess thermodynamic quantities toward equilibrium. The relaxation of the thermodynamic quantities persists until equilibrium is obtained (Li 2006). Because glasses have very large relaxation times, the attainment of equilibrium during physical aging is only achieved within a reasonable experimental time-scale at temperatures slightly below T_g. Figure 2-5 shows aging isotherms for bulk polystyrene aged at different temperatures (Greiner 1984). The T_g of polystyrene is 100 ^{o}C. When aged 3 ^{o}C below T_g, equilibrium is reached after 10^4 sec; when aged 10 ^{o}C below T_g, equilibrium is reached after 10^7 sec.

Aging isotherms typically can show three distinct features: an initial plateau (not shown in Figure 2-5), a linear region and an equilibrium plateau. The equilibrium plateau is only observed when equilibrium is achieved; thus, it is only seen when aging occurs near T_g. The initial plateau occurs before the linear region; it is dependent on both temperature and thermal history (Greiner 1984). The exact cause of the initial plateau is unknown but has been misinterpreted to mean that a system is not aging (Greiner 1984).

The linear regions of the aging isotherms can be used to characterize the rate of volume relaxation (Struik 1978; Kovacs 1979; Greiner 1984). The rate of volume relaxation, r_v, is defined as the slope of the linear portion of the aging isotherms and is given by

$$r_v = -\frac{1}{\upsilon} \cdot \frac{d\upsilon}{d \log t_a} \qquad 2\text{-}13$$

where t_a is aging time. As illustrated from Figure 2-5 for polystyrene, the rate of volume relaxation is dependent on the physical aging temperature. Figure 2-6 shows the temperature dependence of the rate of volume relaxation for polystyrene (PS), poly(vinyl chloride) (PVC), poly(methyl methacrylate) (PMMA) , and polycarbonate (PC) (Greiner 1984). For all systems, the rate of volume relaxation is strongly dependent on temperature. The temperature dependence

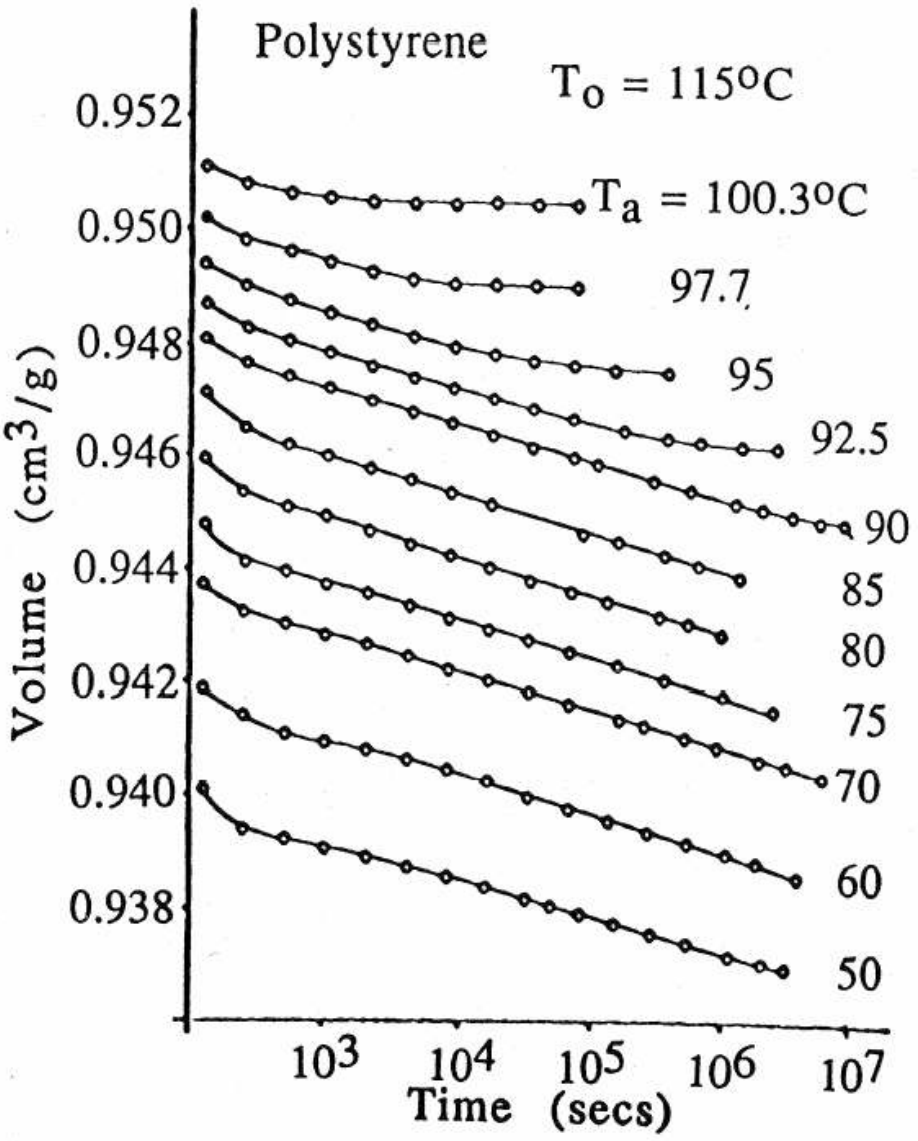

Figure 2-5: Specific volume relaxation for polystyrene at several temperatures below the glass transition temperature. The polymer was annealed at T_o prior to quenching to the specified aging temperature (listed to the right of each curve). Data taken from (Greiner 1984). (With permission.)

of the rate of volume relaxation is a result of competition between the thermodynamnic driving forces for aging and the mobility of the system. The greater is the departure from equilibrium, the greater are the thermodynamic driving forces for aging and the lesser is the molecular mobility. For every system there exists a synergism between the driving forces for aging and mobility at a given temperature. For PS, PVC, and PC a maximum in relaxation rate occurs near T_g. For PMMA, there are maxima in the aging rate near the secondary beta and gamma transitions. The fact that PMMA exhibits a global maximum in aging rate at the beta transition has led to much debate about the impact of the beta transition on physical aging (Guerdoux 1981; Lee 1993; Muzeau 1994). In fact, Struik initially suggested that physical aging did not proceed below the beta transition of polymers (Struik 1978); this suggestion has since been proven incorrect (Greiner 1984; Hodge 1995; Hutchinson 1995).

With increasing physical aging time there is an increase in the average α-relaxation time and a broadening of the α-relaxation dynamics as shown by photobleaching techniques (Thurau 2002a; Thurau 2002b), dielectric spectroscopy (Guerdoux 1981), and dynamic mechanical analysis (Muzeau 1994). A recent theory of the glass transition predicts an increase in the average α-relaxation time and a broadening of the α-relaxation dynamics during physical aging (Merabia 2006). Thus, the α-relaxation dynamics persist below T_g. How physical aging impacts the beta transition (sub-segmental relaxation, non-cooperative relaxation dynamics) has received little attention from the research community. It has been shown that physical aging does not result in a shift of the peak of the β process along the time axis (the dynamics associated with the beta process are not slowed / enhanced by physical aging (Guerdoux 1981; Muzeau 1994)). However, it has been shown that physical aging results in a reduction in the strength / magnitude

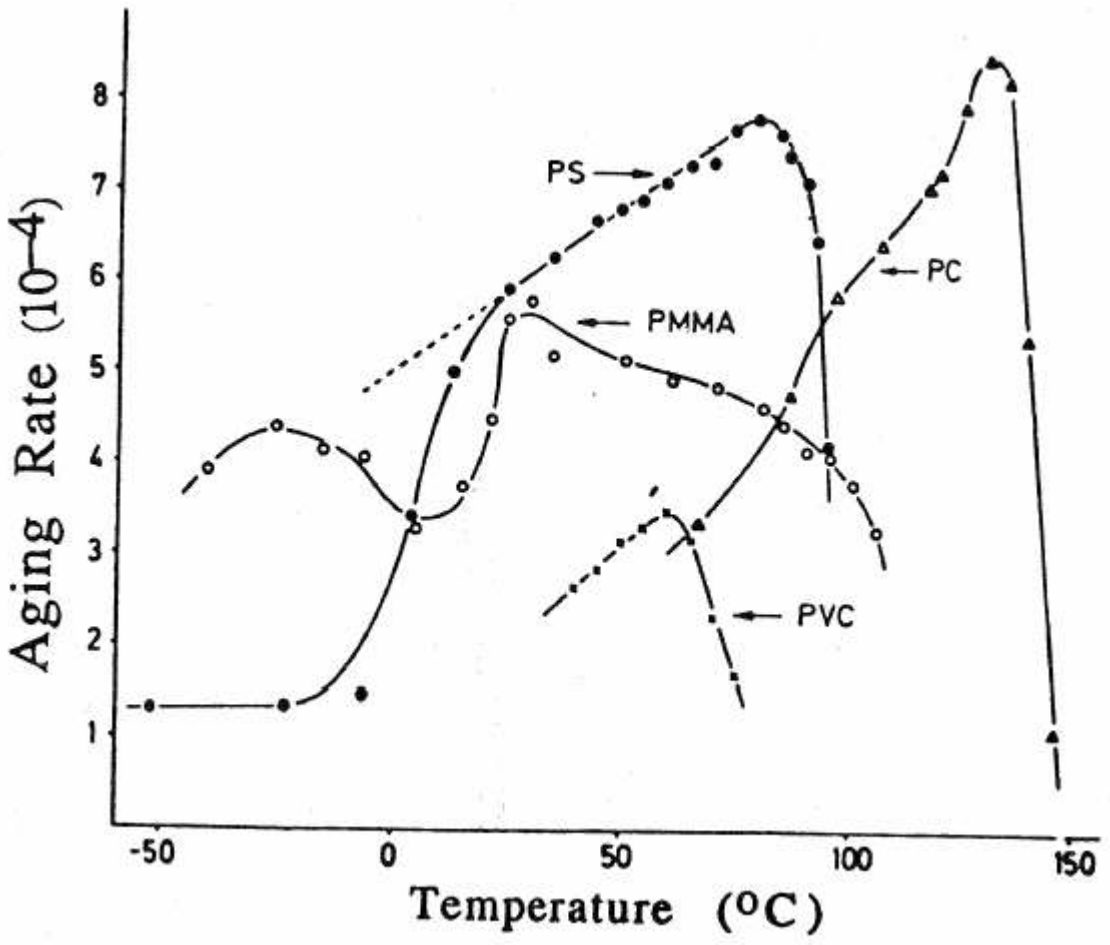

Figure 2-6: Temperature dependence of the physical aging rate of polystyrene, polycarbonate, poly(vinyl chloride), and poly(methyl methacrylate). Aging rates determined from 12 day physical aging experiments. Data taken from (Greiner 1984). (With permission.)

of the β relaxation process (Guerdoux 1981).

Recently, it has been shown that the translational and rotational relaxation times of a probe molecule are impacted differently by physical aging (Thurau 2002a; Thurau 2002b). Following a quench from above T_g to a specific aging temperature, the time required to reach equilibrium is shorter for the translational relaxation time than for the rotational relaxation time (Thurau 2002a; Thurau 2002b). The results indicate that the spatially heterogeneous dynamics present above T_g persist below T_g during aging. The difference in the time required for the translational and rotational relaxation times to reach equilibrium arises because the two variables average over heterogeneous dynamics in different ways (Thurau 2002a). The significance of heterogeneous dynamics during physical aging is that different properties average these dynamics differently; thus, the physical aging characteristics determined via one measurement may not identically translate the physical aging characteristics of another measurement. The difference in how different variables average over heterogeneous dynamics may be the reason why it has been shown that specific volume, specific enthalpy, stress relaxation, and dielectric properties evolve differently during aging (Struik 1978; Matsuoka 1986; McKenna 1989; Simon 2001; Badrinarayanan 2007).

From positron annihilation lifetime spectroscopy (Cangialosi 2003) and absorbance spectroscopy (Victor 1988) studies, it has been shown that free volume decreases with increasing physical aging time. In fact, Struik has suggested a closed-loop scheme for the reduction in free volume with physical aging time as given below:

$$\upsilon_f \rightarrow M \rightarrow \frac{d\upsilon_f}{dt} \qquad \text{2-14}$$

where M is the segmental mobility (Struik 1978). In this picture, the rate of relaxation ($d\upsilon_f / dt$) is determined by the segmental mobility which is itself determined by the free volume. This scheme implies that volume relaxation during physical aging is a non-linear relaxation process (the rate of relaxation depends on the instantaneous state of the system). Thus, the differential equation describing the relaxation process is given by

$$\frac{d\upsilon_f}{dt} = -\frac{\upsilon_f - \upsilon_\infty}{\tau} \qquad 2\text{-}15$$

where υ_∞ is the free volume at equilibrium. The relaxation time, τ, is then a function of temperature and free volume.

Phenomenological models used to describe structural relaxation such as the TNM (Tool 1946; Narayanaswamy 1971; DeBolt 1976) and KAHR (Kovacs 1979) models are based on equation 2-15. In these models the volume departure from equilibrium is usually expressed as

$$\delta = \frac{(\upsilon - \upsilon_\infty)}{\upsilon_\infty} \qquad 2\text{-}16$$

Then equation 2-15 is given as

$$\frac{d\delta}{dt} = -\frac{\delta}{\tau} \qquad 2\text{-}17$$

Note that equations 2-15 and 2-17 assume an instantaneous quench from above T_g to the aging temperature and do not include a term that accounts for cooling. The main difference in the TNM and KAHR models is the expression for τ. However, both models assume τ to be a function of temperature and the instantaneous state of the system. For a detailed summary of both models, the reader is referred to references by McKenna (McKenna 1989), McKenna and Simon (McKenna 2002), Hutchinson (Hutchinson 1995), and Tant and Wilkes (Tant 1981).

While this summary of physical aging has focused on volume relaxation, a substantial amount of work has focused on the impact of aging on the mechanical relaxation of polymers (Struik 1978; Tant 1981; Read 1991). With increasing physical aging time there are substantial changes to the creep response and stress relaxation of polymers. For a thorough review of the impact of aging on the mechanical properties of glasses see the monograph by Struik (Struik 1978).

3 CONFINEMENT EFFECTS ON THE PROPERTIES OF GLASS FORMING LIQUIDS

3.1 Introduction

As the confining dimension is decreased below a certain critical value in thin polymer films (with thickness as the confining dimension) and polymer nanocomposites (with inter-nanoparticle distance as the confining dimension), an increasingly large fraction of polymeric material is directly in contact with interfaces (e.g. air-polymer interface or free surface) and surfaces. Properties can be strongly perturbed by the interfacial interactions and surfaces in confined polymer, and these perturbations to average properties or the distribution of properties within such systems are commonly referred to collectively as the confinement effect.

This chapter provides a review of the literature conducted prior to or during the completion of this thesis related to the impact of confinement on the properties of glass forming liquids, in particular polymers. The properties of interest include the glass transition temperature (T_g), α-relaxation dynamics and physical aging. While there are numerous ways to physically confine a polymer (e.g. thin film geometry, polymer in nanocomposites, polymer in nanopores, minor phase in polymer blends), this chapter will mostly describe the behavior of thin films with some mention of nanocomposites. The goal of the chapter is to provide a survey of important literature and key concepts related to the impact of confinement on the properties of glass forming liquids. The reader is referred to reviews by Alcoutlabi and McKenna (Alcoutlabi 2005),

Roth and Dutcher (Roth 2004), and Dalnoki-Veress and Forrest (Dalnoki-Veress 2001) for a more complete survey of the literature.

3.2 Confinement Effects on Polymer Behavior

3.2.1 Glass Transition Temperature

The first systematic study of T_g values of confined polymers was reported by Keddie *et al.* (Keddie 1994a; Keddie 1994b). They used ellipsometry to measure T_g as a function of film thickness in spin-cast films of polystyrene (PS) and poly(methyl methacrylate) (PMMA) (Keddie 1994a; Keddie 1994b). When supported on silicon wafers, PS exhibited a decrease in T_g with decreasing film thickness for film thicknesses below 40 nm, such that a 20-nm-thick film had a T_g reduced by 17 K compared to T_g(bulk) (Keddie 1994a). To investigate the effect of the substrate on the T_g-nanoconfinement behavior, T_g was measured as a function of film thickness for PMMA films supported on either gold or silicon substrates. PMMA exhibits attractive interactions with silica and non-attractive interactions with gold. It was observed that T_g decreased when the film thickness was decreased below 60 nm for PMMA on gold substrates; in contrast, T_g increased slightly when the film thickness was decreased below 80 nm on silicon substrates. Keddie *et al*. (Keddie 1994a; Keddie 1994b) suggested that the reason for the reduction in T_g for PS ultrathin films supported on silica and PMMA ultrathin films supported on gold was due to the presence of a liquid-like layer at the free surface. For PMMA supported on silica, they proposed that attractive interactions between the polymer and substrate (hydrogen bonding) overwhelm the effects of the free surface and caused an overall increase in T_g.

Over the past decade and a half, the impact of confinement on the T_g of PS and PMMA

has been investigated by numerous techniques including dielectric spectroscopy (Fukao 1999; Fukao 2000; Fukao 2001b; Hartmann 2002; Wubbenhorst 2002; Wubbenhorst 2003; Serghei 2005; Lupascu 2006; Serghei 2006a; Napolitano 2007a; Napolitano 2007b; Fukao 2001a), thermal probe measurements (Fryer 2000), X-ray reflectivity (Lenhart 2002; White 2003; Soles 2004; Bhattacharya 2005), quartz crystal microbalance (Forrest 1998), positron annihilation lifetime spectroscopy (DeMaggio 1997), Raman scattering (Liem 2004), atomic force microscopy (Sills 2004), ellipsometry (Prucker 1998; Grohens 2002; Xie 2002; Kanaya 2003; Pham 2003; Fakhraai 2004; Park 2004; Fakhraai 2005), second harmonic generation (Hall 1997b), and fluorescence methods (Ellison 2002; Ellison 2002a; Ellison 2005; Mundra 2006; Mundra 2007a; Roth 2007a; Mundra 2007b; Roth 2007b). Several manuscripts are highlighted below.

Fryer *et al*. (Fryer 2001) investigated the T_g-nanoconfinement behavior of PS and PMMA films supported on octadecyltrichlorosilane (OTS) deposited silica. Exposure of the OTS deposited silica substrate with X-rays modified the OTS by incorporating oxygen-containing groups on the surface, thereby tuning its interfacial energy (interactions) with PS and PMMA. (Fryer 2001). As measured by local thermal analysis, ellipsometry, and X-ray reflectivity, the T_g-confinement effect depended on the interfacial energies between the polymer and the substrate. At low interfacial energies between the polymer (PS and PMMA) and the substrate, T_g decreased with confinement while at high interfacial energies, T_g increased with confinement. For a constant film thickness of either PS or PMMA, ΔT_g scaled linearly with the interfacial energy between the polymer and the substrate providing evidence that the T_g-confinement effect resulted from interfacial interactions (Fryer 2001).

Park *et al*. (Park 2004) investigated the dependence of T_g on composition of confined random copolymers for PS-PMMA and PS-poly(2-vinyl pyridine) (P2VP) in the thin film geometry. In the case of the homopolymers supported on silica, T_g decreased with confinement of PS and increased with confinement for PMMA and P2VP. By varying the mole % of PS in either a PS-PMMA or a PS-P2VP random copolymer (varying the amount of polymer that can have attractive interactions with the substrate), the T_g-nanoconfinement behavior could be tuned to the point at which T_g was independent of film thickness. The results were qualitatively explained by an approximate cancellation of opposing perturbations to T_g caused by free surface effects and substrate effects.

Prucker *et al*. (Prucker 1998) measured T_g of PMMA films supported on hydrophobic surfaces using ellipsometry (weak to no interactions between PMMA and substrate). Poly(methyl methacrylate) films were prepared by three different methods: spincoating from solution, grafting, and Langmuir-Blodgett-Kuhn. For all films, T_g decreased with decreasing thickness. The results help to support the notion that the T_g-confinement effect was not a result of spincoating itself (spincoating can lead to unrelaxed stresses in a film), as most thin films were prepared via this method.

In work by Keddie *et al*. (Keddie 1994a) and later by Ellison *et al*. (Ellison 2005) , the impact of molecular weight on the T_g-confinement behavior of PS was investigated. It was observed that ΔT_g versus film thickness collapsed to a single curve. The results were used to rule out the origin of the T_g-confinement effect originating from finite size effects. Finite size effects are supposed to occur when the thickness of the film approaches a characteristic length scale of the polymer such as the radius of gyration or a cooperatively rearranging region (CRR)

(McKenna 2000a; McKenna 2000b; McKenna 2003). In the study by Ellison *et al*. (Ellison 2005), the radius of gyration was varied by a factor of over 25, yet the T_g-T_g(bulk) data collapsed on a single curve. Given that the confinement effects on T_g can be observed at length scales greater than 100 nm while the accepted size of a CRR is approximately 1-4 nm, it unlikely that the effects are directly related to the length scale of a CRR. In addition, since the T_g-nanoconfinement effect is independent of molecular weight, the effect is not directly related to chain entanglements or the chain end surface concentration (Ellison 2005).

In a series of papers, Forrest, Dalnoki-Veress, Roth, Dutcher and coworkers (Forrest 1996; Forrest 1997; Forrest 2000; Dalnoki-Veress 2001; Roth 2003; Roth 2006) performed T_g-nanoconfinement studies on free-standing PS and PMMA films using ellipsometry (two free surfaces) and observed a reduction in T_g approximately twice that observed for supported films (one free surface). The results supported the idea of Keddie *et al*. (Keddie 1994a) that the free surface had a liquid-like layer with a reduced T_g and was the cause of confinement effects on the average T_g of polymer films. The freely standing film measurements have been subsequently quantitatively reproduced using X-ray reflectivity (Miyazaki 2007) and dielectric relaxation spectroscopy (film suspended in solution) (Svanberg 2007) and qualitatively reproduced using differential scanning calorimetry (Koh 2006).

While the T_g-nanoconfinement effect was understood to result from interfacial effects (Keddie 1994a; Keddie 1994b), Ellison and Torkelson provided the first direct measurements of T_g at the free surface or substrate interface of thin polymer films (Ellison 2003). The results demonstrated that T_g reductions originating at the free surface can propagate some tens of nanometers into the film interior (Ellison 2003), thereby altering the average film T_g. The results

were obtained using a novel fluorescence / multilayer technique in which only one layer was labeled with a fluorescent probe. The work provided unequivocal evidence that the impact of confinement on T_g was a result of interfacial effects.

3.2.2 α-Relaxation Dynamics

In 2005, Fakhraai and Forrest (Fakhraai 2005) used variable cooling rate ellipsometric measurements to probe the fast and slow relaxation dynamics associated with T_g. For fast cooling rates (> 90 K / min), T_g was nearly independent of film thickness, while for the slow cooling rates (~ 1 K / min), T_g decreased with decreasing film thickness. The results indirectly demonstrated that fast and slow parts of the α-relaxation time distribution (different length scales of cooperativity) were impacted by confinement in different ways.

The first work to directly investigate the α-relaxation dynamics of confined polymer was that of Hall *et al*. (Hall 1997b) who used second harmonic generation to study the dynamics of a Disperse Red 1 (DR1)-methacrylate / isobutyl methacrylate copolymer. The results indicated a broadening in the distribution of α-relaxation times with confinement; however, there was no change in the average α-relaxation time with confinement. For the copolymer system studied, the results indicated that confinement (via interfaces) introduced additional dynamic heterogeneity into the system; conversely, there was no change in T_g with confinement.

Fukao and Miyamoto (Fukao 1999; Fukao 2000) were the first to extensively examine confinement effects on the α-relaxation dynamics of PS films using dielectric relaxation spectroscopy. Via capacitive dilatometry measurements they showed that the T_g of PS decreased with decreasing film thickness in a similar manner as the results of Keddie, Jones, and Cory

(Keddie 1994a). With confinement of PS, a broadening of the distribution of α-relaxation times was observed similar to that of the work by Hall *et al*. (Hall 1997b). In addition, with confinement of PS, the average α-relaxation time decreased, indicating an enhancement in dynamics. The onset thickness at which T_α (peak temperature of the α-relaxation process) began to exhibit deviations from bulk T_α was dependent on the frequency. The slower the frequency, the greater the onset thickness at which deviations from bulk behavior were observed. The results indicated that different length scales (or extents of cooperativity) are impacted by confinement differently.

Work by Lupascu *et al*. (Lupascu 2006), in which they used dielectric spectroscopy to probe the relaxation dynamics of thin PS films, is in agreement with the work of Fukao and Miyamoto (Fukao 2000). The α-relaxation dynamics of PMMA (Hartmann 2002) and poly(vinyl acetate) (Serghei 2006b) are impacted by confinement in a similar manner as that of PS. However, the work Hartmann *et al*. (Hartmann 2002) showed the β process of PMMA was not significantly affected by confinement.

3.2.3 Mobility at Free Surface

The existence of a layer at the free surface of polymers with enhanced mobility has been the subject of intense research and debate (Liu 1997; Hamdorf 2000; Schwab 2000; Forrest 2001; Kerle 2001; Pu 2001; Ellison 2003; Jones 2003; Teichroeb 2003; Sharp 2003a; Herminghaus 2004; Roth 2004; Sharp 2004; Tanaka 2004; Alcoutlabi 2005; Fischer 2005; Fischer 2005; Hutcheson 2005; Gasemjit 2006; Papaleo 2006; Hutcheson 2007; Sharp 2007; Fakhraai 2008). While many literature reports conclude that there exists a region of enhanced

mobility at the free surface (Schwab 2000; Pu 2001; Ellison 2003; Teichroeb 2003; Sharp 2003a; Herminghaus 2004; Tanaka 2004; Gasemjit 2006; Papaleo 2006; Fakhraai 2008), other reports conclude the opposite (Liu 1997; Kerle 2001; Pu 2001; Alcoutlabi 2005; Fischer 2005; Hutcheson 2005). For example, Liu *et al.* (Liu 1997) used near edge x-ray absorption fine spectroscopy (NEXAFS) to investigate the orientation of PS in the first 1 - 10 nm below the free surface. They observed that the orientational dynamics of the chains were identical 1 nm and 10 nm below the free surface and concluded that there is not a free surface layer with enhanced mobility. Schwab *et al*. (Schwab 2000) used optical birefringence measurements to determine the free surface T_g of PS and found a reduction in T_g at the free surface, which supports the idea of enhanced mobility at the free surface. These results are in qualitative agreement with free surface T_g measurements reported by Ellison and Torkelson using fluorescence (Ellison 2003). Pu *et al.* (Pu 2001) used dynamic secondary ion mass spectrometry (DSIMS) and determined that the center of mass diffusion coefficient of the polymer chains was reduced at the free surface compared to the bulk. They concluded that the mobility at the free surface was reduced compared to the bulk. The above papers highlight the controversy in the research area that has arisen in the past years.

While they may appear contradictory, it is possible to rationalize that the conclusions from the above reports are all correct. The different experimental techniques probed the polymer physics on different length scales. NEXAFS, which was used by Liu *et al*., only probed the flipping motion of the phenyl ring on PS, while birefringence measurements used by Schwab *et al*. probed larger molecular motions. Ellison and Torkelson determined T_g by fluorescence that probes environments within the polymer on the nanometer length scale, while the diffusion

coefficients determined by Pu *et al*. probed large scale translational motion. It is likely that different length scales of polymer dynamics are affected differently by the free surface. Work by Fakhraai and Forrest (Fakhraai 2005) and Fukao and Miyamoto (Fukao 2000) have shown that different length scales are affected differently by confinement.

3.2.4 Physical Aging

The effect of confinement on the physical aging response of amorphous polymers has received little attention in the research literature compared to the T_g-nanoconfinement effect. However, a small number of studies have been aimed at identifying the effect of confinement on the physical aging response of polymers from the membrane literature (Pfromm 1995; Dorkenoo 1999; Huang 2004; Zhou 2004; Huang 2005; Huang 2006) and the polymer physics literature (Ellison 2002a; Kawana 2003; Richardson 2003; Richardson 2004; Cangialosi 2005; Fukao 2005). A summary of key results is given below.

Using permeability measurements, Pfromm and Koros (Pfromm 1995) reported an increase in the physical aging rate for free-standing polyimide and polysulfone films of thicknesses below 500 nm. Such a large length scale for a confinement effect had not been previously reported for either T_g or physical aging. Later, Dorkenoo and Pfromm (Dorkenoo 1999) used permeability measurements and reported accelerated physical aging for free-standing polynorbornene films of thicknesses less than 800 nm. They developed a mathematical model based on the KAHR (Kovacs 1979) model to explain their results. By invoking a reduction in T_g of the thin films, they were able to fit their experimental results. However, it should be noted that caution must be taken with using T_g as the fitting parameter. First, nowhere in the research literature has a T_g-nanoconfinement effect been reported for films as thick as 800 nm. Second,

the authors did not report the T_g values used to fit the data. Using permeability measurements (Huang 2004), Huang and Paul recently reported accelerated physical aging for free-standing polysulfone, polyimide, and poly(phenylene oxide) films for thicknesses below 900 nm. However, they found no change in T_g with film thickness down to 290 nm. These results dispute the interpretation by Dorkenoo and Pfromm that a reduction in T_g could explain the physical aging results.

The above studies highlight the effect of film thickness on the physical aging behavior of free-standing polymer films studied by permeation measurements. The polymers used in the investigations all have rigid backbones (not C-C flexible backbones). The large length-scale (h ~ 1 μm) at which the physical aging-nanoconfinement effect is observed may be related to the rigidity of the polymer backbone. At present, the length scale at which physical aging is affected in free-standing polymer films with a C-C chain backbone (e.g., PS and PMMA) is unknown.

Prior to 2005 only two studies had been conducted to address the impact of confinement on physical aging of supported polymer films (Ellison 2002a; Kawana 2003). Kawana and Jones (Kawana 2003) studied the effect of confinement on the physical aging response of PS films with thicknesses between 10-200 nm. Ellipsometry was used to measure overshoots in the expansivity of PS films that were aged at 70 ^{o}C and 80 ^{o}C. For a 10-nm-thick PS film aged at 70 ^{o}C and 80 ^{o}C no expansivity overshoot was detected upon heating the film above T_g(bulk) (100 ^{o}C). The result suggested that the 10 nm thick film was still in an equilibrium state at temperatures 30 ^{o}C below T_g(bulk). Also noteworthy is the observation that 18 nm and 30 nm thick films exhibited expansivity overshoots at 100 ^{o}C (T_g(bulk)), while the average T_gs of the films were 80 ^{o}C and 90 ^{o}C, respectively. This result indicated spatially heterogeneous dynamics

of local physical aging throughout the film. Fukao and Sakamoto recently reported physical aging results of PMMA thin films investigated by dielectric measurements (Fukao 2005). As the film thickness was decreased, the aging rate decreased.

3.2.5 Viscoelastic Properties

The impact of confinement on the viscoelastic properties of polymer has been investigated via novel experimental techniques: nanobubble inflation technique (O'Connell 2005), dewetting technique (Bodiguel 2007), and a buckling technique (Stafford 2006). O'Connell and McKenna reported that the rubbery compliance of a 27-nm-thick PS film was reduced by a factor of 300 compared to the bulk compliance (O'Connell 2005). Subsequently, Bodiguel and Fretigny reported no change in the rubbery compliance of PS films with confinement (Bodiguel 2007). At present, a reconciliation between the two reports remains elusive. Stafford *et al.* (Stafford 2006) reported that the elastic moduli of PS and PMMA films decreased with confinement when supported on poly(dimethyl siloxane) (PDMS). The results are consistent with a reduction of T_g with confinement for PS and PMMA films supported on PDMS.

3.2.6 Nanocomposites

The effects of nanoconfinement on T_g and physical aging of polymers are not unique to the thin-film geometry (Anastasiadis 2000; Ash 2002; Berriot 2002; Lu 2003; Schonhals 2003; Kalogeras 2004; Bansal 2005; Vlasveld 2005; Elmahdy 2006; Narayanan 2006; Rittigstein 2006; Lee 2007; Rittigstein 2007; Srivastava 2007). As with ultrathin polymer films, confinement effects in polymer-nanosphere nanocomposites can lead to decreases or increases in T_g relative to the neat polymer (Ash 2002; Berriot 2002; Rittigstein 2006; Lee 2007; Srivastava 2007). The

change in T_g depends on whether the nanocomposite formation leads to free surfaces between the polymer and nanoparticles or to wetted nanoparticle interfaces with attractive polymer interactions (Rittigstein 2006) and the interparticle spacing between the nanoparticles (Rittigstein 2007; Srivastava 2007). Confinement effects in nanocomposites can also perturb the physical aging response of the polymer. For example, enthalpy relaxation has been reported to be nearly a factor of four smaller during aging of a 10 parts per hundred epoxy-clay nanocomposite compared to that of neat epoxy (Lu 2003). Also, it was recently shown that physical aging deep in the glassy state can be nearly arrested in 0.4 vol% silica-poly(2-vinyl pyridine) (P2VP) nanocomposites (Rittigstein 2006).

3.2.7 Simulations

Although most research in this area has been experimental, simulations (Torres 2000; Starr 2001; Varnik 2002; Baljon 2004; Peter 2006) have reached similar conclusions regarding the roles of free surfaces and attractive polymer-substrate interactions in defining the T_g-confinement effect. Torres *et al*. (Torres 2000) illustrated via molecular simulations that T_g of thin polymer films either decreased or increased with confinement depending on the strength of the polymer-substrate interactions. Peter *et al*. (Peter 2006) explored the T_g-confinement behavior of freely standing films by means of molecular simulations. Via a layer resolved technique they showed that there existed a distribution of relaxation times (T_gs) in freely standing films that originated at the interfaces. The results observed via the simulation study are consistent with experimental work by Ellison and Torkelson (Ellison 2003).

4 MOLECULAR-SCALE TECHNIQUES TO MONITOR GLASS FORMATION AND GLASSY BEHAVIOR OF POLYMERS

4.1 Introduction

This chapter describes the use of fluorescence spectroscopy and dielectric relaxation spectroscopy as analytical tools to monitor the molecular-scale dynamics of polymers. First, basic principles and applications of fluorescence spectroscopy will be provided, followed by the principles and applications of dielectric relaxation spectroscopy.

4.2 Fluorescence as an Analytical Tool

4.2.1 Basic Fluorescence

The basics of fluorescence can be visualized from the Perrin-Jablonski diagram shown in Figure 4-1. The processes illustrated in Figure 4-1 are absorption, internal conversion, and fluorescence. A molecule (probe) is said to be in its electronically excited state when an electron is excited from its ground state orbital to an unoccupied orbital by absorption of a photon. Once the molecule is excited, it can return to the ground state (de-excitation) by several mechanisms, one of which is fluorescence. Absorption of a photon by a molecule promotes the molecule to an electronically excited state vibrational energy level on a time scale of 10^{-15} sec (Lakowicz 1999; Valeur 2002). When a molecule is excited to an energy level higher than the lowest vibrational level of the first electronic state, a spontaneous non-radiative transition between the two

electronic states occurs. This transition is known as internal conversion and relaxes the molecule to the lowest vibrational energy level of the first electronic state via vibrational relaxation on a time scale of 10^{-13}-10^{-11} sec (Lakowicz 1999; Valeur 2002). Fluorescence proceeds by emission of a photon from the lowest energy level of the first electronic state on a time scale of 10^{-8} sec (Lakowicz 1999; Valeur 2002). As a result of internal conversion and emission to higher ground-state vibrational levels, the fluorescence emission spectrum is located at higher wavelengths (lower energy) than the excitation spectrum. The shift between the spectra is called the Stokes shift. Emission and excitation spectra often resemble each other since the differences between vibrational levels are similar in the ground state and the excited state (Lakowicz 1999; Valeur 2002).

Experimentally, fluorescence can be classified into two types of measurements: steady state and time-resolved (Lakowicz 1999). Steady state measurements are performed under constant illumination. The probe is excited at an appropriate wavelength to efficiently promote the electrons to an excited electronic state. The fluorescence emission spectrum is recorded by monitoring the emission intensity as a function of wavelength. The excitation spectrum is obtained by monitoring the emission intensity at a single wavelength while scanning the excitation wavelength.

With time-resolved spectroscopy, it is possible to measure fluorescence intensity decays. Experimentally, the sample is exposed to a pulse of light that is shorter than the decay time. Intensity decay measurements are recorded with a high speed detection system. Time-resolved and steady state measurements are related by the following equation:

$$I_{ss} = \int_0^\infty I_o \cdot \exp(-t/\tau_s) \cdot dt \qquad 4\text{-}1$$

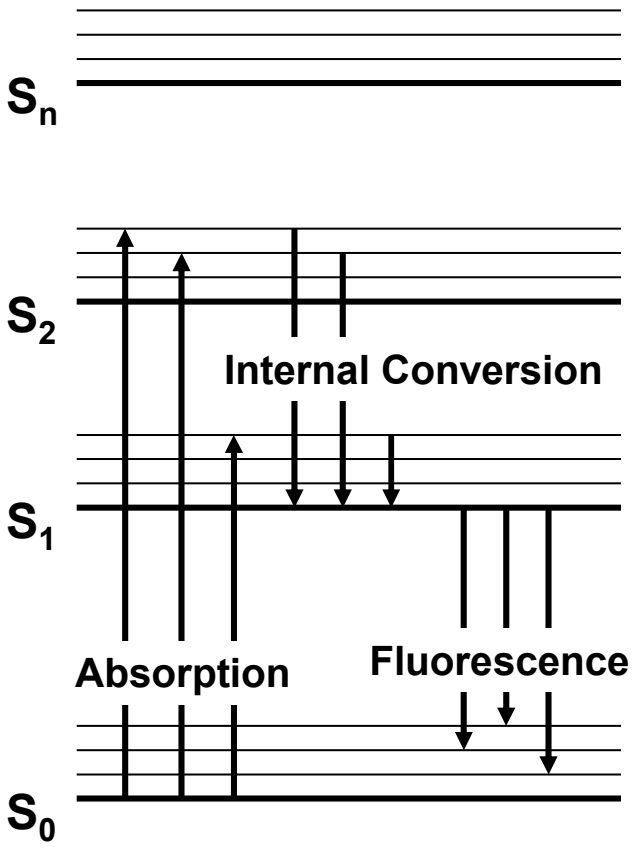

Figure 4-1: Schematic representation of the Perrin-Jablonski diagram and the process of absorption, internal conversion, and fluorescence (phosphorescence not shown).

where I_{ss} is the steady state emission intensity, I_o is a parameter that depends on the probe concentration and a number of instrument parameters, t is time, and τ_s is the average excited-state lifetime. The steady state emission intensity is simply an average of the time-resolved measurements. Although they are more complex experiments, time-resolved measurements are useful for systems that exhibit multiple relaxation times such as polymers.

Two important characteristics of a probe are the quantum yield and the excited-state lifetime. The quantum yield is a ratio of the emitted photons to the number of absorbed photons (Lakowicz 1999; Valeur 2002). The excited-state lifetime of a probe, typically 1-100 ns, is the timescale the molecule is in the excited state. The lifetime determines the amount of time available for the excited state probe to interact with its environment (Lakowicz 1999). Besides fluorescence, excited state molecules can undergo de-excitation via non-radiative pathways such as internal system crossing, vibrational or rotational motions, quenching, intramolecular charge transfer, energy transfer, and conformational changes (Valeur 2002). Figure 4-2 shows a kinetic schematic of the excitation / de-excitation process of a probe. Once excited by absorption of a photon, an excited state probe will undergo de-excitation by fluorescence (a radiative pathway) or a non-radiative pathway. The pathways by which a probe de-excites depend on various parameters such as polarity, pressure, temperature, and viscosity. Thus, the fluorescence of a probe depends on its surrounding medium. Similar to chemical kinetics, after a pulse of light at time zero, the rate of disappearance of an excited-state probe can be expressed by the following equation (Valeur 2002):

$$-\frac{d[A^*]}{dt} = (k_{rad} + k_{non-rad}) \cdot [A^*] \qquad 4\text{-}2$$

where $[A^*]$ is the concentration of excited state probe, k_{rad} is the rate constant for radiative decay,

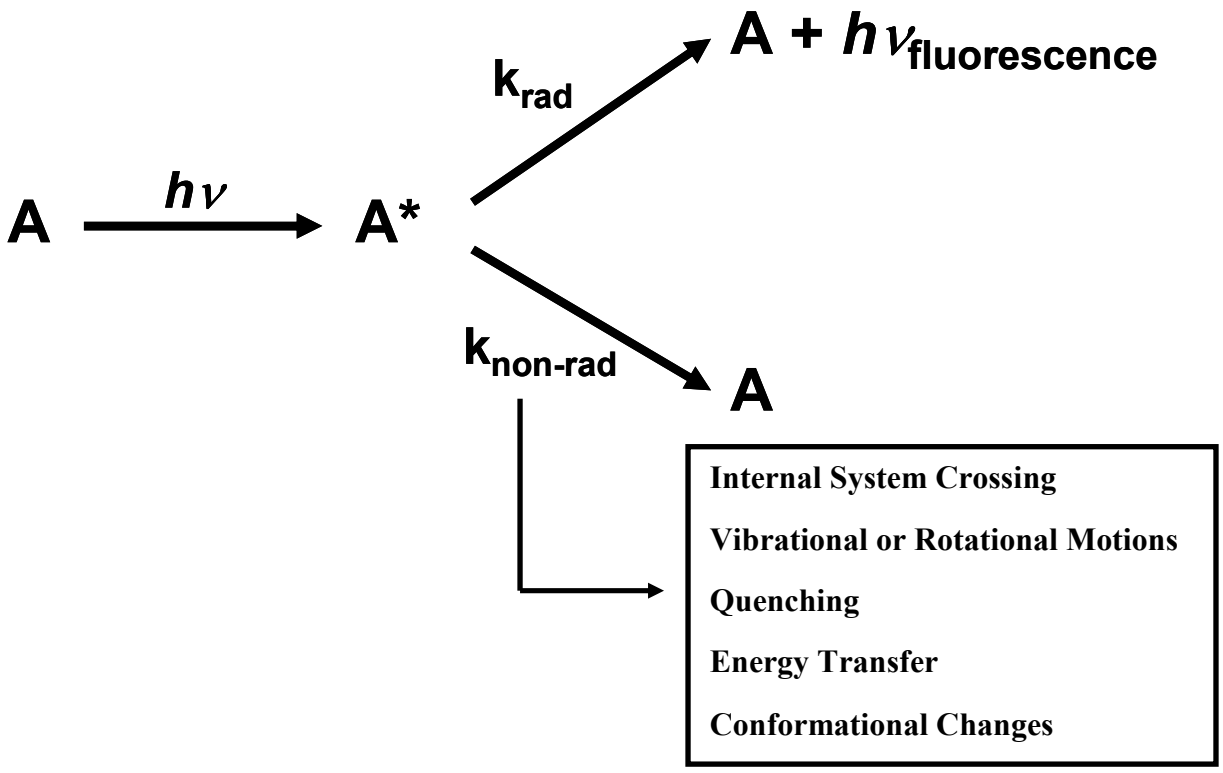

Figure 4-2: Kinetic representation of the excitation and de-excitation of a molecular fluorescent probe. An excited state molecular probe can de-excite via a radiative process that involves fluorescence or a non-radiative process that does not involve fluorescence.

and $k_{non\text{-}rad}$ is the rate constant for non-radiative decay. Integration of equation 4-2 yields the following equation:

$$[A^*] = [A^*]_o \cdot \exp(-t / \tau_s) \qquad 4\text{-}3$$

which provides the time evolution of the concentration of excited state probes. In equation 4-3, $[A^*]_o$ is the concentration of excited-state molecules at time zero after a pulse of light. The average excited state lifetime is defined as:

$$\tau_s = \frac{1}{k_{rad} + k_{non-rad}} \qquad 4\text{-}4$$

As stated above, the quantum yield is the fraction of molecules that de-excite via emission of a photon (radiative path) and is given by the following equation:

$$\Phi = \frac{k_{rad}}{k_{rad} + k_{non-rad}} = k_{rad} \cdot \tau_s \qquad 4\text{-}5$$

For tricyanovinyl-[N(2-hydroxyethyl)-N-ethyl]aniline (TC1), a probe used in this work, the excited-state lifetime and quantum yield in dilute solution of different solvents at room temperature are reported in Loufty 1980.

4.2.2 Intramolecular Charge Transfer Fluorophores

The absorption of a photon by a probe results in the movement of a electron from one orbital to another orbital (Valeur 2002). In some cases, the electronic transition associated with excitation induces an instantaneous change in the dipole moment of the probe (Valeur 2002). Such a probe consists of an electron-donating group (e.g. $–NH_2$, NMe_2, and $–CH_3O$) conjugated to an electron-withdrawing group (-C=O, -CN) (Valeur 2002) and is called an intramolecular charge transfer (ICT) probe. Intramolecular charge transfer probes are also called mobility-

sensitive probes because their emission spectra are sensitive to the medium dynamics in which they are dispersed. Figure 4-3 illustrates the sensitivity of an ICT probe to the molecular mobility of a host medium. In low viscosity polar solvents, the solvent molecules rotate (medium relaxation) during the excited state lifetime of the probe until the solvation shell is in equilibrium with the excited state probe. The resulting relaxed intramolecular charge transfer (ICT) state leads to a reduction in energy prior to fluorescence and causes a red shift in the fluorescence emission spectrum. If the medium viscosity is high, fluorescence will occur from the unrelaxed intramolecular charge transfer state, and there will be no observed red shift in the emission spectrum. The observed shift in the spectrum is an absolute quantity and is not dependent on probe concentration, light intensity, or sample geometry.

During the relaxation towards the ICT state, some probes may experience internal rotation about certain bonds (Valeur 2002). If the internal rotation is around a non-conjugated bond, de-excitation of the probe from its excited state can occur, minimizing fluorescence. Such a probe is commonly referred to as a rotor probe. If the internal rotation is around the bond connecting the donor and accepter moieties (conjugated bond), the molecule will become stable in a twisted intramolecular charge transfer (TICT) state and then fluoresce to the ground state. Thus, the probe will exhibit dual fluorescence from the ICT state and the TICT state (see Figure 4-4) (Valeur 2002). The internal rotation with the fastest rate will control the decay pathway (Loutfy 1981).

In a non-polar medium where the ICT state is not stabilized, isomerization (twisting around the double bond) of the probe becomes the most efficient pathway for non-radiative decay. Essentially the probe relaxes its energy by conformational changes from the trans state to

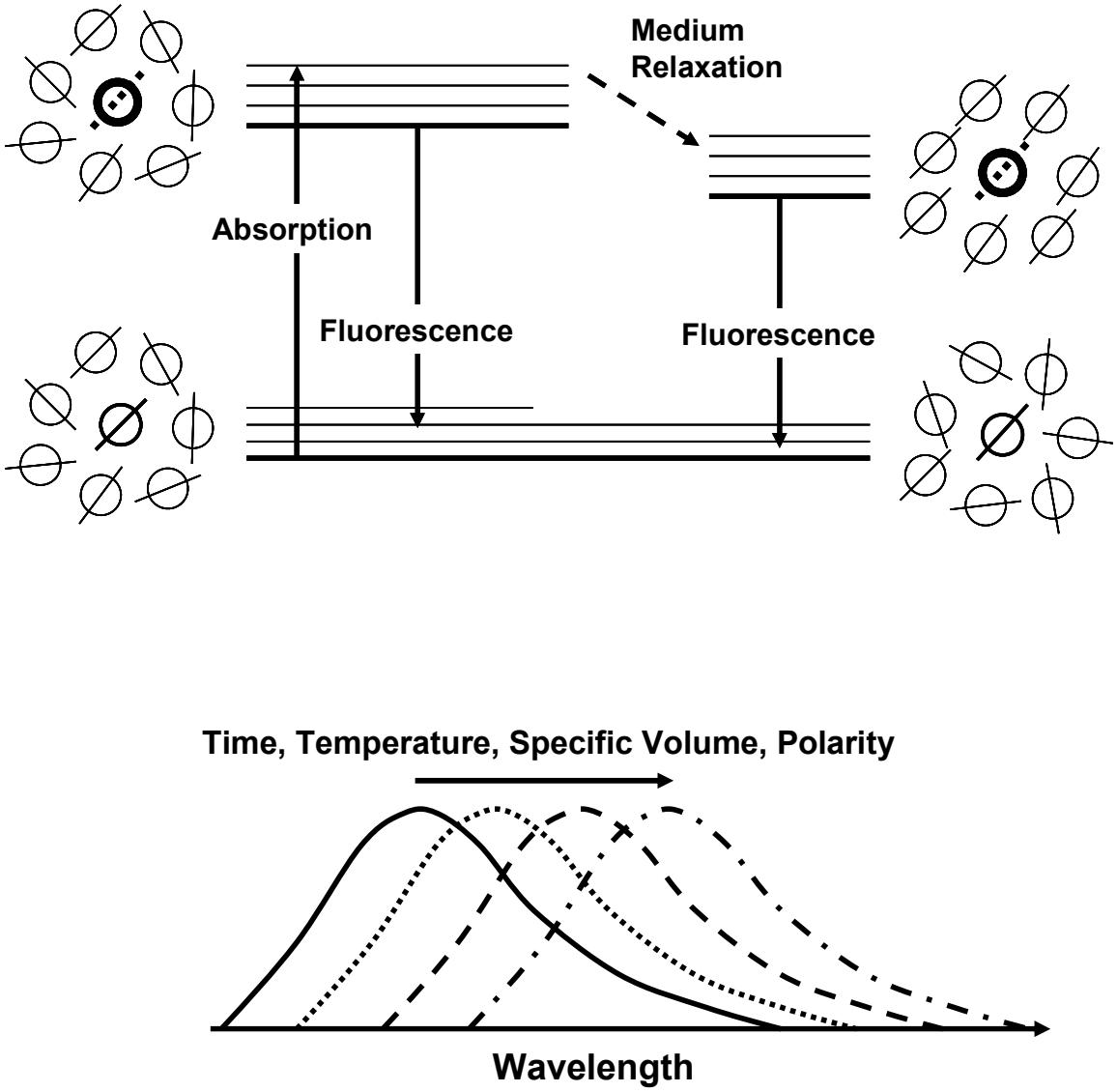

Figure 4-3: Impact of medium mobility on the location of the fluorescence emission spectra of intramolecular charge transfer probes. The greater the medium mobility, the greater the spectral shift. The greater the medium polarity, the greater the spectral shift.

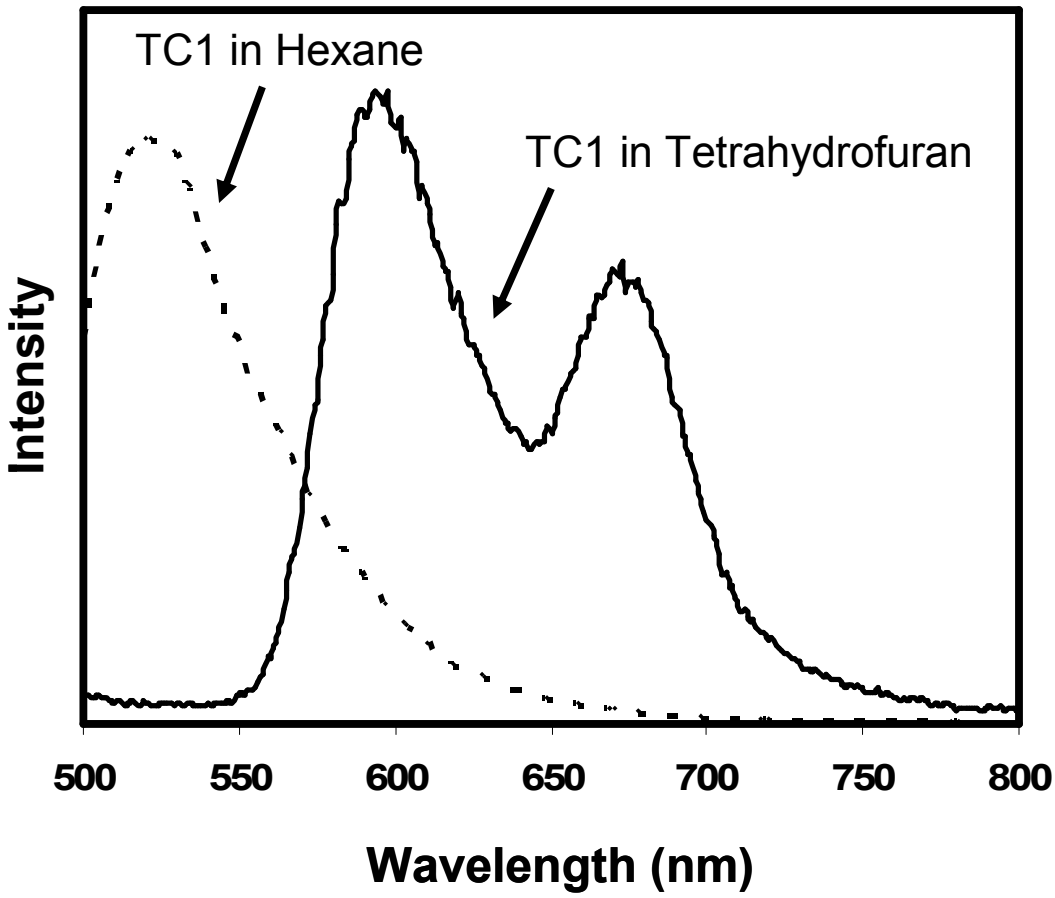

Figure 4-4: The room temperature fluorescence emission spectrum of TC1 dissolved in hexane or tetrahydrofuran. When dissolved in hexane, TC1 exhibits single fluorescence from the ICT state, but when dissolved in tetrahydrofuran, TC1 exhibits dual fluorescence from the ICT and TICT states.

the cis state. For non-radiative decay to occur by rotor motion or isomerization, there must be a certain quantity of free volume to permit such motions (Loutfy 1986). Many polymer properties such as T_g and physical aging have been related to free volume; thus, fluorescent probes exhibiting molecular rotations should provide molecular-level sensitivity to T_g and physical aging.

4.2.3 Polymer Characterization by Fluorescence

Due to the strong influence of the surrounding medium on the fluorescence emission spectrum of fluorescent probe molecules, they are widely used to investigate the properties of chemical, biological, and biochemical systems (Winnik 1986; Lakowicz 1999; Valeur 2002). In the case of polymer science, fluorescence has been used to characterize polymer chain dynamics (Ingratta 2007), monitor polymerization and curing (Loutfy 1981; Jager 1995; Strehmel 1999; Quirin 2003), and sorption and drying (Ellison 2004a). *Photophysical and Photochemical Tools in Polymer Science* provides a collection of studies on the use of fluorescence as a tool to investigate the dynamics of polymers in solution and melts, polymers in the glassy state, and polymer blends (Winnik 1986). Rather than attempt to provide an exhaustive review of the use of fluorescence as a tool in polymer science, an overview of fluorescence as a tool to measure the glass transition temperature and physical aging will be provided.

4.2.3.1 Glass Transition Temperature

The first use of fluorescence spectroscopy to determine the T_g of polymers was shown by Loufty (Loutfy 1981; Loutfy 1986). In his study, the temperature dependence of the fluorescence emission spectrum of a probe doped into poly(methyl methacrylate) was monitored

over a wide temperature range. Plots of the fluorescence emission intensity as a function of temperature provided a route to determine T_g similar to dilatometric methods. At T_g, there was a significant change in the temperature dependence of the fluorescence emission intensity. In particular, the intersection of linear fits in the rubbery and glassy states yielded a T_g value identical to that determined by differential scanning calorimetry (DSC).

The T_g at an epoxy-glass interface was determined by monitoring the emission intensity of a (dimethylamino)nitrostilbene (DMANS) probe as a function of temperature (Lenhart 2001). In the study, DMANS was either doped into the matrix or labeled to a triethoxysilane coupling agent that was grafted to the glass substrate. At T_g, there was a break in the temperature dependence of the fluorescence emission intensity. Additionally, DMANS exhibited a blue-shift in its fluorescence emission spectrum with decreasing temperature. Thus, DMANS can be considered an ICT probe. It was shown that at the epoxy-glass interface, T_g could be higher or lower than the bulk T_g depending on the structure of the silane coupling agent. In addition, the extent of blue-shift observed at the interface depended on the structure of the silane coupling agent. Interestingly, Lenhart *et al*. (Lenhart 2001) suggested that there might exist a gradient in properties at the interface and that their interfacial measurements were just an average of the gradient in properties.

Since 2002, Torkelson and coworkers have extensively used fluorescence spectroscopy to measure the T_g of polymeric systems (Ellison 2002a; Ellison 2002b; Ellison 2003; Ellison 2004b; Ellison 2005; Mundra 2006; Rittigstein 2006; Rittigstein 2007; Mundra 2007a; Priestley 2007a; Roth 2007a; Mundra 2007b; Priestley 2008b; Roth 2007b). In all studies, T_g was determined by monitoring the emission intensity as a function of temperature. The T_g was determined by fitting

linear temperature dependences to both the rubbery state and glassy states, with the intersection of the lines defining T_g. With the appropriate probe, sample preparation and experimental setup, T_g determined via fluorescence was nearly identical to the value determined by DSC for all systems studied by Torkelson and coworkers. A significant reason for the interest by Torkelson and coworkers in using fluorescence spectroscopy to determine T_g was the potential of the technique to monitor T_g of nanoconfined polymers (Ellison 2002b).

Ellison and Torkelson were the first to show the applicability of fluorescence to measure T_g of ultrathin polymer films (Ellison 2002a; Ellison 2002b). The T_gs of ultrathin polystyrene films determined by fluorescence were nearly identical to the T_gs of ultrathin polystyrene films as determined by ellipsometry (Ellison 2002a; Ellison 2002b). In 2003, Ellison and Torkelson developed a fluorescence / multilayer method that allowed for the first determination of a distribution of T_gs at the air-polymer interface of a supported polystyrene film (Ellison 2003). In that 2003 study, a pyrene-labeled polystyrene layer of known thickness was placed atop a neat polystyrene layer of known thickness using a water transfer technique. Thus, fluorescence measurements provided T_g of the labeled layer. Using bilayer and trilayer film geometries, Ellison and Torkelson determined that the T_g of a polystyrene layer at the air-polymer interface was substantially reduced from the bulk T_g when the free-surface layer thickness was less than 30 nm (Ellison 2003).

Recently, Jager *et al*. have shown that a solvatochromic and rigidochromic ICT color-shifting probe could be employed to determine T_g of poly(methyl methacrylate) and polystyrene (Jager 2005). Instead of plotting the emission intensity as a function of temperature, Jager *et al*. determined T_g by plotting the wavelength of the peak maximum as a function of temperature.

Linear fits in both rubbery and glassy states provided a measure of T_g. The T_gs of bulk poly(methyl methacrylate) and polystyrene determined via the color-shifting probe was consistent with those determined via DSC.

To enhance the sensitivity of fluorescent probes to the glass transition and secondary relaxation processes, several studies have plotted the full width half maximum of the fluorescence emission spectrum (Deus 2004; Martins 2006) or the first moment of the fluorescence intensity (Turrion 2005; Corrales 2006) as a function of temperature. A break (slope change) in the temperature dependence of the parameter as a function of temperature provided a measure of the transition temperature. Besides T_g, these approaches have been used, although not convincingly, to determine the beta, gamma, and delta transitions of polymers (Deus 2004; Corrales 2006).

4.2.3.2 Physical Aging

In 1990, the first studies were published on the use of fluorescence spectroscopy as a tool to monitor physical aging of polymers by Meyer *et al*. (Meyer 1990) and Schwab and Levy (Schwab 1990). Meyer *et al*. monitored the isothermal physical aging of poly(vinyl acetate) by measuring the time-dependent change in the emission intensity of Auramine O doped into the matrix (Meyer 1990). With increasing physical aging time, there was an increase in the emission intensity of Auramine O. A comparison of the change in emission intensity with aging time to the increase in the characteristic time for stress relaxation with aging time revealed a linear relationship, indicating consistency between the two measurements (Meyer 1990). Schwab and Levy showed that the emission intensities of the probes malononitrile and nitrostilbene increased with increasing physical aging time when doped into poly(methyl methacrylate) or amine-cured

diglycidyl ether of bisphenol A epoxy (Schwab 1990). After 1000 min of aging, the fluorescence intensity increased by approximately 3 % while the specific volume decreased by less than 0.1 % (Greiner 1984; Schwab 1990). Thus, fluorescence provides enhanced sensitivity to physical aging.

In the early 1990's, Royal and Torkeslon published a series of manuscripts on the use of fluorescence spectroscopy as a tool to monitor physical aging of polymers (Royal 1990; Royal 1992a; Royal 1992b; Royal 1992c; Royal 1993). They monitored physical aging by measuring the emission intensity as a function of physical aging time. Doping the probe julolidenemalononitrile into several amorphous polymers, Royal and Torkelson showed that the physical aging rates determined by fluorescence measurements followed the same temperature dependence as the physical aging rates determined by volume relaxation measurements (Royal 1993). The fluorescence physical aging rate was determined as the slope of the intensity versus log(aging time) plot. The slope of an aging isotherm is given by the following equation:

$$r_f = \frac{1}{f_O} \cdot \frac{df}{d \log t_a} \qquad 4\text{-}6$$

where f_o is the initial fluorescence intensity and f is the fluorescence intensity at aging time t_a. The time required for fluorescence intensities to reach equilibrium after aging was similar to the time required for volume to reach equilibrium after aging using dilatometric measurements (Royal 1993). Besides single-temperature jump isothermal physical aging experiments, Royal and Torkeslon showed that multiple-temperature jump asymmetry and memory physical aging experiments could be monitored using fluorescence spectroscopy (Royal 1992b).

Recently, a wavelength shifting probe was employed to investigate physical aging of polycarbonate and poly(methyl methacrylate) (Berg 2006). For each polymer, a linear

correlation was found between the wavelength at the emission maximum and specific volume. With increasing physical aging time, there was a blue shift in the peak maximum of the fluorescence emission spectrum. A characteristic relaxation time for aging was determined by fitting the relaxation curves to the KWW function. The aging characteristics of the polymers determined via the fluorescence from wavelength shifting probes and other methods were comparable, providing evidence that the fluorescence from wavelength shifting probes is a reliable method to monitor physical aging (Berg 2006).

4.3 Dielectric Relaxation Spectroscopy as an Analytical Tool

4.3.1 Basics of Dielectric Relaxation

Dielectric relaxation spectroscopy is a technique that allows for the investigation of polymer relaxation dynamics over a large temperature range and a wide frequency range. For typical frequency domain measurements, the frequency range is 10^{-3} Hz < f < 10^{7} Hz. Dielectric relaxation spectroscopy probes molecular dynamics by monitoring molecular dipole relaxations as a function of frequency and temperature.

For a small electric field (E), the dielectric displacement (D) within a sample can be expressed as

$$D = \varepsilon_o \varepsilon^* E \qquad 4\text{-}7$$

where ε_o is the dielectric permittivity in vacuum (ε_o = 8.854 x 10^{-12} As V^{-1} m^{-1}) and ε^* is the complex dielectric constant or complex dielectric permittivity. The complex dielectric constant can be a function of time or frequency if time-dependent processes take place within the sample (Schonhals 2003). Within the scope of this work, the time-dependent processes of interest are

those related to fluctuations of dipoles due to individual molecules or groups of molecules moving together.

The complex dielectric constant is given by

$$\varepsilon^*(\omega) = \varepsilon'(\omega) - i\varepsilon''(\omega) \qquad 4\text{-}8$$

where ε' and ε'' are the real and imaginary parts of the complex dielectric constant, respectively, and ω is the radial frequency ($\omega = 2\pi f$, where f is frequency) associated with the periodic electric field applied to the sample. The real and imaginary parts of the complex dielectric constant can provide information about the molecular-scale relaxation dynamics of polymers as a function of radial frequency and temperature. Figure 4-5 shows typical dielectric data for the imaginary part of the dielectric constant versus frequency at a given temperature near T_g. The peaks in the imaginary part of the dielectric constant represent the α-relaxation and β-relaxation processes for a typical polymer. (It is noted that not all polymers exhibit a β-process. Additional relaxation processes that may be observed are omitted from Figure 4-5.) Dielectric measurements as a function of frequency and temperature allow for the determination of the temperature dependence of relaxation processes (Arrhenius plot). As illustrated from Figure 4-5, it is possible via dielectric spectroscopy to access the full relaxation time distribution for a given relaxation process.

Analysis of dielectric spectroscopy data usually involves fitting data similar to Figure 4-5 to a non-Debye relaxation function such as the Havriliak and Negami (Havriliak 1967) function:

$$\varepsilon^*(\omega) = \varepsilon_\infty + \frac{\Delta\varepsilon}{(1 + (i\omega\tau)^\beta)^\gamma} \qquad 4\text{-}9$$

where β and γ are shape parameters that describe the symmetric and asymmetric broadening of

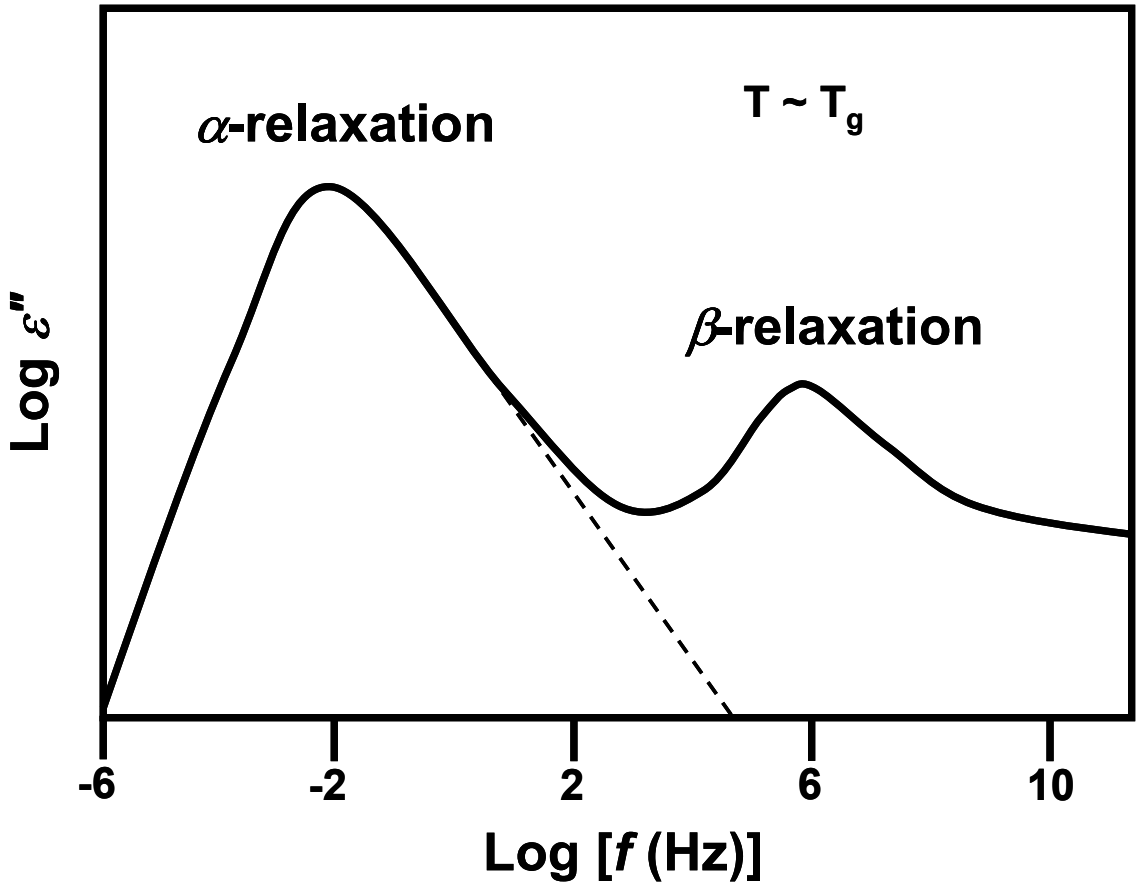

Figure 4-5: The dependence of the loss component of the dielectric constant on the logarithm of the frequency for an amorphous polymer. The peaks of the curve represent the α-relaxation process and the β-relaxation process.

the relaxation process, respectively. From linear response theory, it is possible to determine the relaxation time distribution of a process from measurements conducted in the frequency domain (Schonhals 2003). Figure 4-6 shows transformation relationships for linear dielectric relaxation measurements.

4.3.2 Molecular Dielectric Probes

A prerequisite for the use of dielectric spectroscopy to investigate the dynamics of polymers is the existence of dipoles. Although most polymers contain at least a weak dipole moment, non-polar polymers (e.g. polyolefins) do not contain polar moieties. Thus, the dynamics of these non-polar polymers cannot be investigated by dielectric spectroscopy. However, several studies have shown that the addition of host molecular dielectric probes to the matrix of non-polar polymers provides a route by which their relaxation dynamics can be investigated via dielectric spectroscopy (Hains 1975; Dhinojwala 1993; Dionisio 1994; Dhinojwala 1994b; Berg 2004; Berg 2004b; Berg 2005).

Dhinojwala and Torkelson demonstrated that dielectric spectroscopy of polystyrene (a weakly polar polymer) containing low levels of the molecular dielectric probe Disperse Red 1 (DR1) yielded good determination of the polystyrene relaxation dynamics (Dhinojwala 1994b). In particular, the rotational reorientation dynamics of DR1 are coupled to the α-relaxation dynamics of polystyrene (Dhinojwala 1994b) and other polymers (Dhinojwala 1993). Dhinojwala and Torkelson showed that the average α-relaxation time and the α-relaxation time distribution as determined by dielectric spectroscopy were nearly identical for neat polystyrene and DR1-doped polystyrene (Dhinojwala 1994b).

Using a series of nitro-stilbene probes, the effect of probe size and concentration on the

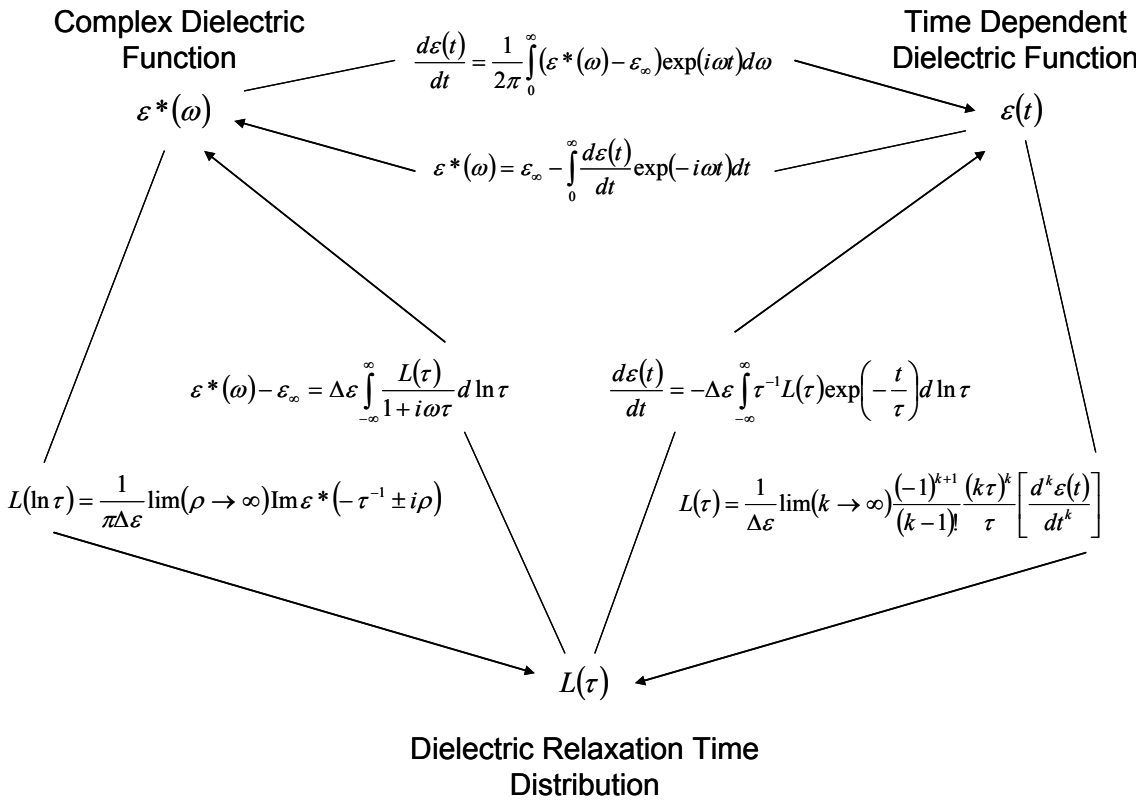

Figure 4-6: Transformation relationships for linear dielectric relaxation spectroscopy data.

dielectric response of polystyrene was investigated (Berg 2005). The length of the probes ranged between 0.6 to 2.0 nm and the concentration ranged between 0.1 to 1.0 weight percent. The polymer used was polystyrene. The incorporation of all nitrostilbenes into the matrix of polystyrene resulted in an amplification of the α-relaxation process that increased linearly with increasing probe concentration (Berg 2005). Interestingly, the smallest probe used (l = 0.6 nm) exhibited an additional relaxation process which was attributed to "free-volume probe relexation" that was not coupled to the dynamics of the polymer. Thus, the minimum probe size required for the coupling of the rotational dynamics of a probe and the α-relaxation dynamics of polystyrene is at least l = 0.6 nm.

PART II: GLASS TRANSITION TEMPERATURE MEASUREMENTS

5 DISTRIBUTION OF GLASS TRANSITION TEMPERATURES OF POLYMER WITH ATTRACTIVE POLYMER-SUBSTRATE INTERACTIONS

5.1 Introduction

The achievement of a complete understanding of the nature of the glass transition in amorphous materials remains one of the most challenging problems in condensed matter physics (Anderson 1995; Angell 1995; Debenedetti 2001). A central tenet of the physics of the glass transition is that of the cooperative rearranging region (CRR) (Adams 1965; Sillescu 1999; Ediger 2000; Donth 2001) which, as defined by Adam and Gibbs (Adams 1965), is "the smallest region that can undergo a requisite transition to a new configuration without a requisite simultaneous configurational change on and outside its boundary." Experimental studies indicate that the size of a CRR is approximately 1-4 nm (Tracht 1998; Ediger 2000; Berthier 2005) and may be considered as the lower limit for the size of a dynamic heterogeneous region (Ediger 2000).

Since the discovery more than a decade ago that confinement of polymer films at the nanoscale can lead to large deviations in T_g compared to the bulk state (Keddie 1994a; Keddie 1994b), many experimental studies (Forrest 1996; vanZanten 1996; DeMaggio 1997; Fukao 1999; Fryer 2000; Dalnoki-Veress 2001; Grohens 2002; Ellison 2003; Park 2004; Ellison 2005; Mundra 2006; Svanberg 2007; Fukao 2001) and simulations (Torres 2000; Varnik 2002; Baljon

2004; Peter 2006; Riggleman 2006) have been carried out in a quest to characterize and explain the observed phenomena. As mentioned in Chapter 3, two prominent explanations accounting for the impact of confinement on T_g are finite size effects and interfacial effects. Finite size effects are hypothesized to occur when the length scale of the system, i.e., film thickness, and the length scale governing T_g, i.e., a CRR, coincide (Fukao 2000; Fukao 2001b). Interfacial effects are expected to increase in significance with an increase in the ratio of interfacial area to volume (Keddie 1994a; Keddie 1994b; Forrest 1996; Ellison 2003).

The definition of a CRR has been used to justify two- and three-layer models that offer explanations of the deviation from T_g(bulk) in nanoscopically confined polymer films (Keddie 1994a; Forrest 2000). These models assume that perturbations to T_g at the free surface (air-polymer interface) or the polymer-substrate interface are limited to length scales roughly the size of a CRR. (By some interpretations, CRRs are always independent of one another and should not impact the dynamics of adjacent CRRs; with these interpretations, perturbations to T_g at the free surface or substrate interface are believed to be limited to a layer thickness of one CRR and unable to propagate from the interface into the film interior.) However, reductions in T_g from T_g(bulk) have been reported for films as thick as 300-400 nm when the films lack attractive interactions with the substrate on which they are supported (Ellison 2005). Because of the large difference in the length scale at which T_g-confinement effects have been observed in polymer films and the length scale of a CRR, it can be concluded that deviations in T_g are not directly related to the size scale of a CRR (Forrest 1996). In addition, it is unclear how perturbations limited to the very small length scale of a CRR can lead to significant changes in the T_g of polymer films with thicknesses that are one or even two orders of magnitude larger than a CRR.

The picture that T_g dynamics are perturbed by interfacial effects only over the length scale of a CRR has been experimentally refuted by a recent study employing a fluorescence/multilayer technique that found that perturbations to T_g at the free surface of a film are able to propagate into the film interior (Ellison 2003). In particular, the study showed that the perturbed T_g dynamics at the free surface of polystyrene (PS) led to T_gs differing from T_g(bulk) at distances of several tens of nanometers from the PS free surface. This behavior was explained to result from the strongly perturbed CRRs in the free-surface layer affecting the average cooperative dynamics in adjoining layers of CRRs, and to a lesser extent the CRRs of the next layer, and so on.

This chapter describes the first study to characterize the distribution of T_gs for polymer films that possess strong attractive interactions with the substrate. The results demonstrate not only that strongly perturbed T_g behavior in an interfacial layer of a polymer film propagates over length scales equivalent to a number of layers of CRR*s* but that perturbations to T_g caused by attractive interactions with the substrate can be observed over length scales of several hundred nanometers.

5.2 Experimental

Poly(methyl methacrylate) (PMMA) was synthesized by free radical polymerization, with *Mn* = 355,000 g/mol and *PDI* = 1.54 obtained by gel permeation chromatography (universal calibration relative to PS standards). The onset T_g = 394 K, as determined by DSC (Mettler Toledo DSC822e) on second heating with a heating rate of 10 K/min. The chromophore 4-tricyanovinyl-[N-(2-hydroxyethyl)-N-ethyl]aniline (TC1) was synthesized by reaction with tetracyanoethylene (TCI America) and 2-(N-ethylaniline)ethanol (TCI America) dissolved in

dimethyl formamide (Fisher) at 55 ^{o}C for 15 min and then recrystallized from glacial acetic acid. The 1-pyrenyl butanol-labeled (Aldrich) and TC1-labeled methacrylate monomers were synthesized through an esterification of 1-pyrenyl butanol and TC1, respectively, with methacryloyl chloride (Aldrich) in the presence of triethylamine (Aldrich) and dichloromethane (Aldrich) at 0 ^{o}C for 2 hr (see Figure 5-1). Labeled PMMA was synthesized by reaction of methyl methacrylate monomer (Aldrich) in the presence of a trace amount of either pyrene-labeled or TC1-labeled methacrylate monomer. The pyrene-labeled PMMA contains 1.22 mol % (1 in 82 repeat units) of pyrene-labeled monomer and the TC1-labeled PMMA contains 1.37 mol% (1 in 73 repeat units) of the TC1-labeled monomer determined by UV-Vis absorbance spectroscopy (Perkin Elmer Lambda 35). For pyrene-labeled PMMA, *Mn* = 456,000 g/mol, *PDI* = 2.0, and the onset T_g = 395 K. For TC1-labeled PMMA, *Mn* = 509,000 g/mol, *PDI* = 1.67, and the onset T_g = 394 K. All polymer was washed by dissolving in toluene (Fisher) and precipitating in methanol (Fisher) at least five times to remove residual solvent and then dried in a vacuum oven at T_g + 15 K for 24 hr.

Single layer films were prepared by spin casting polymer/toluene solutions onto silica slides. The films were allowed to dry in vacuum at T_g + 5 K for 8 hr. Multilayer films were prepared by spin casting polymer/toluene solutions onto either a silica slide or a NaCl salt disk. Films spun cast onto NaCl salt disks were floated on top of films spun cast onto silica slides by submersing the salt disk in a water bath (see Figure 5-2 for illustration of multilayer film preparation). After preparation of a multilayer film, it was dried in vacuum at room temperature for 12 hr and then annealed at T_g + 25 K for 10 min to ensure a completely consolidated film. Film thicknesses were measured with a Tencor P10 profilmeter.

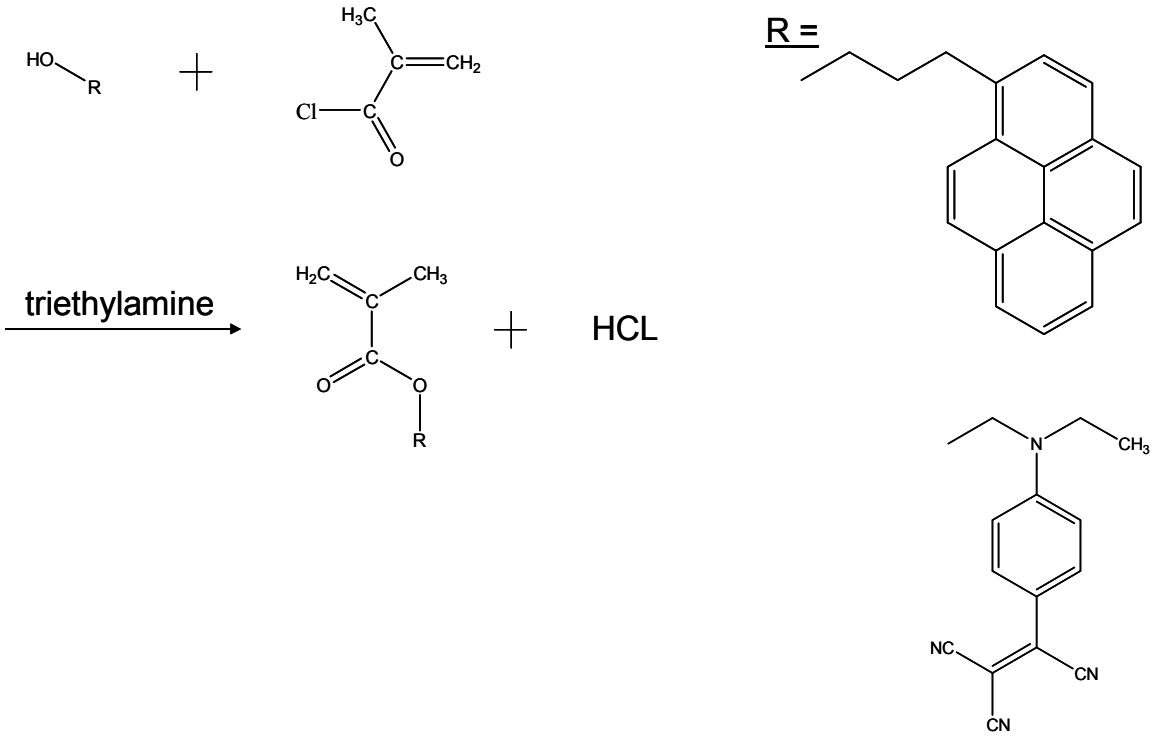

Figure 5-1: Synthesis of pyrene-labeled or TC1-labeled methacrylate monomers.

1. **Spincoat first layer on silica substrate**

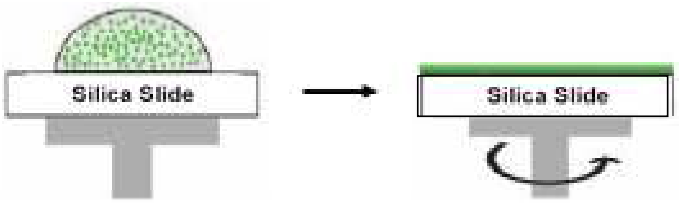

2. **Spincoat second layer on salt disk or mica**

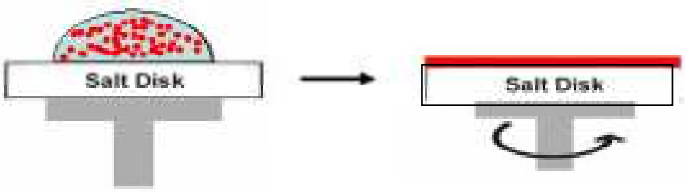

3. **Float second layer on salt disk or mica to water**

4. **Pick up second layer onto first layer**

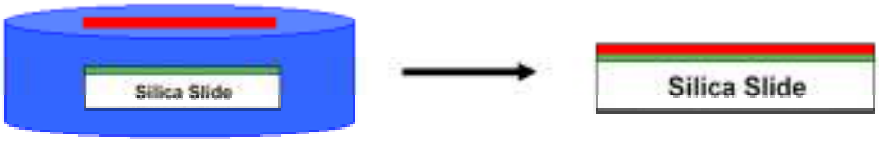

Figure 5-2: Preparation of multilayer films by a water transfer technique.

All polymers were of sufficiently high molecular weight to ensure that interlayer diffusion was at most several nanometers during the experimental time, which includes the time to create a consolidated film. The estimated interlayer diffusion can be determined from nuclear reaction analysis data (Shearmur 1998). For the conditions employed in this work, the total diffusion time of 40 min was much less than the polymer disentanglement time. The disentanglement time can be calculated by the following equation: $\tau_D = (2R_g^2)/(\pi^2 D_s)$, where R_g is the radius of gyration of the polymer and D_s is the bulk self-diffusion coefficient. For PMMA (lowest molecular weight and fastest diffusing component used in these studies) at T_g + 25 K, the disentanglement time was 3850 min using D_s = ~ $3x10^{-18}$ cm^2/s from nuclear reaction analysis diffusion data (Shearmur 1998). Since the total experimental time above T_g was substantially smaller than the disentanglement time (experimental time above T_g was only 1% of disentanglement time), the maximum interlayer penetration distance was substantially less than the PMMA R_g (~18.5 nm), with a reasonable estimate of a few nanometers. It is important to note that the above estimate is an upper limit as the polymer used in the study (355,000 g/mol, 456,000 g/mol and 509,000 g/mol) is of higher molecular weight than that used in (100,000 g/mol and 127,000 g/mol) the interlayer diffusion study (Shearmur 1998).

Steady-state fluorescence emission spectra were taken as a function of temperature (on cooling) using a Photon Technology International fluorimeter in a front-face geometry (with emission at 90^o relative to excitation and the film at an angle of 28^o relative to excitation) with 3.0 mm excitation and emission slits (12 nm bandpass) used for TC1-labeled PMMA experiments and 1.25 mm excitation and emission slits (5 nm bandpass) used for pyrene-labeled PMMA experiments. The wavelength used to excite the TC1 and pyrene were 480 nm and 254

nm, respectively. The emission spectra of TC1 and pyrene were measured at 540-690 and 360-460, respectively. The T_g values of the labeled films were determined by fitting the temperature dependence of the integrated fluorescence intensity to linear correlations in both the rubbery and glassy states. In fitting the data to linear correlations, only data well outside T_g were used in the fitting procedure.

In all cases, T_g data were obtained from fluorescence measurement obtained upon cooling from the equilibrium rubbery or liquid state. Polymer films were heated to the maximum measurement temperature and held for a minimum of 10 min before measuring the fluorescence emission spectrum. Then the temperature was decreased by 5 K where the sample was held for 5 min to ensure thermal equilibrium before again measuring the fluorescence emission spectrum. This "cooling, holding, measuring" protocol was repeated well into the glassy state of each film being measured and has previously been shown to yield T_g measurements in bulk films that are in good agreement with onset T_gs measured by DSC using a 10 K/min heating rate (Ellison 2002b). The good agreement is likely due to the temperature ramping by DSC being within an order of magnitude of the effective average cooling rate of 5 K/5 min (or 1 K/min) used in our fluorescence measurements of T_g. Additional information on the use of fluorescence to monitor T_g is found in (Ellison 2002b; Ellison 2003; Ellison 2005; Mundra 2007a; Roth 2007b).

5.3 Results and Discussion

Figure 5-3 shows the temperature dependence of the fluorescence emission spectrum of a 200-nm-thick TC1-labeled PMMA film supported on silica. A decrease in temperature yields an increase in the fluorescence intensity. The increase in intensity with decreasing temperature (decrease in thermal energy and densification of polymer) is a result of a reduction in the rate of

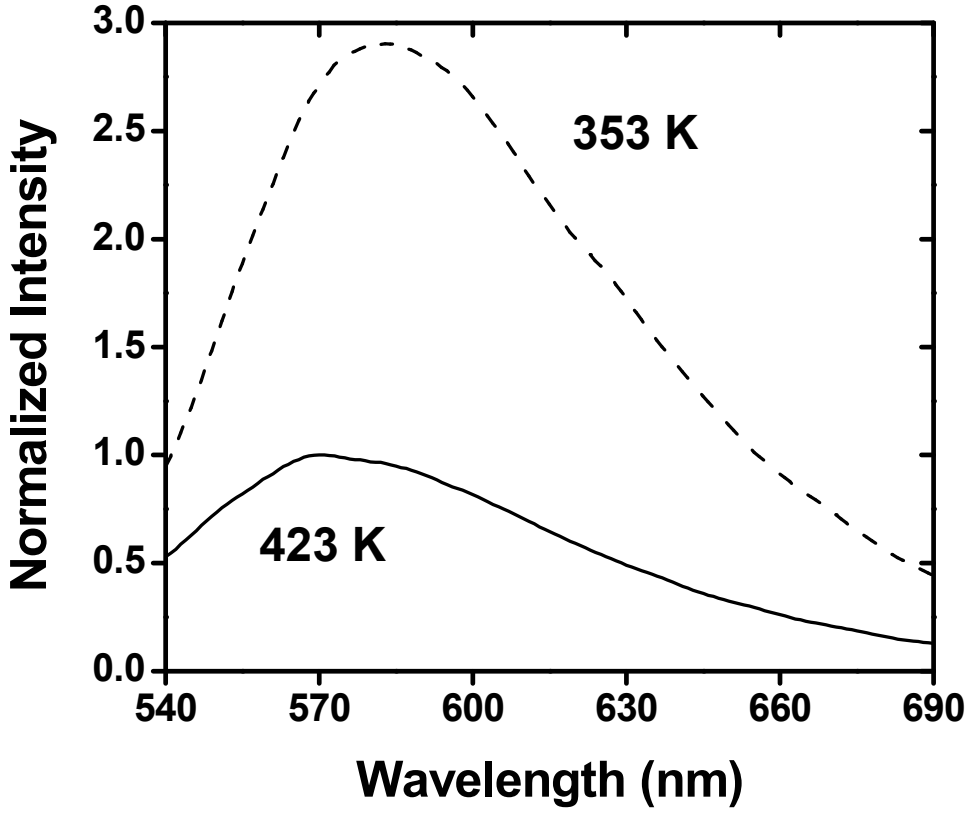

Figure 5-3: Temperature dependence of the fluorescence emission spectrum of a 200-nm-thick TC1-labeled PMMA film supported on quartz.

non-radiative decay (see Chapter 4 for more detail). Figure 5-4 shows the normalized integrated fluorescence intensity as a function of temperature for pyrene-labeled and TC1-labeled PMMA films. Data points were obtained by taking the integrated intensity of the fluorescence emission spectrum of the labeled polymer as a function of temperature. Linear correlations were fit to data points in both the rubbery and glassy states, with the intersection providing a measure of T_g. The T_g values of the 250-nm-thick pyrene-labeled PMMA and 200-nm-thick TC1-labeled PMMA films are 394 K and 395 K, respectively, and are within 1 K of T_g(bulk) determined by DSC of the labeled PMMA.

While the values of T_g obtained using pyrene- and TC1-labeled PMMA are consistent, the slope changes in the temperature dependences of the normalized integrated fluorescence emission intensity are opposite each other (see Figure 5-4). The difference in the change in slope of the temperature dependence of fluorescence intensity for the two probes is related to the different mechanism by which each probe undergoes non-radiative decay from its excited state and is briefly explained below.

Pyrene, a band definition probe, undergoes non-radiative decay by vibrational motions (Lakowicz 1999; Valeur 2002); thus, the emission intensity follows the density of the polymer and the temperature dependence of the emission intensity is smaller below T_g than above T_g. Numerous band definition probes have been used to determine T_g in bulk polymeric glass formers (Meyer 1990; Ellison 2002b; Ellison 2003; Deus 2004; Ellison 2005; Turrion 2005; Mundra 2007a). The TC1 probe, a "rotor" probe, undergoes non-radiative decay by rotational motion as depicted by the inset in Figure 5-3 (Valeur 2002). To facilitate the rotational motion of the probe, a certain amount of free volume is required (Loutfy 1982); thus, it is believed that

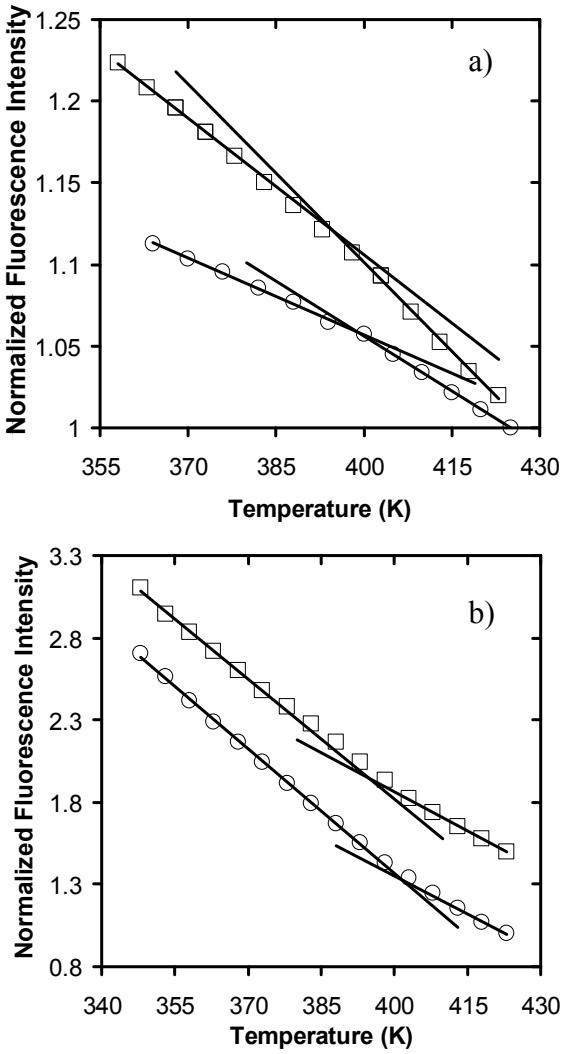

Figure 5-4: Determination of T_g using probes labeled to PMMA. a) Temperature dependence of the normalized integrated fluorescence intensity of 250-nm-thick (squares) and 50-nm-thick (circles) pyrene-labeled PMMA films. The solid lines are fits of the data in both the rubbery and glassy states, with the intersection of the lines defining T_g. b) Temperature dependence of the normalized integrated fluorescence intensity of 200-nm-thick (squares) and 35-nm-thick (circles) TC1-labeled PMMA films. The solid lines are fits of the data in both the rubbery and glassy states, with the intersection of the lines defining T_g.

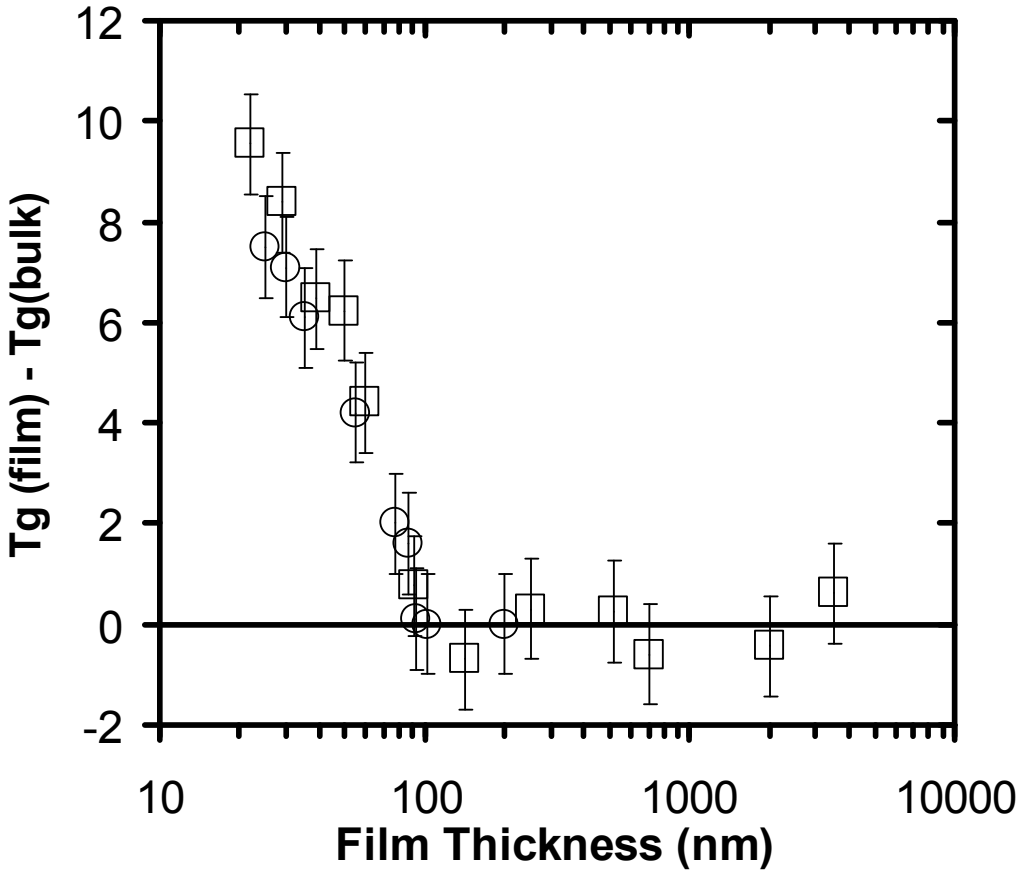

Figure 5-5: T_g(film) - T_g(bulk) of pyrene-labeled PMMA (squares) and TC1-labeled PMMA (circles) single layer films as a function of film thickness. Within experimental error, both probes detect identical increases in T_g of PMMA as a function of film thickness.

changes in polymer density impede the rotational motion to a greater extent in the glassy state than in the liquid state. As a result, the temperature dependence of the emission intensity is greater in the glassy state than the rubbery state. Because of the enhanced sensitivity of "rotor" probes to density changes that occur in the glassy state, they have been used to monitor physical aging of polymeric glass formers (Meyer 1990; Royal 1990; Royal 1992b; Royal 1993; Ellison 2002a).

According to Figure 5-4, the T_gs of a 50-nm-thick pyrene-labeled PMMA film and a 35-nm-thick TC1-labeled PMMA film are 399 K and 402 K, respectively. This indicates that there is an increase in T_g with decreasing film thickness for PMMA films supported on silica. The increase in T_g with decreasing thickness is thought to be related to hydrogen bond formation that can occur between the ester groups on PMMA and the hydroxyl groups on the silica substrate (Keddie 1994b; Fryer 2000; Grohens 2002; Park 2004). The formation of hydrogen bonds is believed to reduce the cooperative segmental mobility of the polymer at and near the silica interface, thus resulting in an increase in T_g with decreasing film thickness as the ratio of interfacial area to volume becomes increasingly large.

Figure 5-5 shows the effect of film thickness on T_g(film) – T_g(bulk) obtained by fluorescence of pyrene- and TC1-labeled PMMA films. The increase in T_g with decreasing film thickness is identical for pyrene- and TC1-labeled PMMA films and is qualitatively consistent with other studies of single layer PMMA films supported on silica substrates (Keddie 1994b; Fryer 2000; Park 2004). For thicknesseses greater than approximately 90 nm, T_g is independent of thickness. For thickness less than approximately 90 nm, T_g increases roughly linearly on a logarithmic scale with decreasing thickness, such that for a 20-nm-thick film, T_g(film) – T_g(bulk)

= 9 K.

The direct impact of the substrate on the local T_g near the polymer-substrate interface of a bulk PMMA film was determined using a bilayer film geometry (see Figure 5-6 inset) in which a labeled PMMA layer of known thickness (h) was sandwiched between the substrate and an unlabeled 240-nm-thick PMMA layer. The overall bilayer film thickness was sufficiently large that T_g(film) = T_g(bulk).

Figure 5-6 shows that T_g(substrate layer) – T_g(bulk) = 10 K for a 12-nm-thick substrate layer. When the thickness of the substrate layer is increased, the value of T_g(substrate layer) – T_g(bulk) gradually approaches zero at h = 70-80 nm. It is noted that a similar experiment conducted with a 14-nm-thick substrate layer in a bulk PS bilayer film found that T_g(substrate layer) – T_g(bulk) = 0 K (Ellison 2003). The difference in the T_g behavior of the PS and PMMA substrate layers can be explained by hydrogen bonding effects that are present at the PMMA/silica substrate interface (Keddie 1994b; Peter 2006) but absent at the PS/silica substrate interface (Keddie 1994b; Ellison 2003).

Placement of a labeled PMMA layer atop a bulk film allowed for local T_g measurements at the free surface of PMMA. Labeled PMMA layers of known h were floated onto the surface of a 240-nm-thick PMMA film supported on silica. The overall bilayer film thickness was sufficiently large that T_g(film) = T_g(bulk). The impact of the free surface on modifying T_g dynamics is opposite that of the silica substrate.

Figure 5-7 shows that T_g(free surface) – T_g(bulk) = - 7-8 K for a 12-nm-thick free-surface layer. When the thickness of the labeled free-surface layer is increased, the value of T_g(free surface) – T_g(bulk) gradually approaches zero at h = 40 nm. For purposes of comparison, the

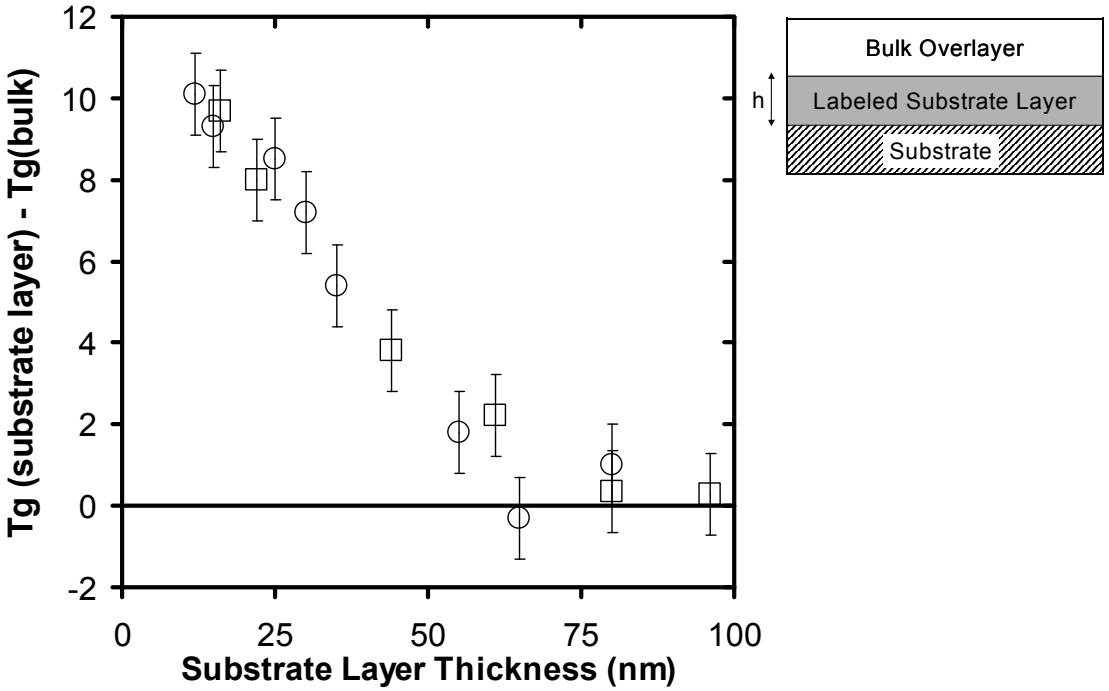

Figure 5-6: Direct measurement of substrate layer T_g values using a bilayer film geometry in which one layer is labeled with either pyrene (squares) or TC1 (circles). T_g(substrate layer) - T_g(bulk) of labeled substrate layer film as a function of the labeled substrate layer film thickness. Film thickness of bulk overlayer film is 240 nm. Film geometry used in experiments is also shown.

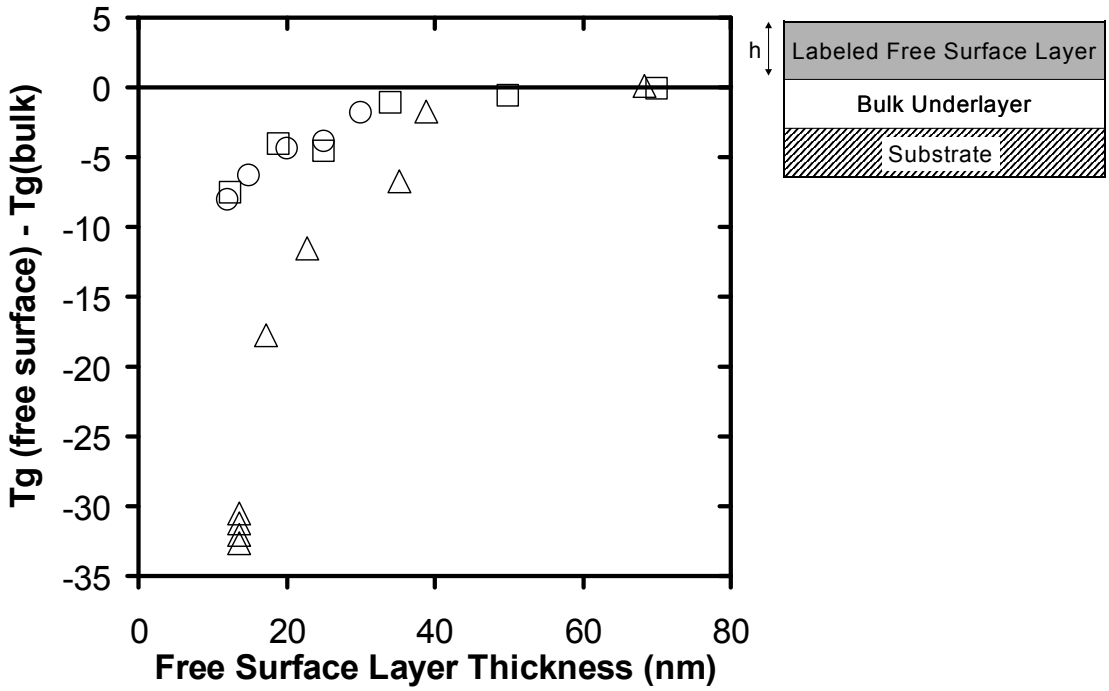

Figure 5-7: Direct measurement of free surface layer T_g values using a bilayer film geometry in which one layer is labeled with either pyrene (squares) or TC1 (circles). T_g(free surface) - T_g(bulk) of labeled free surface layer film as a function of the labeled free surface layer film thickness (h). Film thickness of bulk underlayer film is 240 nm. Film geometry used in experiments is also shown. PS data are taken from (Ellison 2003).

free surface layer T_g measurements of PS from Ellison and Torkelson (Ellison 2003) were replotted in Figure 5-7. As seen in Figure 5-7, the free-surface layer thicknesses at which PMMA and PS begin to exhibit reductions in T_g are approximately the same. However, the magnitude of the reduction in T_g at the free surface is much weaker in PMMA than in PS. These results demonstrate that the ability of a free surface to perturb T_g dynamics is strongly dependent on the chemical structure of the polymer. This observation is in accord with T_g measurements done on 40-nm-thick freely standing (two free surfaces) PMMA (Mn = 718,000 g/mol) and PS (Mn = 690,000 g/mol) films, for which the values of T_g were reduced by ~15 K and ~52 K, respectively, compared to T_g(bulk) (Roth 2003).

Regarding the effects of surfaces and interfaces on T_g shown in Figure 5-6 and Figure 5-7, the increase in T_g near the silica substrate is understood qualitatively to arise from hydrogen bonding interactions between the ester side groups of PMMA and the hydroxyl groups on the silica substrate. In the absence of hydrogen bonding interactions, as in the case of PS films supported on silica substrates, no change in T_g is expected or observed. In contrast, the underlying cause of the large difference in the magnitude of the free surface effects in PMMA and PS films is not yet understood even at a qualitative level. There is no molecular-scale mechanism or theory by which to explain the observations. Further study of the effect of repeat unit structure on perturbations to T_g at free surfaces of films is warranted. (Chapter 6 looks at the effect of chemical structure on the impact that surfaces and interfaces have on T_g of a series of poly(*n*-methacrylate)s.)

Employing a 12-nm-thick labeled middle layer, trilayer films were used to determine the length scale over which the free surface and substrate modify T_g dynamics within bulk PMMA

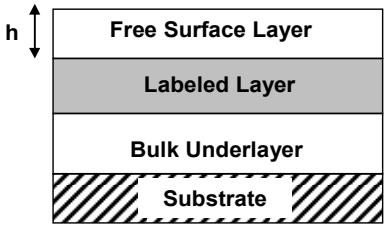

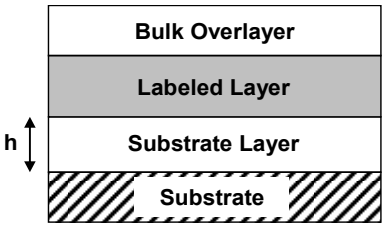

Surface Layer Thickness, h (nm)	Labeled Layer Depth (nm)	T_g (film) - T_g (bulk) (K)
8	8 - 20	-2
12	12 - 24	0

Substrate Layer Thickness, h (nm)	Labeled Layer Depth (nm)	T_g (film) - T_g (bulk) (K)
12	12 - 24	5
26	26 - 36	4
56	56 - 68	1

Figure 5-8: Determination of the distribution of T_gs as a function of depth displaced from either the free surface or the substrate-polymer interface using trilayer films in which the middle layer is labeled with either pyrene or TC1. Labeled middle layer is 12-nm-thick, while the bulk overlayer / underlayer film thickness is 240 nm.

films. As illustrated in Figure 5-8, when an 8-nm-thick unlabeled free-surface layer is placed on top of a 12-nm-thick labeled middle layer (meaning that the labeled-layer depth within the film is 8-20 nm), the T_g of the labeled layer is reduced by only 2 K compared to T_g(bulk). When the unlabeled free surface layer thickness is 12 nm, the labeled middle layer reports T_g(bulk). In the opposite case, when a 12-nm-thick labeled middle layer is displaced 12 nm from the substrate interface, its T_g is increased by 5 K compared to T_g(bulk). As shown in Figure 5-8, it is not until the labeled middle layer is displaced approximately 50-70 nm from the substrate interface that it reports a T_g value that is within experimental error equal to T_g(bulk).

These experiments demonstrate several key points. First, there is a distribution of T_gs near the free surface and substrate interface of bulk PMMA films supported on silica substrates. Second, the results disallow the concept of two- and three-layer models to explain the T_g-confinement effect (Keddie 1994a; Forrest 2000) and instead imply that a distribution of T_gs should be incorporated into any model being used to explain T_g-confinement behavior (Ellison 2003). Third, the length scale over which the substrate interactions modify T_g dynamics within a bulk PMMA film is greater than that associated with free surface effects, consistent with the notion that perturbations to T_g caused by substrate effects are stronger than those caused by free-surface effects for PMMA supported on silica.

Figure 5-9 allows us to quantify the relative strengths of the competing free surface and substrate effects and the length scales over which the stronger substrate effects modify T_g dynamics in confined PMMA films. Specifically, the impact of the substrate on the T_g of a 12-nm-thick labeled free-surface layer is measured as a function of overall film thickness (h'). The length scale separating the 12-nm-thick free-surface layer from the substrate is adjusted by

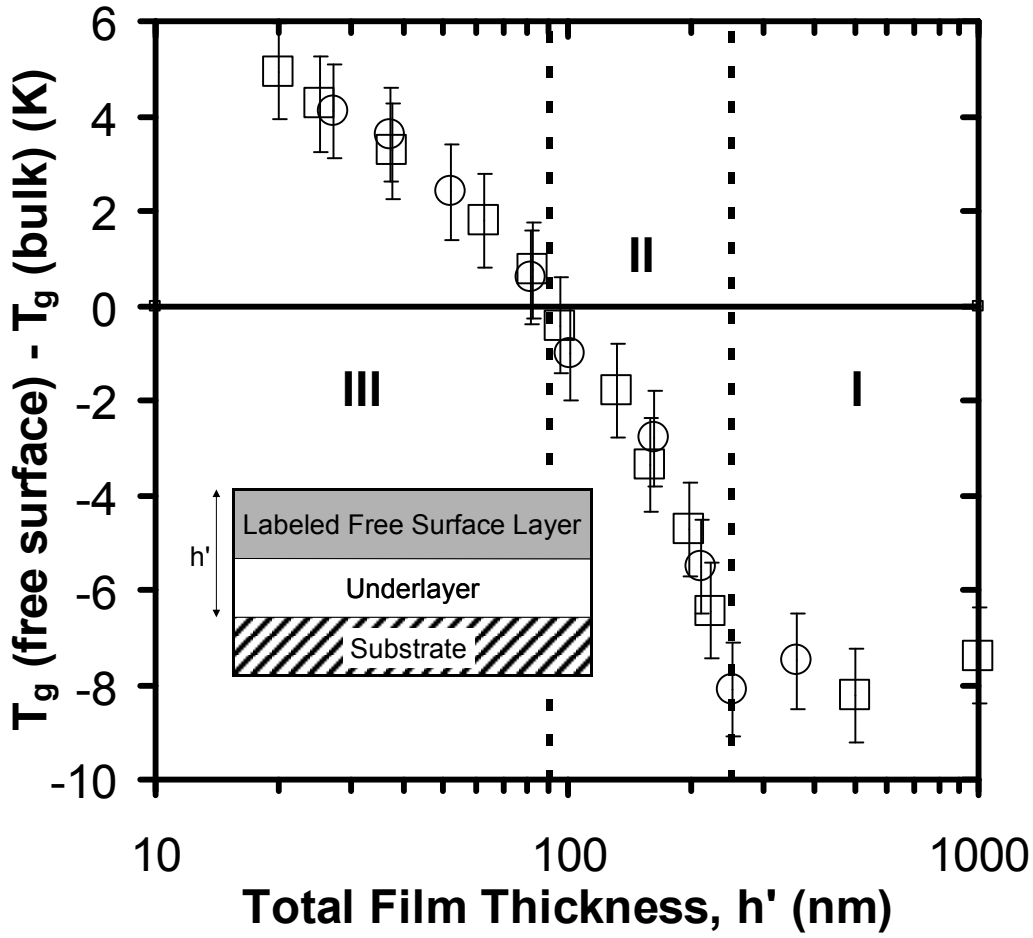

Figure 5-9: T_g(free surface) - T_g(bulk) of pyrene-labeled (squares) or TC1-labeled (circles) PMMA free-surface layer as a function of overall film thickness (*h'*). The labeled free-surface layer thickness is held constant at 12 nm while the underlayer thickness is varied.

controlling the underlayer thickness. As shown in Figure 5-9, when $h' > 250$ nm (**I**), the T_g within the free-surface layer is reduced by 7-8 K from T_g(bulk). At these thicknesses, the free-surface T_g dynamics are unaffected by the increased T_g at the polymer-substrate interface. When 90 nm $< h' <$ 250 nm (**II**), the free-surface layer T_g increases with decreasing h' but remains below T_g(bulk). At these thicknesses, the effects of the strongly reduced cooperative segmental mobility at the polymer-substrate interface percolate across the film, increasing the free-surface layer T_g. When $h' < 90$ nm (**III**), the T_g within the free-surface layer actually exceeds T_g(bulk) and continues to increase with decreasing h'; this means that the perturbed T_g dynamics at the substrate that percolate across the film are sufficiently strong within the free-surface layer to dominate the perturbations to T_g caused by the free surface. Thus, under certain circumstances of confinement with attractive polymer-substrate interactions, the T_g of an ultrathin free-surface layer may exceed T_g(bulk).

Figure 5-10 illustrates the effect of overall film thickness on T_g(substrate layer) – T_g(bulk) of a 12-nm-thick substrate layer within a PMMA bilayer film. When the overall film thickness is 250-260 nm, T_g(substrate layer) – T_g(bulk) = 9-10 K. As shown in Figure 5-10, decreasing the overall thickness results in a decrease in the substrate layer T_g. When the overall thickness of the bilayer film is reduced to 50-60 nm, T_g(substrate layer) – T_g(bulk) = 7 K. Further reduction of the overall thickness to 35-40 nm leads to T_g(substrate layer) – T_g(bulk) = 3-4 K.

According to Figure 5-9 and Figure 5-10, when the overall bilayer film thickness exceeds 250 nm, T_g(free surface) – T_g(bulk) = - 7-8 K for a 12-nm-thick free-surface layer and T_g(substrate layer) – T_g(bulk) = 9-10 K for a 12-nm-thick substrate layer. The difference

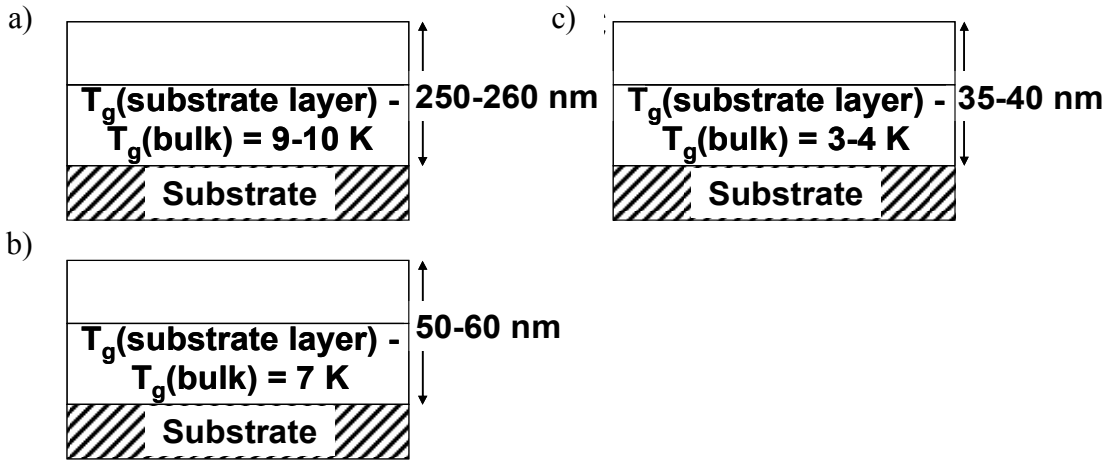

Figure 5-10: Influence of overall film thickness on T_g(substrate layer) - T_g(bulk) of a 12-nm-thick substrate layer within a bilayer film. The overall film thickness is a) 250-260 nm, b) 50-60 nm, and c) 35-40 nm.

between the T_gs at the free surface and substrate is 16-18 K. When the overall bilayer film thickness is reduced to 35-40 nm, T_g(free surface) – T_g(bulk) = 3-4 K for a 12-nm-thick free-surface layer as well as for a 12-nm-thick substrate layer. The difference between the T_gs at the free surface and substrate is 0 K. We also note that in 35- to 40-nm-thick bilayer films, the T_g*s* of the free surface and substrate layers are identical within experimental error to the T_g of a 35- to 40-nm-thick single layer PMMA film (see Figure 5-5). Thus, with increasing nanoscale confinement, the gradient in T_g across a PMMA film is reduced and, within the experimental uncertainty of the multilayer method, can be eliminated under circumstances of extreme confinement. The observation that confinement leads to a reduction in the gradient in T_g across a PMMA film is consistent with similar measurements conducted on PS films (Ellison 2003). The results associated with both PS and PMMA films indicate that below a certain overall thickness the T_g dynamics adjust to satisfy the constraint that the gradient in T_g dynamics across an ultrathin polymer film cannot be too sharp and abrupt (Ellison 2003).

A comparison of Figure 5-5 and Figure 5-6 reveals that T_g(film) – T_g(bulk) = 6 K for a 50-nm-thick single layer PMMA film and T_g(substrate layer) – T_g(bulk) = 2 K for a 50-nm-thick substrate layer in a bulk bilayer PMMA film. This indicates that placing a layer with bulk T_g dynamics over a 50-nm-thick substrate layer can lead to faster cooperative dynamics and a lower T_g in the substrate layer. The observation that the T_g dynamics of a layer are affected by the dynamics of an adjacent layer have been previously reported for PS films (Ellison 2003). For example, the T_g of a 14-nm-thick labeled PS free surface layer in a bulk bilayer film is approximately 5 K higher than the T_g of a 14-nm-thick single layer film. This indicates that placing a PS layer with average bulk T_g dynamics underneath a 14-nm-thick polysytrene layer

results in slower cooperative dynamics and a higher T_g in the free surface layer.

This latter observation has recently been explained in the context of the coupling model (Ngai 2006), which recognizes the importance of many molecule or many segment relaxation dynamics associated with the glass transition. The placement of a bulk layer with slower dynamics underneath a 14-nm-thick surface layer imposes intersegmental constraints on the surface layer. This constraint results in slower dynamics and a higher T_g in the 14-nm-thick free-surface layer than in the 14-nm-thick film (Ngai 2006). A similar explanation can be given for some of the PMMA results. Placement of a layer with bulk T_g dynamics atop a 50-nm-thick substrate layer imposes intersegmental interactions on the substrate layer, resulting in faster dynamics and a lower T_g. However, we note that $T_g - T_g(\text{bulk}) = 9$ K for both a 20-nm-thick single layer film and a 20-nm-thick substrate layer in a bulk bilayer film. Thus, for a 20-nm-thick film in which it is possible for most of the PMMA chains to be pinned at the substrate interface (Baschnagel 2003) via hydrogen bonds, placing a thick layer atop it has no measurable impact on its T_g. This means that the substrate effects are strong enough to dominate the effects of intersegmental constraints imposed by the bulk overlayer film.

The results reported in Figures 5-5, 5-6, 5-7, and 5-8 can occur only if perturbations caused by surfaces or interfaces to T_g dynamics propagate many layers of CRRs within the films. That is, if on average the cooperative dynamics in a layer are perturbed substantially relative to bulk, then, on average, many adjoining layers must also have their dynamics perturbed, albeit to lesser extents. This idea is consistent with simulations (Donati 1998; Glotzer 2000) and experiments (Weeks 2000; Ellison 2003) indicating that glass formers do not typically have abrupt transitions in neighboring regions of local dynamic heterogeneity from very fast dynamics

to slow dynamics and is consistent with dielectric noise studies (Russell 2000) suggesting that a minimum length scale (> 40 nm) is required to obtain the full breadth of the distribution of cooperative relaxation dynamics in polymers near T_g.

From a scientific point of view, the results in Figures 5-5, 5-6, 5-7, and 5-8 associated with T_g behavior that is strongly perturbed by interfacial effects stand in opposition to the simple definition of a CRR offered more than forty years ago (Adams 1965) in which configurational changes within a CRR are assumed to occur independently of neighboring CRRs. Instead, the results highlight the long-range effects of substrate interactions on T_g dynamics and are qualitatively consistent with recent models (Long 2001; Merabia 2004) and simulations (Baljon 2004) suggesting that percolation of slow-relaxing regions associated with attractive polymer-substrate interactions can explain enhancements in average T_gs in confined films.

5.4 Conclusions

The study in this chapter employed an innovative fluorescence/multilayer method to investigate the impact of confinement and interfacial effects on the T_g of PMMA films supported on silica substrates. With single layer PMMA films that were less than 90-nm-thick, T_g increased roughly linearly with decreasing logarithmic thickness. The use of bilayer films revealed that compared to T_g(bulk), T_g was reduced at the free surface by 7-8 K for a 12-nm-thick free surface layer and increased at the substrate interface by 10 K for a 12-nm-thick substrate layer of a bulk film, resulting in a T_g-gradient across the film. Measurements of confined bilayer films revealed that the stronger substrate effects percolate across the film to modify the T_g dynamics at the free surface. Thus, with nanoconfinement, the stronger substrate effects dominate the free surface effects, providing an explanation for the increase in average T_g

with decreasing single layer PMMA film thickness. With extreme confinement, the T_g gradient across the film thickness was suppressed, with both substrate layer and free surface layer T_g*s* exceeding T_g(bulk). These results demonstrate that strongly perturbed T_g dynamics at the interfaces propagate across many layers of CRRs within the films, meaning that configurational changes associated with cooperative segmental dynamics within a CRR do not occur independently of neighboring CRRs. Thus, insight into the fundamental nature of the glass transition may be gained by measuring the nanoscale distributions of T_gs in confined polymers.

6 EFFECTS OF NANOSCALE CONFINEMENT AND INTERFACES ON THE GLASS TRANSITION TEMPERATURE OF A SERIES OF POLY(N-METHACRYLATE) FILMS

6.1 Introduction

It is now known that the chemical structure of a polymer can have a dramatic impact on the effect of nanoscale confinement on T_g of freely-standing films (Roth 2003) and supported films (Ellison 2005). In 2003, Roth and Dutcher (Roth 2003) observed that the T_g of a 40-nm-thick freely-standing poly(methyl methacrylate) (PMMA) films was reduced by approximately 15 K compared to T_g(bulk) while the T_g of a 40-nm-thick freely-standing polystyrene (PS) film was reduced by approximately 52 K compared to T_g(bulk). In a follow up study, Roth and Dutcher ruled out surface tension effects and polarity differences between PMMA and PS as the reason for the difference in the T_g-nanoconfinement effect between the two polymers (Roth 2006). Instead they suggested that the difference in the magnitude of the reduction in T_g for PMMA and PS freely-standing films compared to T_g(bulk) may be related to PMMA having a strong β process and PS having a weak β process. However, no experimental evidence exists to support the claim, and a qualitative reason for the difference in the magnitude of the reduction in T_g for PMMA and PS freely-standing films compared to T_g(bulk) remains elusive.

In 2005, Ellison, Mundra, and Torkelson (Ellison 2005) investigated the impact of slight

modifications to the repeat unit structure of PS on the T_g-confinement effect observed in films supported on silica. In addition to polystyrene (PS), they studied two other systems, including poly(4-methylstyrene) (P4MS) and poly(*tert*-butylstyrene) (PTBS), none of which exhibits any significant attractive interaction with hydroxyl groups on the surface of the silica substrate; this means that all T_g-confinement effects originate at the free surfaces of PS, P4MS, and PTBS films. They observed that the T_g reductions in the ultrathin films increased dramatically with the presence of large, rigid side groups on the phenyl ring. In the case of 25-nm-thick films supported on silica, they obtained the following reductions in T_g relative to bulk T_g: approximately 12 K for PS, approximately 18 K for P4MS, and approximately 47 K for PTBS (Ellison 2005). In addition, the onset thickness for the T_g reduction in PTBS was 300-400 nm, much larger than in PS or P4MS, where the onset thickness for the T_g reductions was approximately 60 nm (Ellison 2005). The results indicated that small changes to the repeat unit structure of the polymer, presumably leading to changes in the packing efficiency of the polymer repeat units and thereby the effective chain stiffness, can lead to substantial tunability in the T_g-confinement effect.

This chapter investigates how the T_g-confinement effect is impacted by slight variations to the side groups of poly(n-methacrylate) films supported on silica, which exhibit both free-surface effects and attractive polymer-substrate interactions. Fluorescence is used to determine T_g values in single-layer films and in bilayer films in which only one layer has polymer labeled with a fluorescence probe. The latter experiments allow us to measure directly the local T_gs in ultrathin free-surface layers and substrate layers. The polymers used in this study include PMMA, poly(ethyl methacrylate) (PEMA), poly(propyl methacrylate) (PPMA), and poly(*iso*-

butyl methacrylate) (PIBMA).

6.2 Experimental

Three unlabeled polymers, PMMA, PEMA, and PIBMA, were synthesized at 70 ^{o}C by bulk free radical polymerization using benzoyl peroxide (Aldrich) as initiator. The synthesis of the probe 4-tricyanovinyl-[N-(2-hydroxyethyl)-N-ethyl]aniline (TC1) and 1-pyrenyl butanol-labeled and TC1-labeled methacrylate monomers was described in Chapter 5.

Probe-labeled versions of PMMA, PEMA, PPMA, and PIBMA were synthesized by bulk free radical polymerization of methyl methacrylate (Aldrich), ethyl methacrylate (Aldrich), propyl methacrylate (Aldrich), and *iso*-butyl methacrylate (Aldrich), respectively, in the presence of trace amounts of pyrene-labeled or TC1-labeled methacrylate monomer. All probe-labeled polymers were washed by dissolving in toluene (Fisher) and precipitating in methanol (Fisher) at least five times to remove residual unreacted labeled monomer and then dried in a vacuum oven at T_g + 15 K for 24 hr. Table 6-1 lists the number average molecular weight (M_n) values, polydispersity indexes (M_w /M_n), bulk T_gs, and label content of the poly(n-methacrylate) samples, and Figure 6-1 shows the repeat unit structures.

The bulk T_g of each polymer was determined using a Mettler-Toledo 822 DSC. Sample masses of 5-10 mg were placed in sealed aluminum pans with a pinhole in the top to allow measurements to be conducted in a nitrogen environment. The T_gs were determined on heating at 10 K/min after annealing the samples at 423 K to erase the prior thermal history. The reported T_gs are onset values.

The M_n value and polydispersity index of each polymer were determined using a Waters Breeze gel permeation chromatograph equipped with refractive index and fluorescence detectors.

Table 6-1: Molecular characterization and bulk T_gs of polymers used in this study.

Material	M_n (g/mol)	M_w/M_n	*Bulk* T_g (K) (onset, DSC)	*Bulk* T_g (K) (fluorescence)	Label Content (mol %)
PMMA	355000[#]	1.54[#]	394	-	-
PEMA	460000[+]	1.70[+]	348	-	-
PIBMA	300000[+]	2.00[+]	337	-	-
TC1-labeled PMMA	509000[#]	1.67[#]	394	395	1.4
Pyrene-labeled PEMA	202000[+]	1.80[+]	348	347	0.6
Pyrene-labeled PPMA	188000[+]	1.78[+]	320	320	0.3
TC1-labeled PIBMA	181000[+]	1.96[+]	337	339	0.6

[#] Determined via gel permeation chromatography using the universal calibration method and appropriate Mark-Houwink parameters.

[+] Determined via gel permeation chromatography relative to PS standards using tetrahydrofuran as eluent.

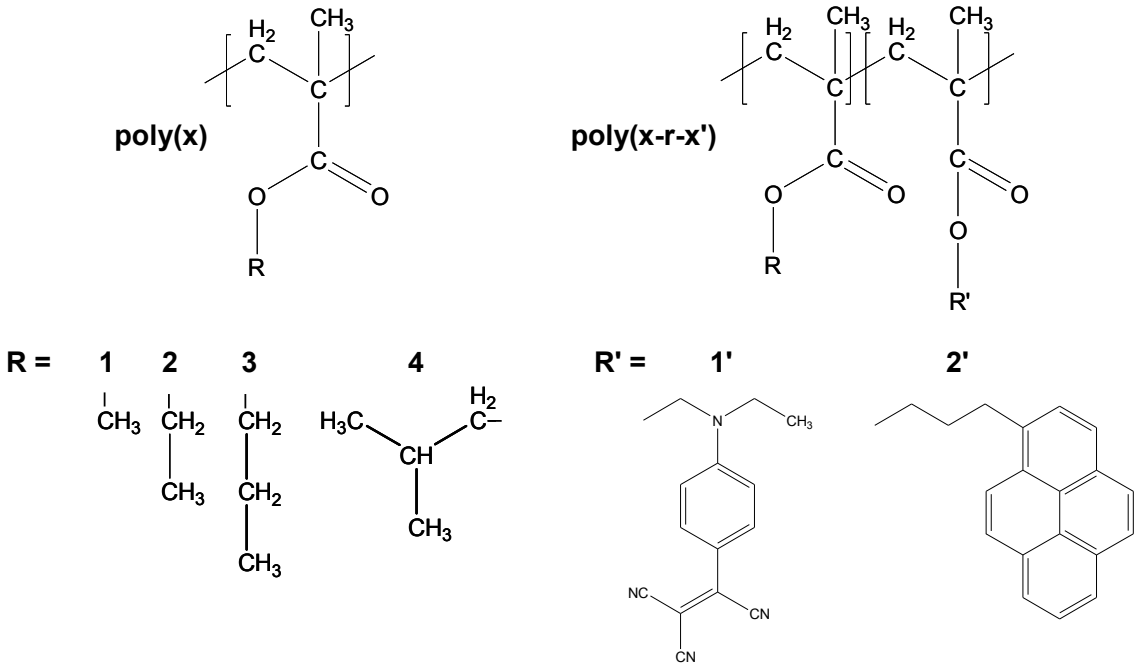

Neat Polymers:
poly(1) = PMMA
poly(2) = PEMA
poly(4) = PIBMA

Labeled Polymers:
poly(1-r-1') = TC1-labeled PMMA
poly(2-r-2') = Pyrene-labeled PEMA
poly(3-r-2') = Pyrene-labeled PPMA
poly(4-r-1') = TC1-labeled PIBMA

Figure 6-1: Structures of polymers used in the present study.

Molecular weight values were determined relative to PS standards or universal calibration using the appropriate Mark-Houwink constants. Tetrahydrofuran was used as the eluent at 30 ^{o}C.

The label content of each labeled polymer was determined using a Perkin-Elmer Lambda 35 UV-Vis absorbance spectrophotometer. Probe-labeled polymer was dissolved in chloroform at a known concentration, and the absorbance spectrum of the solution was measured. Using wavelengths at which only the probe contributes to the absorbance spectrum, the concentration of the probe in the solution, and thereby the label content in the labeled polymer, can be determined using the Beer-Lambert law with measured extinction coefficients for the TC1-labeled monomer and pyrene-labeled monomer. (The technique assumes that the probe attached to the polymer has the same extinction coefficient at its absorbance maximum as the probe-labeled monomer even though the absorbance spectrum of the probe attached to the polymer is shifted by a few nanometers compared to the probe-labeled monomer. The extinction coefficient for each probe-labeled monomer was determined from absorbance measurements taken from solutions containing varying amounts of probe-labeled monomer. The extinction coefficient is the slope of a plot of absorbance vs. concentration.) The label contents were as follows: 1.4 mole% and 0.6 mole% TC1-labeled monomer in PMMA and PIBMA, respectively, and 0.6 mole% and 0.3 mole% pyrene-labeled monomer in PEMA and PPMA, respectively.

Single layer films were prepared by spin casting polymer/toluene solutions onto silica slides using solution concentrations ranging from 0.5 wt% to 4.0 wt% and spin speeds ranging from 100-4000 rpm. The films were allowed to dry in vacuum at T_g + 5 K for 8 hr. Bilayer films were prepared by a water transfer technique that was described in Chapter 5. Film thicknesses were measured with a Tencor P10 profilmeter using an average of at least ten

measurements.

All polymers were of sufficiently high molecular weight to ensure that interlayer diffusion occurred over at most several nanometers during the experimental measurement time, which includes the time to create a consolidated film. Estimation of interlayer diffusion of similar bilayer films was described in Chapter 5.

Steady-state fluorescence emission spectra were measured as a function of temperature (on cooling) using a Photon Technology International fluorimeter or a SPEX Fluorog-2 DM1B fluorimeter with 5 nm bandpass excitation and emission slits used for pyrene-labeled polymer and 12 nm bandpass excitation and emission slits used for TC1-labeled polymer. Excitation wavelengths of 254 nm and 480 nm were used for pyrene-labeled and TC1-labeled polymers, respectively, where there were maxima in absorbance. The emission spectra of pyrene-labeled and TC1-labeled polymers were measured at 360-460 nm and 540-690 nm, respectively. The T_gs of films were determined by fitting the temperature dependence of the integrated fluorescence intensity to linear correlations in both the rubbery and glassy states. In fitting the data to linear correlations, only data well away from T_g were used in the fitting procedure. Additional information on this protocol to determine T_g can be found in Chapter 5 and referemces (Ellison 2002b; Roth 2007b).

6.3 Results and Discussion

Figure 6-2 shows the fluorescence emission spectrum of a pyrene-labeled PEMA film supported on silica as a function of temperature, which consists solely of fluorescence from isolated excited-state pyrenyl units, which is called monomer fluorescence. (When two pyrenyl probes are separated from each other by a several Angstrom distance, it is possible to observe

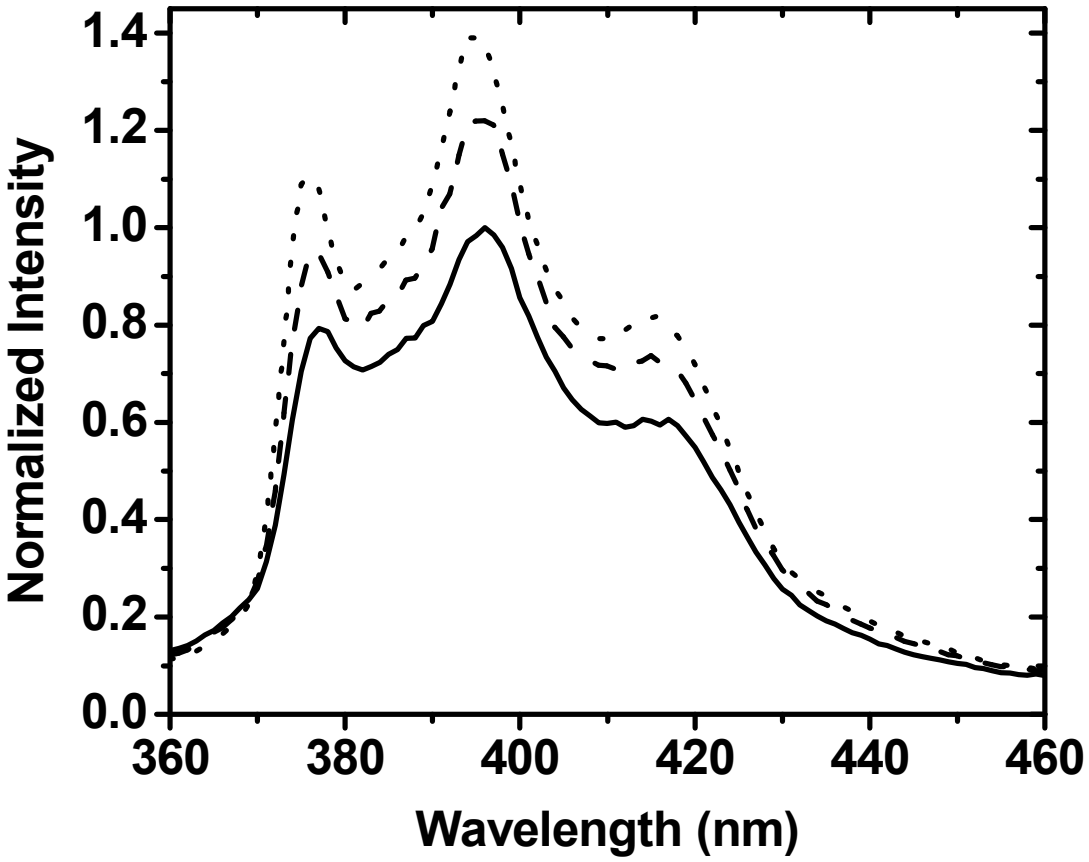

Figure 6-2: Temperature dependence of the fluorescence emission spectrum of a 500-nm-thick pyrene-labeled PEMA film supported on silica: 383 K (solid curve), 348 K (dashed curve), and 308 K (dotted curve). Data have been normalized to one at the maximum peak value at 383 K.

excimer fluorescence or fluorescence from an excited-state dimer, which is a broad, structureless emission centered with a maximum intensity at 480-490 nm (Kim 2002). Such fluorescence is absent in the film measurements done in the current study, indicating that, within error, all pyrenyl probe fluorescence is from single pyrene probes isolated in the polymer matrix.) A decrease in temperature yields an increase in fluorescence intensity. The increase in intensity results because a reduction in temperature leads to reduced thermal energy and densification of the nanoscale medium surrounding the probe, both of which reduce the rate of nonradiative decay from the excited state of the pyrene probe. An increase in intensity with decreasing temperature in the other pyrene-labeled and TC1-labeled polymers used in this study is also observed.

Figure 6-3 shows the temperature dependence of the normalized integrated fluorescence intensity of thin and ultrathin, single-layer pyrene-labeled PEMA and TC1-labeled PIBMA films. The intersection of linear correlations fit to data points deep in the rubbery state and glassy state provides a measure of T_g. There is an interesting difference in fluorescence of pyrene-labeled and TC1-labeled polymers, with pyrene fluorescence yielding a greater temperature dependence in the rubbery state above T_g and TC1 fluorescence yielding a greater temperature dependence in the glassy state below T_g. This difference is related to the different mechanisms by which each probe undergoes nonradiative decay from its excited state and is explained in Chapter 5. Nevertheless, both probes report T_gs for bulk polymers that are in good agreement with T_g values obtained by classic techniques such as differential scanning calorimetry.

Figure 6-3 illustrates that nanoscale confinement leads to a decrease in the T_g of PEMA. The T_g values of the 500-nm-thick and 20-nm-thick pyrene-labeled PEMA films are 347 K and

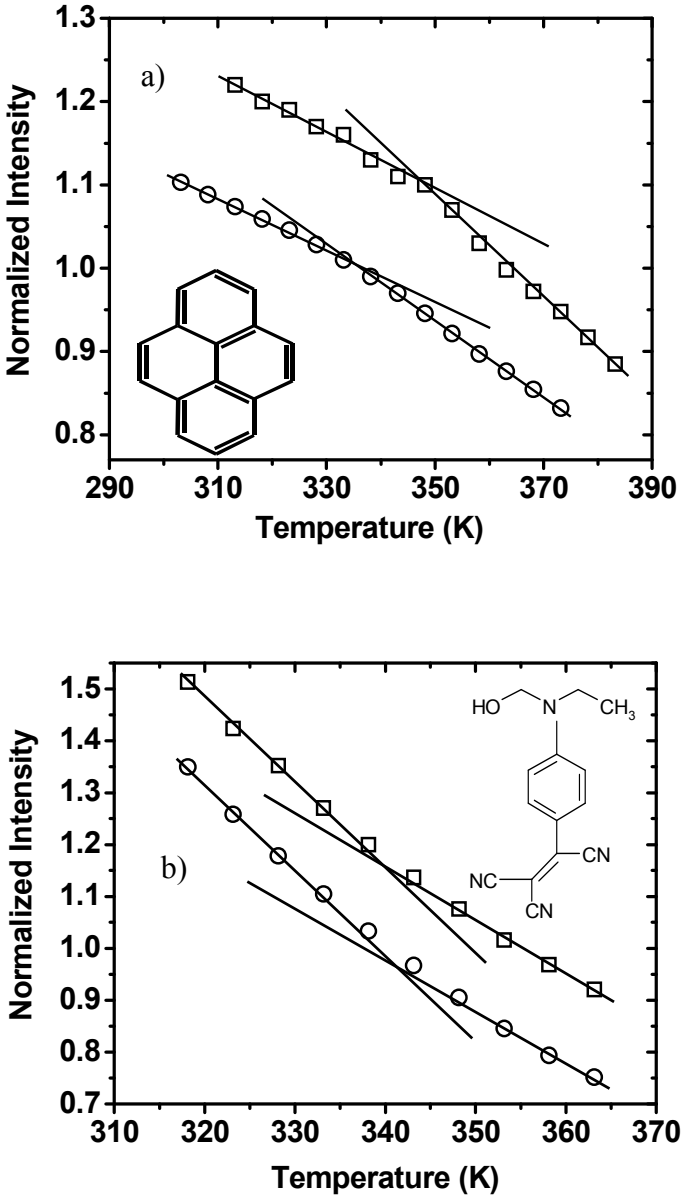

Figure 6-3: a) Temperature dependence of integrated fluorescence intensity of 500-nm-thick (squares) and 20-nm-thick (circles) pyrene-labeled PEMA films. Data have been normalized to T_g and arbitrarily shifted vertically for clarity. Inset shows the structure of pyrene. b) Temperature dependence of integrated fluorescence intensity of 500-nm-thick (squares) and 20-nm-thick (circles) TC1-labeled PIBMA films. Data have been normalized to T_g and arbitrarily shifted vertically for clarity. Inset shows the structure of TC1.

336 K, respectively. In addition, Figure 6-3 shows that nanoscale confinement leads to no change within experimental error (+/- 1 K) in the T_g of PIBMA. The T_g values of the 500-nm-thick and 20-nm-thick TC1-labeled PIBMA films are 339 K and 341 K, respectively. Related measurements of T_g were also obtained in thin and ultrathin PMMA and PPMA films.

Figure 6-4 shows the thickness dependence of the deviation of T_g from bulk T_g for single-layer films of PMMA, PIBMA, PEMA, and PPMA supported on silica. Figure 6-4 reveals that slight modifications to the repeat unit structure of a series of poly(n-methacrylate)s can have a profound impact on how confinement to thicknesses less than 100 nm affects T_g. (Little change, in the case of PPMA, or no change, in the case of PMMA, PIBMA, and PEMA, in T_g is observed as a function of thickness for films with thickness exceeding 100 nm. This is because the perturbations to the T_g response caused by the polymer-air and polymer-substrate interfaces are too small to modify the average T_g response across films that are thicker than 100 nm.) For TC1-labeled PMMA, the increase in T_g with confinement is consistent with previous studies of single layer PMMA films supported on silica (Keddie 1994b; Fryer 2001; Mundra 2007c). The increase in T_g with confinement has been related to attractive hydrogen bonding interactions between the ester side groups of PMMA and the hydroxyl groups on silica that reduce segmental mobility at the substrate interface (Keddie 1994b; Fryer 2001). Changing the side unit off the ester group of PMMA from a methyl unit to an ethyl (PEMA) or propyl (PPMA) unit leads to an opposite effect of confinement on T_g, with T_g decreasing from its bulk value by 11 K in a 20-nm-thick PEMA film and by 17 K in a 30-nm-thick PPMA film. Changing the methyl unit off the ester group of PMMA to an *iso*-butyl unit (PIBMA) leads to a T_g that is, within error, independent of confinement down to a film thickness of 14 nm.

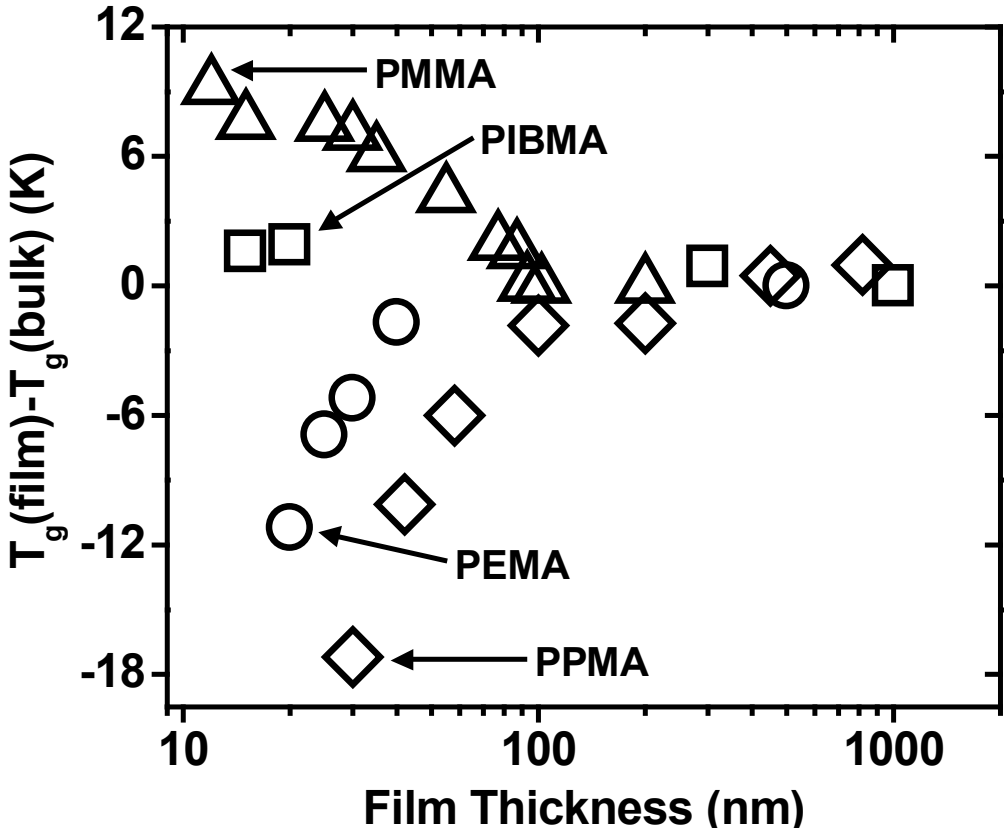

Figure 6-4: Deviation of T_g from bulk T_g as a function of film thickness for TC1-labeled PMMA (triangles), TC1-labeled PIBMA (squares), pyrene-labeled PEMA (circles), and pyrene-labeled PPMA (diamonds) films.

Why do these small modifications to the repeat unit structure have such an enormous impact on how confinement affects T_g in this series of poly(n-methacrylates)? From a comparison of data presented in Chapter 5 and a study by Ellison and Torkelson (Ellison 2003) on the distributions of T_gs for PMMA and PS, respectively, it is known that the free surface and substrate interfaces affect T_g differently in different polymers (Ellison 2003). Here a bilayer fluorescence method is used to investigate directly the local T_gs in the free surface and substrate interface layers of the series of poly(n-methacrylate)s.

Bilayer films consist of a probe-labeled poly(n-methacrylate) layer and an unlabeled poly(n-methacrylate) layer. Bilayer films are constructed in such a manner that an ultrathin labeled layer can be placed at either the free surface or substrate interface. Heating the bilayer films for a short time above T_g produces a consolidated film with only the labeled layer contributing to the fluorescence signal.

Figure 6-5 shows the results of the bilayer film measurements for PMMA, PEMA, and PIBMA where the films are sufficiently thick to yield bulk T_g values if measured as single layer films. In all cases, there is a reduction in T_g at the 12- or 14-nm-thick free surface layers, qualitatively consistent with previous studies (Keddie 1994a; Forrest 1996; Ellison 2003; Sharp 2003a; Papaleo 2006; Svanberg 2007) of how the presence of a free surface perturbs the local T_g. In all cases, there is an increase in T_g at the polymer substrate interface, consistent with expectations for polymers that can undergo hydrogen bonding with hydroxyl groups naturally on the surface of the silica substrates. However, the magnitude of the deviations in T_g at the interfaces depends strongly on chemical structure. For PMMA, the 12-nm-thick substrate layer has a T_g enhanced by 10 K compared to the bulk T_g, while for PEMA and PIBMA the 14-nm-

thick substrate layers have T_gs enhanced by only 5 K compared to the bulk T_gs. The 14-nm-thick free-surface layer of PEMA has a T_g reduced by 14 K compared to its bulk T_g. In contrast, the T_g reductions are only 7 K and 6 K in 12-nm-thick PMMA and 14-nm-thick PIBMA free-surface layers, respectively.

A comparison of Figures 6-4 and 6-5 reveals a correlation between the observed deviations in T_g with confinement for the single layer films (Figure 6-4) and the relative strength of the deviations in T_g in the free surface and substrate interface layers (Figure 6-5) of the poly(n-methacrylate) films. When substrate effects are stronger than free surface effects (as quantified by a greater T_g deviation in the substrate layer than in the free surface layer), the T_gs of single layer films increase with confinement as observed with PMMA films. When free surface effects are stronger than substrate effects, as in the case for PEMA, the T_gs of single layer films decrease with confinement. When free surface and substrate effects are of nearly equal strength, as in case of PIBMA, the T_gs of single-layer films are invariant with confinement.

Regarding the effects of the substrate and free surface on the T_gs of the poly(n-methacrylate) layers shown in Figure 6-5, the increase in T_g in the layer next to the silica substrate is understood qualitatively to arise from hydrogen bonding interactions between the ester groups of the poly(n-methacrylate)s and the hydroxyl groups on the silica surface while the reduction in T_g in the free surface layer is related to how the free surface reduces the requirement for cooperative segmental mobility. PMMA, which has the smallest alkyl side group of the series of poly(n-methacrylate)s studied, exhibits the greatest substrate effect. This is likely because the small methyl units off the ester side groups in PMMA are relatively ineffective relative to the larger ethyl and *iso*-butyl units of PEMA and PIBMA, respectively, in impeding

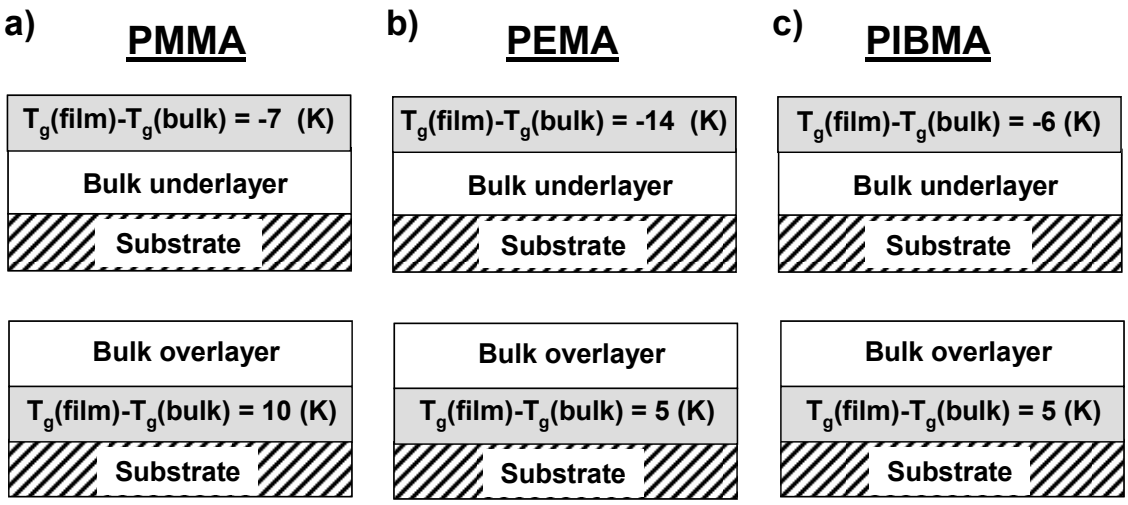

Figure 6-5: Deviation of T_g from bulk T_g in ultrathin free-surface and substrate layers in bilayer films. a) 12-nm-thick TC1-labeled PMMA layer placed at the free surface and substrate interface of PMMA bilayer films. Film thicknesses of bulk overlayer and bulk underlayer are 240 nm. b) 14-nm-thick pyrene-labeled PEMA layer placed at the free surface and substrate interface of PEMA bilayer films. Film thicknesses of bulk overlayer and bulk underlayer are 500 nm. c) 14-nm-thick TC1-labeled PIBMA layer placed at the free surface and substrate interface of PIBMA bilayer films. Film thicknesses of bulk overlayer and bulk underlayer are 500 nm.

hydrogen bonding between the oxygen atoms on the ester side groups and hydroxyl units on the surface of the silica. The detailed cause of the substantially larger effect in the free surface layer of PEMA relative to the effects observed in PMMA and PIBMA is not yet known. However, it likely relates to how the chemical structure of PEMA better supports a strong free-surface effect, with its perturbation of T_g dynamics via a reduction of the requirement for cooperativity at the polymer-air interface. Further experimental, theoretical, and simulation studies are warranted to provide an understanding regarding why the perturbations to T_g at free surfaces are strongly dependent on chemical structure.

6.4 Conclusions

Fluorescence spectroscopy was used to determine the effects of confinement and interfaces on the T_gs and their distributions in PMMA, PEMA, PPMA, and PIBMA films supported on silica. The average T_g across thin and ultrathin films of PIBMA was invariant with confinement, while that of PMMA increased with confinement and those of PEMA and PPMA decreased with confinement. The relative roles of perturbations to the T_g by free surfaces and polymer-substrate interfaces in the presence of hydrogen bonding interactions were determined by a series of bilayer fluorescence experiments. In all cases, reductions in T_g relative to bulk T_g are observed in ultrathin free surface layers while increases in T_g relative to bulk T_g are observed in ultrathin substrate-interface layers. The effects of confinement of the average T_g across single layer films were fully consistent with observed relative strengths of the perturbations caused by free surfaces and polymer-substrate interfaces. When the free surface effect is greater, as in the case of PEMA, the average T_g across a film decreased with nanoscale confinement. When the substrate effect is greater, as in the case of PMMA, the average T_g across a film increased with

nanoscale confinement. When the effects of the substrate and free surface in perturbing T_g are nearly equal, as in the case of PIBMA, within error the average T_g across a film is independent of nanoscale confinement.

PART III: α-RELAXATION DYNAMICS MEASUREMENTS

7 GLASS TRANSITION AND ALHPA-RELAXATION DYNAMICS OF THIN POLYSYTRENE FILMS LABELED WITH A MOLECULAR DIPOLE

7.1 Introduction

The dynamics of thin polymer films have been investigated by many experimental methods such as dynamic light scattering (Forrest 2000), dielectric relaxation spectroscopy (Fukao 1999; Fukao 2000; Fukao 2001b; Hartmann 2002; Wubbenhorst 2002; Serghai 2003; Lupascu 2006; Svanberg 2007), dynamic mechanical measurements (Akabori 2005), and second harmonic generation (SHG) measurements (Hall 1997b). In accordance with the decrease in T_g, the dynamics of the α-process, which are due to the cooperative segmental motions and are directly associated with the glass transition, become faster with decreasing film thickness. Fukao and Miyamoto (Fukao 1999) were the first to use dielectric relaxation spectroscopy (DRS) to investigate the relaxation dynamics of thin polymer films. They applied DRS to the investigation of the dynamics of ultrathin polymer films and provided information about the relaxation dynamics of the α process, the β process and the normal mode in the case of polystyrene (PS), poly(vinyl acetate) (PVAC), poly(methyl methacrylate) (PMMA), and cis-poly(isoprene). Although the glass transition and dynamics of thin films of PS have been investigated intensively, it is very difficult to obtain the dielectric loss signal of the α process due to the very low polarity of PS.

The above studies on the dynamics of thin polymer films are mainly related to the average T_g and the average relaxation time of the α process. Based on results presented in Chapter 5 and work by Ellison and Torkelson (Ellison 2003), it is expected that there exists a distribution or a positional dependence of the relaxation time of the α process within polymer thin films, especially thin supported films. However, the above assertion has never been tested since no method has been developed in which only one layer of a multilayer film is dielectrically active.

There are several studies in the literature (Hains 1975; Dionisio 1994; Berg 2005) that have established that the incorporation of guest dipoles into a nonpolar polymer is a useful method to enhance its dielectric strength. In this chapter, the relaxation dynamics of single layer films of polystyrene labeled with a nonlinear optical probe 4-[N-ethyl-N-(hydroyethyl)]amino-4-nitroazobenzene (Disperse Red 1, DR1) are investigated and compared with those for unlabeled polystyrene in order to provide rationale the possibility of position dependent measurements of the α-relaxation dynamics for a multilayer film.

7.2 Experimental

Polystyrene labeled at a low level with a nonlinear optical probe DR1 is used (DR1-labeled PS). The molecular structure of DR1 is shown in the inset of Figure 7-1. Disperse Red 1-labeled PS is a random copolymer of neat styrene monomer and DR1-labeled monomer synthesized following a procedure outlined by Dhinojwala *et al*. (Dhinojwala 1994a). Thus, the polar DR1 guest molecules are covalently attached, i.e., labeled, to the polymer chains of PS. As determined via UV-visible absorbance spectroscopy, the concentration of DR1 in DR1-labeled PS is approximately 3.0 mol %. As determined by gel permeation chromatography, M_w = 1.34 x

10^4 g/mol and M_w/M_n = 1.65 for the DR1-labeled PS.

The molecular dipole moment of DR1 is approximately 7.0 D (Cheng 1991). It has been established that, when doped in PS, the reorientation dynamics of DR1 as measured by second harmonic generation are coupled to cooperative segmental dynamics (α process) of PS (Dhinojwala 1994b). A related study demonstrated that the reorientation dynamics of DR1 labeled to polymers are also coupled to the α process (Dhinojwala 1994a). The incorporation of DR1 from 0.0 to 3.0 mol % label content in PS results in a linear enhancement of the dielectric response, indicating that probe-probe associations (dipole quenching) do not occur in 3.0 mol % of DR1-labeled PS.

Thin polymer films were prepared by spin-coating from a toluene solution of DR1-labeled PS onto an aluminum (Al)-deposited glass substrate. Film thickness was controlled by changing the concentration of the solution and spin speed of the spin-coater. The thin films obtained by spin-coating were annealed for 48 h at 303 K. After annealing, Al was vacuum-deposited onto the thin films to serve as an upper electrode. Vacuum deposition of Al might increase the temperature of thin polymer films locally; however, no dewetting of polymer films was observed during the vacuum deposition of Al. Therefore, the local heating of thin polymer films by vacuum deposition, if any, would not affect the present experimental results. The thickness of the Al electrode was controlled to be approximately 40 nm, which was monitored by a quartz oscillator. The effective area of an electrode (S) is 8.0 mm^2. The thickness (d) of DR1-labeled PS was evaluated from the electric capacitance after calibration with the absolute thickness measured by an atomic force microscope.

Dielectric measurements were performed using an LCR meter (HP4284A) in the

frequency (f) range from 20 Hz to 1 MHz and an impedance analyzer with a dielectric interface (Solartron Instruments 1260/1296) in the f range from 0.1 Hz to 1 MHz. The temperature of the sample cell was changed between 273 K and 413 K at a constant rate of 1 K/min. The dielectric measurements during the heating and cooling processes were performed repeatedly several times. Data were recorded during all cycles except the first cycle. Good reproducibility of dielectric data were obtained after the first cycle.

7.3 Results

7.3.1 Constant Frequency Measurements

Figure 7-1 shows the real (ε') and imaginary (ε'') components of the complex dielectric constant observed during the cooling process at the frequency of the applied electric field f = 100 Hz for a DR1-labeled PS film and an unlabeled PS film. The thicknesses of the DR1-labeled PS and the unlabeled PS films are 360 nm and 298 nm, respectively, and hence both can be regarded as bulk systems. It is clear that below T_g there is nearly no difference in ε' and ε'' between DR1-labeled PS and unlabeled PS. However, the values of ε' and ε'' above T_g for DR1-labeled PS are enhanced compared to those of the unlabeled PS. As shown in Figure 7-1, the peak height of the dielectric loss (ε'') due to the α process of DR1-labeled PS is approximately 65 times larger than that of the unlabeled PS.

Figure 7-2 shows the temperature dependence of the real part of the complex electric capacitance (C') normalized to the value at 273 K for three different frequencies. The data are observed during the heating process. From Figure 7-2, it is observed that the normalized electric capacitances at the three different frequencies overlap and have linear temperature dependences

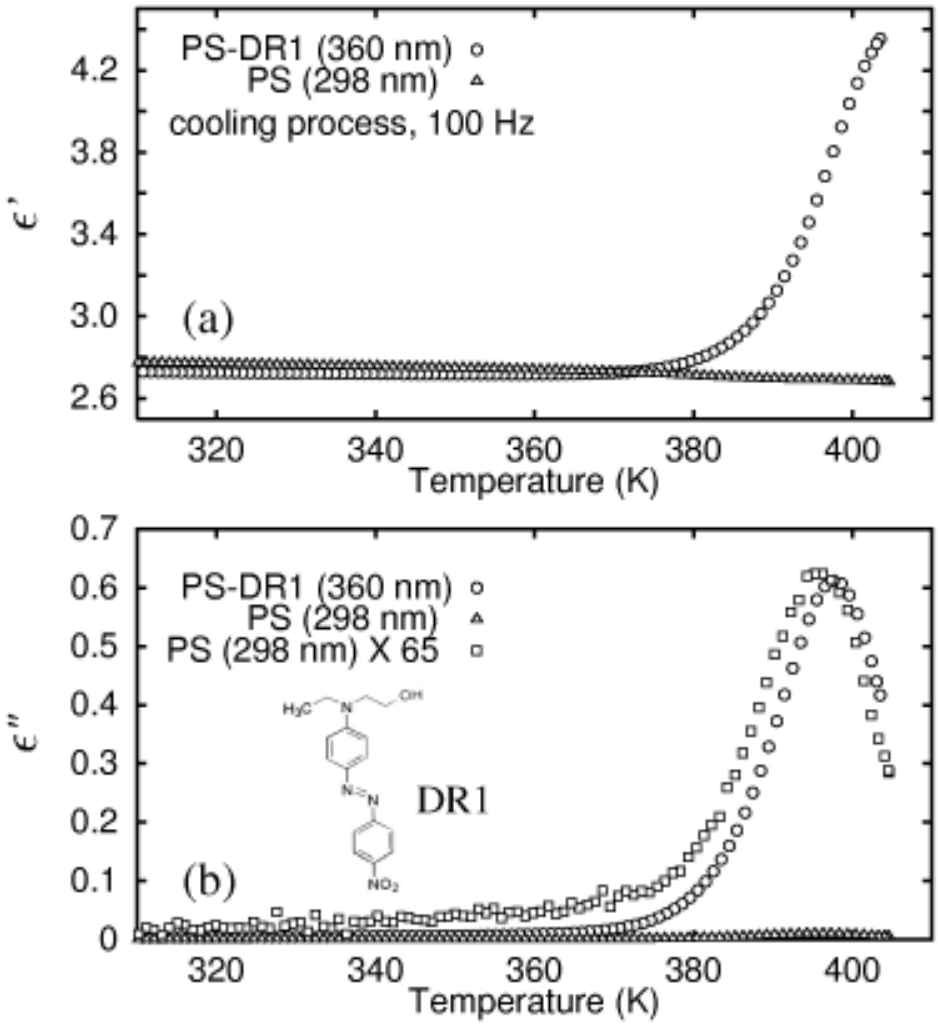

Figure 7-1: Temperature dependence of the real and imaginary parts of the complex dielectric constants for a 360-nm-thick DR1-labeled PS film and a 298-nm-thick unlabeled PS film. Data points are obtained at $f = 100$ Hz.

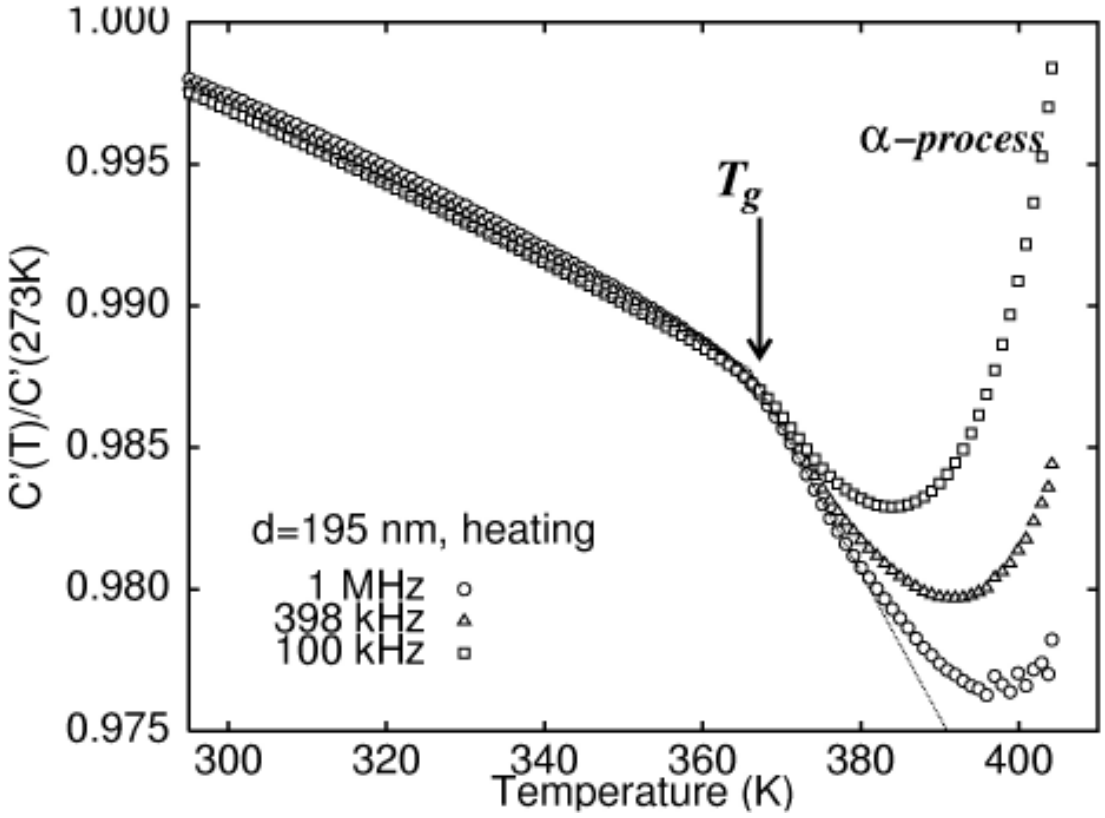

Figure 7-2: Temperature dependence of the real part of the electric capacitance normalized by the value at 273 K for a 195-nm-thick film at three different frequencies. The data are observed during the heating process.

below about 368 K. On the other hand, above 368 K the electric capacitance has a small linear temperature dependence followed by a non-linear temperature dependence. (As discussed in previous studies (Fukao 1999; Fukao 2000), the slopes of the linear portions of the curves correspond to the thermal expansion coefficient normal to the film surface.) Therefore, T_g can be determined by capacitive dilatometry (CD). The T_g determined by CD is 368 K and within experimental error equal to T_g determined by DSC (370 K). The linear thermal expansion coefficients evaluated from Figure 7-2 change from 0.7 x 10^{-4} K^{-1} to 2.5 x 10^{-4} K^{-1} when going from the glassy state to the rubbery state, which agrees well with the literature values of PS. The frequency dispersion of C' above T_g is due to the α-relaxation process.

Figure 7-3 shows the thickness dependence of T_g determined from the temperature dependence of the electric capacitance as mentioned above (see Figure 7-2). Figure 7-3 clearly shows that T_g decreases with decreasing film thickness. The thickness dependence of T_g can be fitted using the following equation:

$$T_g(d) = T_g^{\infty}(1 - a/d) \qquad 7\text{-}1$$

where the best fit parameters are T_g^{∞} = 369.5 ± 2.1 K and a = 1.1 ± 0.2 nm. In Figure 7-3 the thickness dependence of T_g of unlabeled PS is also included. The molecular weights of the two unlabeled PS samples are M_w = 2.8 x 10^5 and 1.8 x 10^6 g/mol. Comparing the thickness dependence of T_g between the DR1-labeled PS and the unlabeled PS, it is found that in both cases T_g decreases with decreasing film thickness in a reasonably similar way, although there is a small difference between the two systems (DR1-labeled PS and unlabeled PS). This difference may be attributed to the difference in molecular weight between DR1-labeled PS and the unlabeled PS samples.

Figure 7-4 shows the temperature dependence of the real and imaginary components of the complex dielectric constant for thin films of DR1-labeled PS with film thickness ranging from 360 nm to 15 nm. The data are obtained during the cooling process at frequency 20 Hz. Figure 7-4 shows that the α process is strongly affected by film thickness. As the thickness decreases, the peak height of the dielectric loss due to the α process decreases and at the same time, the peak temperature of the α process (T_α) shifts to a lower temperature. In Figure 7-5, T_α is plotted as a function of film thickness for f = 20 Hz and 100 Hz. The value of T_α depends strongly on frequency and increases with increasing frequency. With decreasing film thickness, T_α decreases. The decrease in T_α with decreasing film is related to the decrease in T_g with decreasing film thickness, as T_α and T_g are related (see Chapter 2). (At f = 0.01 Hz, the value of T_α is approximately equal to the value of T_g when determined on cooling at 10 K/min.) Therefore, the decrease in T_α with decreasing film thickness at a given frequency is associated with the decrease in T_g and the faster dynamics of the α process in thinner films.

7.3.2 Frequency Sweep Measurements

Figure 7-6 shows the frequency dependence of the real and imaginary components of the complex dielectric constants at various temperatures for 360-nm-thick and 19-nm-thick DR1-labeled PS films. The real part of the complex dielectric constant for the 360-nm-thick film exhibits a gradual step from 4.7 to 2.7, while in the imaginary part there is a maximum at the same frequency where there is the step in ε'. The step change in ε' and the peak in ε'' are associated with the existence of the α process. The peak frequency of ε'' corresponds to the inverse of a characteristic relaxation time of the α process at a given temperature. As shown in

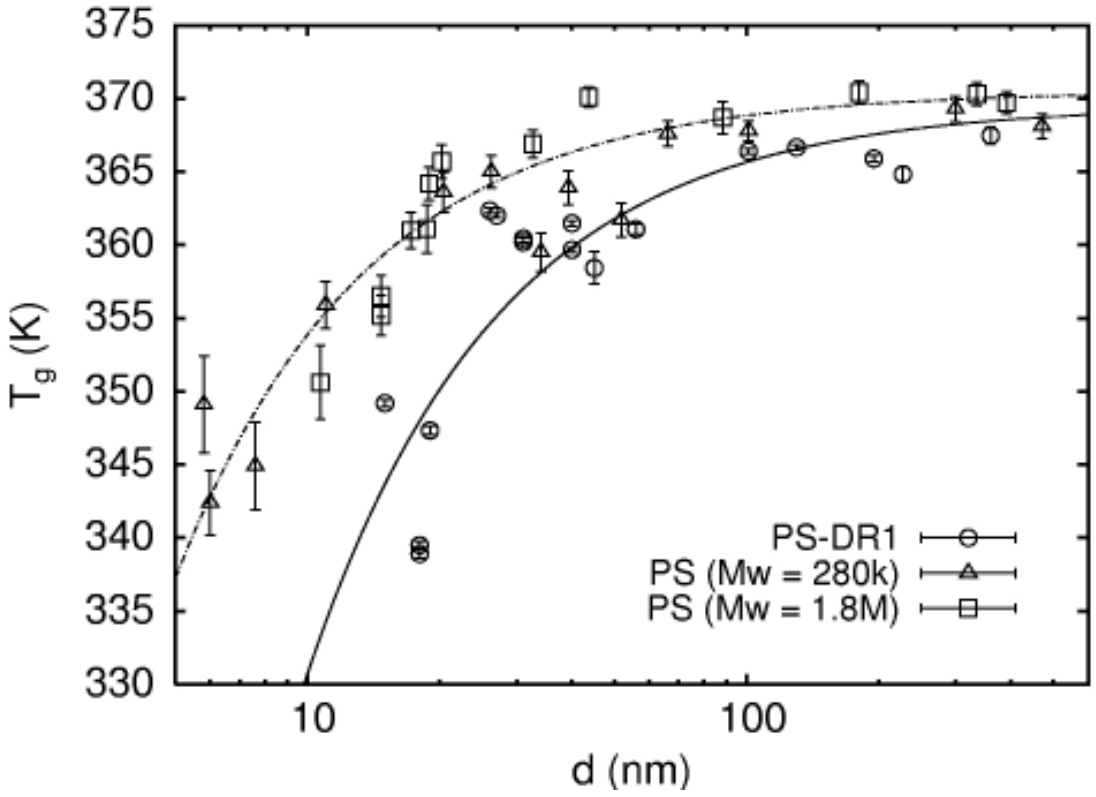

Figure 7-3: Thickness dependence of T_g determined from the crossover temperature as shown in Figure 7-2 for thin films of DR1-labeled PS. The thickness dependence of T_g of unlabeled PS is also plotted (Fukao 2000). The lines are obtained by fitting the observed data points to equation 7-1.

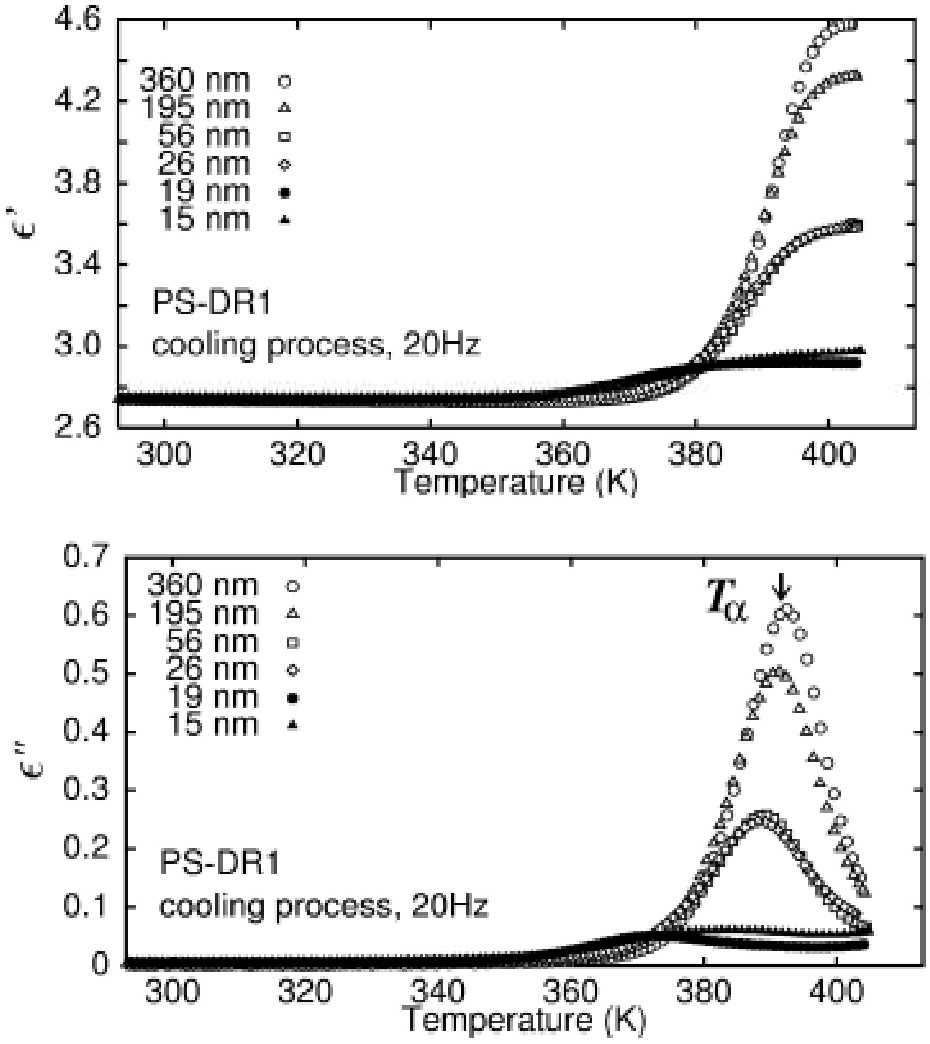

Figure 7-4: Temperature dependence of the real and imaginary components of the dielectric constants at $f = 20$ Hz for several films different thicknesses.

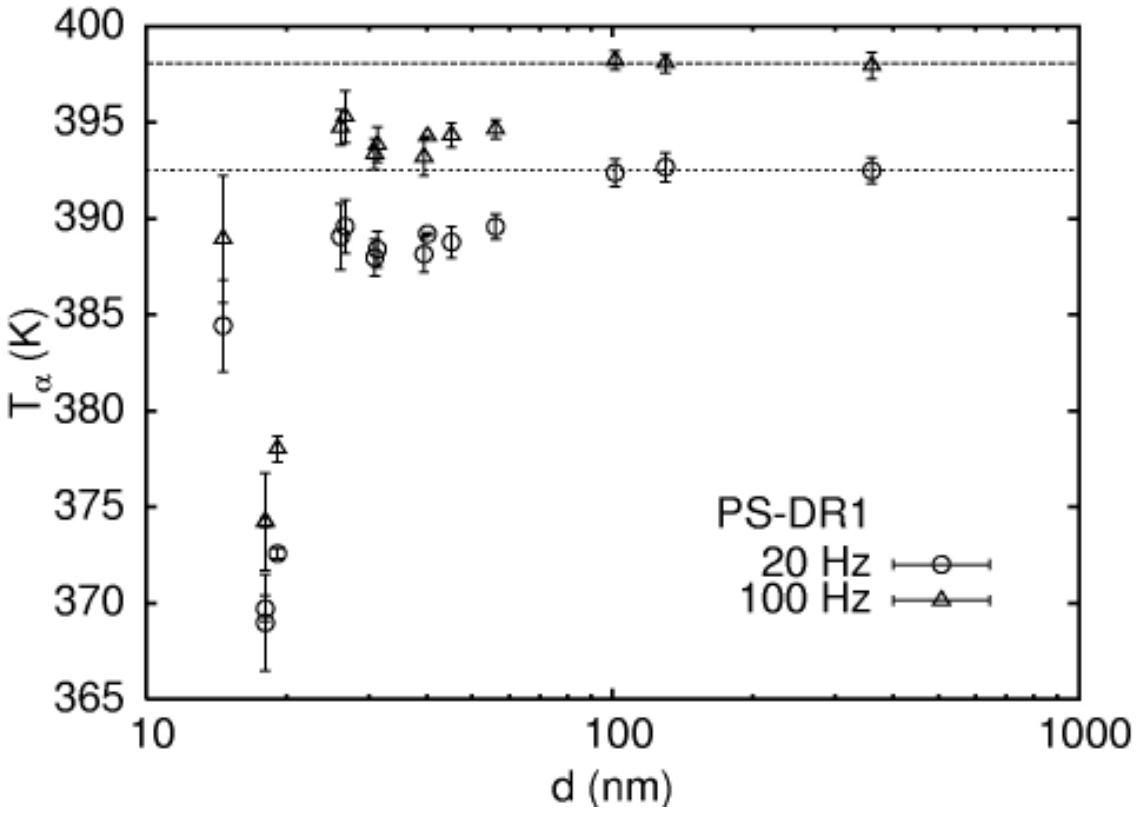

Figure 7-5: Thickness dependence of T_α observed at f = 20 Hz and 100 Hz. The dotted lines correspond to the values observed for bulk PS at f = 20 Hz and 100 Hz.

Figure 7-6, the peak frequency of the α process shifts to a higher frequency with increasing temperature. This shift corresponds to an acceleration of the dynamics of the α process with increasing temperature. (At higher temperatures there is a large increase in ε'' with decreasing frequency. This is usually attributed to contributions from dc conductivity due to space charges or impurities within the polymeric systems.) In comparing the frequency dependences of ε' and ε'' for the 360-nm-thick film and the 19-nm-thick film in Figure 7-6, it is observed that the peak height of ε'' due to the α process for the 19-nm-thick film is much smaller than that of the 360-nm-thick film. A comparison of data at constant temperature (400.0 K for 360-nm-thick film and 400.7 K for 19-nm-thick film) illustrates that the peak shape and the peak position of the 19-nm-thick film is different from that of the 360-nm-thick film.

The solid lines in Figure 7-6 are a fit of the data to the following empirical equation of the complex dielectric constant as a function of frequency:

$$\varepsilon^*(\omega) = \varepsilon_\infty + i\frac{\sigma}{\varepsilon_o}\omega^{-m} + \frac{\Delta\varepsilon}{\left[1+(i\omega\tau_o)^\alpha\right]^\beta} \qquad 7\text{-}2$$

where $\omega = 2\pi f$, ε_o is the permittivity in vacuum and ε_∞ is the permittivity at a very high frequency. The second term is a contribution from space charge (Miyamoto 1984), and this contribution can be attributed to pure dc conductivity if $m = 1$. The third term represents the α process and is usually called the Havriliak-Negami (HN) equation, where $\Delta\varepsilon$ is the relaxation strength, α and β are the shape parameters, and τ_o is the characteristic relaxation time of the α process. Figure 7-6 shows that equation 7-6 can well reproduce the frequency dependence of the observed dielectric constant. Examples of the best-fit parameters of the HN function at 390 K are listed in Table 7-1. In Table 7-1, the value of β_{KWW} (the exponent in the Kohlraush-

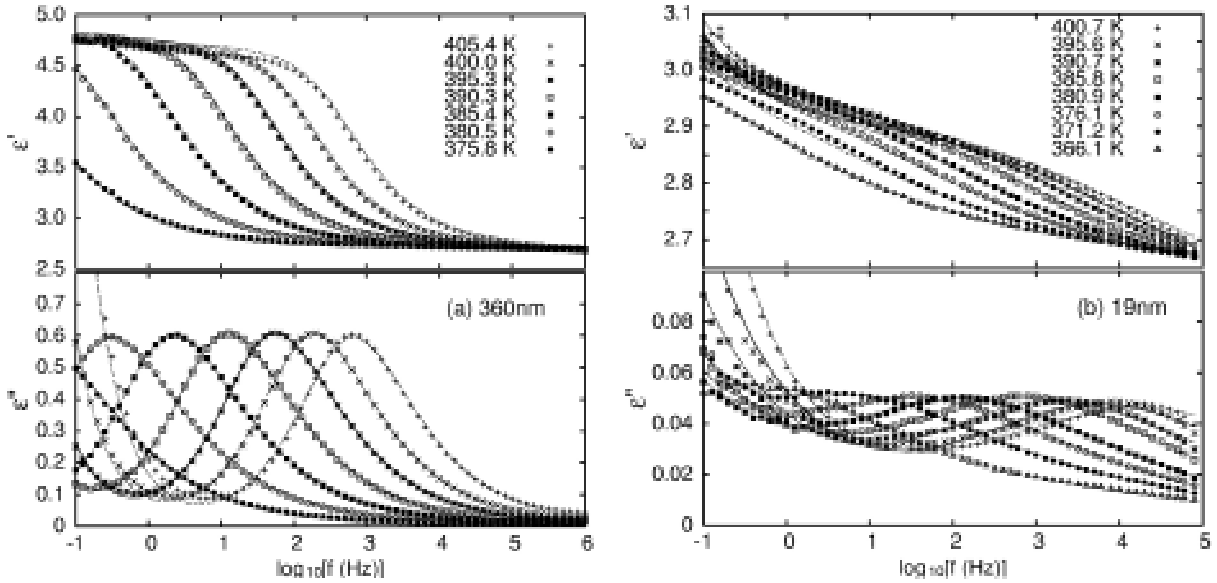

Figure 7-6: The dependence of the complex dielectric constant on the logarithm of the frequency at various temperatures above T_g for a 360-nm-thick film and a 19-nm-thick film. Solid curves are a fit to the data using equation 7-2.

Table 7- 1: Fitting parameters of the HN function for three different DR1-labeled PS films near 390 K.

d (nm)	T (K)	$\Delta\varepsilon$	α_{HN}	β_{HN}	τ_o (s)	β_{KWW}
19	390.7	0.33	0.46	0.48	3.1×10^{-4}	0.29
26	389.8	0.96	0.69	0.52	1.8×10^{-2}	0.43
360	390.3	2.14	0.80	0.57	2.32×10^{-2}	0.53

Williams-Watts equation; see equation 2-1 in Chapter 2) is also listed. The value of β_{KWW} is evaluated from the following relationship (Alvarez 1991):

$$\beta_{KWW} = (\alpha\beta)^{1/1.23} \qquad 7\text{-}3$$

Recall from Chapter 2 that the value of β_{KWW} is a measure of the distribution or breadth of the α-relaxation process, with $\beta_{KWW} = 1$ denoting a single exponential relaxation process and $\beta_{KWW} = 0$ denoting a relaxation process of infinite breadth.

Figure 7-7 shows the Arrhenius plot of the α process for three DR1-labeled PS thin films of thickness 19 nm, 26 nm, and 360 nm. The vertical axis is the logarithm of ($1/2\pi\tau$), where τ is the characteristic relaxation time of the α process and is evaluated from the relationship ($2\pi f_{max}\tau = 1$), where f_{max} is the frequency at which ε'' exhibits a peak due to the α process at a given temperature. The curves are fit to the Vogel-Fulcher-Tammann (VFT) equation:

$$\tau(T) = \tau^{o} \exp\left(\frac{U}{T - T_o}\right) \qquad 7\text{-}4$$

where τ^{o} is a microscopic time scale for the α-process, U is an apparent activation energy of the α process, and T_o is the Vogel temperature (Vogel 1921; Fulcher 1925; Tammann 1926). For each film thickness the relaxation time of the α process can be well described by VFT equation. However, that there is a distinct thickness dependence of τ, that is, the relaxation time of the α process becomes smaller with decreasing film thickness at a given temperature. The best fit parameters from the VFT equation for the three DR1-labeled PS thin films are listed in Table 7-2. It is clear that the Vogel temperature decreases with decreasing film thickness, which is consistent with the fact that T_g decreases with decreasing film thickness as shown in Figure 7-3.

In order to obtain the thickness dependence of the profile of the dielectric loss spectrum,

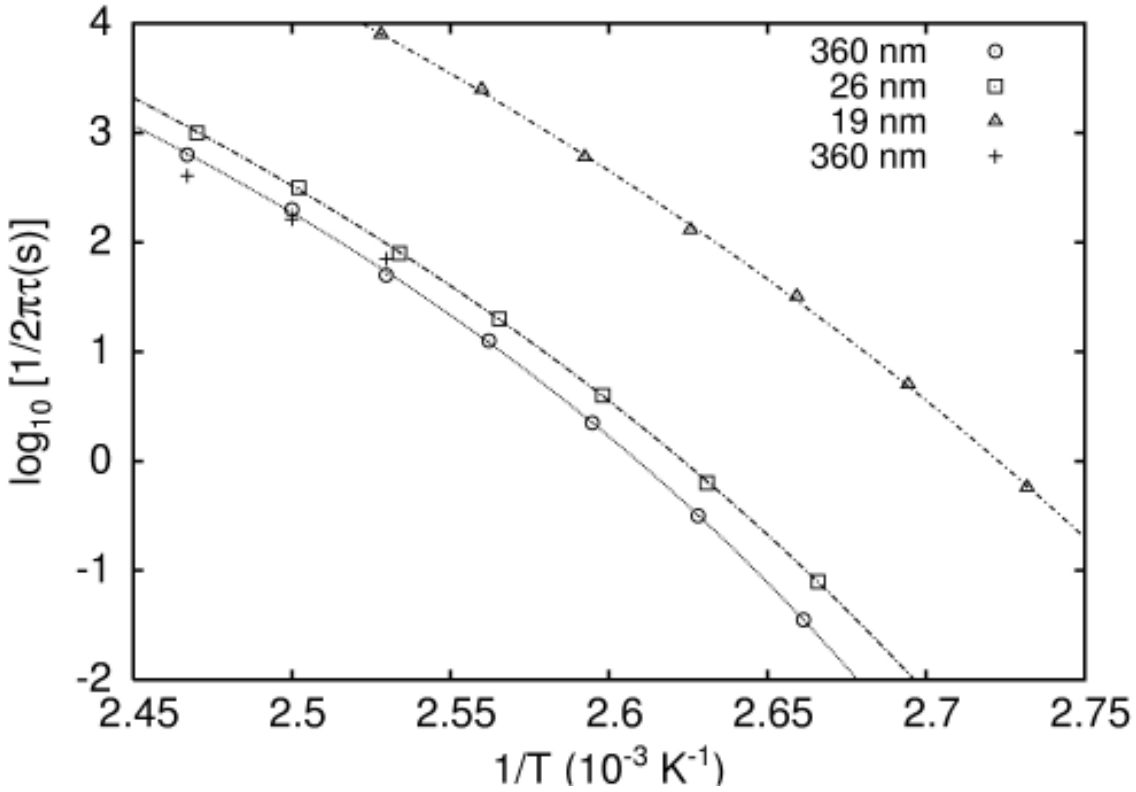

Figure 7-7: Arrhenius plot ($1/2\pi\tau$ vs $1/T$) for the α-relaxation process for DR1-labeled thin films. The curves are a fit of the data to the VFT equation.

Table 7- 2: Fitting parameters of the VFT equation (equation 7-4) to the data presented in Figure 7-7.

d (nm)	$\log[\tau_o\,(\mathrm{s})]$	$U\,(10^3\ \mathrm{K})$	$T_o\,(\mathrm{K})$
360	-11.8	1.6	318
26	-13.3	2.1	306
19	-14.6	2.3	294

the observed loss peaks of ε'' at various temperatures are normalized with respect to the peak position for each temperature in the case for three different film thicknesses, as shown in Figure 7-8. For clarity, data points of the 19-nm-thick and 26-nm-thick films are shifted along the vertical axis by + 0.6 and + 0.3, respectively. From Figure 7-8 it is observed that the width of the α process increases with decreasing film thickness. This suggests that the distribution of the relaxation times of the α process becomes broader with decreasing film thickness. In addition, Figure 7-8 shows that there is a strong contribution of dc conductivity in the low-frequency side of the spectrum, which may disturb the evaluation of the distribution of the relaxation times of the α process. In order to avoid this problem, the best fit parameters of the HN function α, β and τ_o will be used to evaluate the distributions of α-relaxation times. Here, the distribution function $F(\ln\tau)$ of the relaxation time τ is defined by the following relation (see Chapter 4.3 for details):

$$\varepsilon^*(\omega) = \varepsilon_\infty + \Delta\varepsilon \int_{-\infty}^{+\infty} \frac{F(\ln\tau)d(\ln\tau)}{1+i\omega\tau}. \qquad 7\text{-}5$$

If we assume that the shape of the dielectric loss peak is described by the HN function, then the distribution function $F(\ln\tau)$ can be calculated analytically as follows (Schonhals 2003):

$$F(s) = \frac{1}{\pi}(1 + 2e^{\alpha(x_o - s)}\cos(\pi\alpha) + e^{2\alpha(x_o - s)})^{-\beta/2} \cdot \sin[\beta \tan^{-1}(\frac{e^{\alpha(x_o - s)}\sin(\pi\alpha)}{1 + e^{\alpha(xo - s)}\cos(\pi\alpha)})] \qquad 7\text{-}6$$

where $s = \ln\tau$ and $x_o = \ln\tau_o$ (Fukao 2001b; Schonhals 2003). Figure 7-9 shows the distribution of the α-relaxation time for three different film thicknesses at 391 K determined using equation 7-6. It is observed that the peak of the α-relaxation process (which is related to average α-relaxation time) is shifted to smaller times and that the width of the distribution becomes larger (width of distribution increases from two decades for the 360-nm-thick film to eight decades for 19-nm-

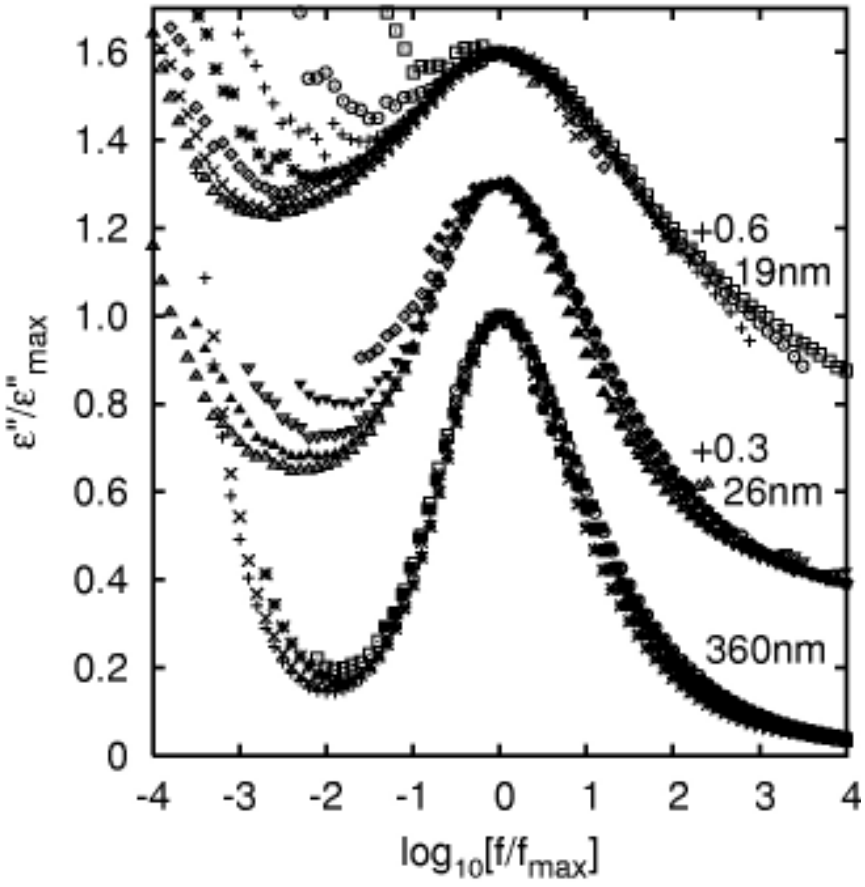

Figure 7-8: The dependence of the normalized dielectric loss of DR1-labeled PS films on the logarithm of the normalized frequency. The data are normalized with respect to the peak position of the α process. Different symbols correspond to different temperature above T_g.

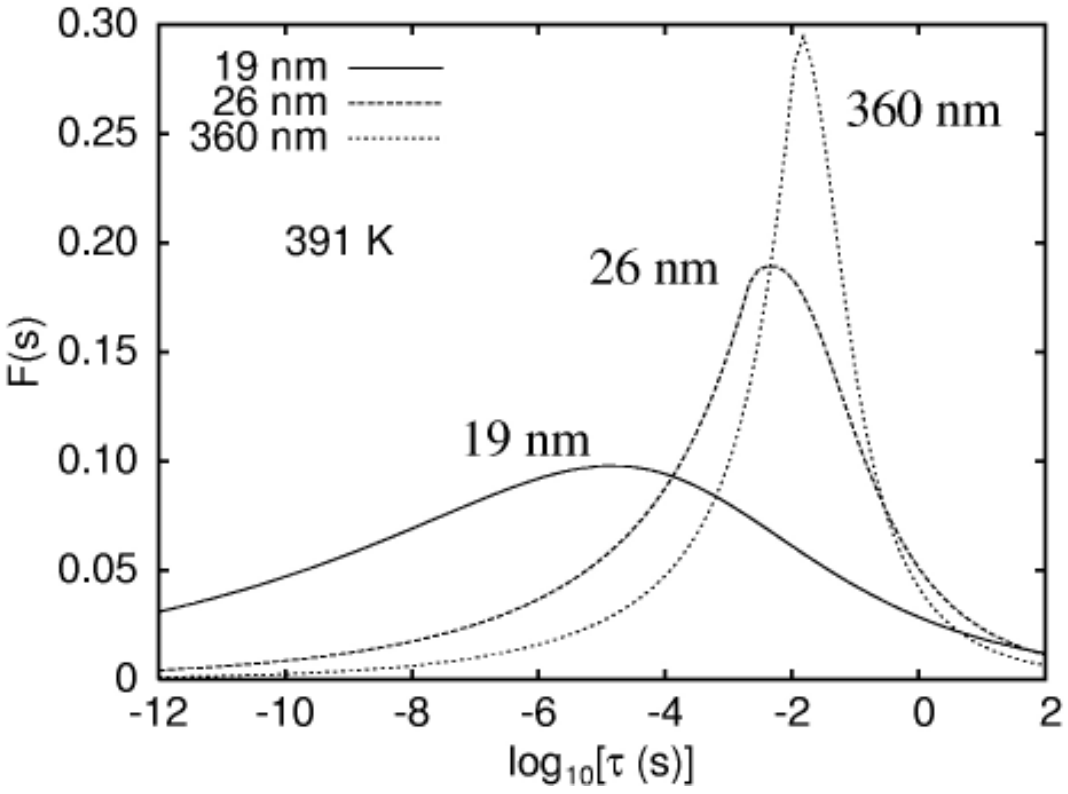

Figure 7-9: Distribution function F(s) of the relaxation times of the α process at 391 K for DR1-labeled PS thin films.

thick film).

7.4 Discussion

In 1994, Dhinojwala *et al*. (Dhinojwala 1994b) investigated the rotational dynamics of DR1 doped at 2 wt. % into polystyrene using second harmonic generation spectroscopy (SHG) and dielectric relaxation spectroscopy. They observed that SHG and dielectric relaxation spectroscopy yielded nearly an identical relaxation time of the rotational dynamics of DR1 doped into PS. In addition, they observed that above the T_g of PS, the temperature dependence of the relaxation time of the rotational dynamics of DR1 doped into PS was well described by the Williams-Landel-Ferry (WLF) equation with appropriate WLF constants. The ability to fit the temperature dependence of the rotational relaxation time of DR1 doped into PS indicated that the rotational dynamics of DR1 are coupled to the α-relaxation process of PS (Dhinojwala 1994b).

As shown in section 7.3, the signal of the dielectric loss can be observed above T_g for DR1-labeled PS using dielectric relaxation spectroscopy. The strength of dielectric loss signal above T_g for DR1-labeled PS is approximately 65 times greater than that of unlabeled PS. As illustrated in Figure 7-7, the rotational dynamics of DR1 labeled to PS can be fit to the VFT equation (the VFT equation is equivalent to the WLF equation). The results are consistent with results presented by Dhinojwala *et al*. (Dhinojwala 1994b). Therefore, the reorientation dynamics of DR1 labeled to PS, which is the microscopic origin of the observed dielectric loss, are coupled to the α-relaxation process of PS.

In many polymeric systems with large polarity such as PMMA and poly(vinyl acetate), it is impossible to determine T_g by capacitive dilatometry (Fukao 2001a). However, as shown in Figure 7-2, T_g of DR1-labeled PS can be successfully determined by capacitive dilatometry.

Furthermore, the thickness dependence of T_g for DR1-labeled PS thin films is consistent with that of the unlabeled PS. The reduction in T_g with decreasing film thickness is believed to be related to a layer at the upper Al-electrode polymer interface with a reduced T_g. Thus, with decreasing film thickness, the layer with a reduced T_g contributes more to the average dynamics of the film, leading to a decrease in the average film T_g.

The observed shapes of the dielectric loss and the distribution of relaxation times of the α-process for thin films of DR1-labeled PS are shown in Figures 7-8 and 7-9. Table 7-1 lists the best fit parameters of the HN equation for three DR1-labeled PS thin films at 390 K. From Figures 7-8 and 7-9 it is observed that the distribution of the α-relaxation times become broader with decreasing film thickness. Such an observation is consistent with previous studies of unlabeled PS (Fukao 1999; Fukao 2000; Fukao 2001b). However, the distribution of α-relaxation times for DR1-labeled PS is narrower than that of unlabeled PS at a fixed thickness and temperature: $\beta_{KWW} = 0.53$ for a 360-nm-thick DR1-labeled PS film and $\beta_{KWW} = 0.44$ for a 408-nm-thick unlabeled PS film. This difference may be related to the fact that the reorientation dynamics of DR1, which are coupled with the α-process of PS, are the observed dielectric relaxation process.

Figure 7-6 shows that with decreasing film thickness there is a reduction in the strength of the α-relaxation process: $\Delta\varepsilon$ changes from 2.14 for a 360-nm-thick film to 0.33 for a 19-nm-thick film. This thickness dependence of $\Delta\varepsilon$ has been previously observed in other polymeric systems such PS, PMMA, and poly(vinyl acetate) (Fukao 2001b; Serghai 2003). A simple model for the reduction in the strength of the α-relaxation process with decreasing film thickness has been recently proposed by Fukao and Miyamoto (Fukao 2001b). The model assumes that

there is a motional unit of which *n* dipole units move or rotate cooperatively. The strength of the relaxation process, $\Delta\varepsilon$, is given by the following relation:

$$\Delta\varepsilon = \frac{N\mu^2}{3k_BT} \qquad 7\text{-}7$$

where N is the number of the motional units and is given by $N = N_o/n$, and μ is the total strength of dipole moments included in a unit and is given by $\mu = n \times \mu_o$. Here, μ_o is the strength of a single dipole moment attached to polymer chains, N_o is the total number of dipole moments in the system. Using N_o and μ_o, equation 7-7 can be rewritten as follows:

$$\Delta\varepsilon = n\frac{N_o\mu_o^2}{3k_BT} \qquad 7\text{-}8$$

If the number of dipole moments within a motional unit or the number of motional units is decreased with decreasing film thickness, then the strength of the α process decreases. The notion of a decrease in the number of dipole moments moving cooperatively is consistent with the existence of a cooperatively rearranging region (CRR).

It is noted that DR1 is a guest molecule in PS (neat PS does not contain traces of DR1). Therefore, there is a possibility that the local structure of PS chains deviates from that of the unlabeled PS and that this deviation in chain structure affects the α-relaxation dynamics of the polymer chains observed by dielectric relaxation spectroscopy. However, it is believed that such deviation, if any, has almost no effect on the segmental motions of DR1-labeled PS, because the α-relaxation dynamics and its thickness dependence are consistent with those of unlabeled PS, as shown in our study. In addition, previous studies conducted using DR1 as a probe either doped or covalently attached to the polymer yielded average α-relaxation times in agreement with those

determined using other techniques for unlabeled PS (Dhinojwala 1993; Dhinojwala 1994b).

7.5 Conclusions

The T_g and α-relaxation dynamics of DR1-labeled PS were investigated using dielectric relaxation measurements. Above T_g, the dielectric strength of DR1-labeled polystyrene was about 65 times greater than that of unlabeled polystyrene. The relaxation dynamics of bulk DR1-labeled PS were consistent with the relaxation dynamics of bulk unlabeled PS. In addition, the effect of confinement on the α-relaxation dynamics of DR1-labeled PS was consistent with the effect of confinement on the α-relaxation dynamics of unlabeled PS. The results suggest that it may be possible to develop a dielectric / multilayer technique to investigate the interfacial relaxation dynamics of PS in a similar manner as the fluorescence / multilayer technique allowed for the investigation of the interfacial T_g. The development a dielectric / multilayer technique will be presented in Chapter 8.

8 GLASS TRANSITION AND ALPHA-RELAXATION DYNAMICS OF THE INTERFACIAL LAYERS OF POLYSTRENE LABELED WITH A MOLECULAR DIPOLE

8.1 Introduction

Over the past decade, many experimental studies (Keddie 1994a; Forrest 1996; Fukao 1999; Fukao 2000; Ellison 2003; Roth 2003; Sharp 2003a; Fakhraai 2005; Lupascu 2006; O'Connell 2006; Mundra 2007a) and simulations (Torres 2000; Starr 2001; Varnik 2002; Peter 2006) have been done to characterize and explain the effect of confinement on polymer properties. Of particular interest has been the impact of confinement on the glass transition temperature (T_g) of thin polymer films. As discussed in Chapter 3, many experimental techniques such as ellispometry (Keddie 1994a; Forrest 1996; Roth 2003), dielectric spectroscopy (Fukao 1999; Fukao 2000; Serghai 2003; Lupascu 2006), fluorescence (Ellison 2002b; Mundra 2007a; Roth 2007b), and other techniques (O'Connell 2005) have been used to investigate the impact of film thickness on T_g of polymers. There is a growing consensus that the effect of thickness on T_g originates from interfacial effects (free surface and substrate interface); as thickness is decreased, the interfacial area to volume ratio increases, leading to interfacial properties contributing more to average film properties (see reviews (Roth 2004; Ngai 2006)).

For freestanding films, decreasing thickness leads to a decrease in T_g of polystyrene (PS) (Forrest 1996) and poly(methyl methacrylate) (PMMA) (Roth 2003). However, for films

supported on silica, decreasing thickness leads to a decrease in T_g of PS (Keddie 1994a; Fukao 1999; Ellison 2003; Fakhraai 2005; Lupascu 2006) and an increase in T_g of PMMA (Keddie 1994b; Fryer 2000; Roth 2003). Using a novel fluorescence method, in which only one layer of a bilayer film was labeled with a fluorescent probe, the impact of the free surface and substrate interface on T_g was directly measured for PS (Ellison 2003) and PMMA (results presented in Chapter 5). At the free surface both PS and PMMA exhibit reductions in T_g, while at the substrate interface the T_g of PS is unchanged and that of PMMA is enhanced. Fluorescence studies, along with other experiments (Forrest 1996; Sharp 2003a; Akabori 2005; Gasemjit 2006; Papaleo 2006) and simulations (Peter 2006), have provided a strong correlation between the impact of confinement on T_g and interfacial effects. Although the glass transition is associated with cooperative segmental (α) relaxation dynamics, the effect of confinement on those dynamics has not been intensely characterized (Fukao 1999; Fukao 2000; Serghai 2003; Lupascu 2006; Svanberg 2007). Dielectric spectroscopy of aluminum (Al)-capped PS films has revealed a reduction in the peak temperature of the α-process (T_α) and a broadening of the α-process with decreasing thickness (Fukao 1999; Fukao 2000; Lupascu 2006). The reduction in T_α and the broadening of the α-process have been attributed to interfacial effects (Fukao 1999; Fukao 2000; Lupascu 2006); however, no direct experimental measurement supports the assertion. A technique is needed that can measure the α-relaxation spectrum within an interfacial layer of a bulk film.

Building on results presented in Chapter 7, this chapter describes the first direct experimental measurements of the α-relaxation dynamics at a polymer/substrate interface using dielectric relaxation spectroscopy. This is achieved using a bilayer film geometry in which one

layer is labeled with a guest dipole that enhances its signal relative to the other layer. In agreement with fluorescence studies showing a reduction in T_g at a free surface, a reduction in T_g at the evaporated-Al/polymer interface is observed; such an interface is known to yield a reduction in T_g in single layer films identical to that of films with one free surface (Fukao 1999; Fukao 2000; Sharp 2003a; Lupascu 2006). For the first time, a slight reduction in T_α and a broadening of the α-process is observed at the interface. The results indicate that the impact of confinement on the α-process originates from interfacial effects just as the T_g-nanoconfinement effect originates from interfacial effects. The reduction of T_α at the interface is shown to be frequency dependent, which is consistent with recent cooling rate-dependent T_g measurements of thin films (Fakhraai 2005).

8.2 Experimental

Polystyrene (Aldrich; M_w = 1800 kg/mol, M_w/M_n = 1.03) was used as received. 4-[N-ethyl-N-(hydroxyethyl)]amino-4-nitroazobenzene (Disperse Red 1)-labeled PS (M_w = 13.4 kg/mol, M_w/M_n = 1.65 by gel permeation chromatography) was synthesized by free radical polymerization of styrene in the presence of a trace amount of Disperse Red 1-labeled methacrylate monomer. The concentration of Disperse Red 1 in the labeled PS was 3 mol % as determined by UV-vis absorbance. Labeled PS was washed and dried to remove residual monomer. Procedures for the synthesis of labeled monomer and labeled polymer follow those of Dhinojwala *et al*. (Dhinojwala 1994a).

Single layer films were prepared by spin-coating polymer from toluene onto Al-deposited glass substrates. Bilayer films were prepared by spin-coating polymer from toluene onto Al-

deposited glass substrates or NaCl salt disks. Films cast onto salt disks were floated atop films cast onto Al-deposited glass substrates. Single layer and bilayer films were dried under vacuum at 303 K for 48 hr. After annealing, Al was vacuum-deposited onto the films to serve as the upper electrode (Chapter 5 describes in more detail the preparation of multilayer films.) The upper and lower electrodes were each 40 nm thick, and the effective area of the capacitor was 8.0 mm^2. Dielectric measurements were performed using an LCR meter (HP 4284A) in the frequency (f) range from 20 Hz to 1 MHz. The temperature of the sample cell was cycled between 273 K and 413 K at a constant rate of 1 K/min. Data were acquired after the first heating cycle above the dilatometric T_g.

8.3 Results and Discussion

Figure 8-1 shows the imaginary component of the complex dielectric constant (ε'') at f = 100 Hz for 298-nm-thick neat PS and 360-nm-thick labeled PS films. By comparison, the dielectric strength of the α-process of the labeled PS is 65 times greater than that of unlabeled PS. Nonetheless, the spectral shape of the α-process is essentially identical for the unlabeled and labeled PS, indicating that the low level of DR1 label does not alter the PS cooperative segmental dynamics (see Chapter 7 for more detail). Second harmonic generation studies (Dhinojwala 1994b) have shown that the rotational reorientation dynamics of DR1 in PS are coupled to the α-relaxation dynamics of PS. Thus, the rotational reorientation dynamics of DR1, which are the microscopic origin of the enhancement in the dielectric signal, are equivalent to the cooperative segmental dynamics of PS. The inset in Figure 8-1 shows the real component of the complex electric capacitance normalized at 300 K as a function of temperature at f = 1 MHz.

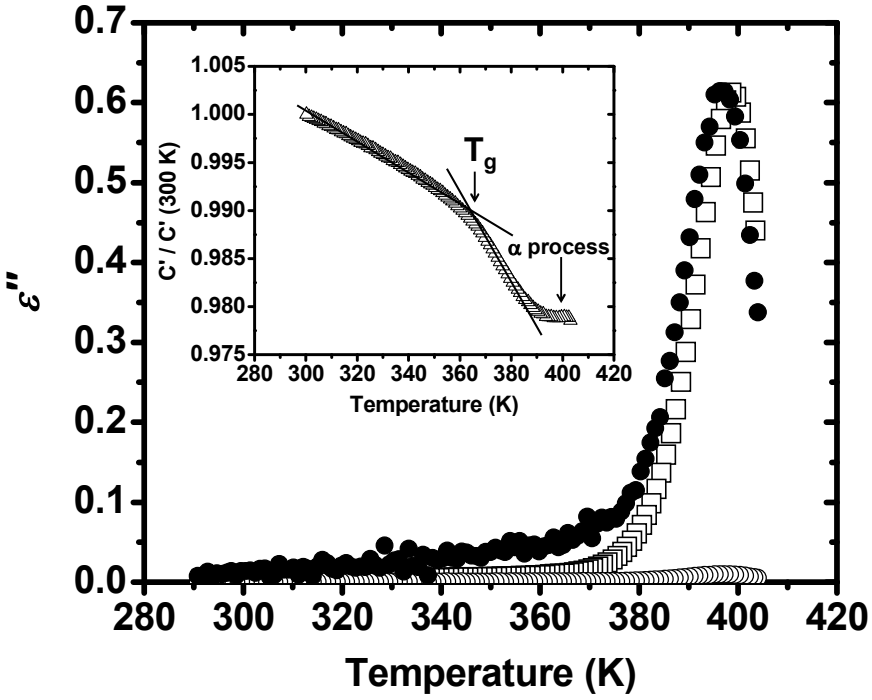

Figure 8-1: Temperature dependence of the imaginary component of the complex dielectric constant at f = 100 Hz for unlabeled PS (○), unlabeled PS x 65 (●), and labeled PS (□). Film thicknesses of unlabeled and labeled PS are 298 nm and 360 nm, respectively. Inset: Temperature dependence of the real component of the complex capacitance at f = 1 MHz of a 360-nm-thick labeled PS film. Data have been normalized to the capacitance value at 300 K.

The intersection of linear fits deep in the rubbery and glassy states provides a measure of the capacitive dilatometric T_g that is identical to the volume dilatometric T_g (Lupascu 2006). The T_g(bulk) value determined by capacitive dilatometry is 368 K, within 1 K of that from differential scanning calorimetry.

Figure 8-2 shows the impact of thickness on T_g of unlabeled and labeled PS films determined by capacitive dilatometry (neat PS data are from a study by Fukao and Miyamoto (Fukao 1999)). Two key points are obtained from Figure 8-2. First, the evaporation of the upper Al electrode as required for dielectric spectroscopy does not mask the effects of the free surface, as evident by the reduction in T_g with decreasing thickness that is similar to techniques that afford a free surface. This is not surprising since it has been previously observed that evaporated-Al capped PS films show a reduction in T_g identical to that of PS films with one free surface (Fukao 1999; Sharp 2003a; Lupascu 2006). In essence, evaporated-Al capped PS films behave as if they have a free surface. Second, the T_g-confinement behavior of labeled PS is similar to that of unlabeled PS. The solid curve in Figure 8-2 is a best fit to the empirical equation $T_g(d) = T_g^{\infty}(1 - a/d)$ where d is the thickness and the fit parameters are $T_g^{\infty} = 369$ K and $a = 0.65$ nm.

Figure 8-3 shows the effect of thickness on the α process of labeled PS at $f = 100$ Hz. The data are normalized with respect to the peak maximum. The α process of labeled PS broadens and the peak temperature of the α process decreases with decreasing thickness in a manner similar to that of unlabeled PS (Fukao 1999; Fukao 2000; Lupascu 2006).

The effect of confinement on the α relaxation dynamics of PS was hypothesized to result from interfacial effects (Fukao 1999; Fukao 2000; Lupascu 2006), with a film consisting of

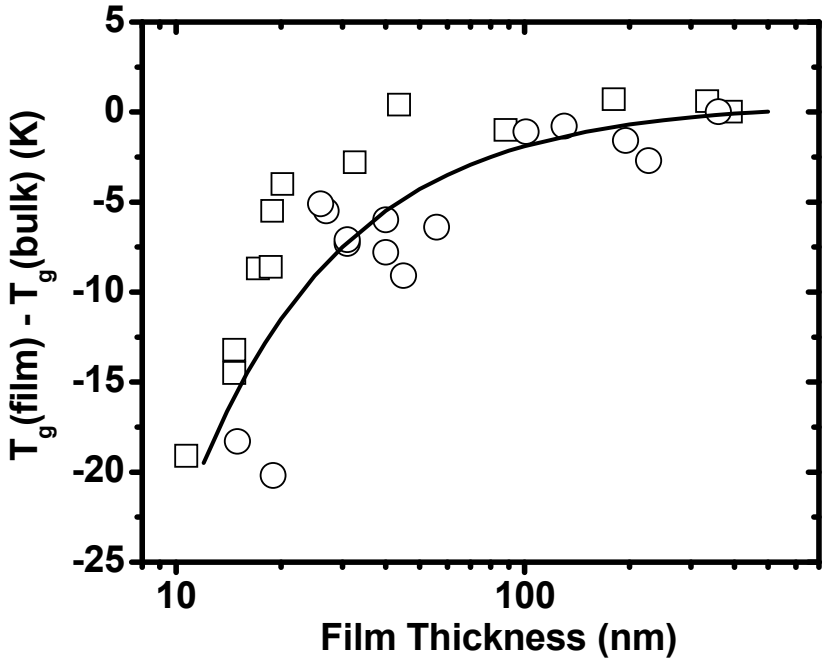

Figure 8-2: Deviation of T_g from T_g (bulk) as a function of thickness for unlabeled PS (□) and labeled PS (○) films. Unlabeled PS data are replotted from reference (Fukao 1999). The solid line is a best fit of the data to the empirical equation $T_g(d) = T_g^{\infty}(1 - a/d)$.

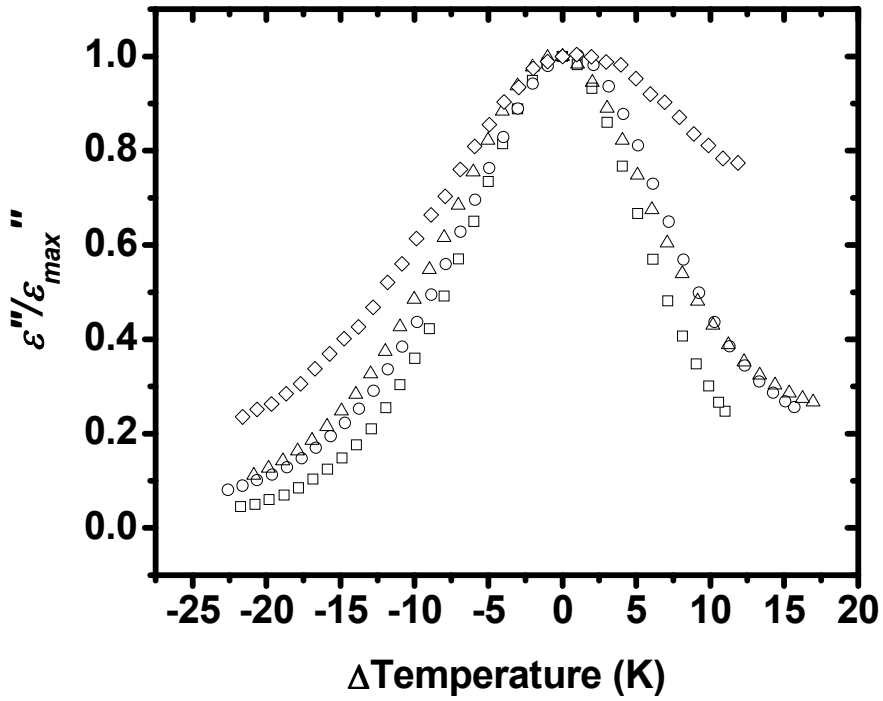

Figure 8-3: Effect of thickness on the width of the α-process for 360-nm-thick (□), 56-nm-thick (○), 30-nm-thick (Δ), and 19-nm-thick (◊) films at f = 20 Hz. Data have been normalized to the peak maximum of the α-process.

regions with bulk dynamics and regions near the evaporated-Al/polymer interface with enhanced dynamics. Thus, a reduction in thickness would lead to an overall broadening in the α process due to a greater contribution of the enhanced interfacial layer dynamics to the overall film dynamics. In turn, this would lead to a reduction in the average T_α across the film with confinement.

To explore the above hypothesis, a bilayer/dielectric spectroscopy technique (see Figure 8-4) has been developed to directly measure the α-relaxation dynamics in an ultrathin layer at the evaporated-Al/polymer interface. As shown in Figure 8-4, when a 15-nm-thick labeled PS layer is placed atop a 293-nm-thick unlabeled PS layer, the peak ε'' value is 0.018 for the bilayer film. When a 19-nm-thick labeled PS layer is placed atop a 251-nm-thick unlabeled PS layer, the peak ε'' value is 0.028. Also shown for comparison are the ε'' data for the unlabeled PS and labeled PS single layer films from Figure 8-1. If the bilayer film geometry is treated as an equivalent series combination of two capacitors, it is possible to extract the signal contribution exclusively from the labeled layer. The total complex electric capacitance (C^*_{total}) is given by $1/C^*_{total} = 1/C^*_{labeled\ PS} + 1/C^*_{neat\ PS}$, where $C^*_{labeled\ PS}$ and $C^*_{neat\ PS}$ are the contributions from the labeled PS layer and neat PS layer, respectively. Knowledge of the complex electric capacitance from the unlabeled layer allows for extracting the signal contribution from the labeled layer at the evaporated-Al/polymer interface.

Figure 8-5 shows the T_g and α-relaxation dynamics of the labeled PS layers at the evaporated-Al/polymer interface. Relative to T_g(bulk) (= 368 K), the 15-nm-thick labeled layer has a T_g reduction of 10 K while the 19-nm-thick labeled layer has a T_g reduction of 6 K. The results are qualitatively consistent with bilayer/fluorescence studies of PS films (Ellison 2003).

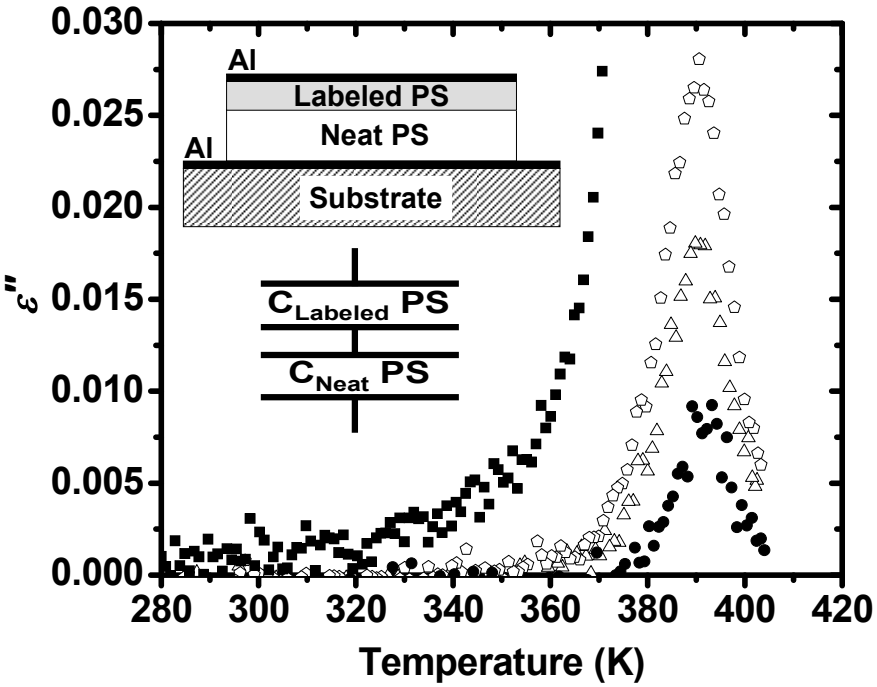

Figure 8-4: Imaginary component of the complex dielectric constant at $f = 20$ Hz for a 298-nm-thick neat PS film (●), a 360-nm-thick labeled PS film (■), a 15-nm-thick labeled PS/293-nm-thick neat PS bilayer film (Δ), and a 19-nm-thick labeled PS/251-nm-thick neat PS bilayer film (⬠). Inset shows film geometry and equivalent series combination of two capacitors.

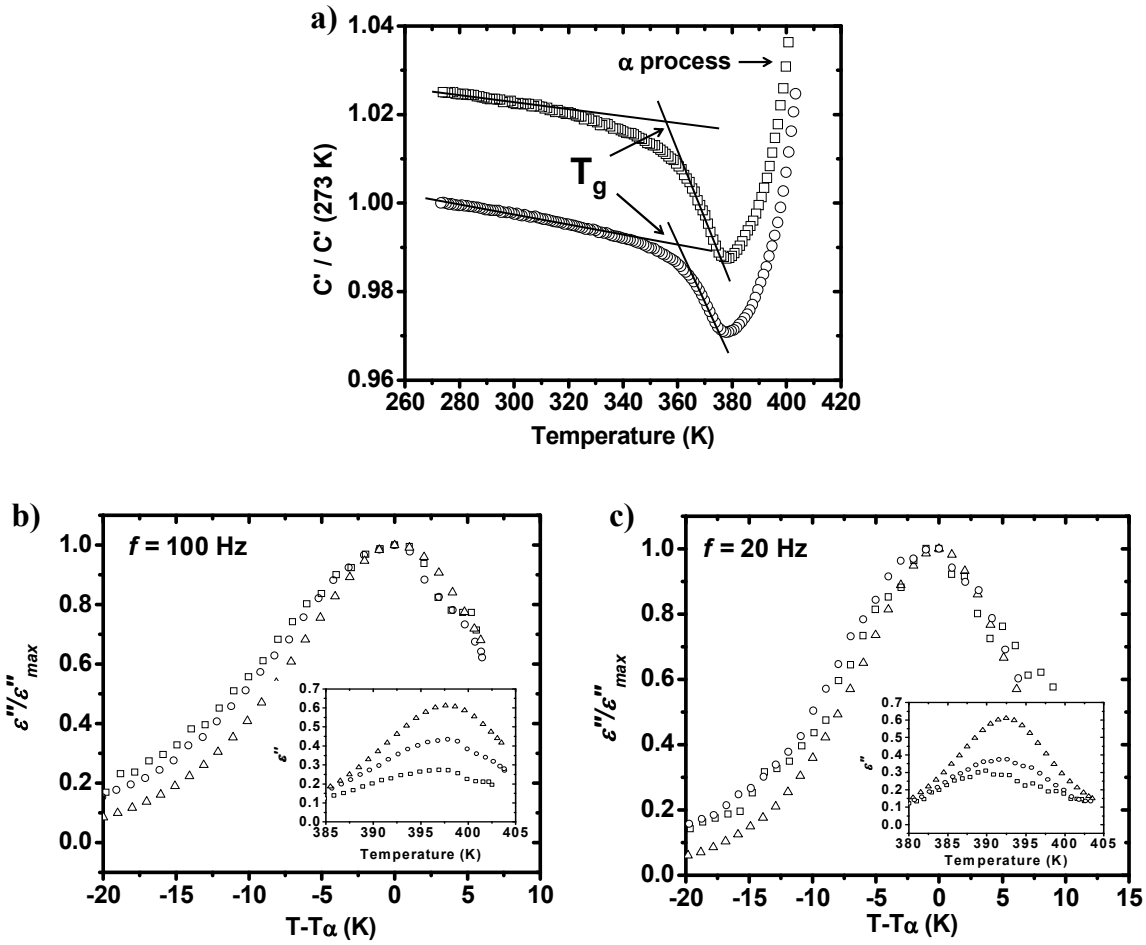

Figure 8-5: a) Temperature dependence of the real component of the complex capacitance for a 15-nm-thick labeled layer (□) and a 19-nm-thick labeled layer (○) within bilayer films. Data have been normalized to the capacitance value at 273 K and arbitrarily shifted for clarity. Imaginary component of the complex dielectric constant at f = 100 Hz b) and f = 20 Hz c) normalized with respect to the peak value for a 360-nm-thick labeled PS film (Δ), a 15-nm-thick labeled layer (□), and a 19-nm-thick labeled layer (○).

A possible reason for the quantitative difference (~32 K reduction in T_g reported by fluorescence for a 14-nm-thick labeled layer) may be due to the difference in M_w of the labeled PS used here (13.4 kg/mol) and that used in the fluorescence study (760 kg/mol). (Previous T_g measurements of freestanding PS films showed that low M_w PS has a weaker T_g-confinement effect compared to high M_w PS, and it is possible that such an effect is present at the free surface of PS films (Dalnoki-Veress 2001).) Besides the observed reduction in T_g at the interface, a comparison of Figure 8-5a and the inset in Figure 8-1 illustrates that the glass transition is broadened in the interfacial layer compared to the bulk film.

Figures 8-5b and 8-5c show the effect of the evaporated-Al interface on the α-process. At f = 100 Hz and 20 Hz, the α-relaxation dynamics are broader in the ultrathin labeled layers at the evaporated-Al interface than in a 360-nm-thick single layer film. The asymmetric broadening of the lower temperature side of the relaxation spectrum of the interfacial layers indicates the existence of enhanced dynamics of the cooperative segmental motions at the evaporated-Al/polymer interface. A potential reason for the enhancement in cooperative segmental dynamics at the interface is a reduction in the requirement for cooperativity (Ellison 2003). Interestingly, at f = 100 Hz the peak of the α process is identical (T_α = 397.5 K) for 19-nm-thick and 15-nm-thick interfacial layers and a 360-nm-thick film. However, at f = 20 Hz, T_α = 392.5 K for a 19-nm-thick thick interfacial layer and a 360-nm-thick film while T_α = 390 K for a 15-nm-thick thick interfacial layer. The results suggest that the impact of the interface on the α-process is frequency dependent and greater at lower frequency (equivalent to a longer time-scale or probing greater cooperativity). This observation is consistent with a recent study (Fakhraai 2005) demonstrating that the effect of confinement on T_g increases with decreasing cooling rate

in thin PS films.

8.4 Conclusions

In summary, a novel bilayer/dielectric spectroscopy technique has been developed to investigate the T_g and α-relaxation dynamics at the interface of polymer films. The study provided evidence for the enhancement of cooperative segmental (alpha) relaxation dynamics at the evaporated-Al polymer interface, which previous studies (Fukao 1999; Sharp 2003a; Lupascu 2006) have shown acts like a free surface (polymer-air interface) in the T_g behavior of thin films. The study is also consistent with models (Fukao 1999; Fukao 2000) suggesting that the acceleration of the α-process with decreasing film thickness is a result of enhanced dynamics at the evaporated-Al polymer interface.

PART IV: PHYSICAL AGING MEASUREMENTS

9 PHYSICAL AGING OF THIN AND ULTRATHIN SUPPORTED POLYMER FILMS PROBED BY FLUORESCENCE INTENSITY

9.1 Introduction

Nanoscopically confined polymers often exhibit a deviation in glass transition temperature (T_g) from that of the bulk material as discussed in Chapter 3 (Forrest 2001; Baschnagel 2003; Roth 2004; Alcoutlabi 2005; Ngai 2006). With confined, supported films, there is evidence that a depression in T_g is due to enhanced mobility near the air-polymer surface (Forrest 1996; Kajiyama 1997; Fryer 2000; Schwab 2000; Ellison 2003) while an increase in T_g is associated with attractive polymer-substrate interactions (vanZanten 1996; Fryer 2000; Park 2004) that may overwhelm the free-surface effects (Ellison 2003).

Potentially of equal scientific and technological importance as the T_g is the physical aging of nanoconfined glasses. In the case of polymers, physical aging is the structural relaxation below T_g of the chains from their non-equilibrium conformations to an overall conformational state at equilibrium (Greiner 1984; McKenna 1989; Hodge 1995; Hutchinson 1995). With bulk systems, this leads to time-dependent properties including increases in density, modulus, and yield stress and decreases in specific enthalpy, impact strength, fracture energy, and ultimate elongation (Struik 1978; Tant 1981). Besides work from the membrane literature discussed in Chapter 3, there are few reports on physical aging of confined glasses (Simon 2002; Ellison

2002a; Kawana 2003; Lu 2003; Cangialosi 2005; Fukao 2005; Vlasveld 2005; Fukao 2007). Kawana and Jones (Kawana 2003) used ellipsometry to study polystyrene (PS) supported on silicon; at 30 K below the bulk glass transition temperature (T_g(bulk)), an 18-nm-thick film exhibited aging while a 10-nm-thick film did not. Interestingly, Kawana and Jones showed that while ultrathin PS films exhibited reductions in T_g compared to T_g(bulk), they exhibited enthalpy recovery peaks (aging recovery peaks) at T_g(bulk). Lu and Nutt (Lu 2003) reported reduced enthalpy relaxation for epoxy-clay nanocomposites compared to that of neat epoxy. They suggested that the reduction in physical aging (reduced enthalpy relaxation) of the nanocomposites compared to the neat matrix was related to a reduction in molecular mobility at the epoxy-clay interface. In contrast, Simon *et al*. (Simon 2002) reported that the enthalpy relaxation of a low molecular weight glass-former confined to nanopores was faster than in bulk due to the combined effects of isochoric aging and the fact that confinement had reduced the T_g.

This chapter provides the first characterization of physical aging as a function of polymer-substrate interactions, attractive in the case of poly(methyl methacrylate) (PMMA)/silica substrate films and non-attractive in the case of PS/silica substrate films, in nanoconfined polymers. Fluorescence of mobility-sensitive or rotor probes is employed to monitor aging of ultrathin films (Chapter 4 describes the use of fluorescence to monitor physical aging of bulk polymers), similar to methods used to characterize physical aging in bulk polymer (Meyer 1990; Royal 1990; Schwab 1990; Royal 1992b; Royal 1993; Berg 2004a). As discussed in Chapter 4, rotor probes exhibit an increase in fluorescence emission intensity with a decrease in local mobility or free volume, which accompanies densification during physical aging. Royal and Torkelson (Royal 1993) found that the temperature dependence of the physical aging rate

measured by julolidene malononitrile (JMN) doped in a variety of polymers agreed qualitatively with the temperature dependence of the rate of volume relaxation (Greiner 1984). Using 4-tricyanovinyl-[N(2-hydroxyethyl)-N-ethyl]aniline (TC1), with a higher quantum yield than JMN (Hooker 1995), Ellison *et al*. (Ellison 2002a) extended this approach to monitor aging at T_g(bulk) – 25 K in ultrathin poly(isobutyl methacrylate) (PIBMA) films supported on silica. They found that the aging rate was roughly independent of thickness down to 10 nm. In the present study, TC1 is employed as a dopant (in a simple mixture with PS, without covalent attachment to the polymer) or as a label covalently attached at trace levels to PMMA. Using thin (500-nm-thick) and ultrathin (20-nm-thick) PS and PMMA films supported on silica, it is demonstrated that aging in confined systems can be suppressed at temperatures below T_g(bulk) or induced at temperatures above T_g(bulk), depending on the level of attractive polymer-substrate interactions. In addition, work in this chapter will show that confinement can affect the temperature dependence of the aging rate below T_g(bulk).

9.2 Experimental

Polystyrene was synthesized by free radical polymerization (FRP): M_n = 354,000 g/mol, M_w/M_n = 1.76 by gel permeation chromatography (GPC) relative to PS standards; onset T_g = 376 K (DSC, 10 K/min heating rate, second heating). PMMA was synthesized by FRP: M_n = 355,000 g/mol, M_w/M_n = 1.54, by GPC universal calibration; onset T_g = 394 K. The probe TC1 was synthesized using procedures in ref. (McKusick 1958). Following ref. (Deppe 1996), PMMA was synthesized incorporating a trace of TC1-labeled methacrylate monomer: M_n = 150,000 g/mol, M_w/M_n = 1.60, by GPC universal calibration; onset T_g = 393 K; 0.24 mol % TC1 label (UV-vis absorbance). Polymers were thoroughly washed and dried prior to use. (Probe

concentrations, either doped or labeled, are sufficiently low to avoid probe aggregation and to ensure that the excitation of the probes occurs evenly across the thickness of the film. A study by White *et al*. (White 2003) demonstrated that probes in polymer films did not segregate to the interfaces of ultrathin polymer films, indicating that the probes remain distributed across the thickness of the film.)

Films were spin cast from toluene solutions onto quartz slides (Hall 1998b). Doped films contained less than 0.50 wt% TC1; labeled PMMA films contained 0.24 mol % TC1. Films were dried under vacuum at T_g(bulk) + 5 K for 8 hr. Thickness was measured by profilometry, taking the average of at least four measurements. Prior to each aging experiment, the thermal history was erased by annealing at T_g(bulk) + 25 K for 20 min. Films were quenched using a temperature-controlled cell holder preset to the aging temperature. Fluorescence was recorded using a Photon Technology International fluorimeter in front-face geometry with 3.0 mm excitation and emission slits (12.0 nm bandpass) and a 480 nm excitation wavelength. Physical aging was monitored by measuring the maximum intensity (at 550-555 nm for TC1-doped PS and at 560-565 nm for TC1-labeled PMMA).

9.3 Results and Discussion

Figure 9-1 shows the emission spectrum of a 500-nm-thick, TC1-labeled PMMA film. After absorption of light and promotion of an electron to an excited singlet state, TC1 returns to the ground state by internal conversion (energy loss by vibrational and rotor motions) or by fluorescence (Loutfy 1980; Valeur 2002). The film densifies upon aging, suppressing internal conversion and yielding an increase in fluorescence intensity. The 38% increase in intensity over 460 min of physical aging at 305 K (T_g(bulk) – 88 K) exceeds that observed in various

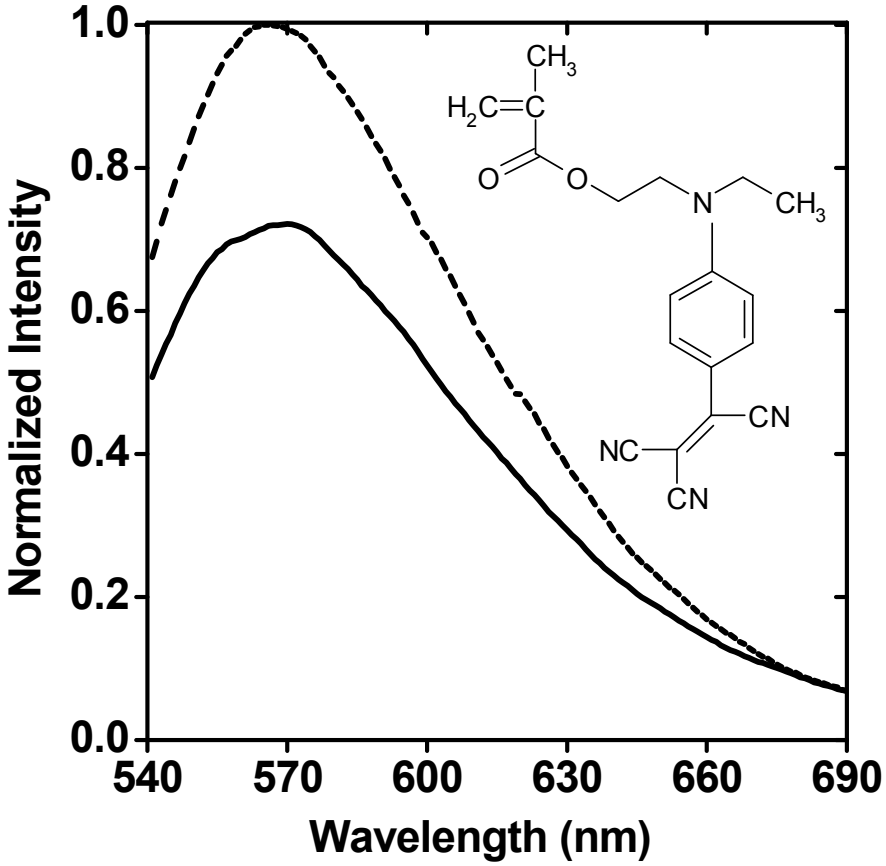

Figure 9-1: Fluorescence emission spectrum of a 500-nm-thick TC1-labeled PMMA film as a function of physical aging time after a temperature jump from above T_g(bulk) to T_g(bulk) – 88 K: 10 min (solid line); 460 min (dashed line). Inset: molecular structure of TC1-labeled methacrylate monomer used in the labeling procedure.

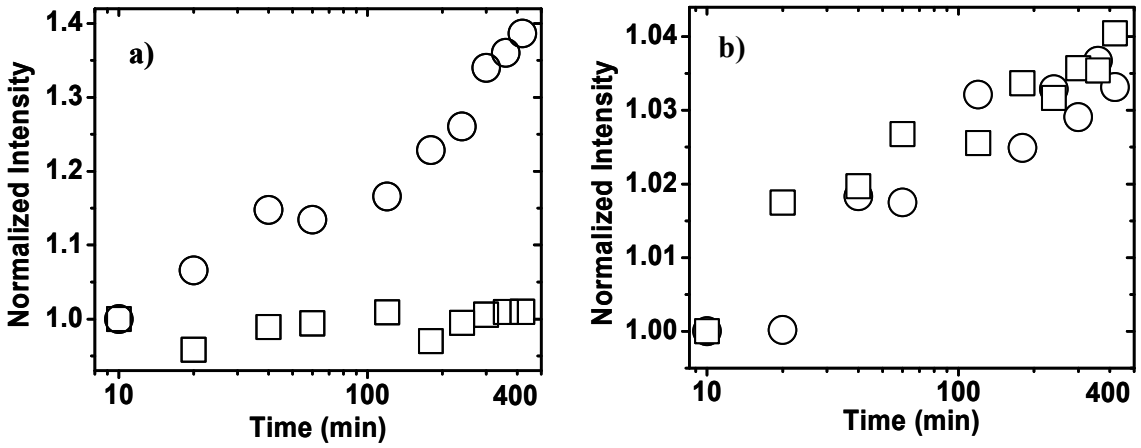

Figure 9-2: Normalized fluorescence intensity of a 500-nm-thick TC1-labeled PMMA film as a function of logarithmic aging (or annealing) time after quenching from T_g(bulk) + 25 K to the following temperature: T_g(bulk) – 88 K (305 K) (circles); T_g(bulk) + 7 K (400 K) (squares). b) Normalized fluorescence intensity of a 20-nm-thick TC1-labeled PMMA film as a function of logarithmic aging or annealing time after quenching from T_g(bulk) + 25 K to the following temperature: T_g(bulk) – 88 K (circles); T_g(bulk) + 7 K (squares).

JMN-doped polymers (Royal 1993) as well as in TC1-labeled PIBMA (Ellison 2002a). By comparison, TC1-doped PMMA yields a 6-7% increase in intensity at the same conditions used in Figure 9-1. When TC1 is used as a label instead of a dopant, its quantum yield increases as a result of the more restricted mobility associated with covalent attachment to the polymer. It is postulated that this is the reason that TC1-labeled PMMA exhibits an unusually high sensitivity to physical aging.

Figure 9-2 compares the effects of aging temperature and nanoconfinement on the physical aging of TC1-labeled PMMA. Intensities are normalized at 10 min after quenching from well above T_g(bulk) to ensure that thermal equilibrium had been achieved in the films aged at T_g(bulk) + 7 K as well as those annealed at T_g(bulk) - 88 K. When the 500-nm-thick film is aged below T_g(bulk), there is a roughly linear increase in intensity with logarithmic aging time, similar to aging monitored by enthalpy recovery (Royal 1992b) and density (Tant 1981; Greiner 1984). When the thin film is aged above T_g(bulk), there is no increase in intensity, consistent with the film being at equilibrium. (As previously illustrated from fluorescence studies used to monitor physical aging, there is some correlation between the rate of change of fluorescence intensity and the rate of change in specific volume (Royal 1993) and some correlation between the times to achieve equilibrium in systems aged slightly below T_g as quantified by fluorescence and enthalpy relaxation (Royal 1992a).)

In contrast to the thin film, the ultrathin film exhibits a much smaller, 4% increase in intensity over 460 min of aging at T_g(bulk) – 88 K. Furthermore, unlike the 500-nm-thick film, the 20-nm-thick film exhibits aging when annealed at T_g(bulk) + 7 K, a clear indication that the ultrathin film in not at equilibrium. Several factors may contribute to these effects. First, as a

result of attractive PMMA-substrate interactions, the ultrathin film has a T_g that exceeds T_g(bulk) (Keddie 1994b; Park 2004), thereby allowing for aging at temperatures above T_g(bulk). Evidence for the enhanced T_g is obtained from a break in the temperature dependence of the fluorescence intensity of the ultrathin film of TC1-labeled PMMA at 407 K or T_g(bulk) + 14 K; in contrast, the 500-nm-thick TC1-labeled PMMA exhibited a break in the temperature dependence of fluorescence intensity at 393 K, exactly the value of T_g(bulk) for the PMMA. (As discussed in Chapters 4-6, the break in the temperature dependence of the fluorescence of a trace amount of fluorescent probe or label yields accurate T_g values in both bulk and nanoconfined polymer films.) This also means that the thin and ultrathin films aged deep in the glassy state at 305 K have been aged at different temperatures relative to their own T_g values; physical aging is known to depend on quench depth below T_g (Struik 1978; Greiner 1984). Second, it is postulated that attractive polymer-substrate interactions may significantly retard structural relaxation in ultrathin films. Hydrogen-bonding interactions that can occur between the ester side groups of PMMA and the hydroxyl groups that are normally found at the surface of silica may reduce conformational relaxation processes that are associated with physical aging. This interfacial effect is expected to result in measurable differences in ultrathin films from bulk behavior observed in a 500-nm-thick film. (Chapter 10 investigates the direct impact of interfaces on physical aging of thin films.) A final potential contributing factor may be related to the effect of confinement on the sub-T_g β-relaxation, which has long been understood to be correlated with the presence of physical aging (Struik 1978). At present, there are several reports (Fukao 2001b; Hartmann 2002; Kalogeras 2004) regarding the impact of nanoconfinement on the β-relaxation of PMMA. However, due to differences in sample tacticity and substrate interaction, there is

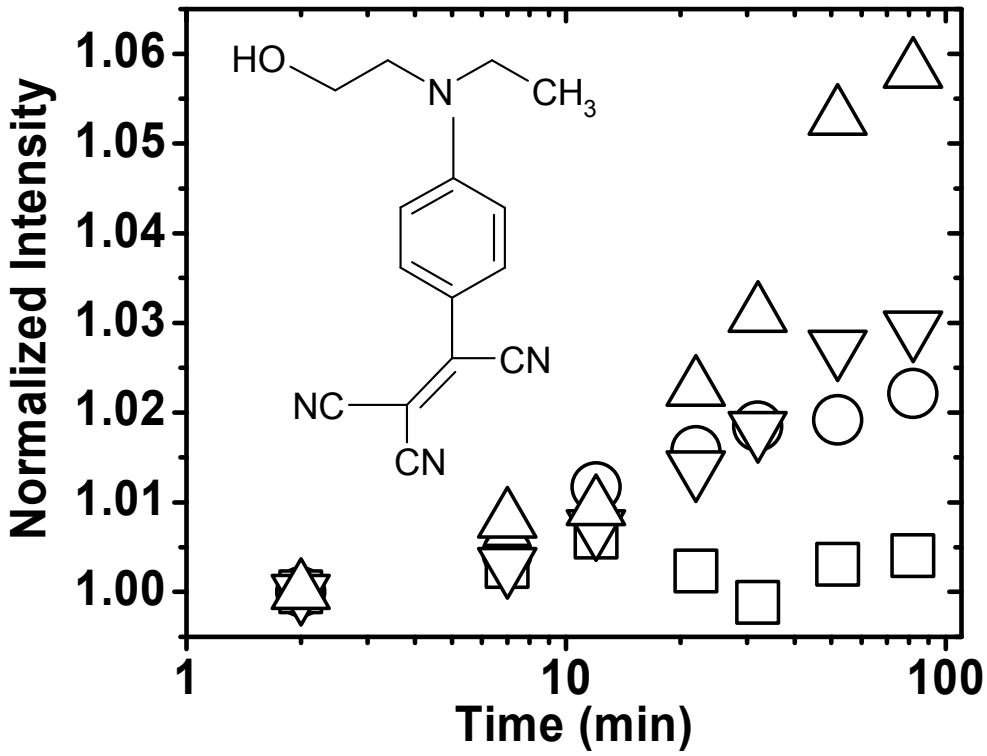

Figure 9-3: Normalized fluorescence intensity as a function of logarithmic aging or annealing time for 500-nm-thick TC1-doped PS films at T_g(bulk) – 10 K (366 K) (triangles up) and T_g(bulk) – 71 K (305 K) (triangles down) and for 20-nm-thick TC1-doped PS films at T_g(bulk) – 10 K (366 K) (squares) and T_g(bulk) – 71 K (305 K) (circles). Physical aging was initiated by a temperature jump from T_g(bulk) + 25 K to the temperature of interest. Inset: molecular structure of TC1.

not a consensus among these reports on the effect of nanoconfinement on the β-relaxation. Further study of this issue and its correlation with physical aging in confined polymers is warranted.

Figure 9-3 compares the effects of temperature and nanoconfinement on physical aging of TC1-doped PS over an 80-min aging time. In agreement with previous studies of bulk PS (Greiner 1984; Royal 1990), the 500-nm-thick film ages faster at T_g(bulk) – 10 K than at T_g(bulk) – 71 K. At T_g(bulk) – 71 K, the 20-nm-thick PS film exhibits about the same physical aging as the 500-nm-thick PS film. However, when annealed at T_g(bulk) – 10 K, the ultrathin film exhibits, within error, no physical aging. This evidence of structural equilibrium in a PS ultrathin film below T_g(bulk) agrees with findings by Kawana and Jones (Kawana 2003), who observed no structural relaxation in a 10-nm-thick PS film aged at T_g(bulk) – 30 K. The absence of physical aging in nanoconfined PS films at a temperature below T_g(bulk) may be explained by the fact that such films exhibit strong T_g depressions. Data by Ellison *et al*. (Ellison 2002b) and Keddie *et al*. (Keddie 1994a) indicate that a 20-nm-thick PS film exhibits a T_g that is depressed by 14-17 K relative to T_g(bulk); extrapolations of the same data suggest that a 10-nm-thick PS film has a T_g depressed by much more than 30 K relative to T_g(bulk).

Figure 9-4 compares the effect of aging temperature on the "fluorescence aging rate", r_f, in thin and ultrathin PMMA films; Figure 9-4a does so as a function of aging temperature whereas Figure 9-4b does so as a function of $T_g - T_{aging}$ (this is the quench depth below T_g). By analogy to specific volume aging rate (Struik 1978), r_f is defined as (Royal 1993):

$$r_f = \left(1 \Big/ F_o \right) \left(dF \Big/ d \log t_a \right) \qquad 9\text{-}1$$

where F (F_o) is fluorescence intensity at aging time t_a (at the assumed start of aging). Over the

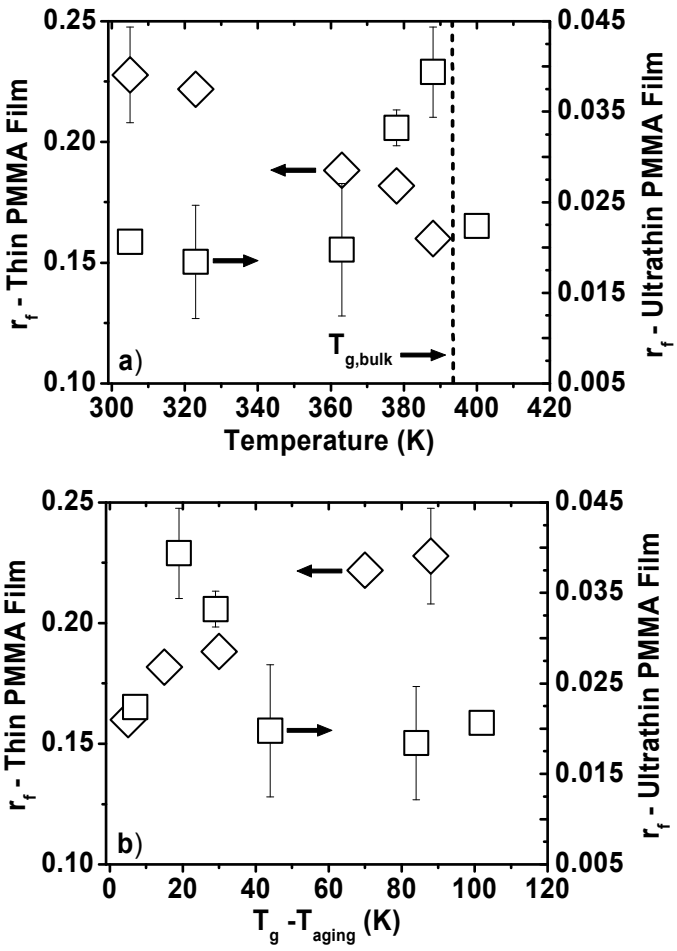

Figure 9-4: Fluorescence aging rate, r_f, as a function of physical aging temperature for thin (500-nm-thick) (diamonds) and ultrathin (20-nm-thick) (squares) TC1-labeled PMMA films. b) Fluorescence aging rate, r_f, as a function of aging quench depth below T_g for thin (500-nm-thick) (diamonds) and ultrathin (20-nm-thick) (squares) TC1-labeled PMMA films.

temperature range and aging time studied, the aging rate of the 500-nm-thick PMMA film exhibits a maximum near 305-320 K (~73-88 K below T_g of the 500-nm-thick film) and decreases with increasing temperature approaching T_g(bulk). This is in reasonable agreement with the specific volume aging rate of bulk PMMA (Greiner 1984) and characterization of r_f of bulk PMMA using JMN (Royal 1993). The aging rate changes dramatically in two ways when PMMA is confined in the 20-nm-thick film. First, below T_g(bulk), r_f is reduced dramatically relative to the 500-nm-thick film. Second, the maximum in r_f is observed near 388 K (~19 K below T_g of the 20-nm-thick film) and is more than a factor of two higher than the r_f values at 320-365 K. The vastly reduced aging rate in the ultrathin film may be rationalized by polymer-substrate interactions reducing the rate of structural relaxation. A postulate for the increase in aging rate with increasing temperature from 363 K to 388 K in the 20-nm-thick film is that the thermal energy at higher temperature may overcome some of the polymer-substrate interactions (hydrogen bonding), enhancing the structural recovery. Figure 9-4b shows that the differences in physical aging rate observed in the 500-nm-thick and 20-nm-thick films cannot be ascribed to differences in T_g with film thickness. Obviously, the maximum aging rate is observed to occur much closer to T_g in the ultrathin film, and at no value of $T_g - T_{aging}$ does the aging rate of the ultrathin film approach or exceed that of the thin film.

9.4 Conclusions

Fluorescence spectroscopy has been used to investigate for the first time the impact of interfacial effects on physical aging of thin and ultrathin polymer films. In the case of PMMA films supported on silica, for which attractive polymer-substrate interactions are exhibited, physical aging was reduced with decreasing film thickness when aged deep in the glassy state.

In the case of PS films supported on silica, for which there are no attractive polymer-substrate interactions, physical aging was found to be independent of film thickness when aged deep in the glassy state. The direct impact of interfaces on physical aging of ultrathin films will be presented in the next chapter (Chapter 10).

10 DISTRIBUTION OF PHYSICAL AGING RATES ACROSS PMMA FILMS SUPPORTED ON SILICA

10.1 Introduction

As discussed in Chapters 3, 5, and 6, there is now significant evidence that the origin of the T_g-nanoconfinement effect is related to surfaces and interfaces modifying relevant T_g dynamics in the interior regions of polymers. Chapter 9 provided the first study of the impact of interfacial effects (attractive polymer-substrate interactions versus non-attractive polymer-substrate interactions) on physical aging of polymer glasses. (See Chapter 4 for more information about physical aging.) In agreement with a previous study (Lu 2003), Chapter 9 provided evidence that attractive polymer-substrate interactions lead to reduced physical aging in nanoconfined polymer. To further understand the effect of confinement on physical aging, this chapter details the first study to directly measure physical aging at surfaces and interfaces of thin polymer films.

10.2 Experimental

Poly(methyl methacrylate) (PMMA) (M_n = 355,000 g/mol, M_w/M_n = 1.54 by gel permeation chromatography using PS standards and universal calibration) synthesized by free radical polymerization was used to examine the effects of surfaces and interfaces on physical aging. The onset T_g = 394 K, as determined by differential scanning calorimetry on second heating with a heating rate of 10 K/min. The probe 4-tricyanovinyl-[N-(2-hydroxyethyl)-N-

ethyl]aniline (TC1) was synthesized by the procedure described in Chapter 5. TC1-labeled PMMA was synthesized by reaction of MMA monomer (Aldrich) in the presence of a trace amount of TC1-labeled methacrylate monomer. By UV-Vis absorbance spectroscopy (Perkin Elmer Lambda 35), the resulting labeled PMMA contained 0.24 mol% TC1-labeled methacrylate. For the TC1-labeled PMMA, M_n = 150,000 g/mol, M_w/M_n = 1.60, and the onset T_g = 393 K. All polymers were thoroughly washed by dissolving in toluene (Fisher) and precipitating in methanol (Fisher) at least five times to remove residual monomer and placed in a vacuum oven at T_g + 15 K for 24 hr to dry.

Films were spin-cast from toluene solutions onto either quartz slides or NaCl salt disks where film thickness was controlled by changing the solution concentration and spin speed. Film thicknesses were obtained by profilometry (Tencor P10), taking the average of at least four measurements on a second film spun at the same time. For single-layer films, the solution was spin-cast onto a glass substrate and then allowed to dry in vacuum at T_g + 5 K for 8 hr. Upon receipt the glass was cleaned with a 70/20/10 ethanol/water/sodium hydroxide solution, which lightly etched the glass surface; the glass was solvent washed with toluene between experiments. Multilayer films were prepared by floating a layer from a NaCl salt disk on top of a single layer film (see experimental section in Chapter 5 for more detail on multilayer film preparation). After preparation of a multilayer film, it was placed in vacuum at room temperature for 12 hr to ensure that the film was completely dried and then annealed at T_g + 25 K for 25 min to create a completely consolidated film.

Both the TC1-labeled and unlabeled PMMA are of sufficiently high *MW* to ensure that interlayer diffusion of the polymer chains during our annealing procedures above T_g (to create a

consolidated film and to erase thermal history prior to physical aging) is at most several nanometers. For the conditions employed in this study, the total diffusion time (45 min total at 419 K) is much less than the polymer chain disengagement time. The disengagement time (τ_D) may be calculated by the equation $\tau_D = (2R_g^2)/(\pi^2 D_s)$ where R_g is the radius of gyration of the polymer and D_s is the bulk self-diffusion coefficient. For the TC1-labeled PMMA at ~ 418 K (the lowest molecular weight and fastest diffusing component used in these studies), R_g ~12.0 nm and $D_s \sim 3\text{x}10^{-18}$ cm^2/s (Shearmur 1998) resulting in τ_D = 1620 min. Since the disengagement time (or reptation time) is substantially longer than the annealing time above T_g (annealing time is only 3% of the disengagement time), the maximum interlayer penetration distance is significantly less than R_g (~12 nm), with a reasonable estimate being several nanometers or less. In addition, the polymer used in this study (150,000 g/mol TC1-labeled PMMA and 355,000 g/mol unlabeled PMMA) is of significantly higher molecular weight than that used for estimation (Shearmur 1998) (100,000 g/mol and 127,000 g/mol) of the interlayer diffusion.

Steady-state fluorescence emission spectra were taken as a function of aging time using a Photon Technology International fluorimeter in a front-face geometry (with emission at 90^o relative to excitation and the film at an angle of 28^o relative to excitation) with 3.0 mm excitation and emission slits (6 nm bandpass). The wavelength used to excite the TC1 was 480 nm. The emission intensity was monitored at the emission maximum as a function of aging time and then normalized to unity 15 min after the quench (well after thermal equilibrium had been achieved). Prior to all structural relaxation experiments, the thermal history was erased by annealing at T_g(bulk) + 25 K for 20 min. Films were then quenched using a temperature-controlled cell holder preset to the aging temperature. The T_g value reported for an individual layer was

determined using the procedure outlined in Chapter 5.

10.3 Results and Discussion

Figure 10-1 shows the increase in normalized fluorescence intensity during physical aging at 305 K of a 400-nm-thick TC1-labeled PMMA film (T_g(bulk) = 393 K). As described in Chapter 9, monitoring the peak intensity as a function of aging time provides a measure of physical aging (Royal 1993). The inset in Figure 10-1 plots the normalized intensity as a function of logarithmic aging time. In agreement with specific volume and enthalpy relaxation measurements during physical aging of bulk polymer (Greiner 1984; Hutchinson 1995), the fluorescence intensity is roughly linear with logarithmic aging time. The intensity increases 16% (after a quench from 418 K to 305 K) as aging time increases from 15 min to 200 min. In analogy to physical aging rates based on volume relaxation (Greiner 1984; Royal 1993; Hutchinson 1995), it is possible to define a physical aging rate, R_f, based fluorescence intensity (see equation 9-1). Aging rates are a nonlinear function of temperature and typically exhibit a maximum. The maximum aging rate is a result of the competition between thermodynamic driving forces for aging, which is highest at temperatures well below T_g, and the sub-segmental mobility which increases with temperature (Greiner 1984).

The impact of film thickness on the physical aging rate as defined by equation 9-1 is provided in Table 10-1. (Results in Table 10-1 were obtained by fitting data similar to the inset of Figure 10-1 equation 9-1.) Table 10-1 shows that the aging rate at 305 K increases by a factor of approximately four upon increasing film thickness from 35 nm to 300 nm. For film thicknesses $\geq$ 300 nm, R_f is thickness-independent and equal to the physical aging rate of 0.15 obtained for a several-μm-thick TC1-labeled PMMA film, representative of bulk. (All values of

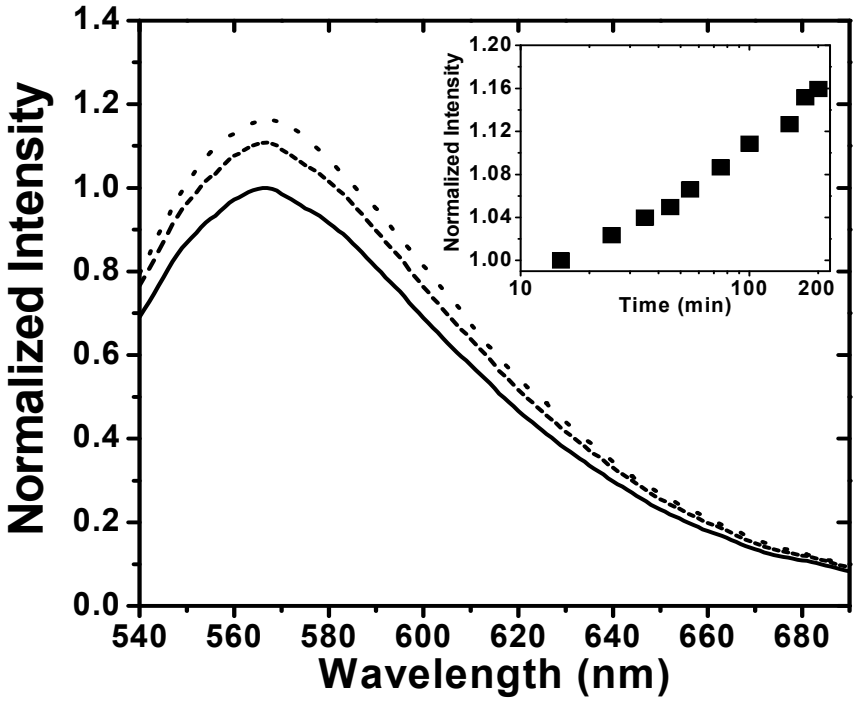

Figure 10-1: Physical aging in single-layer PMMA films monitored via fluorescence. Fluorescence emission spectrum of a 400-nm-thick TC1-labeled PMMA film after quenching from 418 K to 305 K taken after 15 min (solid curve), 100 min (dashed curve) and 200 min (dotted curve) of aging time. Inset: Normalized fluorescence intensity at the maximum as a function of aging time.

Table 10- 1: Fluorescence physical aging rate defined by equation 9-1 as a function of film thickness for TC1-labeled PMMA at 305 K.

Film Thickness (nm)	Physical Aging Rate
35	0.04
65	0.07
250	0.10
300	0.15
400	0.15
500	0.15

the relaxation rate, R_f, which is unitless, are determined via equation 9-1 with aging time t_a in units of minutes.) While the sensitivity of TC1 fluorescence to aging is tied to volume relaxation (minute increases in local density near TC1 reduce the rate of nonradiative decay from the TC1 excited state, resulting in enhanced fluorescence (Royal 1993)), the physical aging rate determined via TC1 fluorescence is amplified by orders of magnitude relative to that determined from volume relaxation. For example, the specific volume relaxation rate, R_v, of bulk PMMA is ~ 0.00055 during aging at 305 K (Greiner 1984). Over an aging time from 20 min to 200 min, this means that bulk PMMA at 305 K undergoes a 0.055% reduction in specific volume. Relative to R_v, R_f is approximately a factor of 275 greater during physical aging at the same conditions.

Multilayer films are used to explore the influence of a confining substrate and free surface on glassy-state relaxation. Figure 10-2a provides physical aging data from a 25-nm-thick TC1-labeled PMMA middle layer sandwiched between two 1000-nm-thick PMMA layers. Figure 10-2b provides structural relaxation data from a 25-nm-thick TC1-labeled free-surface layer sitting atop a 1000-nm-thick PMMA underlayer. Figure 10-2c provides physical aging data from a 25-nm-thick TC1-labeled substrate layer sandwiched between a 1000-nm-thick PMMA overlayer and the substrate. At 305 K the physical aging rate is greatest in the middle layer, yielding $R_f = 0.14$, within error equal to that in bulk. The physical aging rate is reduced by a factor of two at the free surface. The substrate layer exhibits the slowest relaxation rate of 0.01 at 305 K, indicating that physical aging is almost totally suppressed next to the substrate.

At an aging temperature of 388 K, the free-surface layer exhibits almost no physical aging. This near absence of aging is consistent with the notion that much of the 25-nm-thick

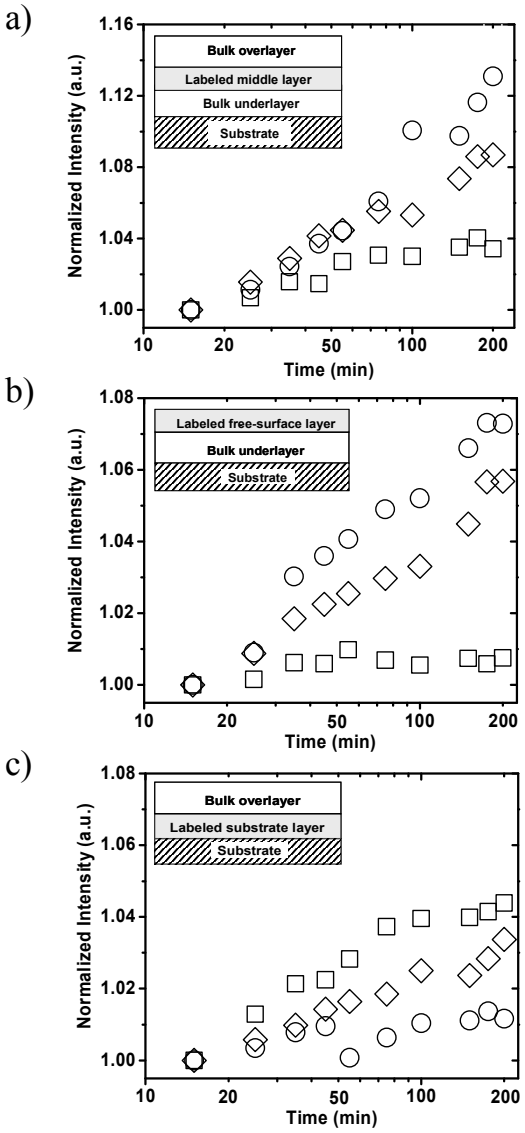

Figure 10-2: Physical aging monitored by fluorescence in multilayer PMMA films with 25-nm-thick TC1-labeled layers and 1000-nm-thick unlabeled bulk overlayers/underlayers. Insets show schematics of the film arrangement. The normalized fluorescence intensity as a function of aging time for (a) a trilayer film and (b) and (c), two bilayer films aged at various temperatures: 305 K (circles), 348 K (diamonds) and 388 K (squares). (Data points are averages of two runs.)

a)

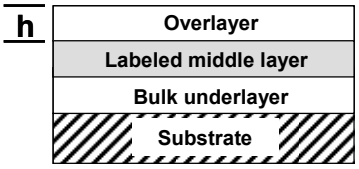

b)

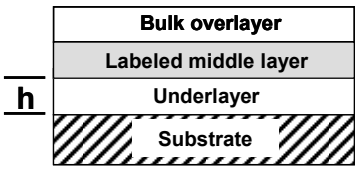

PMMA Overlayer Film Thickness (h) (nm)	Aging Rate
0	0.07
25	0.08
100	0.11
250	0.15

PMMA Underlayer Film Thickness (h) (nm)	Aging Rate
0	0.01
25	0.10
100	0.12
250	0.14

Figure 10-3: Physical aging rates at 305 K for PMMA multilayer films with a 25-nm-thick TC1-labeled layer. The trilayer films characterize physical aging rates at known distances from free surfaces and substrate interfaces. Bulk overlayers and underlayers are 700-nm-thick for trilayer films and 1000-nm-thick for bilayer films. Fluorescence physical aging rate of a TC1-labeled layer placed (a) at the free surface or at distances below the free surface (25 nm, 100 nm, and 250 nm) and (b) at the substrate or at distances from the substrate (25 nm, 100 nm, and 250 nm). (Results in (a) and (b) are averages of two runs with standard deviations of 0.01 or less.)

free-surface layer has a T_g that is equal to or below 388 K and suggests there is a rubbery equilibrium layer at the free surface (Ellison 2003). As the aging temperature is decreased, physical aging becomes more pronounced at the free surface but is always substantially less than that in the interior of the film. In contrast, the substrate layer exhibits an increasing physical aging rate with increasing temperature and at 388 K has nearly the same physical aging rate as the middle layer. The additional thermal energy at higher temperatures approaching T_g likely reduces the ability of interfacial hydrogen bonds to suppress physical aging.

Further understanding of the impact of confinement on physical aging is obtained via buried-layer experiments, where 25-nm-thick TC1-labeled middle layers are placed a distance from the free surface or substrate interface. Figure 10-3 shows results from trilayer studies at 305 K. Figure 10-3a indicates that as a 25-nm-thick layer is moved from the free surface to a buried layer, there is a smooth increase in relaxation rate, from 0.07 at the free surface to 0.08, 0.11 and 0.15 when buried 25, 100, and 250 nm, respectively, below the free surface. Within error (± 0.01), the physical aging rate in the layer buried 250 nm below the free surface is identical to bulk. Figure 10-3b reveals a sharp increase in the physical aging rate from 0.01, when a 25-nm-thick layer is located next to the substrate, to 0.10 when located 25 nm from the substrate. Further displacement results in a smooth increase in physical aging rate, from 0.12 to 0.14 when the layer is located 100 nm and 250 nm, respectively, from the substrate. Thus, the substrate and free surface affect the physical aging rate in supported PMMA films over similar distances, but the substrate interactions perturb the structural relaxation to a greater extent.

Figure 10-4 provides a schematic of the surface- and interface-induced gradients in relaxation that is consistent with the present results. At a distance of at least 100 nm but less

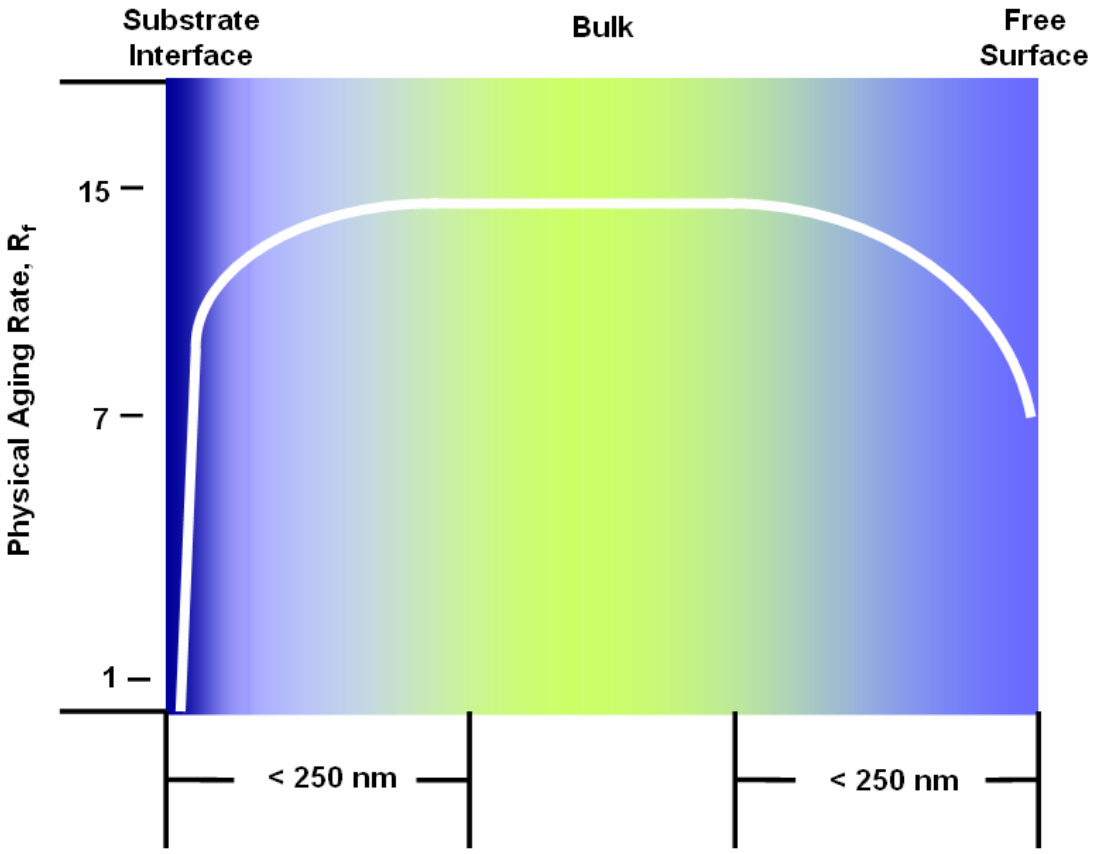

Figure 10-4: Illustration representing the effect of the substrate interface and the free surface on the distribution of physical aging rates in PMMA at 305 K. Both the substrate interface and the free surface perturb the physical aging rate at least 100 nm but less than 250 nm into the film interior. Relative to bulk behavior, a 25-nm-thick layer at the free surface exhibits a factor-of-two reduction in physical aging rate. In contrast, a 25-nm-thick layer at the substrate interface exhibits a factor-of-15 reduction in physical aging rate relative to bulk, i.e., almost a complete arresting of physical aging.

than 250 nm from the free surface, there begins a smooth factor-of-two reduction in structural relaxation rate between the bulk and the free surface. At a distance of at least 100 nm but less than 250 nm from the substrate interface, there begins a factor-of-15 reduction in relaxation rate from the bulk to the interface, the vast majority of which occurs within 25 nm of the interface. The origins of the perturbations near the free surface and substrate differ. Near the free surface, there is enhanced cooperative segmental mobility and a reduced T_g (Ellison 2003), resulting in a reduced thermodynamic driving force for physical aging. At the substrate interface, hydrogen bonds suppress cooperative segmental mobility and lead to an increased T_g (Keddie 1994b; Park 2004). Hence, there is an enhanced thermodynamic driving force for structural relaxation. However, the interfacial hydrogen bonds also suppress molecular motions associated with physical aging, which deep in the glassy state can result in near elimination of physical aging within 25 nm of the substrate and retardation of physical aging relative to bulk at a distance of at least 100 nm from the substrate. The manner in which retardation in physical aging occurs over distances of at least 100 nm from a substrate or free surface is not yet understood, but it may relate to the percolation of slowly relaxing dynamic heterogeneities that has been hypothesized as an explanation for the effect of confinement on T_g (Long 2001; Baljon 2004; Merabia 2004) and that is expected to result in long-range changes in dynamics induced by surfaces and interfaces (Long 2001). There is no theory or model that directly addresses the effect of confinement on physical aging.

Finally, it is important to note that the distribution of physical aging rates obtained in this study is distinct from the distribution of T_g values in supported PMMA films (see Chapter 5). Relative to T_g(bulk) (= 393 K), a 25-nm-thick layer at the free surface of a 1000-nm-thick film

exhibits a 5-6 K reduction in T_g while a 25-nm-thick layer at the substrate of a 1000-nm-thick film exhibits a 12 K increase in T_g. However, the T_g of a 25-nm-thick layer that is located 100 nm from either the substrate interface or the free surface in an 800-nm-thick multilayer film is identical within error (+/- 1 K per sample) to the T_g of bulk TC1-labeled PMMA. Thus, while interfacial effects perturb physical aging rates 100 nm from the substrate, they do not perturb T_g values over the same length scale. This is possibly due to the fact that T_g is associated with larger scale motions of cooperative segmental mobility (α-relaxation processes) while physical aging may be associated with different, smaller scale dynamics (β-relaxation processes) (Struik 1978). Experiments need to be developed to characterize directly how α- and β-relaxation dynamics near T_g are separately affected by surfaces and interfaces. These results suggest that surface and interfacial effects may potentially be tailored to control the structural relaxation of high performance materials that have a large fraction of polymer near surfaces and interfaces, as with polymer nanocomposites (see Chapter 12).

10.4 Conclusions

A fluorescence/multilayer spectroscopy technique was used for the first time to directly measure the physical aging rate in the interior of a film, at the free surface of a film, and at the polymer-substrate interface of a film. Relative to that of bulk PMMA, the physical aging rate was reduced by a factor of two at the free surface and a factor of fifteen at the substrate interface, when aged at 305 K. Increasing the physical aging temperature towards T_g(bulk) resulted in a weakening of interfacial effects on physical aging. The distribution in aging rates extended more than 100 nm into the film interior, a distance greater than that over which interfaces affected T_g.

11 FLUORESCENCE INTENSITY RATIO AS A NOVEL METHOD TO MONITOR PHYSICAL AGING

11.1 Introduction

Results presented in Chapters 9 and 10 illustrated the dramatic impact of nanoconfinement on physical aging of thin polymer films. In the previous two chapters, physical aging was measured by monitoring the fluorescence emission intensity of 4-tricyanovinyl-[N-(2-hydroxyethyl)-N-ethyl]aniline (TC1) either doped into or labeled to a polymer as a function of aging time. In agreement with volume dilatometry measurements, enthalpy relaxation measurements, and mechanical measurements, the fluorescence emission intensity increased roughly linearly on a logarithmic time scale (Struik 1978; Tant 1981; Greiner 1984). As described in Chapter 9, a fluorescence physical aging rate could be determined from a plot of fluorescence intensity versus the logarithm of the aging time. Previous work by Royal and Torkelson (Royal 1990; Royal 1992a; Royal 1992b; Royal 1992c; Royal 1993), using similar probes as TC1, showed that the temperature dependence of the fluorescence physical aging rate and the time required to reach equilibrium as determined by fluorescence intensity were in agreement with volume dilatometry and calorimetry results.

A limiting factor of fluorescence intensity measurements is that they are dependent on sample geometry, probe concentration and light source. In addition, because of the temperature dependence of the fluorescence emission intensity of TC1 and other rotor probes (the slope of the glassy-state line is greater than the slope of the liquid-state line), the theoretical equilibrium

glassy-state line cannot be determined by extrapolating the liquid-state line into the glassy state. As a result, the fluorescence intensity at equilibrium in the glassy state cannot be determined unless equilibrium is achieved (Li 2006), limiting the analysis of physical aging.

In this chapter, a ratio of fluorescence intensities (absolute quantity, independent of sample geometry, probe concentration and light source) is used for the first time to characterize physical aging in bulk and nanoconfined polymer films. The use of fluorescence intensity ratio allows for the extrapolation of the liquid-state line into the glassy state; thus, the extent of physical aging can be determined. This chapter provides the first study to compare quantitatively the extents of physical aging toward equilibrium in bulk and ultrathin polymer films and to provide evidence that glass formation in rapidly quenched, ultrathin films is closer to isochoric (constant volume) than isobaric. Using a charge resonance probe, van den Berg *et al.* (Berg 2006) showed that the emission wavelength at maximum intensity can be used to monitor physical aging in bulk polymer. Here an intramolecular charge transfer (ICT) probe is used to measure physical aging by monitoring the change in shape of the emission spectrum via a ratio of emission intensities below and above the wavelength of maximum emission.

11.2 Experimental

4-tricyanovinyl-[N-(2-hydroxyethyl)-N-ethyl]aniline (TC1)-labeled PMMA [M_n = 509,000; M_w/M_n = 1.67 by gel permeation chromatography (universal calibration with polystyrene standards); T_g = 394 K by differential scanning calorimetry, second heat at 10 K/min, 1.37 mol% (UV-vis absorbance)] was synthesized by the procedure outlined in Chapter 5. The TC1-labeled PMMA was washed by multiple dissolving/precipitating steps in toluene/methanol and dried in vacuo at 410 K for 24 hr. Films were spin coated from toluene solutions onto silica

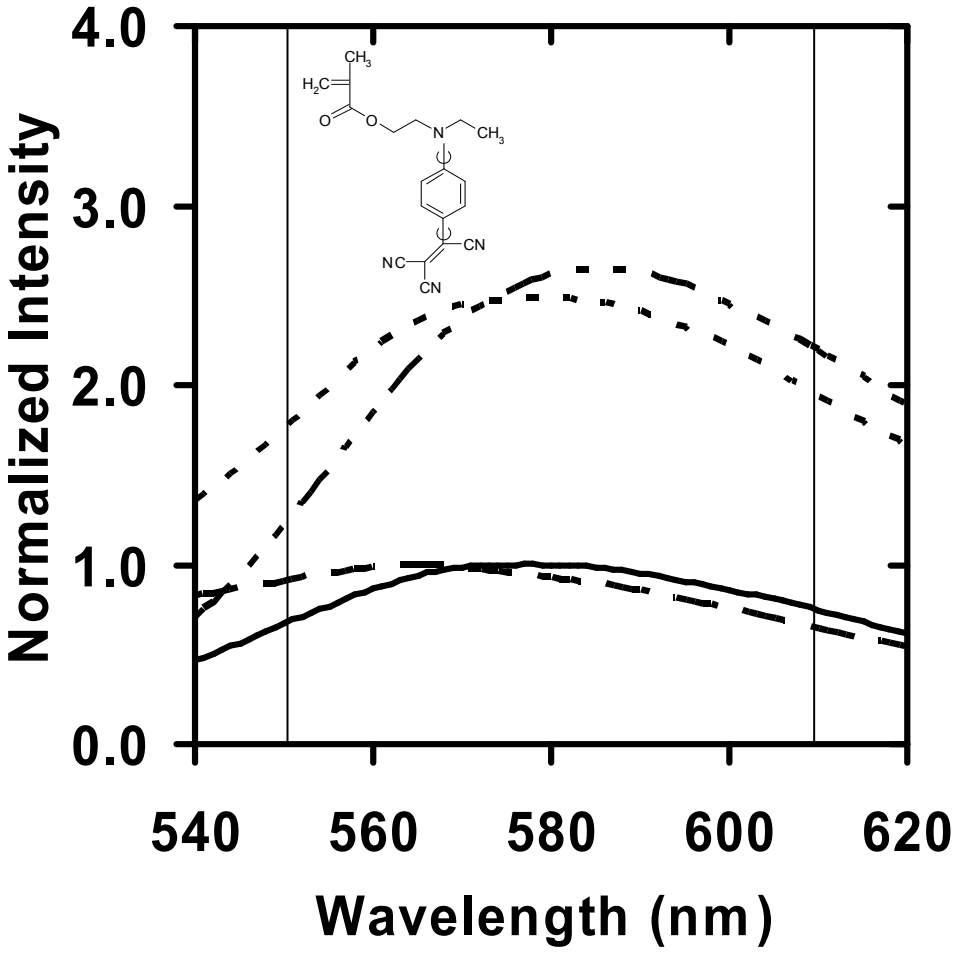

Figure 11-1: Fluorescence spectrum of bulk and 35-nm-thick TC1-labeled PMMA films as a function of temperature: 423 K (solid curve: bulk film, dashed curve: 35-nm-thick film) and 348 K (dashed/dotted curve: bulk film, dotted curve: 35-nm-thick film). Data normalized to maximum intensity at 423 K. Vertical lines at 550 nm and 610 nm. Inset: Molecular structure of TC1-labeled methacrylate used in making TC1-labeled PMMA.

and dried in vacuo at 400 K for 8 hr. Thicknesses were measured with a Tencor P10 profilometer.

The T_gs were determined by measuring fluorescence as a function of temperature upon cooling. Samples were annealed at T_g + 25 K for 20 min and cooled in 5 K increments, holding at each temperature for 5 min prior to taking an emission scan. Physical aging was monitored by measuring fluorescence as a function of aging time. A Photon Technology International fluorimeter was used with excitation at 480 nm and emission monitored from 540 nm to 620 (or 650) nm. Before an aging measurement, thermal history was erased by holding the film at T_g + 25 K for 20 min and rapidly quenching (quench time ~ 60 sec) to the aging temperature, T_{aging}. Greater detail about the use of fluorescence spectroscopy to measure T_g and monitor physical aging can be found in Chapters 4, 5, and 9.

11.3 Results and Discussion

The temperature dependences of fluorescence for bulk and 35-nm-thick TC1-labeled PMMA films are shown in Figure 11-1. A decrease in temperature yields an increase in intensity and a spectral red shift. The increase in intensity is due to a densification of the nanoscale medium surrounding the TC1 probe, with a slightly denser environment yielding a higher intensity due to a reduced rate of non-radiative decay. The red shift is due to combined effects of densification and the ICT nature of TC1. Upon excitation, TC1 exhibits an instantaneous change in its dipole moment due to the presence of an electron-donating group conjugated to an electron-withdrawing group (Valeur 2002). Hence, excited-state TC1 is not in equilibrium with its surrounding medium. If the surrounding medium reorients within the TC1 excited-state lifetime (~ 1 ns), then TC1 goes to its ICT state, which is of reduced energy,

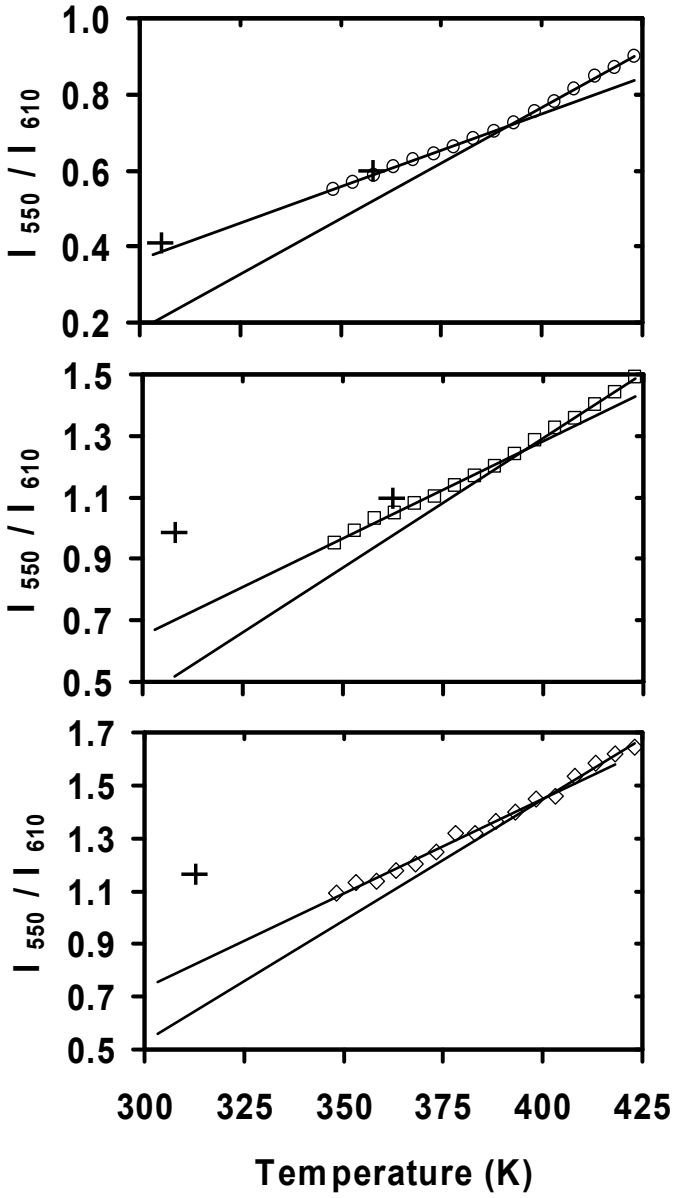

Figure 11-2: I_{550} / I_{610} of TC1-labeled PMMA as a function of temperature: (○) bulk film, (□) 35-nm-thick film and (◇) 20-nm-thick film. Intersection of linear fits in the rubbery and glassy states provides a measure of T_g. Crosses show intensity ratio values of quenched glass prior to aging.

resulting in a spectral red shift. (Reorientation is a function of medium polarity; resulting in ICT dyes being solvatochromatic (see Chapter 4).) With decreasing temperature, the nanoscale medium surrounding TC1 is less mobile. Other things being equal, this would reduce medium reorientation during the TC1 excited-state lifetime, resulting in a spectral blue shift. However, also accompanying a decrease in temperature is an increase in the TC1 excited-state lifetime, which increases the time scale for medium reorientation to result in an ICT state. On balance, the effect of increasing excited-state lifetime with decreasing temperature is sufficient to yield an increase in reorientation of the surrounding medium leading to relaxation of TC1 to an ICT state and a spectral red shift.

The effect of temperature in shifting the spectrum can be quantified using a ratio of any two intensities at wavelengths well below and above the spectral maximum (accurate T_gs were determined for intensity ratios at wavelengths ranging from 540–570 nm / 610–650 nm). As shown in Figure 11-1, the temperature dependence of intensity at 550 nm is smaller than that at 610 nm. The temperature dependence of the ratio of intensity at 550 nm to intensity at 610 nm (I_{550} / I_{610}) is plotted in Figure 11-2 for bulk, 35-nm-thick, and 20-nm-thick TC1-labeled PMMA films. It must be noted that I_{550} / I_{610} at a given temperature increases with decreasing thickness, indicating a spectral blue shift with confinement. Thus, there is less medium reorientation during the excited-state lifetime of TC1 in ultrathin films than in the bulk, yielding less relaxation to an ICT state. This effect is consistent with hydrogen bond formation at the PMMA-silica interface, which affects ultrathin film behavior. For all films, I_{550} / I_{610} exhibits linear temperature dependences in the rubbery and glassy states with the intersection yielding a measure of T_g. From the data in Figure 11-2, the T_g(bulk) is 392 K, T_g of the 35-nm-thick film is 396 K, and T_g

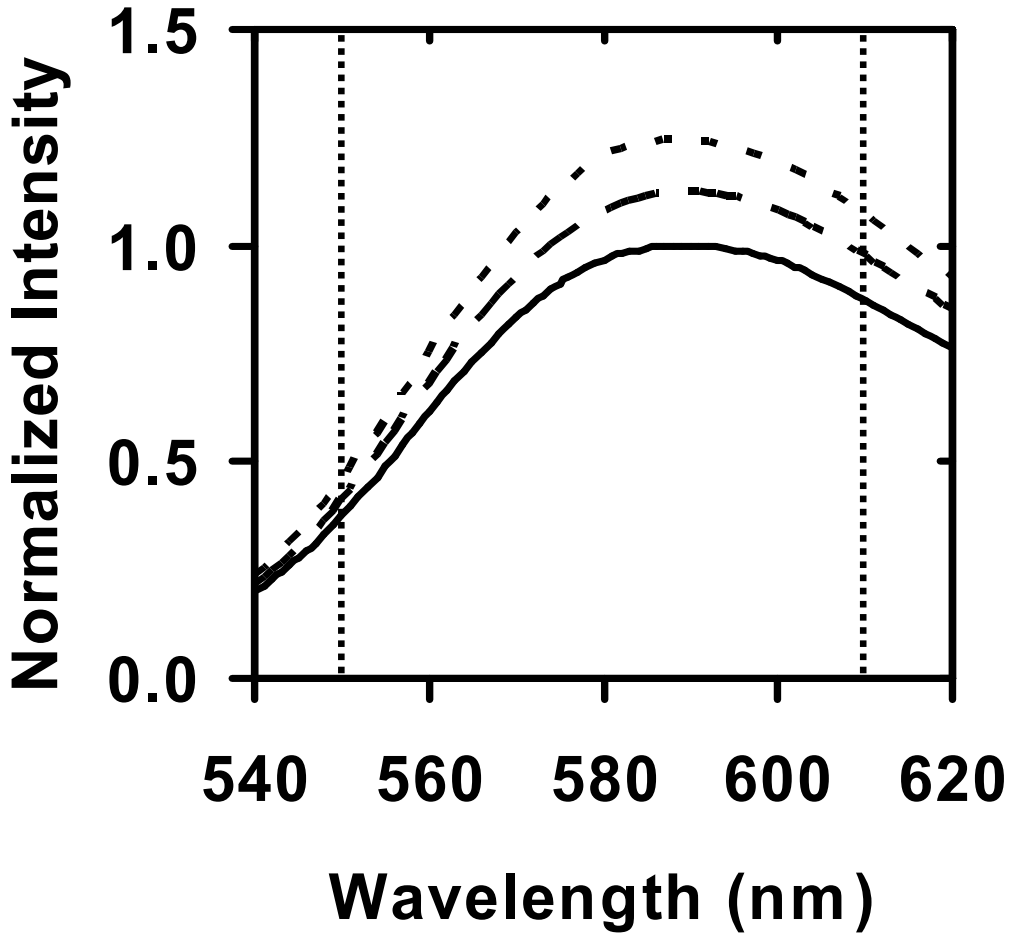

Figure 11-3: Fluorescence spectrum of bulk TC1-labeled PMMA at $T_{g,film} - T_{aging}$ = 87 K as a function of aging time: 40 min (solid curve), 1860 min (dashed curve), and 3780 min (dotted curve). Data normalized to maximum intensity at 40 min. Vertical lines at 550 nm and 610 nm.

of the 20-nm-thick film is 400 K. The increase in T_g with decreasing thickness is in agreement with previous studies of PMMA supported on silica (Keddie 1994b; Fryer 2000; Roth 2003; Park 2004). Similar results have been obtained using the temperature dependence of fluorescence intensity to define T_g in various polymer films (Ellison 2002a; Ellison 2002b; Ellison 2004b; Ellison 2005; Mundra 2006; Rittigstein 2006; Rittigstein 2007; Mundra 2007a; Roth 2007a; Mundra 2007b; Roth 2007b). However, there is an advantage in using intensity ratio to define T_g as it is an intensive variable that is independent of sample geometry, excitation intensity, dye and concentration as previously mentioned. Recently, Jager and co-workers (Berg 2006) determined the T_g of bulk polymers by monitoring the temperature dependence of the wavelength at maximum intensity, also an intensive variable, of a charge resonance probe.

The linear natures of the temperature dependences of I_{550} / I_{610} above and below T_g indicate that, for a given film thickness, a correlation can be made with the temperature dependence of specific volume, which is linear in both the rubbery and glassy states (Greiner 1984). Thus, the rubbery-state intensity ratio may be extrapolated to lower temperature to provide the values of I_{550} / I_{610} of the apparent equilibrium state. By comparing the change in I_{550} / I_{610} during aging to the maximum change defined by the difference in I_{550} / I_{610} of the quenched and apparent equilibrium glasses, a measure can be obtained of the extent of aging toward equilibrium.

Figure 11-3 shows an increase in intensity and a slight spectral red shift with aging of bulk TC1-labeled PMMA. Densification during aging restricts the internal rotational motions of TC1, increasing de-excitation of its excited state by fluorescence. The red shift can be attributed to an increase in the TC1 excited-state lifetime, similar to that with decreasing temperature (see

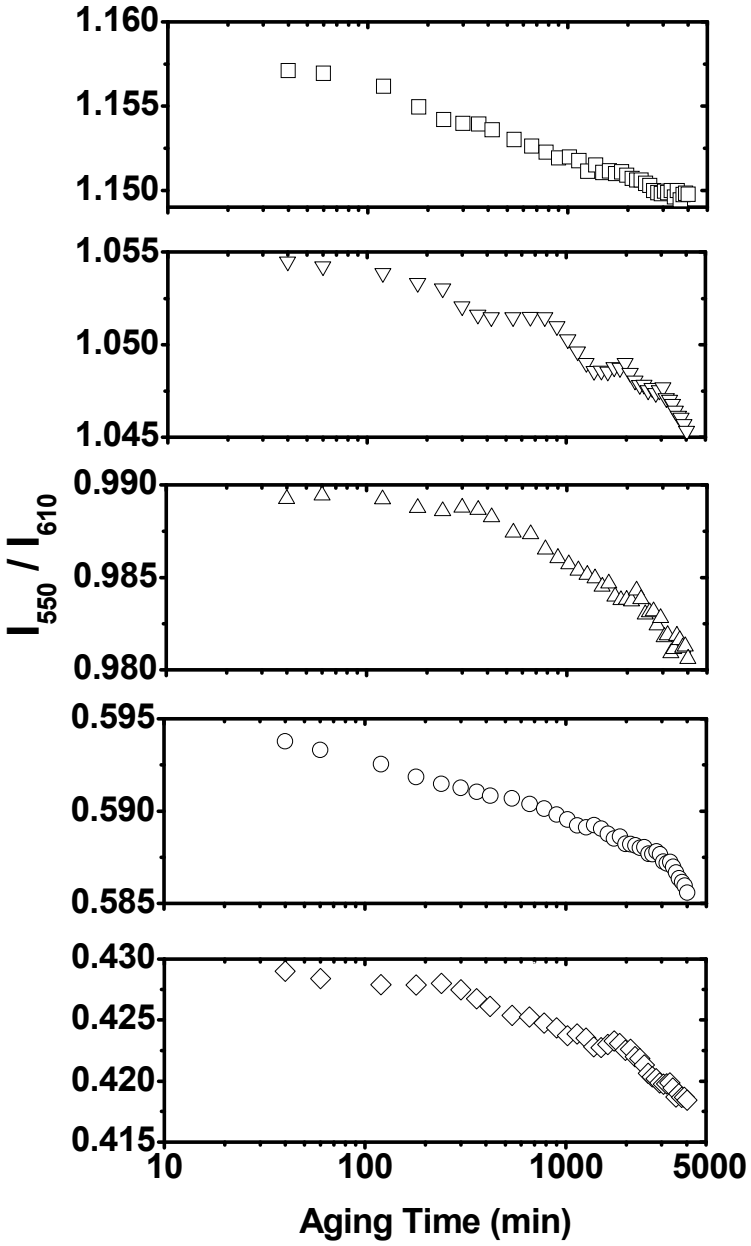

Figure 11-4: I_{550} / I_{610} of TC1-labeled PMMA as a function of logarithmic physical aging time: (◇) bulk film, $T_{g,film} - T_{aging}$ = 87 K; (○) bulk film, $T_{g,film} - T_{aging}$ = 34 K; (△) 35-nm-thick film, $T_{g,film} - T_{aging}$ = 87 K; (▽) 35-nm-thick film; $T_{g,film} - T_{aging}$ = 34 K; and (□) 20-nm-thick film, $T_{g,film} - T_{aging}$ = 87 K.

Chapters 4 and 9 for more information on the sensitivity of TC1 to physical aging).

Figure 11-4 shows I_{550} / I_{610} as a function of logarithmic aging time for bulk, 35-nm-thick, and 20-nm-thick films at $T_{aging} = T_{g,film}$ - 87 K and bulk and 35-nm-thick films at $T_{aging} = T_{g,film}$ - 34 K. The intensity ratios in all films show an initial near invariance followed by roughly linear decreases. The shapes of the relaxation curves obtained by fluorescence are qualitatively consistent with those obtained by volume relaxation of bulk polymer (Struik 1978; Greiner 1984; Hutchinson 1995). By analogy to volume relaxation aging rate (Struik 1978; Greiner 1984), a fluorescence physical aging rate based on intensity ratio measurements can be defined by

$$r_f = -\left(1/F_o\right)\left(dF/d\log t_a\right) \qquad 11\text{-}1$$

where F_o is the initial intensity ratio and F is the intensity ratio at t_a. (The difference in equations 9-1 and 11-1 is a negative sign. With increasing physical aging time, fluorescence intensity increases while fluorescence intensity ratio decreases.) At $T_{aging} = T_{g,film}$ - 87 K and for aging times over which I_{550} / I_{610} changes in Figure 11-4, the fluorescence aging rate is 0.090 for the bulk film, 0.060 for the 35-nm-thick film and 0.040 for the 20-nm-thick film (calculations of aging rates are done with aging time in units of minutes). The decrease in aging rate with confinement is consistent with results presented in Chapters 9 and 10 that determined aging rates using fluorescence intensity. As illustrated in Chapter 10, the reduction in aging rate with confinement for PMMA films supported on silica is a result of interfacial effects. Compared to the interior of a bulk film, the aging rate is reduced at the substrate-polymer and air-polymer interfaces. The reduction in aging rate may result from reduced mobility caused by attractive interactions at the substrate-polymer interface and in part from a reduced thermodynamic driving force for aging caused by a decrease in T_g at the air-polymer interface (see Chapter 10 for more

detail).

As indicated by the crossbars in Figure 11-2, rapidly quenched glasses form differently in bulk and ultrathin films. The intensity ratios of the quenched, bulk glasses at T_{aging} fall very close to the glassy state line (and its extrapolation) determined during the T_g measurement (slowly cooled by 5 K jumps every 5 min). However, the intensity ratios of the quenched, ultrathin films at $T_{aging} = T_{g,film}$ - 87 K are much higher than the extrapolated glassy state line. Since there is a linear relationship of intensity ratio with temperature in both the rubbery and glassy states of the films measured at slow cooling rate, this indicates that intensity ratio is related to specific volume in each film. Hence, when an ultrathin film is rapidly vitrified, the glass is formed with a higher specific volume than the glass formed at slow cooling rate. However, the bulk film has a nearly identical specific volume when formed with a rapid quench or a slow cooling rate.

Close inspection of Figure 11-2 indicates that the rapidly quenched, 35-nm-thick and 20-nm-thick PMMA films result in glass formation that is closer to isochoric than isobaric. This is evident from the moderate difference between the intensity ratios of the 35-nm-thick PMMA film at T_g ($I_{550} / I_{610} = 1.205$) and the quenched 35-nm-thick PMMA film at T_{aging} ($I_{550} / I_{610} = 0.989$). The difference in intensity ratios of 0.216 is less than 40% of the difference in intensity ratios of the glass at T_g and the glass extrapolated from the T_g measurement data to $T_{aging.}$ This implies that, relative to its value at T_g, the decrease in specific volume at T_{aging} experienced by the quenched glass is less than 40% that of the glass made by slow cooling. It should be noted that Simon *et al.* (Simon 2002) reported isochoric glass formation of ortho-terphenyl (o-TP) confined in nanopores. They found differences in the equilibrium state (at T_{aging}) in confined and

Table 11- 1: Physical aging characteristics of TC1-labeled PMMA films aged for 4000 min.

Film Thickness	Bulk Film		35 nm		20 nm
T_{aging} (K)	305	358	309	362	313
$T_{g,film} - T_{aging}$ (K)	87	34	87	34	87
Initial Quenched Glassy State I_{550} / I_{610} at T_{aging}	0.429	0.594	0.989	1.054	1.157
Apparent Equilibrium State I_{550} / I_{610} at T_{aging}	0.210	0.519	0.475	0.922	0.575
Aged Glass I_{550} / I_{610} after 4000 min	0.418	0.585	0.981	1.045	1.150
Extent of Aging toward Apparent Equilibruim State	5.0 %	12.0 %	1.6 %	6.8 %	1.2 %

bulk o-TP due to the presence of a negative pressure in the confined state. In the present study, when an ultrathin film vitrifies during slow cooling, it is under isobaric conditions as revealed by Figure 11-2. However, when the ultrathin film is rapidly quenched to T_{aging}, the glass formation is more isochoric, which may result from attractive interactions at the PMMA-silica interface.

The data in Figures 2 and 4 can be used to compare quantitatively the extent of aging toward the apparent equilibrium state in bulk and ultrathin films (see Table 11-1). The initial departure from the apparent equilibrium state at T_{aging} is given by the difference in I_{550} / I_{610} between the initial quenched glassy state and the apparent equilibrium state; when aged at $T_{aging} = T_{g,film}$ - 87 K, this difference is 0.219 in bulk, 0.514 in the 35-nm-thick film, and 0.582 in the 20-nm-thick film. After 4000 min aging time, the aged glass intensity ratio is reduced by 0.011 in bulk, 0.008 in the 35-nm-thick film, and 0.007 in the 20-nm-thick film. Thus, the bulk film ages 5.0%, the 35-nm-thick film 1.6%, and the 20-nm-thick film 1.2% of the extent needed to reach their apparent equilibrium states. Table 11-1 reveals a similar trend for the bulk and 35-nm-thick films at $T_{aging} = T_{g,film}$ - 34 K. Other things being equal, the greater departure from equilibrium due to the more isochoric formation of the ultrathin films suggests that ultrathin films should age more quickly than the bulk film; however, the extent of aging toward equilibrium is reduced in ultrathin films. Thus, the attractive substrate interactions that result in ultrathin films undergoing more isochoric glass formation and having a greater departure from equilibrium also result in the films having reduced aging through restricted segmental mobility.

11.4 Conclusions

This chapter illustrated for the first time that a ratio of fluorescence intensities could be used to monitor physical aging in bulk and nanoconfined polymer films. In agreement with

Chapters 9 and 10, the rate of physical aging for PMMA films supported on silica decreased with decreasing film thickness. An advantage of using a ratio of fluorescence intensities over fluorescence intensity measurements to monitor physical aging is that the extent of physical aging toward the theoretical equilibrium glassy state can be determined. With confinement, it was shown that the extent of physical aging was reduced. The reduction in the extent of aging is believed to result from retarded structural relaxation and the isochoric formation of the glass in the confined state, both a result of attractive polymer-substrate interactions.

12 ORIGIN OF THE MOLECULAR-SCALE SUPPRESSION OF PHYSICAL AGING IN NANOCONFINED POLYMER

12.1 Introduction

As illustrated in Chapters 9, 10, and 11, nanoscale confinement can have a strong impact on the sub-T_g relaxation "physical aging" of polymer films. As previously defined, physical aging is the observed spontaneous change in properties as a function of annealing time below T_g (Struik 1978; Kovacs 1981; Greiner 1984; McKenna 1989; Hutchinson 1995). In bulk polymers, this leads to time-dependent properties including increases in density, modulus, and yield stress and decreases in specific enthalpy, impact strength, fracture energy, and ultimate elongation. The molecular motions associated with physical aging are believed to be the small scale subsegmental flexible groups in the polymer backbone or the flexible side groups (Struik 1978). These motions are considered to be the manifestation of the β relaxation process in polymers (see Chapter 2 for a description of the β relaxation process).

As described in Chapter 3, the effects of nanoconfinement on physical aging of polymers are not unique to the thin-film geometry (Lu 2003; Rittigstein 2006; Rittigstein 2007). As with ultrathin polymer films, confinement effects in nanocomposites lead to a substantial reduction in the physical aging response of the polymer. For example, enthalpy relaxation has been reported to be nearly a factor of four smaller during aging of a ten parts per hundred epoxy-clay nanocomposite compared to that of neat epoxy (Lu 2003). Also, it was recently shown that

physical aging deep in the glassy state can be nearly arrested in 0.4 vol% silica-poly(2-vinyl pyridine) (P2VP) nanocomposites (Rittigstein 2006).

This chapter describes the first study to characterize quantitatively the effect of confinement both in strongly suppressing physical aging and in modifying the polymer α and β relaxation dynamics, i.e., cooperative segmental mobility associated with T_g and small-scale, sub-segmental secondary relaxations, respectively. In this study, silica-PMMA nanocomposites, in which 10-15 nm diameter silica nanospheres, present at 0.4 vol% or less, were used. Fluorescence spectroscopy was used to provide a measure of physical aging rate while dielectric relaxation spectroscopy was used to characterize the polymer α and β relaxation dynamics. At room temperature deep in the glassy state, the presence of 0.4 vol% silica nanospheres dispersed in PMMA reduced the physical aging rate by more than a factor of 20. The results of our dielectric studies indicated that a reduction in the strength of the β relaxation dynamics (in the case of PMMA, the mobility of the ester side groups) was the molecular-scale origin of this remarkable suppression of physical aging by confinement effects involving attractive polymer-substrate or polymer-nanofiller interactions.

12.2 Experimental

12.2.1 Fluorescence Spectroscopy

The fluorescence probe 4-tricyanovinyl-[N-(2-hydroxyethyl)-N-ethyl]aniline (TC1) was synthesized following the proceddure outlined in Chapter 5. PMMA was synthesized by free radical polymerization, incorporating a trace level of TC1-labeled methacrylate monomer (M_n = 150,000 g/mol, M_w/M_n = 1.60, by gel permeation chromatography using universal calibration

with polystyrene standards; 0.24 mol% TC1-labeled methacrylate monomer incorporated in the polymer, by UV-vis absorbance). The T_g was measured by differential scanning calorimetry (DSC) (Mettler-Toledo DSC 822, second heat, onset method, 10 K/min heating rate) and also via fluorescence, which were found to yield an identical value of 393 K (T_g(bulk)). Silica nanospheres (colloidal silica in methyl ethyl ketone, Nissan Chemical Industries, reported diameter of 10-15 nm) were used as received.

Thin films of neat PMMA (with TC1 label) and of silica-PMMA (with TC1 label) nanocomposites were prepared by spin coating (Hall 1998b) dilute solutions of labeled PMMA in methyl ethyl ketone (MEK), with or without nanofiller, on quartz slides. Solutions containing nanofiller were sonicated (Branson 1200 sonicator) for 40 min prior to spin coating. Resulting films were at least 1 μm thick as determined using a Tencor P10 profilometer. Films were dried in a chemical fume hood for at least 2 days at room temperature prior to performing fluorescence measurements. The T_g of the 0.4 vol% silica-PMMA nanocomposite system was determined to be 399 K, as previously reported (Rittigstein 2006). This method of preparing silica-polymer nanocomposites yields well-dispersed silica nanoparticles in polymers such as P2VP and PMMA (Rittigstein 2006).

Before each physical aging experiment, the thermal history was erased by annealing at 423 K for 1 hr. Films were quenched to the aging temperature of 296 K using a temperature-controlled cell holder preset to the aging temperature. Fluorescence was measured using a Photon Technology International fluorimeter in front-face geometry with 2.5 mm excitation and emission slits (5 nm band-pass) and an excitation wavelength of 480 nm. Fluorescence was monitored by measuring the maximum emission intensity, 560-565 nm for neat PMMA (with

TC1 label) and 584-588 nm for the 0.4 vol% silica-PMMA (with TC1 label) nanocomposite, as a function of aging time after quenching the films from 423 K to the aging temperature of 296 K.

12.2.2 Dielectric Spectroscopy

Poly(methyl methacrylate) was synthesized by free radical polymerization (M_n = 355,000 g/mol, M_w/M_n = 1.54, by gel permeation chromatography using PS standards and universal calibration). The T_g(bulk) = 394 K, as determined by DSC (Mettler-Toledo DSC 822, second heat, onset method, 10 K/min heating rate). Silica nanospheres are identical to those described above in section 12.2.1.

Films of neat PMMA and PMMA nanocomposites were prepared by spin coating (Hall 1998b) dilute solutions of PMMA in MEK, with or without silica nanospheres, onto Al-deposited glass substrates. Solutions containing nanofiller were sonicated for 40 min prior to spin coating. The films were then annealed in vacuum for 12 hr at 413 K. After annealing, Al was vacuum deposited on top of the films to serve as an upper electrode. Vacuum deposition of Al might increase the temperature of the films locally, which could cause dewetting. However, this issue is avoided in the present study since all films are greater than 3 μm in thickness. Film thickness (d) was measured using profilometry (Tencor P10) by taking the average of three measurements near the top electrode of the sample.

Dielectric relaxation spectroscopy measurements were performed using an LCR meter (HP4284A) in the frequency range from 20 Hz to 1 MHz. The sample cell was cycled from 253 K to 433 K at a constant rate of 0.5 K/min. Dielectric measurements during heating and cooling were performed repeatedly. All data were reproducible after the first heating and cooling cycles. Data are reported from the second cooling cycle.

The geometrical capacitance is given by $C_o = \varepsilon_o(S/d)$, where ε_o is the permittivity of vacuum and S is the effective area of the electrode (S = 1.55 X 10^{-5} m^2). From the geometrical capacitance, the loss component of the permittivity of a film (ε'') can be determined from $C'' = \varepsilon'' C_o$, where C'' is the loss component of the complex electrical capacitance.

12.3 Results and Discussion

12.3.1 Fluorescence Spectroscopy

Figure 12-1a shows the emission spectrum of a bulk, neat TC1-labeled PMMA film at two physical aging times after quenching from above T_g to an aging temperature of 296 K. After absorption of light and promotion of an electron to an excited electronic state, the 'rotor' probe TC1 returns to the ground state by internal conversion (energy loss by vibrational and rotor motions) or fluorescence (see Chapters 4, 9, and 10). Slight densification of the material occurs upon aging, reducing the internal conversion and yielding an increase in fluorescence intensity.

Figure 12-1b compares the change in the fluorescence of the TC1 labels as a function of logarithmic physical aging time for films of neat PMMA and 0.4 vol% silica-PMMA nanocomposites at 296 K. At this aging temperature (which is $T_{g,bulk}$ – 97 K for the PMMA film and $T_{g,bulk}$ – 103 K for the nanocomposite film), the neat PMMA film shows a ~31% increase in fluorescence intensity over 8 hr. However, there is a much reduced effect of aging time on fluorescence in the 0.4 vol% silica-PMMA nanocomposite, which exhibits a ~1% increase in fluorescence intensity over 8 hr.

From the plot in Figure 12-1b, a fluorescence physical aging rate, R_f, can be defined in analogy with a physical aging rate based on volume relaxation, R_v, as described in Chapter 9 (see

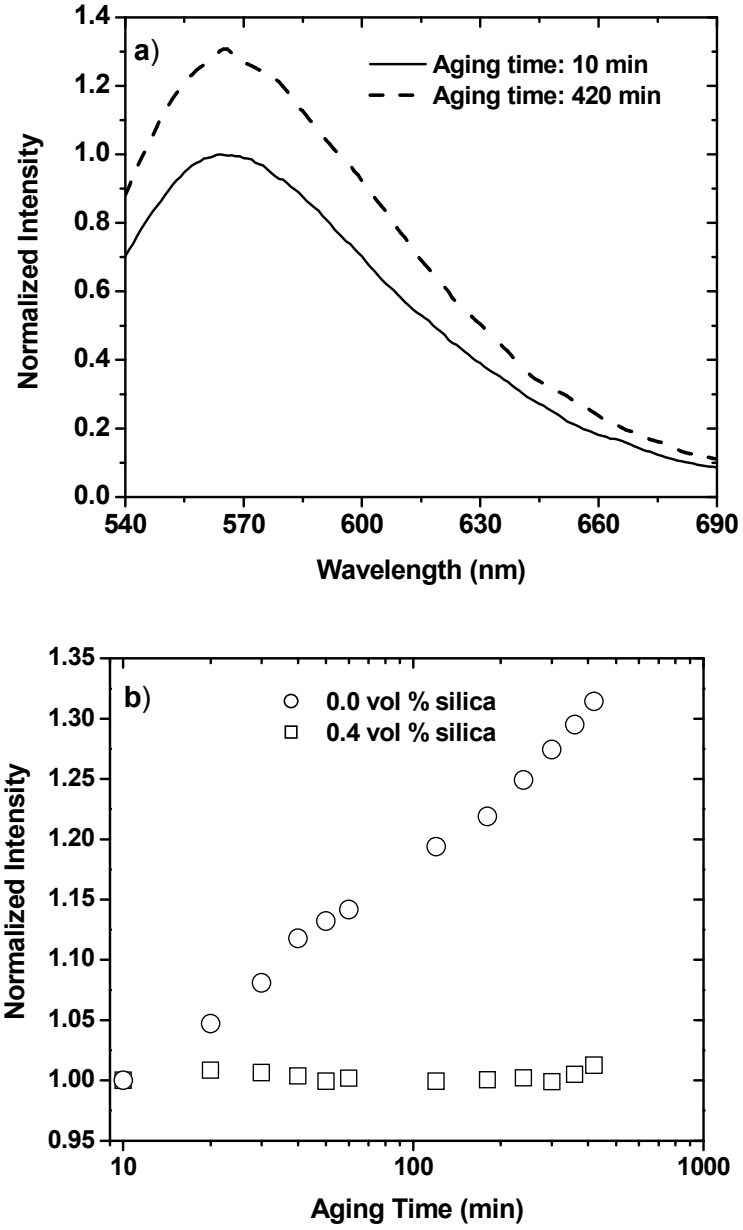

Figure 12-1: **a)** Fluorescence emission spectrum of a bulk TC1-labeled PMMA film after quenching from 423 K to 296 K taken after aging times of 10 min (solid curve) and 420 min (dashed curve). **b)** Normalized fluorescence intensity as a function of logarithmic aging time for both neat PMMA (circles) and 0.4 vol% silica-PMMA nanocomposite (squares) aged at 296 K.

equation 9-1). Using equation 9-1, we find that the physical aging rate at 296 K is reduced by more than a factor of 20 in the 0.4 vol% silica-PMMA nanocomposites relative to neat PMMA. Specifically, with the units of t_a in minutes, $R_f = 0.19$ in PMMA, while $R_f = 0.008$ in the 0.4 vol% silica-PMMA nanocomposite. This extraordinary suppression in aging rate is consistent with a previous report of arrested physical aging in 0.4 vol% silica-P2VP nanocomposites (Rittigstein 2006) and with results presented in Chapters 9 and 10 that examined the physical aging rates, both average values and their distributions, across thin PMMA films supported on one side by silica slides. Such effects of arrested or suppressed aging are not found in ultrathin PS films (see Chapter 9). The results strongly indicate that the arrested or suppressed physical aging is correlated to hydrogen bonds that can form between hydroxyl units that are naturally on the surface of silica slides or silica nanoparticles and groups on the polymer (*e.g.*, the oxygen atoms in the ester side group in PMMA or the nitrogen atom in the ring structure in P2VP). When attractive polymer-substrate or polymer-nanofiller interactions are not possible, as in the case of PS, which contains no atoms that will form hydrogen bonds with hydroxyl groups, no suppression of aging is evident within experimental error.

While the correlation between attractive polymer-nanofiller (substrate) interactions and suppressed physical aging is clear, there has been no molecular-level explanation for how physical aging rates can be so strongly suppressed throughout polymer nanocomposites (thin films), including regions where the polymer segments are some tens of nanometers removed from the polymer-nanofiller (substrate) interface. Dielectric relaxation spectroscopy measurements of silica-PMMA nanocomposites are used to address this issue.

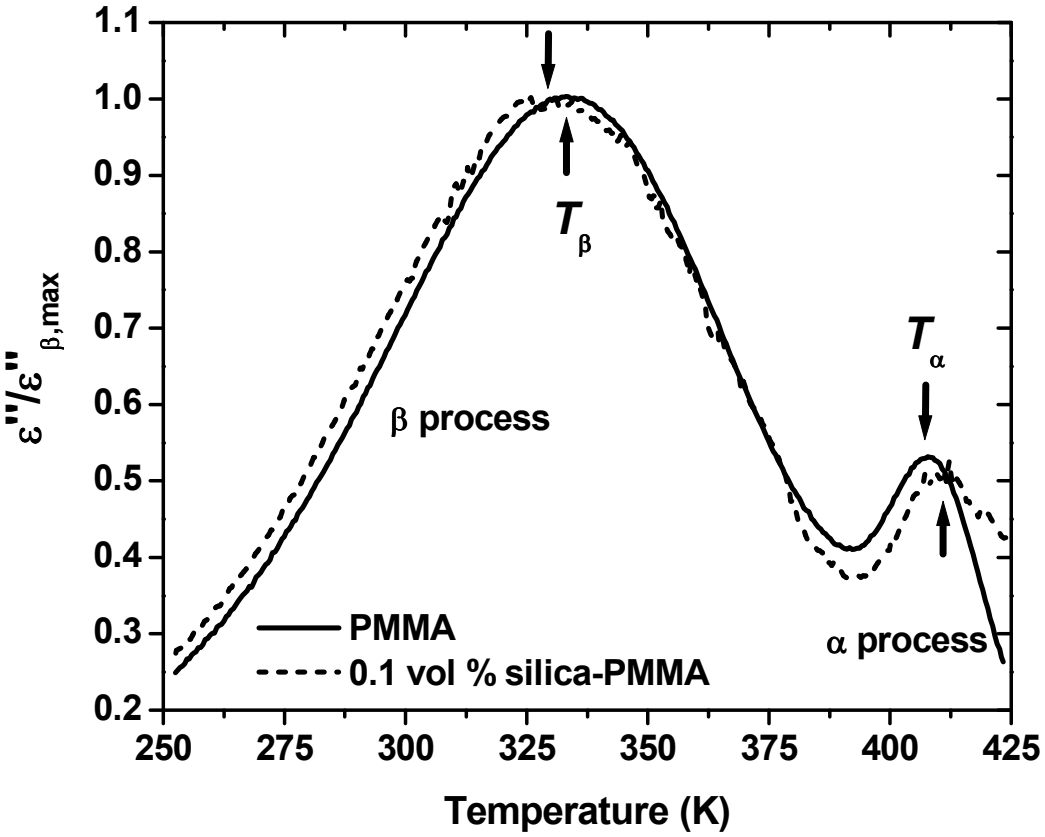

Figure 12-2: Temperature dependence of the imaginary component of the complex dielectric constant at 100 Hz for both neat PMMA (solid curve) and 0.1 vol% silica-PMMA nanocomposite (dashed curve). The vertical axis is normalized to the maximum value of each curve.

12.3.2 Dielectric Spectroscopy

Figure 12-2 shows the temperature dependence of the imaginary component of the complex dielectric constant (ε'') at a fixed frequency (f = 100 Hz) for both a neat PMMA and a 0.1 vol% silica-PMMA nanocomposite. The value of ε'' is normalized to the maximum value for each curve. Due to the presence of both the α and β processes, the imaginary part of the dielectric constant exhibits two maxima, with the peak temperatures denoted as T_α and T_β. In general, the molecular motions associated with the α process are attributed to cooperative segmental motions of the polymer, while the motions of the β process are associated with smaller, sub-segmental flexible groups in the polymer chain or flexible side groups (Struik 1978; Fukao 2001a). As can be seen in Figure 12-2, the values of both T_α and T_β are impacted by the addition of silica nanofiller into PMMA. When f = 100 Hz, T_α = 409 K and T_β = 331 K for neat PMMA, and T_α = 411 K and T_β = 329 K for 0.1 vol% silica-PMMA nanocomposite. In addition, the widths of both the α and β processes increase slightly with the addition of nanofiller. (To obtain the most precise values employing data of the type in Figure 12-2, the peak temperatures of the α and β processes and their widths ΔT_α and ΔT_β were extracted by fitting the imaginary component of the dielectric constant as a function of temperature by the sum of two Lorentzian functions (Fukao 2000): $\varepsilon_i''/(1+[(T-T_i)/\Delta T_i]^2)$ where $i = \alpha,\beta$.)

For ultrathin PMMA films supported between two Al electrodes, it has been reported that the value of T_α decreases with decreasing film thickness (Hartmann 2002; Fukao 2001a). In these studies the decrease in T_α with confinement was attributed to interfacial regions with enhanced dynamics compared to the bulk. Here, the films are at least 3 μm thick; therefore,

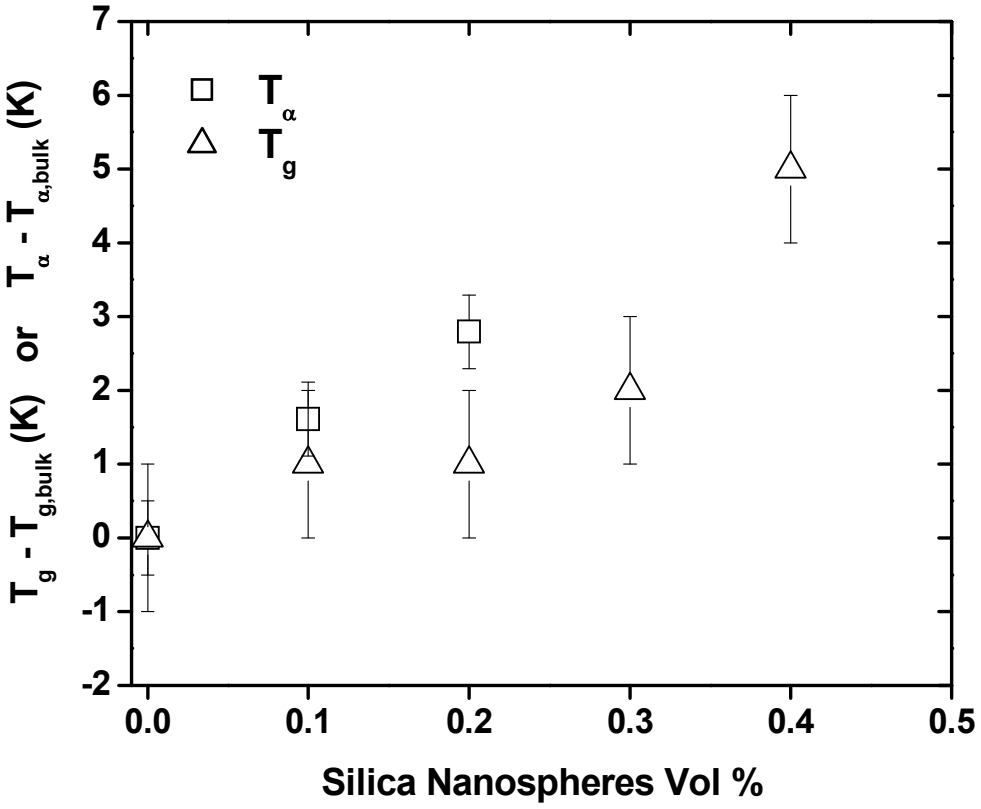

Figure 12-3: Effect of silica nanosphere content on T_α and T_g of PMMA. T_g data are from (Rittigstein 2006). For neat PMMA, T_α = 409 K and T_g = 393 K.

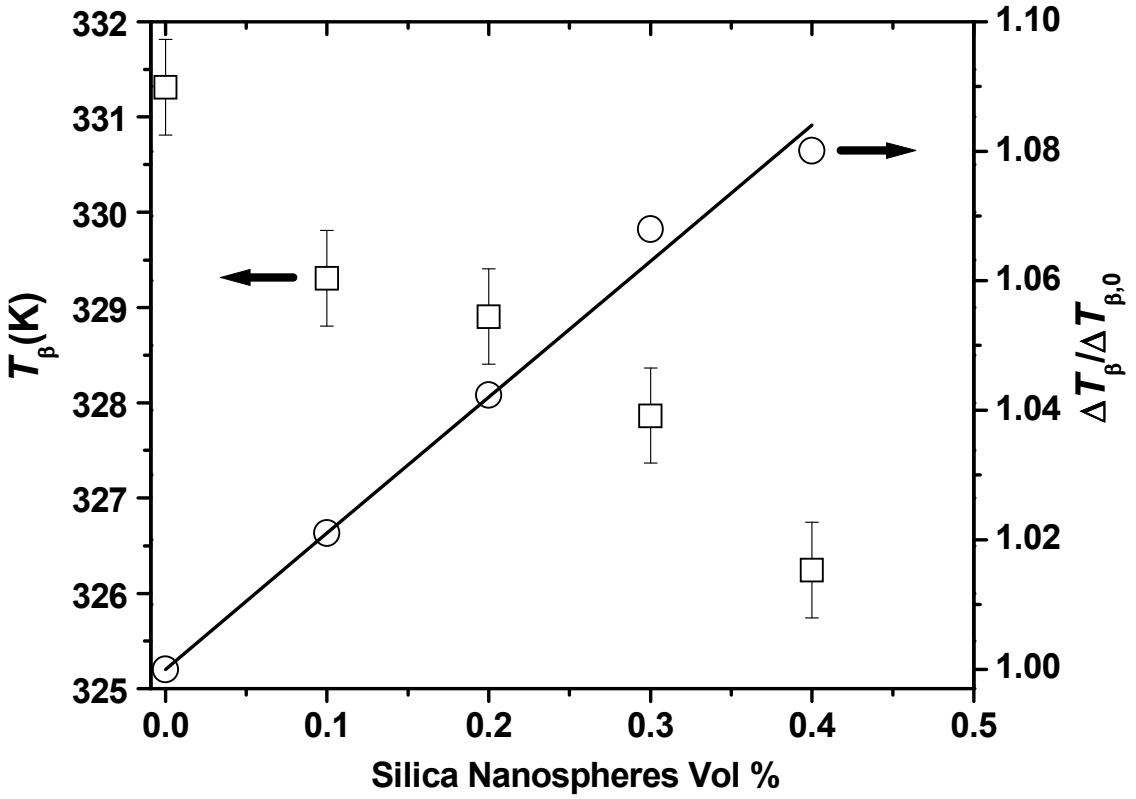

Figure 12-4: Effect of silica nanosphere content on T_β (squares) and the width of the β process normalized to that present in neat PMMA $\Delta T_\beta/\Delta T_{\beta,0}$ (circles). The solid line is a fit of the data to $\Delta T_\beta(\phi) = \Delta T_{\beta,0}(1+\phi/a)$, where $\Delta T_{\beta,0}$ = 47 K, a = 4.7 vol%, and ϕ is the volume percent of silica nanofiller in the nanocomposite.

the increase in T_α is related to the presence of the silica nanospheres. The increase in T_α with a simultaneous decrease in T_β of silica-PMMA nanocomposites is consistent with earlier reports of an increase in T_α and a decrease in T_β of PMMA confined in silica nanopores (Kalogeras 2004; Kalogeras 2005). For ultrathin atactic PMMA films supported between two Al electrodes, a decrease in T_β and broadening of T_β have been reported, both of which are consistent with the results presented in Figure 12-2 (Fukao 2001a).

Figure 12-3 compares the effects of increasing silica content, i.e., increasing confinement, on T_α data obtained in the present study with T_g data determined previously using fluorescence spectroscopy (Rittigstein 2006). (Due to enhanced direct-current conductivity in 0.3 vol % and 0.4 vol % silica-PMMA nanocomposites, the α relaxation peak was broadened, making it impossible to accurately determine T_α.) Both T_α (f = 100 Hz) and T_g increase slightly with the addition of silica nanofiller into PMMA. The increases in T_α and T_g with increasing silica content are consistent with previous reports of ultrathin PMMA films supported on silica substrates that show an enhanced T_g relative to the bulk value (Keddie 1994b; Fryer 2000) and with data presented in Chapters 5 and 6. The increases in T_α and T_g may result from a reduction in mobility due to the hydrogen bonding interactions of the PMMA ester groups and the hydroxyl groups on silica (Keddie 1994b).

The impact of silica nanofiller content on T_β and ΔT_β is given in Figure 12-4. The width of the β process for each nanocomposite, ΔT_β, is normalized to that of neat PMMA, $\Delta T_{\beta,0}$. With increasing silica content, i.e., increasing confinement, the width of the β process increases while T_β slightly decreases. These findings are consistent with earlier work reported for thin PMMA films (Fukao 2001a) and PMMA confined in silica nanopores (Kalogeras 2004; Kalogeras 2005).

The solid line in Figure 12-4 is a fit of the data to the following equation

$$\Delta T_{\beta}(\phi) = \Delta T_{\beta,0} \cdot \left(1 + \frac{\phi}{a}\right) \qquad 12\text{-}1$$

where $\Delta T_{\beta,0}$ = 47 K, a = 4.7 vol%, and ϕ is the volume percent of silica nanofiller in the nanocomposite. This equation is analogous (with a/d replacing ϕ/a) to one used earlier (Fukao 2001a) in analyzing the β process in thin and ultrathin PMMA films. Our value of $\Delta T_{\beta,0}$ obtained from the fit agrees well with that measured for the neat PMMA film employed in this study and that obtained in earlier work on thin and ultrathin PMMA films (Fukao 2001a).

The broadening of ΔT_{β} with increasing silica content is likely related to an addition to the polymer dynamic heterogeneity inherently present in neat PMMA resulting from the attractive polymer-silica interactions reducing the mobility of some PMMA ester groups. This is consistent with Figure 12-2 which shows that addition of silica to PMMA leads to some broadening in the low temperature side of the β process. The slight reduction in T_{β} (shift to lower temperature of the peak maximum in Figure 12-2) with increasing silica content may be related to the *faster* component of the β process having a relatively more intense contribution to the overall relaxation process, since slower components of the relaxation may be hindered or completely immobile as discussed below (Kalogeras 2004).

Finally, in order to examine the impact of nanofiller content on the strength of the β process, ε'' is evaluated as a function of temperature at a fixed frequency (f = 100 Hz). See Figure 12-5. While the addition of silica nanofiller into PMMA leads to a slight decrease in T_{β}, it results in a major reduction in the value of ε'' over all temperatures accessed in this study. In particular, when 0.4 vol% silica is dispersed in PMMA, the maximum value of ε'' is reduced by

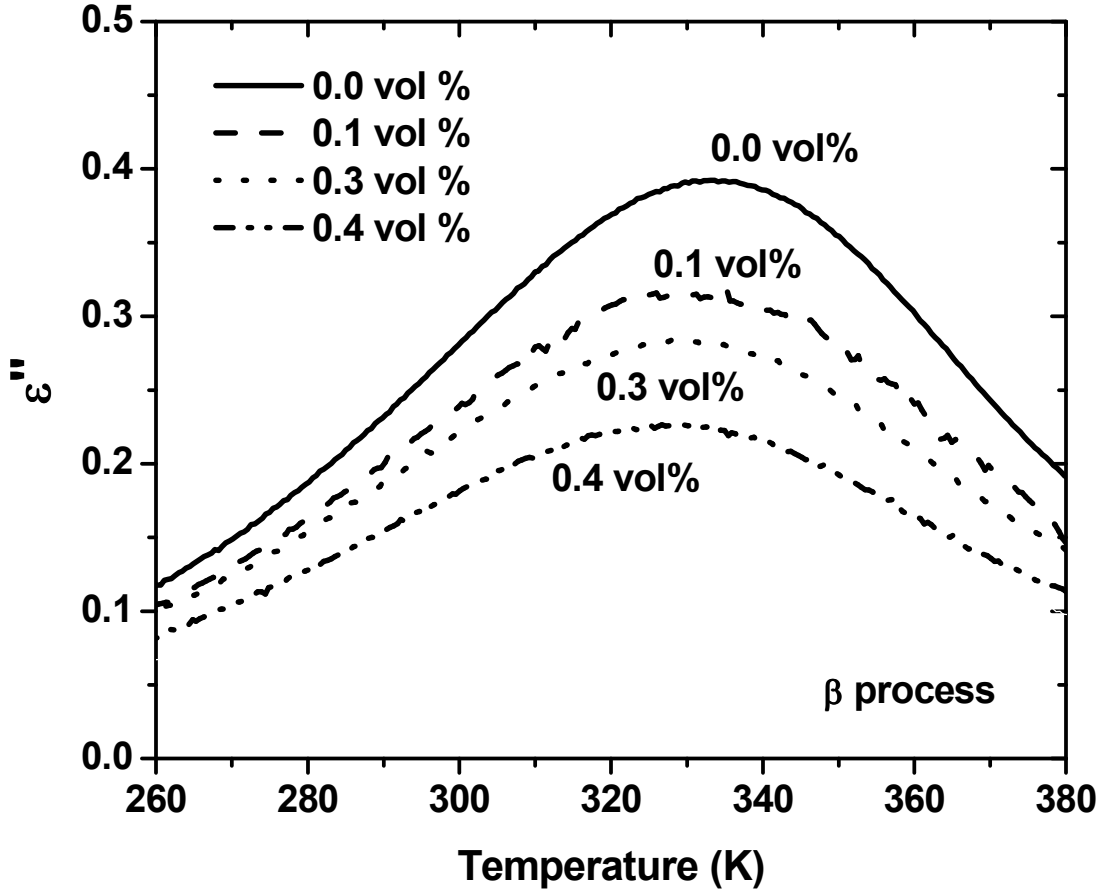

Figure 12-5: Effect of temperature on the dielectric loss constant of the β process for neat PMMA (solid curve), 0.1 vol% silica-PMMA nanocomposite (dashed curve), 0.3 vol% silica-PMMA nanocomposite (dotted curve), and 0.4 vol% silica-PMMA nanocomposite (dashed/dotted curve).

nearly 50 % relative to the value in neat PMMA. The strength of the ε'' signal, i.e., its magnitude, is related to a combination of the density of fluctuating dipoles, the extent to which each dipole is able to fluctuate and to the dipole moment of PMMA. Since the dipole moment of PMMA remains unchanged when 0.4 vol% silica is added to PMMA, the decrease in ε'' results from a combined effect, with some dipoles having hindered motion and some being immobile on the time scale being probed at a frequency of 100 Hz. (It is noted that while there is the slight decrease in T_β with increasing silica content, which, other things being equal, suggests a slight increase in the dynamics of the β process, the strength of the β process is vastly reduced. Thus, there is a major reduction in the extent to which the β relaxation occurs.)

The notion that the molecular motions associated with the β process are hindered or immobilized supports the idea that strong, attractive polymer-silica substrate interactions (in the case of thin films) and strong, attractive polymer-silica nanofiller interactions (in the case of nanocomposites) impede the relaxations associated with physical aging, giving rise to the remarkable reduction in aging rate observed in these nanoconfined systems. The hydrogen bonding interactions that occur between PMMA and silica involve the ester side groups on PMMA and the hydroxyl groups on silica. If the flexible side group motions of PMMA that contribute to physical aging are hindered or immobilized by the presence of silica, it is logical to interpret that the reduction in physical aging rate observed in both PMMA films supported on silica (Chapters 9, 10, and 11) and silica-PMMA nanocomposites is a consequence of a reduction in the mobility of the flexible side groups (motions associated with the β process). The concept that relaxations accompanying physical aging are linked to the β relaxation process was established in bulk polymers nearly 30 years ago (Struik 1978). For PMMA, it is noted that a

reduction in the strength of the β process was observed with decreasing film thickness for films supported between two Al electrodes (Wubbenhorst 2002; Fukao 2001a). The reduction in the strength of the β process was attributed to a modification of the chain equilibrium conformational statistics (Wubbenhorst 2002). This suggests that the reduced strength of the β process in the silica-PMMA nanocomposites may be due to a combination of effects related to the reduced mobility of the flexible side groups caused by hydrogen bonding interactions and by modified chain conformational statistics. Further study is warranted to address this issue.

While the presented results have made a strong connection between the reduced strength of the β process with the suppression of physical aging in PMMA-silica nanocomposites, the mechanism by which the β process and thereby physical aging is hindered over length scales of tens of nanometers away from the polymer-silica interface is as yet unknown. (If an idealized dispersion is assumed and the nanospheres are arranged in a cubic array, the theoretical interparticle distance of 0.4 vol% silica (10-15 nm in diameter) is ~50 nm. Since the dispersion is not ideal, the average interparticle distance must be greater than ~50 nm.) Does the long-range propagation of interfacial effects that hinder the β process and physical aging have its origin in the fact that numerous silica nanoparticles distributed within 10-50 nm will impact the dynamics of a single polymer segment? Is there an effect of temperature relative to T_g on the length scale over which the effects of attractive interfacial interactions propagate away from the interface? These are but a few of the scientific questions associated with this behavior. Besides the important scientific issues, the suppressed aging observed in polymer nanocomposites with attractive polymer-substrate interactions also has very important technological implications. In particular, this behavior suggests that it may be possible to produce glassy materials consisting of

polymer with traces of nanofiller which exhibit little or no physical aging although the polymer itself is a non-equilibrium glass that ages significantly in the neat state.

12.4 Conclusions

Fluorescence spectroscopy has been used to determine the impact of silica nanofiller on the rate of physical aging of PMMA, while dielectric relaxation spectroscopy has been used to determine the impact of silica nanofiller on the α and β relaxation processes. At room temperature, the addition of 0.4 vol% silica nanofiller into PMMA resulted in nearly a total arrest of physical aging during the experimental time scale measured. This addition of silica nanofiller also greatly reduced the strength of the β process in PMMA. The results presented in this chapter suggest that these two effects are strongly correlated and that the reduction in the PMMA ester side group mobility that is the cause of the reduced strength of the β process is also a major part of the molecular-scale origin of the suppression of physical aging in the silica-PMMA nanocomposites.

PART V: SUMMARY

13 CONCLUSIONS AND FUTURE WORK

This work has investigated the impact of confinement and interfaces on the structural relaxation of polymers over a wide temperature range relative to the glass transition temperature (T_g). After the Introduction, the manuscript was divided into five sections. Section I provided background information necessary to understand the work presented in this thesis. Section II (which includes Chapters 2-4) investigated the impact of confinement and interfaces on T_g. Section III investigated the impact of confinement and interfaces on the α-relaxation dynamics. Section IV investigated the impact of confinement and interfaces on physical aging. Lastly, Section V provides key conclusions and future work.

Section II

Work presented in Chapters 5 and 6 (Section II) provided substantial evidence that the T_g-nanoconfinement effect is a result of interfacial effects. In Chapter 5, it was shown that the observed increase in T_g with confinement for poly(methyl methacrylate) (PMMA) films supported on silica was a result of competing interfacial effects. In addition, it was observed that substrate effects can propagate more than 200 nm across a film to impact free surface T_g dynamics. The results highlighted the extremely long range nature of interfacial effects.

Chapter 6 extended the study of Chapter 5 by examining confinement and interfacial effects on a series of poly(n-methacrylate)s supported on silica. The study provided a correlation between the T_g-nanoconfinement behavior and the relative strength of interfacial effects (strength of interfacial effects is a measure of the deviation in T_g). More importantly, the study revealed

that small changes to the repeat unit structure of a polymer can have a dramatic effect on the ability of interfaces to perturb T_g dynamics. A molecular-level model explaining such an effect is warranted.

Section III

Chapters 7 and 8 provided further understanding of confinement and interfacial effects on the α-relaxation dynamics of polystyrene (PS) via dielectric relaxation spectroscopy (DRS). Chapter 7 explored the utility of using PS labeled with a molecular dipole to investigate confinement effects on the α-relaxation dynamics. It was observed that the molecular dipole Disperse Red 1 was coupled to the α-relaxation dynamics of PS and provided an enhanced signal of the relaxation process compared to neat PS. Confinement impacted the α-relaxation dynamics of labeled PS and neat PS in a similar manner. With confinement, labeled PS exhibited faster α-relaxation dynamics and a broadening in the distribution of α-relaxation times. In earlier work, Fukao *et al*. (Fukao 2000) observed similar results for neat PS and proposed a multilayer model to explain their results. In the model, the dynamics at the evaporated aluminum (Al)-polymer interface exhibited enhanced dynamics compared to the film interior.

Chapter 8 tested the model previously proposed by Fukao *et al*. (Fukao 2000). In the chapter a novel multilayer / DRS method was used to provide the first direct measurement of α-relaxation dynamics at the evaporated Al-polymer interface (the Al-polymer interface behaves as a free surface). In agreement with the model proposed by Fukao *et al*. (Fukao 2000), the α-relaxation dynamics of a layer at the evaporated Al-polymer interface were enhanced and broadened compared to the bulk.

Section IV

The objective of Section IV (which includes Chapters 9, 10, 11, and 12) was to investigate confinement and interfacial effects on the physical aging response of polymer glasses. Chapter 9 explored the impact of interfacial effects (weak versus strong) on the physical aging rate of thin polymer films. It was observed that when attractive polymer-substrate interactions existed aging was suppressed; however, when attractive polymer-substrate interactions did not exist, aging was not greatly affected by confinement.

Chapter 10 provided further understanding of the impact that interfacial effects have on physical aging. Poly(methyl methacrylate) films supported on silica were investigated. Using the multilayer / fluorescence technique, for the first time aging was monitored exclusively at the interfaces of a thin polymer film. It was observed that when aged well below T_g(bulk), the aging response at the free surface was reduced compared to the bulk and at the substrate nearly completely suppressed. At aging temperatures closer to T_g(bulk), aging did not occur at the free surface, which indicated the existence of a glass with rubbery behavior at the free surface.

Chapter 11 explored for the first time the possibility of using a ratio of intensities to monitor physical aging in bulk and ultrathin polymer films. Poly(methyl methacrylate) labeled with TC1 was the system investigated. As a result of being an intramolecular charge transfer probe, TC1 exhibited a spectral shift during aging. Monitoring the spectral shift via a ratio of intensities provided a measure of aging similar to that of volume dilatometry. From this method, it was determined that the extent of aging toward equilibrium (theoretical equilibrium) was reduced with confinement.

While Chapters 9, 10, and 11 provided evidence that the polymer-substrate interface was

partially responsible for the aging-confinement effect (reduction in aging rate with confinement), Chapter 12 aimed at providing a molecular origin for the suppression of aging. The β-relaxation dynamics of silica-PMMA nanocomposites were investigated using DRS. Poly(methyl methacrylate) and silica exhibit attractive hydrogen bonding interactions with one another. It was observed that with increasing silica content the aging rate was reduced and the strength of the β process was reduced. As a result, it was concluded that the suppressed aging response in silica-PMMA nanocomposites was a result of a reduced β process that resulted from the attractive polymer-nanofiller interactions.

Future Work

While this work has provided valuable information about the impact of confinement and interfaces on the relaxation dynamics of polymers above, below and at the glass transition, much remains to been conducted. This section will highlight a few opportunities for future work.

Section II of this work investigated the impact of confinement on T_g of polymer films that possessed attractive interactions with the substrate using fluorescence. This work could be potentially extended in two ways. First, fluorescence can be developed to allow for T_g measurements of freely standing films. This would enable the study of the effects of molecular weight and chemical structure on the T_g-nanoconfinement behavior of freely standing films. In addition, fluorescence may provide a route to conduct T_g-nanoconfinement studies of polymer confined to nanopores. This seems plausible if the nanoporous glass could be made of quartz. Labeled polymer can be placed within the nanopores via solution processing or in situ polymerization. Varying the average diameter of the nanopores would provide a way to study confinement effects. Varying the polymer and the surface of the glass would provide a way to

study interfacial effects. It may be possible to label the nanoporous glass with fluorescent probes and conduct T_g measurements on neat polymer. Such a study would provide information about the interfacial T_g. Investigating the interfacial T_g while changing the diameter of the nanoporous glass provides another way to measure confinement effects on T_g.

In a series of studies from Dutcher and coworkers (Forrest 1997; Roth 2006), it was shown that the T_g-nanoconfinement effect of freely standing films was dependent upon the polymer molecular weight. However, it was shown by Keddie *et al*. (Keddie 1994a) and Ellison *et al*. (Ellison 2005) that the T_g-nanoconfinement effect of supported films was independent of the polymer molecular weight. Given the ability of fluorescence to provide an interfacial layer T_g, it should be tested whether or not there is a molecular weight dependence of the T_g of a free surface layer or a substrate layer. Such a study may provide a possible origin for the difference in behavior of freely standing films and supported films.

Section III of this work focused on investigating the impact of confinement and interfaces on the α-relaxation dynamics of polymers. To enhance the dielectric signal of PS a molecular dipole, Disperse Red 1 (DR1), was labeled to PS. The molecular dipole enhanced the dielectric signal of PS by a factor of 65. Work by Dhinojwala *et al*. (Dhinojwala 1994b) demonstrated that the reorientational relaxation dynamics of DR1 were coupled to the α-relaxation dynamics of PS. Future studies should be conducted to examine the impact of the dipole size and concentration on the ability to couple to the α-relaxation dynamics of PS and other polymers. It may be possible to identify probes that couple to β-relaxation dynamics. In addition, work presented in Chapters 7 and 8 should be expanded to high molecular weight polymer. It may be possible to access the relaxation dynamics at the polymer-substrate interface by chemically grafting molecular dipoles

to a substrate. Dielectric relaxation spectroscopy provides a route to examine the relaxation dynamics of polymer filled systems. A novelty may be to label the nanofiller with molecular dipoles, thereby providing a route to probe the interfacial relaxation dynamics of nanocomposites. Work by Rittigstein and Torkelson (Rittigstein 2006) illustrated the importance of wetted versus non-wetted polymer-nanofiller interfaces on T_g. The impact of wetted versus non-wetted polymer-nanofiller interfaces on the relaxation dynamics of polymer should be investigated via DRS.

Section IV investigated the impact of confinement and interfaces on the physical aging of polymers. While studies were able to be conducted on supported films and nanocomposites, no studies were performed on freely standing films. It may be possible to use fluorescence to investigate the physical aging response of freely standing films. Besides conducting such studies on PS and PMMA it would be worthwhile to conduct such measurements on stiffer polymers such as poly(phenylene oxide) (PPO) and poly(ethylene terepthalate) (PET). Besides freely standing films, additional aging measurements should be conducted on model nanocomposites (films supported on both sides).

Chapter 11 introduced the ability of a ratio of fluorescence intensities to monitor physical aging in bulk and ultrathin films. Further studies should be conducted to determine other probes suitable for such measurements. As the ratio of intensities is sensitive to the rigidity of a system, it may be possible to extract information about chain stiffness. Intensity ratio is an absolute quantity that is independent of sample geometry, light source and probe concentration. The life time of a probe, another absolute quantity, may be used to monitor aging in bulk and ultrathin films.

Besides fluorescence, aging-confinement studies can be conducted using DRS and ellipsometry. With DRS, it may be possible to investigate the impact that confinement and interfaces have on the relaxation dynamics during aging. Additionally, such studies can be carried out in nanocomposite systems.

REFERENCES

Adams, G. and Gibbs, J. H. (1965). *Journal of Chemical Physics* **43**: 139.

Akabori, K., Tanaka, K., Nagamura, T., Takahara, A. and Kajiyama, T. (2005). *Macromolecules* **38**: 9735.

Alcoutlabi, M. and McKenna, G. B. (2005). *Journal of Physics: Condensed Matter* **17**: R461.

Alvarez, F., A.Alegria and Colmenero, J. (1991). *Physical Review B* **44**: 7306.

Anastasiadis, S. H., Karatasos, K., Vlachos, G., Manias, E. and Giannelis, E. P. (2000). *Physical Review Letters* **84**: 915.

Anderson, P. E. (1995). *Science* **267**: 1615.

Angell, C. A. (1995). *Science* **267**: 1925.

Angell, C. A. (1995). *Proceeding of the National Academy of Sciences* **92**: 6675.

Angell, C. A., Ngai, K. L., McKenna, G. B., McMillan, P. F. and Martin, S. W. (2000). *Journal of Applied Physics* **88**: 3133.

Ash, B. J., Schadler, L. S. and Siegel, R. W. (2002). *Materials Letters* **55**: 83.

Badrinarayanan, P. and Simon, S. L. (2007). *Polymer* **48**: 1464.

Baljon, A. R. C., Billen, J. and Khare, R. (2004). *Physical Review Letters* **93**: 255701.

Bansal, A., Yang, H., Li, C., Cho, K., Benicewicz, B. C., Kumar, S. K. and Schadler, L. S. (2005). *Nature Materials* **4**: 693.

Baschnagel, J., Meyer, H., Varnik, F., Metzger, S., Aichele, M., Muller, M. and Binder, K. (2003). *Interfacial Science* **11**: 159.

Berg, O. v. d., Cangialosi, D., Jager, W. F., Veen, A. v. and Picken, S. J. (2004a). *Polymeric*

Materials Science and Engineering **90**: 611.

Berg, O. v. d., Jager, W. F., Cangialosi, D., Turnhout, J. v., Verheijen, P. J. T., Wubbenhorst, M. and Picken, S. J. (2006). *Macromolecules* **39**: 224.

Berg, O. v. d., Jager, W. F., Sengers, W. G. F., Wubbenhorst, M. and Picken, S. J. (2004b). *Polymeric Materials: Science and Engineering* **90**: 603.

Berg, O. v. d., Sengers, W. G. F., Jager, W. F., Picken, S. J. and Wubbenhorst, M. (2004). *Macromolecules* **37**: 2460.

Berg, O. v. d., Wubbenhorst, M., Picken, S. J. and Jager, W. F. (2005). *Journal of Non-Crystalline Solids* **351**: 2694.

Berriot, J., Montes, H., Lequeux, F., Long, D. and Sotta, P. (2002). *Macromolecules* **35**: 9756.

Berthier, L., Biroli, G., Bouchaud, J. P., Cipelletti, L., Masri, D. E., L'Hote, D., Ladieu, F. and Pierno, M. (2005). *Science* **310**: 1797.

Bhattacharya, M., Sanyal, M. K., Geue, T. and Pietsch, U. (2005). *Physical Review E* **71**: 041801.

Bodiguel, H. and Fretigny, C. (2007). *Macromolecules* **40**: 7291.

Cangialosi, D., Schut, H., Veen, A. v. and Picken, S. J. (2003). *Macromolecules* **36**: 142.

Cangialosi, D., Wubbenhorst, M., Groenewold, J., Mendes, E. and Picken, S. J. (2005). *Journal of Non-Crystalline Solids* **351**: 2605.

Cheng, L.-T. (1991). *Journal of Chemical Physics* **95**: 10631.

Corrales, T., Villaviega, M. M., Peinado, C. and Bosch, P. (2006). *Journal of Photochemistry and Photobiology A: Chemistry* **182**: 52.

Dalnoki-Veress, K., Forrest, J. A., Murray, C., Gigault, C. and Dutcher, J. R. (2001). *Physical Review E* **63**: 031801.

Debenedetti, P. G. and Stillinger, F. H. (2001). *Nature* **410**: 259.

DeBolt, M. A., Easteal, A. J., Macedo, P. B. and Moynihan, C. T. (1976). *Journal of the American Ceramic Society* **59**: 16-21.

DeMaggio, G. B., Frieze, W. E., Gidley, D. W., Zhu, M., Hristov, H. A. and Yee, A. F. (1997). *Physical Review Letters* **78**(1524).

Deppe, D. D., Dhinojwala, A. and Torkelson, J. M. (1996). *Macromolecules* **29**: 3898.

Deus, J. F. d., Souza, G. P., Corradini, W. A., Atvars, T. D. Z. and Akcelrud, L. (2004). *Macromolecules* **37**: 6938.

Dhinojwala, A., Hooker, J. C. and Torkelson, J. M. (1994a). *Journal of Non-Crystalline Solids* **172**: 286.

Dhinojwala, A., Wong, G. K. and Torkelson, J. M. (1993). *Macromolecules* **26**: 5943.

Dhinojwala, A., Wong, G. K. and Torkelson, J. M. (1994b). *Journal of Chemical Physics* **100**: 6046.

DiMarzio, E. A. (1981). *Annals of the New York Academy of Sciences* **371**: 1.

Dionisio, M. S., Moura-Ramos, J. J. and Williams, G. (1994). *Polymer* **35**: 1705.

Donati, C., Douglas, J. F., Kob, W., Plimpton, S. J., Poole, P. H. and Glotzer, S. C. (1998). *Physical Review Letters* **80**: 2338.

Donth, E. (2001). *The Glass Transiton* Berlin, Springer.

Doolittle, A. K. (1951). *Journal of Applied Physics* **22**: 1471.

Dorkenoo, K. D. and Pfromm, P. H. (1999). *Journal of Polymer Science: Part B: Polymer Physics* **37**: 2239-2251.

Ediger, M. D. (2000). *Annual Reviews of Physical Chemistry* **51**: 99.

Ediger, M. D., Angell, C. A. and Nagel, S. R. (1996). *Journal of Physical Chemistry* **100**: 13200.

Ellison, C. J., Kim, S. D., Hall, D. B. and Torkelson, J. M. (2002a). *European Physical Journal E* **8**: 155-166.

Ellison, C. J., Miller, K. E. and Torkelson, J. M. (2004a). *Polymer* **45**: 2623.

Ellison, C. J., Mundra, M. K. and Torkelson, J. M. (2005). *Macromolecules* **38**: 1767.

Ellison, C. J., Ruszkowski, R. L., Fredin, N. J. and Torkelson, J. M. (2004b). *Physical Review Letters* **92**: 095702.

Ellison, C. J. and Torkelson, J. M. (2002). *Journal of Polymer Science: Part B: Polymer Physics* **40**: 2745.

Ellison, C. J. and Torkelson, J. M. (2002b). *Journal of Polymer Science: Part B: Polymer Physics* **40**: 2745.

Ellison, C. J. and Torkelson, J. M. (2003). *Nature Materials* **2**: 695.

Elmahdy, M. M., Chrissopoulou, K., Afratis, A., Floudas, G. and Anastasiadis, S. H. (2006). *Macromolecules* **39**: 5170.

Fakhraai, Z. and Forrest, J. A. (2005). *Physical Review Letters* **95**: 025701.

Fakhraai, Z. and Forrest, J. A. (2008). *Science* **319**: 600.

Fakhraai, Z., Sharp, J. S. and Forrest, J. A. (2004). *Journal of Polymer Science Part B Polymer Physics* **42**: 4503.

Fischer, H. (2005). *Macromolecules* **38**: 844.

Flory, P. J. (1953). *Principles of Polymer Chemistry* Ithaca, NY, Cornell University Press.

Forrest, J. A. and Dalnoki-Veress, K. (2001). *Advances in Colloid and Interface Science* **94**: 167.

Forrest, J. A., Dalnoki-Veress, K. and Dutcher, J. R. (1997). *Physical Review E* **56**: 5705.

Forrest, J. A., Dalnoki-Veress, K., Stevens, J. R. and Dutcher, J. R. (1996). *Physical Review Letters* **77**: 2002.

Forrest, J. A. and Mattsson, J. (2000). *Physical Review E* **61**: R53.

Forrest, J. A., Svanberg, C., Revesz, K., Rodahl, M., Torell, L. M. and Kasemo, B. (1998). *Physical Review E* **58**: R1226.

Fryer, D. S., Nealey, P. F. and Pablo, J. J. (2000). *Macromolecules* **33**: 6439.

Fryer, D. S., Peters, R. D., Kim, E. J., Tomaszewski, T. E., Pablo, J. J., Nealey, P. F., White, C. C. and Wu, W. L. (2001). *Macromolecules* **34**: 5627.

Fukao, K. and Koizumi, H. (2007). *European Phyics Journal Special Topics* **141**: 199.

Fukao, K. and Miyamoto, Y. (1999). *Europhysics Letters* **46**: 649.

Fukao, K. and Miyamoto, Y. (2000). *Physical Review E* **61**: 1743.

Fukao, K. and Miyamoto, Y. (2001b). *Physical Review E* **64**: 011803.

Fukao, K. and Sakamoto, A. (2005). *Physical Review E* **71**: 041803.

Fukao, K., Uno, S., Miyamoto, Y., Hoshino, A. and Miyaji, H. (2001a). *Physical Review E* **64**: 051897.

Fulcher, G. S. (1925). *Journal of the American Ceramic Society* **8**: 339.

Gasemjit, P. and Johannsmann, D. (2006). *Journal of Polymer Science Part B Polymer Physics* **44**: 3031.

Gibbs, J. H. and DiMarzio, E. A. (1958). *Journal of Chemical Physics* **28**: 373.

Glotzer, S. C. (2000). *Journal of Non-Crystalline Solids* **274**: 342.

Greiner, R. and Schwarzl, F. R. (1984). *Rheologica Acta* **23**: 378.

Grohens, Y., Hamon, L., Reiter, G., Soldera, A. and Holl, Y. (2002). *European Physical Journal*

E **8**: 217.

Guerdoux, L. and Marchal, E. (1981). *Polymer* **22**: 1199.

Hains, P. J. and Williams, G. (1975). *Polymer* **16**: 725.

Hall, D. B., Dhinojwala, A. and Torkelson, J. M. (1997a). *Physical Review Letters* **79**: 103.

Hall, D. B., Hooker, J. C. and Torkelson, J. M. (1997b). *Macromolecules* **30**: 667-669.

Hall, D. B., Underhill, P. and Torkelson, J. M. (1998b). *Polymer Engineering and Science* **38**: 2039.

Hamdorf, M. and Johannsmann, D. (2000). *Journal of Chemical Physics* **112**: 4262-4270.

Hartmann, L., Gorbatschow, W., Hauwede, J. and Kremer, F. (2002). *European Physical Journal E* **8**: 145.

Havriliak, S. and Negami, S. (1967). *Polymer* **8**: 161.

Herminghaus, S., Seemann, R. and Landfester, K. (2004). *Physical Review Letters* **93**: 017801.

Hodge, I. A. (1995). *Science* **267**: 1945.

Hooker, J. C. and Torkelson, J. M. (1995). *Macromolecules* **28**: 7683.

Huang, Y. and Paul, D. R. (2004). *Polymer* **45**: 8377.

Huang, Y. and Paul, D. R. (2005). *Macromolecules* **38**: 10148.

Huang, Y. and Paul, D. R. (2006). *Macromolecules* **39**: 1554.

Hutcheson, S. A. and McKenna, G. B. (2005). *Physical Review Letters* **94**: 076103.

Hutcheson, S. A. and McKenna, G. B. (2007). *European Physical Journal E* **30**: 1.

Hutchinson, J. M. (1995). *Progress in Polymer Science* **20**: 703.

Ingratta, M. and Duhamel, J. (2007). *Macromolecules* **40**: 6647.

Jager, W. F., Berg, O. v. d. and Picken, S. J. (2005). *Macromolecular Symposium* **230**: 11.

Jager, W. F., Volkers, A. A. and Neckers, D. C. (1995). *Macromolecules* **28**: 5153.

Jerome, B. and Commandeur, J. (1997). *Nature* **386**: 589.

Jones, R. A. L. (2003). *Nature Materials* **2**: 645.

Kajiyama, T., Tanaka, K. and Takahara, A. (1997). *Macromolecules* **30**: 280.

Kalogeras, I. M. (2005). *Acta Materials* **53**: 1621.

Kalogeras, I. M. and Neagu, E. R. (2004). *European Physical Journal E* **14**: 193.

Kanaya, T., Miyazaki, T., Watanabe, H., Nishida, K., Yamano, H., Tasaki, S. and Bucknall, D. B. (2003). *Polymer* **44**: 3769.

Kauzmann, W. (1948). *Chemical Review* **43**: 219.

Kawana, S. and Jones, R. A. L. (2003). *European Physical Journal E* **10**: 223.

Keddie, J. L., Jones, R. A. L. and Cory, R. A. (1994a). *Europhysics* **27**: 59.

Keddie, J. L., Jones, R. A. L. and Cory, R. A. (1994b). *Faraday Discussions* **98**: 219.

Kerle, T., Lin, Z., Kim, H.-C. and Russell, T. P. (2001). *Macromolecules* **34**: 3484.

Kim, S. D. and Torkelson, J. M. (2002). *Macromolecules* **35**: 5943.

Koh, Y. P., McKenna, G. B. and Simon, S. L. (2006). *Journal of Polymer Science Part B Polymer Physics* **44**: 3518.

Kohlrausch, R. (1874). *Annuals of Physical Chemistry* **91**: 179.

Koros, W. J. and Fleming, G. K. (1993). *Journal of Membrane Science* **83**: 1.

Kovacs, A. J. (1981). *Annals of the New York Academy of Sciences* **371**: 21.

Kovacs, A. J., Aklonis, J. J., Hutchinson, J. M. and Ramos, A. R. (1979). *Journal of Polymer Science: Polymer Physics Edition* **17**: 1097.

Lakowicz, J. R. (1999). *Principles of Fluorescence Spectroscopy* New York, Plenum.

Lee, H. H.-D. and McGarry, F. J. (1993). *Polymer* **34**: 4267.

Lee, J.-Y., Su, K. E., Chan, E. P., Zhang, Q., Emrick, T. and Crosby, A. J. (2007). *Macromolecules* **40**: 7755.

Lenhart, J. L. and Wu, W.-l. (2002). *Macromolecules* **35**: 5145.

Lenhart, J. L., Zanten, J. H. v., Dunkers, J. P. and Parnas, R. S. (2001). *Macromolecules* **34**: 2225.

Li, Q. and Simon, S. L. (2006). *Polymer* **47**: 4781.

Liem, H., Cabanillas-Gonzalez, J., Etchegoin, P. and Bradley, D. D. C. (2004). *Journal of Physics Condensed Matter* **16**: 721.

Liu, Y., Russell, T. P., Samant, M. G., Stohr, J., Brown, H. R., Cossy-Favre, A. and Diaz, J. (1997). *Macromolecules* **30**: 7768.

Long, D. and Lequeux, F. (2001). *European Physical Journal E* **4**: 371.

Loutfy, R. O. (1981). *Macromolecules* **14**: 275.

Loutfy, R. O. (1986). *Pure and Applied Chemistry* **58**: 1239.

Loutfy, R. O. and Arnold, B. A. (1982). *Journal of Physical Chemistry* **86**: 4205.

Loutfy, R. O. and Law, K. Y. (1980). *Journal of Physical Chemistry* **84**: 2803.

Lu, H. and Nutt, S. (2003). *Macromolecules* **36**: 4010.

Lupascu, V., Picken, S. J. and Wubbenhorst, M. (2006). *Journal of Non-Crystalline Solids* **352**: 5594.

Martins, T. D., Gulmine, J. V., Akcelrud, L., Weiss, R. G. and Atvars, T. D. Z. (2006). *Polymer* **47**: 7414.

Matsuoka, S. (1986). *Journal of Rheology* **30**: 869.

McKenna, G. B. (1989). *Glass Formation and Glassy Behavior, Comprehensive Polymer Science*: *Polymer Properties* Oxford, Pergamon.

McKenna, G. B. (2000a). *Journal of Physics. IV France* **10**: 343.

McKenna, G. B. (2000b). *Journal of Physics IV France* **10**: 53.

McKenna, G. B. (2003). *European Physical Journal E* **12**: 191.

McKenna, G. B. and Simon, S. L. (2002). *The Glass Transition and Underlying Physics, Handbook of Thermal Analysis and Calorimetry* **3**, S.Z.D. Cheng, Ed. Elsevier Science.

McKusick, C. B., Heckert, R. E., Clairns, T. L., Coffman, D. D. and Mower, H. F. (1958). *Journal of American Chemical Society* **80**: 2806.

Merabia, S. and Long, D. (2006). *Journal of Chemical Physics* **25**: 234901.

Merabia, S., Sotta, P. and Long, D. (2004). *European Physical Journal E* **15**: 189.

Merolle, M., Garrahan, J. P. and Chandler, D. (2005). *Proceeding of the National Academy of Sciences* **102**: 10837.

Meyer, E. F., Jamieson, A. M., Simha, R., Palmen, J. H. M., Booij, H. C. and Maurer, F. H. J. (1990). *Polymer* **31**: 243-247.

Miyamoto, Y. (1984). *Polymer* **25**: 63.

Miyazaki, T., Inoue, R., Nishida, K. and Kanaya, T. (2007). *European Physical Journal Special Topics* **141**: 203.

Mundra, M. K., Donthu, S. K., Dravid, V. P. and Torkelson, J. M. (2007a). *Nano Letters* **7**: 713.

Mundra, M. K., Ellison, C. J., Behling, R. E. and Torkelson, J. M. (2006). *Polymer* **47**: 7747.

Mundra, M. K., Ellison, C. J., Rittigstein, P. and Torkelson, J. M. (2007b). *European Phyics Journal Special Topics* **141**: 143.

Mundra, M. K., Ellison, C. J., Rittigstein, P. and Torkelson, J. M. (2007c). *European Phyics Journal Special Topics* **141**: 143.

Muzeau, E., Vigier, G. and Vassoille, R. (1994). *Journal of Non-Crystalline Solids* **172**: 575.

Nagai, K., Masuda, T., Nakagawa, T., Freeman, B. and Pinnau, I. (2001). *Progress in Polymer Science* **26**: 721.

Napolitano, S., Prevosto, D., Lucchesi, M., Pingue, P., D'Acunto, M. and Rolla, P. (2007b). *Langmuir* **23**: 2103.

Napolitano, S. and Wubbenhorst, M. (2007a). *Journal of Physical Chemistry B* **111**: 9197.

Narayanan, R. A., Thiyagarajan, P., Lewis, S., Bansal, A., Schadler, L. S. and Lurio, L. B. (2006). *Physical Review Letters* **97**: 075505.

Narayanaswamy, O. S. (1971). *Journal of the American Ceramic Society* **54**: 491.

Ngai, K. L. (2006). *Journal of Polymer Science Part B Polymer Physics* **44**: 2980.

Ngai, K. L. and Capaccioli, S. (2007). *Journal of Physics Condensed Matter* **19**: 205114.

O'Connell, P. A. and McKenna, G. B. (2005). *Science* **307**: 1760.

O'Connell, P. A. and McKenna, G. B. (2006). *European Physical Journal E* **20**: 143.

Papaleo, R. M., Leal, R., Carreira, W. H., Barbosa, L. G., Bello, I. and Bulla, A. (2006). *Physical Review B* **74**: 094203.

Park, C. H., Kim, J. H., Ree, M., Sohn, B.-H., Jung, J. C. and Zin, W.-C. (2004). *Polymer* **45**: 4507.

Peter, S., Meyer, H. and Baschnagel, J. (2006). *Journal Polymer Science Part B Polymer Physics* **44**: 2951.

Pfromm, P. H. and Koros, W. J. (1995). *Polymer* **36**: 2379.

Pham, J. Q. and Green, P. F. (2003). *Macromolecules* **36**: 1665.

Priestley, R. D., Mundra, M. K., Barnett, N., Broadbelt, L. J. and Torkelson, J. M. (2007a). *Australian Journal of Chemistry* **60**: 765.

Priestley, R. D., Mundra, M. K., Rittigstein, P., Broadbelt, L. J. and Torkelson, J. M. (2008b). *Manuscript in Preparation*.

Prucker, O., Christian, S., Bock, H., Ruhe, J., Frank, C. W. and Knoll, W. (1998). *Macromolecular Chemistry and Physics* **1999**: 1435.

Pu, Y., Rafailovich, M. H., Sokolov, J., Gersappe, D., Peterson, T., Wu, W.-L. and Schwarz, S. A. (2001). *Physical Review Letters* **87**: 206101.

Quirin, J. C. and Torkelson, J. M. (2003). *Polymer* **44**: 423.

Read, B. E. (1991). *Journal of Non-Crystalline Solids* **131**: 408.

Richardson, H., C.Carelli, Keddie, J. L. and Sferrazza, M. (2003). *European Physical Journal E* **12**: 437.

Richardson, H., Lopez-Garcia, I., Sferrazza, M. and Keddie, J. L. (2004). *Physical Review E* **70**: 051805.

Riggleman, R. A., Yoshimoto, K., Douglas, J. F. and Pablo, J. J. (2006). *Physical Review Letters* **97**: 045502.

Rittigstein, P., Priestley, R. D., Broadbelt, L. J. and Torkelson, J. M. (2007). *Nature Materials* **6**: 278.

Rittigstein, P. and Torkelson, J. M. (2006). *Journal of Polymer Science Part B Polymer Physics* **44**: 2935.

Roth, C. B. and Dutcher, J. R. (2003). *European Physical Journal E* **12**: S103.

Roth, C. B. and Dutcher, J. R. (2004). *Mobility on Different Lenth Scales in Thin Polymer Films, Soft Materials: Structure and Dynamics*, J.R. Dutcher & A.G. Marangoni, Eds. Marcel Dekker.

Roth, C. B., McNerny, K. L., Jager, W. F. and Torkelson, J. M. (2007a). *Macromolecules* **40**: 2568.

Roth, C. B., Pound, A., Kamp, S. W., Murray, C. A. and Dutcher, J. R. (2006). *European Physical Journal E* **20**: 441.

Roth, C. B. and Torkelson, J. M. (2007b). *Macromolecules* **40**: 3328.

Royal, J. S. and Torkelson, J. M. (1990). *Macromolecules* **23**: 3536.

Royal, J. S. and Torkelson, J. M. (1992a). *Macromolecules* **25**: 4792.

Royal, J. S. and Torkelson, J. M. (1992b). *Macromolecules* **25**: 1705.

Royal, J. S. and Torkelson, J. M. (1993). *Macromolecules* **26**: 5331.

Royal, J. S., Victor, J. G. and Torkelson, J. M. (1992c). *Macromolecules* **25**: 729.

Russell, E. W. and Israeloff, N. E. (2000). *Nature* **408**: 695.

Schonhals, A., Goering, H., Schick, C., Frick, B. and Zorn, R. (2003). *European Physical Journal E* **12**: 173.

Schonhals, A. and Kremer, F. (2003). *Broadband Dielectric Spectroscopy* Berlin, Springer-Verlag.

Schwab, A. D., Agra, D. M. G., Kim, J.-H., Kumar, S. and Dhinojwala, A. (2000). *Macromolecules* **33**: 4903-4909.

Schwab, S. D. and Levy, R. L. (1990). *Advances in Chemistry Series* **227**: 397-408.

Serghai, A. and Kremer, F. (2003). *Physical Review Letters* **91**: 165702.

Serghei, A., Huth, H., Schellenberger, M., Schick, C. and Kremer, F. (2005). *Physical Review E* **71**: 061801.

Serghei, A. and Kremer, F. (2006a). *Review of Scientific Instruments* **77**: 116108.

Serghei, A., Tress, M. and Kremer, F. (2006b). *Macromolecules* **39**: 9385.

Sharp, J. S. and Forrest, J. A. (2003a). *Physical Review Letters* **91**: 235701.

Sharp, J. S., Forrest, J. A., Fakhraai, Z., Khomenko, M., Teichroeb, J. H. and Dalnoki-Veress, K. (2007). *European Physical Journal E* **35**: 8.

Sharp, J. S., Teichroeb, J. H. and Forrest, J. A. (2004). *European Physical Journal E* **15**: 473.

Shearmur, T. E., Clough, A. S., Drew, D. W., Grinten, M. G. D. v. d. and Jones, R. A. L. (1998). *Polymer* **39**: 2155.

Sillescu, H. (1999). *Journal of Non-Crystalline Solids* **243**: 81.

Sills, S., Overney, R. M., Chau, W., Lee, V. Y., Miller, R. D. and Frommer, J. (2004). *Journal of Chemical Physics* **120**: 5334.

Simon, S. L., Park, J. Y. and McKenna, G. B. (2002). *European Physical Journal E* **8**: 209.

Simon, S. L., Sobieski, J. W. and Plazek, D. J. (2001). *Polymer* **42**: 2555.

Sinnathamby, K. S., Oukris, H. and Israeloff, N. E. (2005). *Physical Review Letters* **95**: 067205.

Smith, G. D., Bedrov, D. and Borodin, O. (2003). *Physical Review Letters* **90**: 226103.

Soles, C. L., Douglas, J. F., Jones, R. L. and Wu, W.-L. (2004). *Macromolecules* **37**: 2901.

Srivastava, S. and Basu, J. K. (2007). *Physical Review Letters* **98**: 165701.

Stafford, C., Vogt, B. D., Harrison, C., Julthongpiput, D. and Huang, R. (2006). *Macromolecules* **39**: 5095.

Starr, F. W., Schroder, T. B. and Glotzer, S. C. (2001). *Physical Review E* **64**: 021802.

Strehmel, B., Strehmel, V. and Younes, M. (1999). *Journal of Polymer Science: Part B: Polymer Physics* **37**: 1367.

Struik, L. C. E. (1978). *Physical Aging of Amorphous Polymers and Other Materials* Amsterdam, Elsevier.

Svanberg, C. (2007). *Macromolecules* **40**: 312.

Tammann, G. and Hesse, W. (1926). *Zeitschrift fur Anorganische und Allgemeine Chemie* **156**: 245.

Tanaka, K., Tateishi, Y. and Nagamura, T. (2004). *Macromolecules* **37**: 8188.

Tant, M. R. and Wilkes, G. L. (1981). *Polymer Engineering and Science* **21**: 874.

Teichroeb, T. H. and Forrest, J. A. (2003). *Physical Review Letters* **91**: 016104.

Thurau, C. T. and Ediger, M. D. (2002a). *Journal of Chemical Physics* **116**: 9089.

Thurau, C. T. and Ediger, M. D. (2002b). *Journal of Polymer Science: Part B: Polymer Physics* **40**: 2463.

Tool, A. Q. (1946). *Journal of the American Chemical Society* **29**: 240.

Torres, J. A., Nealey, P. F. and Pablo, J. J. d. (2000). *Physical Review Letters* **85**: 3221.

Tracht, U., Wilhelm, M., Heuer, A., Feng, H., Schmidt-Rohr, K. and Spiess, H. W. (1998). *Physical Review Letters* **81**: 2727.

Turnbull, D. and Cohen, M. H. (1961). *Journal of Chemical Physics* **34**: 120.

Turrion, S. G., Olmos, D., Ekizoglou, N. and Gonzales-Benito, J. (2005). *Polymer* **45**: 4023.

Valeur, B. (2002). *Molecular Fluorescence: Principles and Applications* Weinheim, Wiley-VCH.

vanZanten, J. H., Wallace, W. E. and Wu, W. L. (1996). *Physical Review E* **53**: R2053.

Varnik, F., Baschnagel, J. and Binder, K. (2002). *Journal of Non-Crystalline Solids* **307**: 524.

Victor, J. G. and Torkelson, J. M. (1988). *Macromolecules* **21**: 3490.

Vlasveld, D. P. N., Bersee, H. E. N. and Picken, S. J. (2005). *Polymer* **46**: 12539.

Vogel, H. (1921). *Physik in unserer Zeit* **22**: 645.

Weeks, E. R., Crocker, J. C., Levitt, A. C., Schofield, A. and Weitz, D. A. (2000). *Science* **287**: 627.

White, C., Wu, W.-L., Pu, Y., Rafailovich, M. and Sokolov, J. (2003). *Polymer Engineering and Science* **43**: 1241-1249.

Williams, G. and Watts, D. C. (1970). *Transactions of the Faraday Society* **66**: 80.

Williams, M. L., Landel, R. F. and Ferry, J. D. (1955). *Journal of the American Chemical Society* **77**: 1471.

Winey, K. I. and Vaia, R. A. (2007). *MRS Bulletin* **32**: 314.

Winnik, M. A., Ed. (1986). *Photophysical and Photochemical Tools in Polymer Science* Dordrecht, Holland, D. Reidel Publishing Company.

Wubbenhorst, M., Murray, C. A. and Dutcher, J. R. (2003). *European Physical Journal E* **12**: s109.

Wubbenhorst, M., Murray, C. A., Forrest, J. A. and Dutcher, J. R. (2002). *11th International Symposium on Electrets* **11**: 401.

Xie, F., Zhang, H. F., Lee, F. K., Du, B., Tsui, O. K. C., Yokoe, Y., Tanaka, K., Takahara, A. and Kajiyama, T. (2002). *MAcromolecules* **35**: 1491.

Zhou, C., Chung, T.-S., Wang, R. and Goh, S. H. (2004). *Journal of Applied Polymer Science* **92**: 1758-1764.